

ISOTOPE DIAGENESIS AND PALAEOFLUID MOVEMENT:
MIDDLE JURASSIC BRENT SANDSTONES, NORTH SEA

A thesis submitted for the degree of
Doctor of Philosophy

by John Forsyth Brint B.Sc (Aberdeen)

Department of Applied Geology,
University of Strathclyde.

April 1989

**CONTAINS
PULLOUTS**

ABSTRACT

The Middle Jurassic deltaic Brent Group sandstones, northern North Sea, have a complicated diagenetic sequence which may be simplified to kaolinite - Fe,Ca carbonates - quartz overgrowths - Fe,Mg carbonates - illite. High porosities and permeabilities have existed in the Etive, Ness and Tarbert Formation sandstones throughout diagenesis. By contrast, the highly micaceous and relatively finer grained Rannoch Formation sandstones have good porosities but very poor permeabilities due to burial compaction and carbonate cementation. Oxygen and hydrogen isotope studies indicate that early diagenesis occurred in a dominantly meteoric pore water ($\delta^{18}\text{O} = -7\%$). The early diagenetic cements of siderite, vermicular kaolinite and calcite started to precipitate at 14, 26 and 32°C respectively. With the onset of burial, below 1.2 km, the Brent sequence eventually became sealed off from the meteoric 'head' by Lower Cretaceous sediments. Blocky kaolinite precipitated and by the end - Cretaceous quartz overgrowth formation commenced. Fluid inclusions in the overgrowths indicate formation from a warm, dominantly low salinity water (1 - 5 wt.% eq. NaCl). Homogenisation temperatures range from 73 to 131 °C. Illite precipitation is cogenetic with the latest stages of quartz overgrowth precipitation (K/Ar illite date, 58Ma.) and has reduced porosity and permeability markedly in different locations prior to oil migration. The depth of burial at which this last cementation event occurred is 2.3 km. Fluid inclusion microthermometry indicates that quartz overgrowth and latest ankerite precipitation occurred in a geothermal gradient of 70°C/km. After this heat excursion the reservoirs have cooled back to present day temperatures of 85 - 115°C. Water values computed from the mineral cements indicate precipitation from a porefluid which has gradually evolved isotopically to its present day composition ($\delta^{18}\text{O} = -7$ to $+2\%$ SMOW) in an isotopic system that has become closed during burial. However the quartz and ankerite suggest one unusual episode of open system hot fluid input.

ACKNOWLEDGEMENTS

I thank Dr. Stuart Haszeldine for giving me the opportunity to undertake this project and for his supervision throughout. My thanks also go to Dr. Jo Hamilton, Dr. Tony Fallick, Peter Ainsworth and the technical staff for their help at the Isotope Geology Unit, S.U.R.R.C., East Kilbride. Dr. Stewart Brown at the Hydrocarbons Unit, B.G.S., is thanked for his help and advice throughout the project. I wish to express my thanks to the British Geological Survey and Britoil plc for making core available. Thin section and polished wafer preparation was provided by John Gilleece and Peter Wallace. Assistance with geochemical techniques was provided by Murdoch MacLeod and Dugie Turner. I thank Dr. George Bowes for his help with computing. Access to the Britoil S.E.M and the canteen by Dr. Graham Blackburn is gratefully acknowledged. Fruitful discussions took place with Dr. Lynton S. Land (Univ. of Texas), Andrew Hogg, Andrew Robinson (British Petroleum) and with members of the Department of Applied Geology. I thank Tom McKie, Dave Banks and Hanni Mills for their help within the department and to my parents for their support throughout. This research was carried out during the tenure of a N.E.R.C postgraduate studentship which is gratefully acknowledged.

CONTENTS

ABSTRACT

ACKNOWLEDGEMENTS

Chapter 1	INTRODUCTION	1
1.1	Thesis structure	1
1.2	Diagenesis	4
1.3	The Brent group	5
1.4	Basin formation - The East Shetland basin and the North Viking Graben	6
1.5	Previous work	8
1.6	Project outline	10
1.7	Methodology	10
1.8	Stable Isotopes	11
1.9	Strontium and rubidium isotopes	17
1.10	Conclusions	19
1.11	References	22
1.12	Figure Captions and Figures	32
Chapter 2	OXYGEN ISOTOPIIC ANALYSIS OF DIAGENETIC QUARTZ OVERGROWTHS FROM THE BRENT SANDS: A COMPARISON OF TWO PREPARATION METHODS	43
2.1	Abstract	44
2.2	Introduction	45
2.3	Initial Preparation	45
2.4	Method One - Technique and Preparation	46
2.5	Method One - Results and Discussion	47
2.6	Method One - Conclusions	48
2.7	Method Two - Technique and Preparation	49
2.8	Method Two - Results and Discussion	50
2.9	Method Two - Conclusions	50
2.10	Final Remarks	51
2.11	Acknowledgements	52
2.12	References	53
2.13	Figure Captions and Figures	55

Chapter 3	ISOTOPE DIAGENESIS AND PALAEOFLUID MOVEMENT IN THE BRENT SANDSTONES, NORTHERN NORTH SEA	64
3.1	Abstract	65
3.2	Introduction	66
3.3	Geological Setting	67
3.4	Analytical Techniques	71
3.5	Petrography	73
3.6	Diagenesis	74
3.7	Reservoir Quality	79
3.8	Porosity Development	80
3.9	Pressure Solution	81
3.10	Closed or Open Diagenesis	82
3.11	Fluid Inclusion Data: Quartz overgrowths	82
3.12	Oxygen Isotopic Studies	86
3.13	Discussion of Oxygen Isotopes	88
3.14	Hydrogen Isotope Studies	92
3.15	K/Ar Illite Dating	96
3.16	Synthesis	97
3.17	Conclusions	102
3.18	Acknowledgements	104
3.19	References	105
3.20	Figure captions and Figures	115
Chapter 4	THE FORMATION AND ORIGIN OF CARBONATE CEMENTED ZONES IN BRENT SANDSTONES OF THE DUNLIN FIELD, NORTHERN NORTH SEA.	169
4.1	Abstract	170
4.2	Introduction	171
4.3	Geological Setting	172
4.4	Analytical Techniques	173
4.5	Sandstone Petrology	175
4.6	Cement - Porosity Relationships	177
4.7	Subsurface Depth of Growth	178
4.8	Carbonate Cement Composition: Microprobe Analysis	180
4.9	Stable Isotopes	181
4.10	Strontium Isotopes	187
4.11	Synthesis	192
4.12	Conclusions	196

4.13	Acknowledgements	199
4.14	References	200
4.15	Figure Captions and Figures	206
Chapter 5	A SULPHUR ISOTOPE STUDY OF LATE DIAGENETIC PYRITE, MIDDLE JURASSIC BRENT SANDSTONES, NORTHERN NORTH SEA.	239
5.1	Abstract	240
5.2	Introduction	241
5.3	Geology	241
5.4	Petrography and Diagenesis	242
5.5	Sulphur Isotopes	243
5.6	Discussion	244
5.7	Precipitation Mechanism for Pyrite	245
5.8	Conclusions	248
5.9	Acknowledgements	250
5.10	References	251
5.11	Figure Captions and Figures	255
Appendices		
A	Well logs and sample points	264
B	Microthermometric studies	276
C	Electron Microprobe analyses	284

CHAPTER 1

The format of this thesis consists of an introduction to the nature of the study and relevant background information on the aspects of the thesis. It also contains a summary of conclusions of the overall study. Chapters 2 - 5 are presented in a "paper style" format, each with their own introduction, reference list and acknowledgements. The papers fulfill the requirements made for submission to the journal specified, see relevant chapters. For practical use within the thesis, numbered sections and sub-sections have been added.

Chapter 2 (Paper 1), is a techniques paper which arose whilst diagenetic mineral separation was undertaken and assesses which preparation technique is most suitable for isolation of quartz overgrowths, which form a major diagenetic cement in the sequence. The isotopic analysis of the overgrowths would facilitate a clearer understanding of burial diagenesis of the sandstones. Direct measurement of the quartz overgrowths by etching overgrowth/detrital grain boundaries with weak HF acid and ultrasonic agitation to split them off failed due to contamination of the sieved fractions with detrital material. It was hoped that the finest size fractions of quartz would contain abundant overgrowths and hence give a direct $\delta^{18}\text{O}$ composition. The failure of this technique resulted in the use of a second method. This second method requires dissolution of overgrowths from the detrital grain by HF acid leaching. The $\delta^{18}\text{O}$ value for detrital grains is combined with a value for quartz plus overgrowths using the mass balance equation below,

$$\delta^{18}\text{O}_T = \delta^{18}\text{O}_C \cdot X_C + \delta^{18}\text{O}_{OG} \cdot X_{OG}$$

T = Total sample (Quartz + overgrowths)

C = Detrital Core

OG = Overgrowth

X = Mole Fraction (from Fisher 1982)

and knowing the percentage of quartz overgrowths, to obtain a $\delta^{18}\text{O}$ value for the quartz overgrowths. The $\delta^{18}\text{O}$ values

obtained were typical for quartz overgrowths which have precipitated at sedimentary temperatures.

Chapter 3 (Paper 2), illustrates the diagenetic sequence throughout the Brent sandstones studied. The multidisciplinary approach indicates that early diagenetic cements precipitated in a meteoric dominated open system at low temperatures. Late, burial related cements precipitated at higher temperatures from an evolving meteoric water, which shows the expected $\delta^{18}\text{O}$ - shift with water/rock interaction as the system became closed on the scale of the Brent Group. Fluid inclusion microthermometry on quartz overgrowths indicate formation temperatures and K/Ar dating of illite constrains the age of the event. Although most of late diagenesis was a subsidence/temperature driven process, the later phases of ankerite, and the majority of quartz overgrowth grew at excessively warm temperatures. This indicates that either a) a high conductive geothermal gradient existed or b) influx of hot fluids occurred.

Chapter 4 (Paper 3), investigates the origin of the carbonate cemented horizons present in the sandstone. Carbon and oxygen isotope studies on the carbonates indicate a mixed source of bicarbonate for siderite and calcite formation in a meteoric dominated fluid at low temperatures and shallow depths of burial. Ankerite formed during late "burial" diagenesis with a mixed bicarbonate source in an isotopically evolving porefluid. Again the application of an integrated study (stable, radiogenic isotopes, microprobe analysis) is used to constrain the diagenetic regime of an early meteoric dominated influx through the Brent resulting in carbonate formation with high $^{87}\text{Sr}/^{86}\text{Sr}$ ratios due to water/rock interaction with biotite detritus. During later diagenesis the porefluid became progressively less enriched in radiogenic Sr as carbonate supply became dominated by shell material (dissolution and reprecipitation). The latest ankerite growth may have had an input of carbon and strontium from surrounding mudrocks and formed at abnormally high temperatures. Electron microprobe analyses indicate that the porewater was fluctuating with respect to concentrations of Ca, Mg, Fe and Mn.

Chapter 5 (Paper 4), is a short paper on the sulphur isotope signature of late "burial" diagenetic pyrite. Using information from cogenetic mineral cements, constraints were placed on the temperature

interval and porefluid conditions. However the limited data available made characterisation of the sulphur source problematic, the high $\delta^{34}\text{S}$ values for the late pyrite do suggest formation by sulphate reduction in a partially closed system, i.e. where the loss of sulphate by reduction into pyrite exceeds replenishment of sulphate.

1.2.1. GENERAL ASPECTS

The study of diagenesis encompasses the physical and chemical processes which act upon sediments in the subsurface. Diagenetic processes commence immediately after deposition and continue until metamorphism takes over, when mineral reactions and transformations occur at elevated temperatures and/or pressures. Blatt (1979) defines the range of physical and chemical conditions included in diagenesis as between 0-200°C, 1-2000 kg/cm² and with water compositions from fresh to hypersaline. These numerical values vary not only with depth but also areally at any single depth. The word "diagenesis" was first used by Von Gumbel in 1868, and the basic concept of diagenesis first defined by Walther (1893-1894). The transition from diagenesis to metamorphism is however a nebulous point (Blatt 1979), and has been recognised as such since Walther's days and by Grubenmann & Niggli (1924), (Dunoyer de Segonzac 1968). Typically, workers in inorganic and organic diagenesis and in metamorphism define the transition differently (Deverin 1924, Grubenmann & Niggli 1924, Fyfe et al. 1958, Dunoyer de Segonzac 1968, Tissot & Welte 1984). Pettijohn (1957) concluded that there was a real continuity between diagenesis and metamorphism and if an arbitrary limit had to be drawn, only the temperature factor (Coombs 1961) can be reasonably used. This study is concerned with inorganic clastic diagenesis and does not consider organic material which itself undergoes diagenetic/catagenetic/metagenetic transformations over the same temperature/depth interval, (Tissot & Welte 1984).

The important physical processes of diagenesis are compaction and pressure solution, both largely dependent on depth of burial. Chemical processes may cause inherently unstable grains and minerals within the sediment to recrystallise (i.e. this is when the crystal fabric is altered but the mineralogy remains unchanged). Grains may also undergo dissolution and/or be replaced by new minerals. Chemical processes include the precipitation of new minerals within the pore spaces of the sediment. This is referred to as authigenesis (Kalkowsky 1886), and if a mineral cement precipitates in sufficient quantities, cementation of the sediment ensues.

Diagenetic processes essentially modify a sediment in terms of its texture, and also have a considerable effect on a sediment's porosity and permeability. Of the many factors which affect sandstone diagenesis, the depositional environment and sedimentary facies, composition and texture of the sediment together with the porewater composition are primary factors (Tucker 1981), with pore fluid migrations and the burial history affecting the course of diagenesis with time. Diagenesis occurs in an aqueous medium and is halted when hydrocarbons fill the pore space.

Sediment diagenesis is usually considered in terms of 1) Early and 2) Late conditions. Early diagenesis embraces processes occurring from deposition into the shallow burial realm (<1 - 1.5km), whilst Late diagenesis is concerned with the processes affecting the sediments at deeper levels.

1.2.2. DIAGENESIS AND ITS USE IN PETROLEUM STUDIES

The application of diagenesis to petroleum studies becomes self evident considering that the growth of diagenetic minerals i.e. carbonates, clays and quartz infills porosity and reduces permeability and hence limits the quantity of hydrocarbons accumulated. Initial porosity values ($\approx 50\%$) and permeabilities (several darcies) (Pryor 1973) have suffered reduction to porosities of < 25% and permeabilities of only a few millidarcies by the time of hydrocarbon emplacement into reservoir sandstones. Therefore prediction of sediment diagenesis, and hence reservoir quality in a well or across an oilfield, requires an understanding of the processes controlling diagenesis, their extent and timing in the basin history (Milliken et al. 1981, Haszeldine et al. 1984a,b, Fisher & Land 1986).

1.3

THE BRENT GROUP

The Middle Jurassic Brent Group is the single most productive hydrocarbon reservoir in the offshore U.K. continental shelf. The Brent Province is situated ≈ 150 km northeast of the Shetland Islands in the northern North Sea (Fig.1.1) and is the site of many major hydrocarbon producing fields (Fig.1.2). The province occurs in the East Shetland Basin and occupies an area of ≈ 6000 km². The oil is

reservoired in the Brent sandstones, and underlying Triassic Statfjord Formation sandstones, in dominantly westerly dipping fault blocks (Fig.1.3) (Brown 1984). The reservoirs are capped by Upper Jurassic and Lower Cretaceous sequences, with the oil sourced from the Upper Jurassic Kimmeridge Clay Formation (Goff 1983).

1.4 BASIN FORMATION - THE EAST SHETLAND BASIN AND NORTH VIKING GRABEN

The East Shetland Basin is a series of faulted terraces which are developed on the western edge of the N-S trending Viking Graben. The Graben itself is part of a larger complex graben system which runs the length of the North Sea (Fig.1), (Ziegler 1980, 1982a,b). Taking a broader view, Northwest Europe has undergone a long and complex geological evolution during which its megatectonic setting has changed repeatedly (Ziegler 1982a,b). Explanation of the formation of the North Viking Graben has made use of extensional basin models e.g. a) uniform stretching (McKenzie 1978, LePichon & Sibuet 1981, Barr 1987), which assumes instantaneous stretching of the crust and mantle lithosphere by the same stretching factor (β), b) depth dependent stretching (Royden & Keen 1980, Rowley & Sahiagan 1986), which involves greater stretching of the mantle lithosphere than the crust during the rifting stage, and c) the simple shear model of Wernicke 1985, a non-uniform stretching model, where stretching of the crust at the proximal end of the shear dominates with little or no thinning of underlying mantle lithosphere, see Fig.1.4. In all three models, basin formation occurs via a two-stage process: - firstly, extension (rifting) and secondly thermal subsidence (driven by an isostatic response to contraction of the mantle lithosphere as it cools and replaces slightly less dense asthenosphere). The model which is the most applicable to the formation of the North Viking Graben is contentious. Gibbs (1987) favours the interpretation that the Viking Graben system is developed on an easterly dipping shear zone (Fig.1.4) by "simple shear" of the lithosphere as proposed by Wernicke (1985) and not by pure shear as previously suggested by other workers (e.g. McKenzie 1978). However, Badley et al. (1988) cite the vertical stacking of syn-rift and post rift sediments from two individual stages of rifting and thermal subsidence (see later) which precludes the application of the non-uniform stretching models (Wernicke 1985) which predict laterally

offset rifting and thermal subsidence phase basins. Badley et al. (1988) also preclude the application of uniform pure shear models due to variations in extension across the basin which are illustrated by differing values at the centre and edges of the basin. They do indicate that the Rowley & Sahiagan (1986) model of continuous, non-uniform depth dependent stretching can accommodate the features observed during the evolution of the northern Viking Graben. White & McKenzie (1988) propose a similar non-uniform stretching model to explain the steer's head geometry and associated post rift stratigraphic onlap in the North Viking Graben, where the mantle lithosphere is stretched over a greater region than the crust.

The Mesozoic basin of the Viking Graben overlies a basement which was involved in Caledonian collision tectonics (Matthews & Cheadle 1986), and many studies have put the onset of rifting and graben system formation in the North Sea within the Permian (Ziegler 1980, 1982a,b, Glennie 1984, Badley et al. 1988). However Gibbs (1987) suggested that the North Sea Devonian basins developed on reactivated Caledonian detachments throughout the area, and that basin symmetry would be directly controlled by the pre-existing Caledonide structures. Such a model would therefore suggest development of a Devonian, and also possibly a Carboniferous precursor to the Viking Graben. Haszeldine & Russell (1987) consider that a pre-Permian rifting event may have occurred in the North Sea and that Carboniferous sediments may exist at depth in many of the Mesozoic basins. Badley et al. (1988) using seismic lines across the North Viking Graben recognise two rifting events - 1) Late-Permian/Early Triassic, with the ensuing thermal subsidence lasting until the Bathonian (Middle Jurassic), when it was succeeded by the second rifting episode. Thermal subsidence was accommodated on the major normal faults, and Jurassic Dunlin and Brent Group sediments indicate thickness variations from basin centre (1000 and 850m respectively) to the margins (100 and 180m), (Badley et al. 1988). 2) - The second rifting event began in the early Bathonian with the subsidence immediate. The greatest subsidence and stretching occurred over the early rift phase axis. The nature of the tilted Jurassic fault blocks was controlled by the pre-existing fault pattern. Badley et al. (1988) consider that rifting (individual block rotation) ceased synchronously over the whole of the graben during

the Ryazanian and thermal subsidence subsequently occurred throughout the Cretaceous. Only basin margin faults remained active into the early Tertiary, when flexural subsidence affected the whole basin.

1.5 PREVIOUS WORK

The initial studies on the Brent Group illustrated both the sedimentology/structural aspects as well as diagenesis. Bowen (1975) defined the Brent stratigraphy into three units as follows - a) Lower unit; a basal coarse sand overlain by fine grained micaceous coastal-shallow marine sheet sands, followed by coarse grained channel sands, b) Middle unit; deltaic plain sands with interbedded siltstones, shales and coals, c) Upper unit; Massive coastal to shallow marine sands. In contrast, Eynon (1981) subdivided the Brent sequence into a 1) basal sand, 2) the Bajocian delta lobe, 3) the lower Bathonian delta lobe and 4) the upper Bathonian delta lobe. The standard lithostratigraphy accepted today consists of five formations; Broom, Rannoch, Etive, Ness and Tarbert, (Fig.1.5), (Deegan & Scull 1977). Many studies have examined and defined the sedimentology and structure of the Brent Group (Hodson 1975, Albright et al. 1980, Kirk 1980, Budding & Inglin 1981, Eynon 1981, Parry et al. 1981, Simpson & Whitley 1981, Brown 1984, Richards & Brown 1986, Brown et al. 1987, Graue et al. 1987, Richards et al. 1988).

The Broom Formation (Kirk 1980, Budding & Inglin 1981, Eynon 1981) is typically a medium - coarse grained sandstone which is locally bioturbated and argillaceous. Richards et al. (1988) have indicated that the Broom may be a separate fan delta unit. The micaceous sandstones of the Rannoch Formation (Hodson 1975) are considered to represent storm influenced shallow marine delta front or shoreface deposits (Richards & Brown 1986). The basal Rannoch Formation consists of parallel laminated heterolithic beds which are locally bioturbated, overlain by laminated and hummocky cross stratified micaceous (very fine - fine grained) sandstones (Richards & Brown 1986). In the north of the East Shetland Basin, the basal Rannoch Formation is a mudstone, locally bioturbated with sandy lenses. The overlying Etive Formation is typically a structureless medium grained, mica poor sandstone with localised thin basal coarse lag deposits and at the top, rootlet zones (Brown et al. 1987). The Etive forms a near-continuous unit across the basin and has been

interpreted as a barrier bar complex (Budding & Inglis 1981), as mouth bar sands (Albright et al. 1980) and as distributary channel sands (Parry et al. 1981). Brown et al. (1987) consider that the lateral continuity of the Etive and underlying Rannoch Formation and the presence of superjacent marine and brackish salinity muds of the Ness Formation tend to favour the first hypothesis. The Ness Formation, which overlies the Etive, is considered to be a back barrier delta plain consisting of interbedded sandstones, siltstones, mudstones and coals (Brown et al. 1987). Finally the Tarbert Formation represents the marine transgression that drowned the progradational deltaic sediments. It consists of locally bioturbated, vertically stacked coarsening upwards units, which exhibit hummocky cross stratification and storm/fairweather couplets similar to that observed in the Rannoch.

For the purposes of this study, the Brent may be considered as a sand dominated deltaic sequence which has laterally uniform depositional facies over a wide area.

The initial diagenetic studies recognised cements and the paragenetic sequence (Blanche & Whitaker 1978, Hancock & Taylor 1978, Sommer 1978). Some workers considered further the effect of cements on reservoir quality (Blanche & Whitaker 1978, Sommer 1978). Sommer (1978) dated illite at 55 Ma and also suggested the possible origins of the cements. Bjorlykke et al. (1979) modified the initial paragenetic sequence and made further suggestions as to the origin of cements, indicating that early diagenesis was affected by meteoric water flowing through the subaerally exposed sandstones (Sommer 1978) and that late (burial) diagenesis was an essentially closed system. More recent studies have looked at particular aspects of Brent diagenesis e.g. Malley et al. (1986) examined fluid inclusions in quartz overgrowths, Bjorlykke & Brendsdal (1986) examined particular aspects of diagenesis i.e. mica-kaolinite transformations, calcite cements, whilst Jourdan et al. (1987) linked illite age dates with fluid inclusion microthermometry. Stable isotope studies of carbonates (Lonoy et al. 1986, Hamilton et al. 1987a,b) have increased the understanding of the overall diagenetic scenario.

This project is a study of sandstone diagenesis areally across part of the Brent sandstones using publically available "released" core material from the British Geological Survey, Edinburgh and Britoil plc., Glasgow. Core samples were taken from wells in the Thistle, Dunlin and Murchison oilfields and the Alwyn area (Fig.1.2) in major sandbodies between depths of 8624 ft - 12459ft (2.63 - 3.80 km), true vertical depth subsea (TVD SS.), over a wide geographical extent. This allowed the similarity/variability in sandstone diagenesis to be assessed with minimal complications from varying depositional facies. The study has examined the three dimensional distribution of diagenetic cements for the first time using groups of wells from different areas within the East Shetland Basin with the aims of the project being -

1) to study the sequence and volume of diagenetic minerals and their relationship to porosity and permeability, i.e. reservoir quality;

2) to constrain the timing and temperatures of mineral cementation and the origin of the porefluid from which cements precipitated, and

3) to integrate the individual aspects of palaeofluid origin and movement, and to illustrate this within a geological scenario compatible with the burial history of the basin, and the association of diagenetic and tectonic events.

A multidisciplinary approach was applied to this study of diagenesis, with optical microscopy supplemented by scanning electron microscopy and cathodoluminescence to elucidate petrographic relationships. X -ray diffraction analysis aided mineral identification and electron probe microanalysis facilitated geochemical analysis of carbonates (see Appendix A). Microthermometric studies of fluid inclusions trapped within quartz overgrowths provided data on the temperature of formation and the chemical composition of the porefluids (Crawford 1981, Roedder 1979a, 1984), (see Appendix B). Stable isotope ratio studies ($^{18}\text{O}/^{16}\text{O}$, D/H, $^{13}\text{C}/^{12}\text{C}$, $^{34}\text{S}/^{32}\text{S}$) on pure

diagenetic separates allowed -

a) characterisation of porefluids ($^{18}\text{O}/^{16}\text{O}$, D/H),

b) oxygen isotopes permit the calculation of formation temperatures due to their temperature dependent mineral-water fractionation factors,

c) measurement of $^{13}\text{C}/^{12}\text{C}$ and $^{34}\text{S}/^{32}\text{S}$

indicates the source of carbon and sulphur during cementation.

Similarly, radiogenic isotopes (via $^{87}\text{Sr}/^{86}\text{Sr}$, $^{87}\text{Rb}/^{85}\text{Rb}$ ratios) were used to elucidate porewater origin and its interaction with other phases. K/Ar dating was used for an absolute timing of cementation events.

1.8

STABLE ISOTOPES

With the use of several isotope systems, it is worthwhile expanding at this point of the thesis on important aspects of their principles and their application.

1.8.1. PRINCIPLES

Stable isotope values are reported in the δ notation in parts per thousand (% permill). The value is defined as

$$\delta = \left[\frac{R(\text{sample}) - R(\text{standard})}{R(\text{standard})} \right] \cdot 1000$$

$$\delta = \left[\frac{R(\text{sample})}{R(\text{standard})} - 1 \right] \cdot 1000$$

where $R = ^{18}\text{O}/^{16}\text{O}$, D/H, $^{13}\text{C}/^{12}\text{C}$ and $^{34}\text{S}/^{32}\text{S}$.

The δ values for oxygen and hydrogen are reported as permill enrichments or depletions relative to the Standard Mean Ocean Water (SMOW), the international standard (Craig 1961). For carbon isotopes, all data are reported with respect to PDB, the Chicago Pee Dee Belemnite standard. Oxygen isotope values associated with carbonates are normally reported in PDB also. These are converted to SMOW by -

$$\delta^{18}\text{O}_{(\text{SMOW})} = 1.03086 \delta^{18}\text{O}_{(\text{PDB})} + 30.86$$

(Friedman & O'Neil 1977).

Sulphur isotopes are reported as depletions or enrichments

relative to the Canyon Diablo Troilite (CDT), the sulphur standard.

1.8.2. OXYGEN ISOTOPE GEOTHERMOMETRY

The stable isotope equilibrium fractionation factor (α) for two phases, A and B is defined as -

$$\alpha_{A-B} = R_A/R_B$$

Mineral and fluid oxygen isotope values and temperature can be related by the relevant equations -

$$1000 \ln \alpha_{\text{Mineral} - \text{H}_2\text{O}} = A \cdot 10^6 \cdot T^{-2} - B$$

where α is the oxygen isotope equilibrium fractionation factor between A and B and T is temperature, °K. The temperature dependence of α forms the basis of oxygen isotope geothermometry (Bigelsein & Mayer 1947, Urey 1947).

1.8.3. CONTROLS ON ISOTOPIC EXCHANGE IN DIAGENETIC MINERALS

The oxygen and hydrogen isotope composition of a mineral forming during diagenesis is a function of -

- 1) temperature of formation
- 2) the isotopic composition of the fluid present during mineral authigenesis
- 3) the mass balance of oxygen and hydrogen between the mineral and the fluid
- 4) the stable isotope equilibrium fractionation factor between the mineral and the fluid phase
- 5) the extent to which isotopic equilibrium was maintained during mineral authigenesis
- 6) the extent and nature of isotopic exchange between the mineral and fluids following crystallisation.

Longstaffe (1983)

At temperatures normal for sedimentary environments, most minerals do not experience significant isotopic exchange with the surrounding fluids. Isotopic exchange between minerals and fluids occurs only during dissolution and reprecipitation. Only as temperature rises does isotopic exchange begin at significant rates. The rate of isotopic exchange between minerals and fluids depends upon the temperature of the system, the chemistry and structure of

the mineral and its grain size. Quartz is highly resistant to isotopic exchange subsequent to crystallisation (Yeh & Savin 1977, Savin 1980, 1982). Clay minerals can exchange isotopes with water under certain conditions (Savin 1967). Exchange of oxygen and hydrogen isotopes between water and structural sites in clay minerals is normally unimportant over short timescales at temperatures typical of sedimentary environments (James & Baker 1976, O'Neil & Kharaka 1976, Savin 1980, Savin & Yeh 1981). As temperature rises, the rate of exchange increases, with notable exchange of hydrogen achieved at $\approx 100^{\circ}\text{C}$ and oxygen exchange by 300°C (O'Neil & Kharaka 1976). Carbonates such as calcite exchange oxygen isotopes with water much more readily and at lower temperatures than do silicate minerals (Clayton 1959).

1.8.4. CARBON ISOTOPE SIGNATURES

Irwin et al. (1977) developed a depth defined model for carbonate cements, characterising the $\delta^{13}\text{C}$ values generated by different processes (Fig.1.6) during diagenesis. Low $\delta^{13}\text{C}$ values (-25%) are generated by the processes of bacterial oxidation and bacterial sulphate reduction of organic matter in the first few metres of the sediment. The reaction ceases as the porewater sulphate is exhausted with depth. Organic fermentation reactions then take over producing isotopically heavy carbon dioxide ($+15\%$) and this zone is believed to extend down to 1km. Subsequent carbon dioxide production at greater depths is by inorganic thermal processes breaking down any remaining organic material which give rise to low carbon isotope values (-10 to -25%).

1.8.5. SULPHUR ISOTOPE SIGNATURES

In sulphur isotope geochemistry, sulphur phases from different sources have characteristic $\delta^{34}\text{S}$ values (Fig.1.7). Meteoritic, lunar and terrestrial igneous sulphur have similar $^{34}\text{S}/^{32}\text{S}$ ratios, and by convention, the $\delta^{34}\text{S}$ of troilite (FeS) in meteorites has been given a value of 0% (Canyon Diablo Troilite). The principal reaction leading to separation of sulphur isotopes in nature is the dissimilatory reduction of sulphate by anaerobic bacteria. Biological processes introduce a kinetic isotope

fractionation on reduction of sulphate to sulphide, the magnitude of which is variable depending on the reaction rate, temperature and the sulphur species available. The reaction itself produces H_2S which is enriched in ^{32}S . Hence pyrite precipitated in the near surface diagenetic environment has very low $\delta^{34}\text{S}$, (Fig.1.7), relative to the $\delta^{34}\text{S}$ of seawater sulphate due to the large fractionation involved. Seawater sulphate is enriched in ^{34}S compared to the primordial composition of the earth's sulphur and present day seawater sulphate has a $\delta^{34}\text{S}$ of +20‰. However over geologic time the $\delta^{34}\text{S}$ value has varied (Claypool et al. 1980) due to the global balance between oxidised and reduced reservoirs, in the Jurassic the $\delta^{34}\text{S}$ was +16‰. Oceanic sulphate $\delta^{34}\text{S}$ variations are recorded in open-ocean, marine evaporites.

As well as bacterial reduction, non-biological reduction processes may cause fractionation of sulphur isotopes i.e. iron reduction and hydrocarbon reduction processes. Bacterial reduction occurs mostly at temperatures of <80 C (Orr 1975). Above these temperatures the isotopic signature of sulphur compounds may be influenced by hydrocarbons (Orr 1975), (Fig.1.7), and by thermochemical sulphate reduction (Krouse et al. 1988). The sulphur values generated have a broad range in $\delta^{34}\text{S}$ as they are controlled by the initial sulphur source and the degree of fractionation.

1.8.6. ISOTOPIC TRENDS WITH WATER-ROCK INTERACTION

In water the ratios $^{18}\text{O}/^{16}\text{O}$ and D/H provide two individual and sometimes independent tracers of its origin. In rocks, oxygen is usually the most abundant element (up to 50% by weight) whilst hydrogen is normally a trace element (<2000 ppm) (Sheppard 1986). This difference between oxygen and hydrogen concentrations in rocks and waters is of consequence. In water/rock interactions, both oxygen and hydrogen isotope exchange may occur between the phases. In systems where the water is of external origin, water is generally the dominant hydrogen reservoir and so will control the D/H ratio of the system. The $^{18}\text{O}/^{16}\text{O}$ ratio of the water is constrained by the amount of exchangeable mineral oxygen and the temperature of exchange unless water to rock ratios are very large or the exchange reactions are ineffective for kinetic or other reasons. So in meteoric water,

seawater or hydrothermal systems using these waters, the δD of the waters is often essentially constant, or undergoes only limited mineral-water exchange reactions. This is in contrast to the oxygen isotope composition of the water, which undergoes an " ^{18}O shift" away from its initial value. The characteristic " ^{18}O shift", which is generally to higher $\delta^{18}O$ values, is a result of the water trying to attain oxygen isotope equilibrium with the ^{18}O -rich silicates and carbonates. Sheppard (1986) indicates that the size of the shift is related to -

a) the ratio of the quantity of oxygen in the exchangeable minerals to that in the water,

b) the temperature of exchange (i.e. the size of the mineral-water fractionation factors) and

c) the initial chemical and isotopic composition of the phases.

Consequently the oxygen isotope composition of the water does not retain its original source signature. Therefore the D/H ratio for the water is often a more definitive parameter than $^{18}O/^{16}O$ for determination of the source of the water. Hence combination of oxygen and hydrogen isotope data can give information on both the source and evolution of the water.

1.8.7. DIAGENETIC POREFLUIDS

Understanding the origin and evolution of the porefluid present during formation of authigenic minerals is assisted by combining stable isotope analysis (which indicate the origin of the porefluid i.e. meteoric, seawater etc.), with chemical data i.e. salinity using fluid inclusion microthermometry and formation water analyses. Several terms are used within this thesis for the water present and are defined below:

Meteoric water:- water derived from rain, snow, water courses and other bodies of surface water that percolates into rocks and displaces the interstitial water.

Saline water:- defined here as water containing 1 - 35 g/l of dissolved solids.

Fresh water:- water containing 0 - 1.0 g/l dissolved solids (Davis 1964, Freeze & Cherry 1979).

Formation/Pore water:- water present in the rocks prior to

drilling.

Marine water: water defined here as seawater/ocean water (salinity of $\approx 35\text{g/l}$ dissolved solids).

1.8.8. STABLE ISOTOPE VARIATIONS IN WATER

Unmodified ocean (marine) water ($\delta\text{D} = 0$, $\delta^{18}\text{O} = 0$) has probably not varied much in its isotopic composition throughout geologic time, at least since the Precambrian (Knauth & Epstein 1976). Modification is possible by dilution with meteoric (fresh) water or extreme evaporation. Meteoric waters reveal a wide and systematic variation in isotopic composition (i.e. $\delta^{18}\text{O} = -50$ to 0 ; $\delta\text{D} = -400$ to 0 , Longstaffe 1983). The isotopic behaviour of meteoric waters may be described by the present day meteoric water line, expressed by (Craig 1961) as -

$$\delta\text{D} = 8.\delta^{18}\text{O} + 10 (\text{‰}).$$

This relationship is generated as a result of evaporation and condensation cycles. With equilibrium, ^{18}O and D are enriched in water condensed from the vapour phase (Taylor 1974, Hoefs 1980,), the liquid - vapour isotopic fractionation increases with decreasing temperature. Therefore water initially evaporated from the ocean becomes progressively depleted in ^{18}O and D as it participates in successive evaporation - condensation cycles. This Rayleigh type distillation creates distinct latitude and altitude dependencies of $\delta^{18}\text{O}$ and δD , with meteoric waters becoming depleted in the heavier isotope at higher altitudes and latitudes (Dansgaard 1964, Friedman et al. 1964, Hitchon & Krouse 1972).

With this knowledge of the regularity of δD and $\delta^{18}\text{O}$ in present day meteoric waters, the isotopic variations in porefluids present in sandstone reservoirs may prove to be of particular interest in helping to promote an understanding of the reservoir in terms of time and its diagenetic evolution. Clayton et al. (1966), Hitchon & Friedman (1969) and Kharaka et al. (1973) have illustrated that meteoric water occurs to varying degrees in oilfield formation waters, however they do not have $\delta^{18}\text{O}/\delta\text{D}$ values that plot along the meteoric water line (Fig.1.8). Instead the formation waters from different basins have $\delta^{18}\text{O}/\delta\text{D}$ values that trend away from the meteoric water line towards higher values of $\delta^{18}\text{O}$ and δD , so

illustrating the oxygen and hydrogen isotope enrichment trend alluded to earlier. Formation waters in sedimentary basins at high latitudes plot on trends that intersect the meteoric water line at lower $\delta^{18}\text{O}$ and δD than formation waters from sedimentary basins at low latitudes (Fig.1.8). This deviation of the $\delta^{18}\text{O}$ and δD values of the formation waters from the meteoric water line can result from a number of different processes which include isotopic exchange between water and ^{18}O - rich and D - rich minerals, mixing of meteoric and connate waters due to dispersion - type processes, dewatering of clay minerals during burial and isotopic fractionation due to diffusion of water through micropore systems in shales and mudstones (Clayton et al 1966, Hitchon & Friedman 1969, Coplen & Hanshaw 1973, Fleischer et al. 1977, Schwartz & Muehlenbachs 1979, Knauth et al. 1980, Land & Prezbindowski 1981 and Graf 1982).

1.9

STRONTIUM AND RUBIDIUM ISOTOPES

As stated earlier in the methodology section (1.7), strontium and rubidium isotopes were used to elucidate porewater origin and interaction with other phases.

The isotopic composition of strontium in circulation in the hydrosphere depends on the $^{87}\text{Sr}/^{86}\text{Sr}$ ratios of the rocks that interact with the water at or near the earth surface. The strontium released into solution is homogenised isotopically by mixing during transport, and arrives in the oceans or continental basins (Faure 1986). From there strontium reenters the rock cycle primarily by coprecipitation with calcium carbonate. So sedimentary carbonate and evaporite rocks of the world have preserved a record of changing isotope composition of Sr in the oceans and on the continents throughout Proterozoic and Phanerozoic time.

The isotopic composition of strontium in the oceans of the world is homogeneous with a $^{87}\text{Sr}/^{86}\text{Sr}$ ratio of 0.70910, (Burke et al. 1982), at present. The variation in $^{87}\text{Sr}/^{86}\text{Sr}$ ratios in the oceans during the Phanerozoic is indicated in Figure 1.9, (taken from Burke et al. 1982), with Middle Jurassic marine water having a ratio of 0.7068.

Chemical weathering and leaching of rocks and minerals on the continents releases strontium with high $^{87}\text{Sr}/^{86}\text{Sr}$ into

solution in lakes, rivers and groundwater. The isotopic composition of this strontium is variable and depends on the age, Rb/Sr ratios of the rocks and the relative solubilities of the different minerals present. Faure et al.(1963) demonstrated that strontium released by weathering of Precambrian gneisses is enriched in radiogenic ^{87}Sr compared to the oceans. The input of strontium derived from the continents tends to increase the $^{87}\text{Sr}/^{86}\text{Sr}$ ratios of the oceans (i.e. marine carbonate) whilst basaltic rocks lower the ratio (Faure 1986). The weathering of old rocks composed of silicate minerals gives rise to solutions with low strontium concentrations and high $^{87}\text{Sr}/^{86}\text{Sr}$ ratios compared to water derived from basins underlain by marine carbonate or evaporitic rocks, which have high strontium concentrations and lower $^{87}\text{Sr}/^{86}\text{Sr}$ ratios. This relationship allows the use of strontium as a natural tracer in the study of groundwater movement in the subsurface as well as on the surface as streams flow across varying rock types.

Calculated $^{87}\text{Sr}/^{86}\text{Sr}$ values have to be corrected for the radioactive decay of ^{87}Rb to ^{87}Sr between formation of the mineral and the present day; $^{87}\text{Sr} = ^{87}\text{Rb}(e^{\lambda t} - 1)$, in order to calculate the initial $^{87}\text{Sr}/^{86}\text{Sr}$ ratio of the mineral at the time of precipitation -

$$(^{87}\text{Sr}/^{86}\text{Sr})_{\text{radiogenic}} = (^{87}\text{Rb}/^{86}\text{Sr})_{\text{measured}} \cdot (e^{\lambda t} - 1)$$

$$(^{87}\text{Sr}/^{86}\text{Sr})_{\text{measured}} = (^{87}\text{Sr}/^{86}\text{Sr})_{\text{initial}} + (^{87}\text{Rb}/^{86}\text{Sr}) \cdot (e^{\lambda t} - 1)$$

$$(^{87}\text{Sr}/^{86}\text{Sr})_{\text{measured}} - (^{87}\text{Rb}/^{86}\text{Sr}) \cdot (e^{\lambda t} - 1) = (^{87}\text{Sr}/^{86}\text{Sr})_{\text{initial}}$$

$$\lambda = 1.42 \cdot 10^{-11} \text{ a}^{-1}, t = \text{age of formation.}$$

The major conclusions of the thesis are summarised in the following points.

1. In a comparison of two preparation techniques for oxygen isotope analysis of quartz overgrowths, the first technique, which entailed direct measurement of separated overgrowths, failed due to unsuccessful separation of the overgrowths from the detrital cores. The cause of this was probably the lack of "interfacial material" at the overgrowth/detrital grain boundary for HF to attack and so weaken the contact prior to ultrasonic agitation and sieving. The lack of interfacial material resulted in HF attacking imperfections, i.e. fractures, within the detrital grains. So rendering detrital particles into all the sieved size fractions analysed.

The second method requires that the overgrowths are dissolved off the detrital grains, and a mass balance calculation made to obtain the $\delta^{18}\text{O}$ composition of the porefluid. Values obtained by this method are typical of quartz overgrowths but the compositions have a much greater potential error ($\pm 2\%$) than the direct measurement of isolated quartz overgrowths.

2. The Brent sandstone diagenetic sequence may be simplified to kaolinite - Fe, Ca-carbonates - kaolinite - quartz overgrowths - Fe, Mg-carbonates - illite. The sequence of events is identical throughout the area studied, with the volume of cements (particularly quartz overgrowths and illite) enhanced in the Alwyn area, due to the greater depth of burial at which the Brent sequence is encountered (12459' TVD) compared to the other locations studied (8624 - 10331' TVD.SS).

3. Diagenesis in the sandstones of the Tarbert, Ness and Etive Formations with their good poroperm and 3-dimensional connectivity was controlled by fluid flow. In contrast, the micaceous, finer grained Rannoch Formation sandstones which have good porosity but poor depositional permeability have suffered marked reduction in reservoir quality at an early stage. This resulted in restrictions on late diagenetic events.

4. Isotopic studies on the early diagenetic cements indicate that the

porefluid was dominantly meteoric ($\delta^{18}\text{O} = -7\text{‰ (SMOW)}$). Vermicular kaolinite developed in all formations whilst siderite and calcite, which forms concretions in places, precipitated in the Rannoch, Ness and Tarbert Formations. Isotopic derived temperatures indicate formation of siderite commencing at around 14°C , kaolinite 26°C and calcite 32°C .

5. Progressive marine burial of the Brent Group through the Cretaceous sealed the sequence from continued meteoric influxes. During this burial phase, kaolinite authigenesis continued and saw a change in morphology to a more blocky, booklet habit. Quartz overgrowth authigenesis began towards the end Cretaceous, at a minimum temperature of 72.4°C (fluid inclusion microthermometry) in an isotopically evolving porewater. Homogenisation temperatures indicate that quartz authigenesis occurred up to about 131°C . Fluid inclusion studies also indicate that the warm porewater present at this time was dominantly of low salinity. Illite is cogenetic with the latest stages of quartz overgrowths and is dated at 58 Ma (Early Tertiary).

6. The system from early diagenesis to late "burial" diagenesis has evolved from one that was open during kaolinite, siderite and calcite precipitation to a closed system, on the scale of the Brent Group, during illite growth. However reservoir temperatures reached 131°C during quartz overgrowth formation, which is markedly higher than expected for the burial depth of the Brent at the Early Tertiary ($\approx 2.3\text{km}$) assuming a normal geothermal gradient ($35^{\circ}\text{C}/\text{km}$). The proximity of faults and evidence of silicification of micro cracks suggest the movement of hotter fluids up faults and through sandstones in an "open" system style of fluid movement from deeper in the basin. These hot fluids also carried hydrocarbons which were being generated from the Kimmeridge Clay source rock deeper in the basin.

7. After this heat excursion the reservoir has cooled back to its present day temperatures ($85 - 115^{\circ}\text{C}$, at 8624' to 12459' TVD. subsea) and formation water analyses indicate a low salinity (17,000 ppm) porewater (cf. seawater, 35,000 ppm) with $\delta^{18}\text{O}$ values of between 0 and $+2\text{‰ (SMOW)}$ and $\delta\text{D} = -24$ to -27‰ (SMOW) . Calculated water isotopic compositions from the latest mineral cements of illite

indicate similar values of $\delta^{18}\text{O} = +1$ to $+2\%$ and $\delta\text{D} = -31$ to -36% (SMOW). Analysis of all the mineral cements indicates an isotopic porewater evolution trend from deposition to burial, in terms of oxygen, $\delta^{18}\text{O} = -7\%$ to $+2\%$ (SMOW) with only limited δD exchange; -48 to -28% (from kaolinite) to -36 to -31% (SMOW). The porewater throughout diagenesis has remained of low salinity.

8. The early carbonates, i.e. siderite, formed at the sites of degrading biotites. These have acted as a nucleation site for the more extensive calcite concretions, so reducing porosity at a very early stage of diagenesis.

9. The bicarbonate supply for the siderite and calcite is from variable admixtures of shell debris and the oxidation of organic matter by iron and sulphate reduction processes. As stated above, oxygen isotopes indicate a dominantly meteoric fluid at this time. Strontium isotope ratios indicate incorporation of radiogenic strontium from the silicate detritus (e.g. degraded biotite etc.) into the siderites with correspondingly low strontium concentrations. Calcite has lower $^{87}\text{Sr}/^{86}\text{Sr}$ ratios but higher concentrations due to the dissolution of aragonitic shell debris with calcite authigenesis. This information appears to support the earlier statements of meteoric water involvement during early diagenesis in the non-marine (Ness) and marine (Tarbert) Formations. The meteoric influxes leach the silicate detritus and shell material to release radiogenic strontium and high concentrations of strontium respectively for incorporation into the cements. Diagenesis at this stage would be open system.

10. Ankerite growth occurred during burial diagenesis 1.1 to 1.7 km, with a mixed bicarbonate supply from fermentation and abiotic processes. Oxygen isotopes indicate formation in an evolving porewater system with the latest stages of growth occurring in an abnormally warm porewater (relative to the burial depth). Strontium ratios indicate the dominance of radiogenic strontium.

11. Sulphur isotope ratios for late cubic/octahedral pyrite have very high $\delta^{34}\text{S}$ values. Formation occurred at temperatures up to 80°C in a system that was effectively closed from further sulphate supply from the surface. This lack of replenishment led to sulphur precipitating with high $\delta^{34}\text{S}$ values.

- ALBRIGHT, W.A., TURNER, W.L., and WILLIAMSON, K.R., 1980, Ninian Field, U.K. sector, North Sea, in Halbouty, M.T., ed., Giant Oil and Gas Fields of the Decade: 1968 - 1978, Am. Assoc. Petroleum Geologists Mem. 30. Tulsa, Oklahoma, p. 173 - 194.
- BADLEY, M.E., PRICE, J.D., DAHL, C.R., and AGDESTAIN, T., 1988, The structural evolution of the northern Viking Graben and its bearing upon extensional modes of basin formation: Jour. Geol. Soc. London, v. 145, p. 455 - 472.
- BARR, D., 1987, Lithospheric stretching, detached normal faulting and footwall uplift, in Coward, M.P., Dewey, J.F., and Hancock, P.L., eds., Continental Extensional Tectonics, Spec. Pub. Geol. Soc. London, 28, p. 75 - 94.
- BIGELEISEN, J., and MAYER, M.G., 1947, Calculation of equilibrium constants for isotopic exchange reactions: Jour. Chem. Physics, v. 15, p. 261 - 267.
- BJORLYKKE, K., ELVERHOI, A., and MALM, A.O., 1979, Diagenesis in Mesozoic sandstones from Spitsbergen and the North Sea - A Comparison: Geologische Rundschau, v. 68, p. 1152 - 1171.
- BJORLYKKE, K., and BRENDSDAL, A., 1986, Diagenesis of the Brent sandstone in the Statfjord Field, North Sea, in Gautier, D.L., ed., Roles of Organic Matter in Sediment Diagenesis, Soc. Econ. Palaeontologists Mineralogists Spec. Publ. No. 38, p.157 - 167.
- BLANCHE, J.B., and Whitaker, J.H.McD., 1978, Diagenesis of part of the Brent Sand Formation (Middle Jurassic) of the northern North Sea Basin, Jour. Geol. Soc. London, v. 135, p. 73 - 82.
- BOWEN, J.M., 1975, The Brent Oilfield, in, Woodland, A.W., ed., Petroleum Geology of the Continental Shelf of Northwest Europe, v. 1, Geology, Applied Science Publishers, Barking, p. 353 - 362.
- BROWN, S., 1984, Jurassic, in Glennie, K.W., ed., Introduction to the Petroleum Geology of the North Sea, Blackwell Scientific Publications, p. 133 - 160.
- BROWN, S., RICHARDS, P.C., and THOMSON, A.R., 1987, Patterns in the

deposition of the Brent Group (Middle Jurassic) UK North Sea, in Brooks, J., and Glennie, K.W., eds., Petroleum Geology of North West Europe, Graham & Trotman, London, p. 899 - 913.

BUDDING, M.C., and INGLIN, H.F., 1981, A reservoir geological model of the Brent sands in Southern Cormorant, in Illing, L.V., and Hobson, G.D., eds., Petroleum Geology of the Continental Shelf of North - West Europe, Heyden & Son, London, p. 326 - 334.

CLAYPOOL, G.E., HOLSER, W.T., KAPLAN, I.R., SAKAI, H., and ZAK, I., 1980, The age curves of sulphur and oxygen isotopes in marine sulphate and their mutual interpretation: Chemical Geology, v. 28, p. 199-260.

CLAYTON, R.N., 1959, Oxygen isotope fractionation in the system calcium carbonate - water: Jour. Chem. Physics, v. 30, p. 1246 - 1250.

CLAYTON, R.N., FRIEDMAN, I., GRAF, D.L., MAYEDA, T.K., MEENTS, W.F., and SHIMP, N.F., 1966, The origin of saline formation waters. 1. Isotopic composition: Jour. Geophys. Research, v. 71, p. 3869 - 3882.

COOMBS, D.S., 1961, Some recent work on the lower grades of metamorphism: Australian Jour. Science, v. 24, p. 203-215.

COPLEN, T.B., and HANSHAW, B.B., 1973, Ultrafiltration by a compacted clay membrane-1. Oxygen and hydrogen isotopic fractionation: Geochim. Cosmochim. Acta, v. 37, p. 2295 - 2310.

COWARD, M.P., 1986, Heterogeneous stretching, simple shear and basin development: Earth and Planetary Science Letters, v. 80, p. 325 - 336.

CRAIG, H., 1961, Isotopic variations in meteoric waters: Science, v. 13, p. 1702 - 1703.

CRAWFORD, M.L., 1981, Phase equilibria in aqueous fluid inclusions, in, Hollister, L.S., and Crawford, M.L., eds., Short Course in Fluid Inclusions: Applications to Petrology, Mineralogical Association of Canada, p. 75 - 100.

DANSGAARD, W., 1964, Stable isotopes in precipitation: Tellus, v. 16,

p. 436 - 468.

DAVIS, S.N., 1964, The chemistry of saline waters by Kreiger, R.A., - discussion: Ground water, v. 2, 51p.

DEEGAN, C.E., and SCULL, B.J., 1977, (Compilers), A standard lithostratigraphic nomenclature for the Central and Northern North Sea: Rept. Inst. Geol. Sci. 77/25, HMSO Publications, London, 36p.

DEVERIN, L., 1924, L'etude lithologique des roches sedimentaires: Schweiz. Mineral. Petrog. Mitt., v. 4, p. 29-50.

DUNOYER DE SEGONZAC, G., 1968, The birth and development of the concept of diagenesis (1866-1966): Earth Sci. Rev., v. 4, p. 153-201.

EYNON, G., 1981, Basin development and sedimentation in the Middle Jurassic of the northern North Sea, in Illing, L.V., and Hobson, G.D., eds., Petroleum Geology of the Continental Shelf of North-West Europe, Heyden & Son, London, p. 196 - 204.

FAURE, G., 1986, Principles of Isotope Geology, 2nd ed., Wiley & Sons, New York, 589 p.

FAURE, G., HURLEY, P.M., and FAIRBAIRN, W.H., 1963, An estimate of the isotopic composition of strontium in rocks of the Precambrian Shield of North America: Jour. Geophys. Res., v. 68, p.2323-2329.

FISHER, R.S., 1982, Diagenetic history of Eocene Wilcox sandstones and associated formation waters, South-Central Texas: Ph.D dissertation, Univ. of Texas, 185 p.

FLEISCHER, E., GOLDBERG, M., GAT, J.R., and MAGARITZ, M., 1977, Isotopic composition of formation waters from deep drillings in southern Israel: Geochim. Cosmochim. Acta, v. 41, p. 511 - 525.

FREEZE, R.A., and CHERRY, J.A., 1979, Ground water: Englewood Cliffs, N.J., Prentice-Hall, Inc., 604p.

FRIEDMAN, I., REDFIELD, A.C., SCHOEN, B., and HARRIS, J., 1964, The variation in the deuterium content of natural waters in the hydrologic cycle: Rev. Geophysics, v. 2, p. 177 - 224.

FRIEDMAN, I., and O'NEIL, J.R., 1977, Compilation of stable isotope

fractionation factors of geochemical interest, in, Fleischer, E., ed., Data of Geochemistry, U.S. Geol. Survey Prof. Paper, 440 - KK, 6th ed.

FYFE, W.S., TURNER, F.J., and VERHOOGEN, J., 1958, Metamorphic reactions and metamorphic facies: Geol. Soc. America Mem., v. 73, 259p.

GIBBS, A.D., 1987, Deep seismic profiles in the northern North Sea, in Brooks, J., and Glennie, K.W., eds., Petroleum Geology of North West Europe, Graham & Trotman, London, p. 1025 - 1028.

GLENNIE, K.W., 1984, The Structural Framework and the Pre-Permian History of the North Sea Area, in Glennie, K.W., ed., Introduction to the Petroleum Geology of the North Sea, Blackwell Scientific Publications, London, p. 25 - 62.

GOFF, J.C., 1983, Hydrocarbon generation and migration from Jurassic source rocks in the East Shetland Basin and Viking Graben of the northern North Sea: Jour. Geol. Soc. London. v. 140, p. 445 - 474.

GRAF, D.L., 1982, Chemical osmosis, reverse chemical osmosis and the origin of subsurface brines: Geochim. Cosmochim. Acta, v. 46, p. 1431 - 1448.

GRAUE, E., HELLAND-HANSEN, W., JOHNSEN, J., LOMO, L., NOTTVEDT, A., RONNING, K., RYSETH, A., and STEEL, R., 1987, Advance and retreat of Brent Delta System, Norwegian North Sea, in Brooks, J., and Glennie, K.W., eds., Petroleum Geology of North West Europe, Graham & Trotman, London, p. 915 - 937.

GRUBENMANN, V., and NIGGLI, P., 1924, Die Gesteinsmetamorphose, 1. Allgemeiner Teil, Borntraeger, Berlin, 539 p.

HAMILTON, P.J., FALLICK, A.E., MACINTYRE, R.M., and ELLIOTT, S., 1987, Isotopic tracing of the provenance and diagenesis of Lower Brent Group sands, North Sea, in Brooks, J., and Glennie, K.W., eds., Petroleum Geology of North West Europe, Graham & Trotman, London, p. 939 - 949.

HAMILTON, P.J., BRINT, J., HASZELDINE, R.S., FALLICK, A.E., and BROWN, S., 1987, Formation of calcite cemented zones, Brent Group, North Sea: Terra Cognita, v. 7, p. 342.

HANCOCK, N.J., and Taylor, A.M., 1978, Clay mineral diagenesis and oil migration in the Middle Jurassic Brent Sand Formation: Jour. Geol. Soc. London, v. 135, p. 69 - 72.

HASZELDINE, R.S., SAMSON, I.M., and CORNFORD, C., 1984a, Dating diagenesis in a petroleum basin: a new fluid inclusion method: Nature, v. 307, p. 354 - 357.

HASZELDINE, R.S., SAMSON, I.M., and CORNFORD, C., 1984b, Quartz diagenesis and convective fluid movement: Beatrice oilfield U.K. North Sea: Clay Minerals, v. 19, p. 391 - 402.

HASZELDINE, R.S., and RUSSELL, M.J., 1987, The Late Carboniferous northern North Atlantic Ocean implications for hydrocarbon exploration from Britain to the Arctic, in Brooks, J., and Glennie, K.W., eds., Petroleum Geology of North West Europe, Graham & Trotman, London, p. 1163 - 1175.

HITCHON, B., and FRIEDMAN, I., 1969, Geochemistry and origin of formation waters in the western Canada sedimentary basin - 1. Stable isotopes of hydrogen and oxygen: Geochim. Cosmochim. Acta, v. 33, p. 1321 - 1349.

HITCHON, B., and KROUSE, H.R., 1972, Hydrogeochemistry of surface waters of the Mackenzie River drainage basin, Canada. III. Stable isotopes of oxygen, carbon and sulphur: Geochim. Cosmochim. Acta, v. 36, p. 1337 - 1358.

HODSON, G.M., 1975, Some aspects of the geology of the Middle Jurassic in the Northern North Sea with particular reference to electro-physical logs: in Jurassic Northern North Sea Symposium, Stavanger, Norw. Petrol. Soc. p. 16/1 - 39.

HOEFS, J., 1980, Stable Isotope Geochemistry, 2nd ed., Springer-Verlag, New York, Heidelberg, Berlin, 208 p.

IRWIN, H., COLEMAN, M.L., and CURTIS, C.D., 1977, Isotope evidence for several sources of carbonate and distinctive diagenetic processes in organic rich Kimmeridgian sediments: Nature, v. 269, p. 209 - 213.

JAMES, A.T., and BAKER, D.R., 1976, Oxygen isotope exchange between illite and water at 22 C: Geochim. Cosmochim. Acta, v. 40, p. 235 -

239.

JOURDAN, A., THOMAS, M., BREVART, O., ROBSON, P., SOMMER, F., and SULLIVAN, M., 1987, Diagenesis as the control of the Brent sandstone reservoir properties in the Greater Alwyn area (East Shetland Basin), in Brooks, J., and Glennie, K.W., eds., Petroleum Geology of North West Europe, Graham & Trotman, London, p. 951 - 961.

KALKOWSKY, E., 1886, Elemente der Lithologie, Winter, Heidelberg. 316p.

KAPLAN, I.R., 1983, Stable isotopes of sulphur, nitrogen and deuterium in recent marine environments, in Arthur, M.A., Anderson, T.F., Kaplan, I.R., Veizer, J., and Land, L.S., eds., Stable Isotopes in Sedimentary Geology, Soc. Econ. Palaeontologists Mineralogists, Short Course No. 10, Dallas, p.2-1, 2 - 108.

KHARAKA, Y.K., BERRY, A.F., and FRIEDMAN, I., 1973, Isotopic composition of oil-field brines from Kettleman North Dome, California and their geological implications: Geochim. Cosmochim. Acta, v. 37, p. 1899 - 1908.

KIRK, R.H., 1980, Statfjord Field: a North Sea giant, in Halbouty, M.T., ed., Giant Oil and Gas Fields of the Decade: 1968 - 1978, Am. Assoc. Petroleum Geologists Mem., 30, Tulsa, Oklahoma, p. 95 - 116.

KNAUTH, L.P., and EPSTEIN, S., 1976, Hydrogen and oxygen isotope ratios in nodular bedded cherts: Geochim. Cosmochim. Acta, v. 40, p. 1095 - 1108.

KNAUTH, L.P., KUMAR, M.B., and MARTINEZ, J.D., 1980, Isotope geochemistry of water in Gulf Coast salt domes: Jour. Geophys. Research, v. 85, p. 4863 - 4871.

KROUSE, H.R., VIAU, C.A., ELIUK, L.S., UEDA, A., and HALAS, S., 1988, Chemical and isotopic evidence of thermochemical sulphate reduction by light hydrocarbon gases in deep carbonate reservoirs: Nature, v. 333, p. 415-519.

LAND, L.S., and PREZBINDOWSKI, D.R., 1981, The origin and evolution of saline formation water, Lower Cretaceous carbonates, south-central Texas: Jour. Hydrology, v. 54, p. 51 - 74.

LEEDER, M.R., 1982, Sedimentology: process and product: Allen & Unwin, London, 344p.

Le PICHON, X., and SIBUET, J.C., 1981, Passive margins; a model for formation: Jour. Geophysical Research, v. 86, p. 3708 - 3720.

LONGSTAFFE, F.J., 1983, Diagenesis 4, Stable isotope studies of diagenesis in clastic rocks: Geoscience Canada, v. 10, p. 43 - 58.

LONDOY, A., AKSELSEN, J., and RONNING, K., 1986, Diagenesis of a deeply buried sandstone reservoir: Hild field, Northern North Sea: Clay Minerals, v. 21, p. 497 - 512.

MALLEY, P., JOURDAN, A., and WEBER, F., 1986, Etudes des inclusions fluides dans les nourrisages siliceux des gres reservoirs de Mer du Nord: une nouvelle lecture possible de l'histoire diagenetique du Brent de la region d'Alwyn: Comptes Rendu. Acad. Sci. Paris, v. 302, p. 653 - 658.

MATTHEWS, D.H., and CHEADLE, M.J., 1986, Deep reflections from the Caledonides and Variscides west of Britain and comparison with the Himalayas, in Barazangi, M., and Brown L., eds., Reflection Seismology: a Global Perspective, American Geophysics Union, Geodynamics Series, no. 13, p. 5 - 19.

McKENZIE, D.P., 1978, Some remarks on the development of sedimentary basins: Earth Planet. Sci. Letters, v. 40, p. 25 - 32.

O'NEIL, J.R., and KHARAKA, Y.K., 1976, Hydrogen and oxygen exchange reactions between clay minerals and water: Geochim. Cosmochim. Acta, v. 40, p. 241 - 246.

ORR, W.L., 1975, Geologic and geochemical controls on the distribution of hydrogen sulphide in natural gas, in Advances in Organic Geochemistry, Proc. of 7th International Meeting on Organic Geochemistry, Madrid, p.571-597.

PALMER, A.R., 1983, The Decade of North American geology. 1983 geologic time scale: Geology, v. 11, p. 504 - 505.

PARRY, C.C., WHITLEY, P.K.J., and SIMPSON, R.D.H., 1981, Intergration of palynological and sedimentological methods in facies analysis of the Brent Formation, in Illing, L.V., and Hobson, G.D., eds.,

- Petroleum Geology of the Continental Shelf of North-West Europe, Heyden & Son, London, p. 205 - 215.
- PARSLEY, A.J., 1984, North Sea Hydrocarbon Plays, in Glennie, K.W., ed., Introduction to the Petroleum Geology of the North Sea. Blackwell Scientific Publications, London, p. 205 - 230.
- PETTIJOHN, F.J., 1957, Sedimentary Rocks: Harper, New York, N.Y., 2nd. Ed., 718p.
- PRYOR, W.A., 1973, Permeability - Porosity patterns and variations in some Holocene sandbodies: Am. Assoc. Petroleum Geologists Bull., v. 57, p. 162 - 189.
- RICHARDS, P.C., and BROWN, S., 1986, Shoreface storm deposits in the Rannoch Formation (Middle Jurassic), North West Hutton Oilfield: Scott. Jour. Geology, v. 22, p. 367 - 375.
- RICHARDS, P.C., BROWN, S., DEAN, J.M., and ANDERTON, R., 1988, A new palaeogeographic reconstruction for the Middle Jurassic of the northern North Sea: Jour. Geol. Soc. London, v. 145, p.883 - 885.
- ROEDDER, E., 1979, Fluid inclusions as samples of ore fluids, in Barnes, H.L., ed., Geochemistry of Hydrothermal Ore Deposits, 2nd Ed., Wiley & Sons, New York, p. 684 - 737.
- ROEDDER, E., 1984, Fluid Inclusions, in, Ribbe, P.H., ed., Reviews in Mineralogy, v. 12, Mineralogical Society of America, 644p.
- ROWLEY, D.B., and SAHIAGAN, D., 1986, Depth dependent stretching: a different approach: Geology, v. 14, p. 32 - 35.
- ROYDEN, R.D.H., and KEEN, C.E., 1980, Rifting processes and thermal evolution of the continental margin of eastern Canada determined from subsidence curves: Earth Planet. Sci. Letters, v. 51, p. 343 - 361.
- SAVIN, S.M., 1980, Oxygen and hydrogen isotope effects in low-temperature mineral-water interactions, in Fritz, P., and Fontes, J.C., eds., Handbook of environmental isotope geochemistry, v. 1, The terrestrial environment, A, p. 283 - 327.
- 1982, Oxygen isotopic studies of diagenetic clay minerals: implications for geothermometry, diagenetic reaction mechanisms, and fluid migration: Am. Assoc. Petroleum Geologists Bull., v. 66, p.

1447, (abstract).

SAVIN, S.M., and YEH, H., 1981, Stable isotopes in ocean sediments, in Emiliani, C., ed., *The Sea*, v. 7, *The Oceanic Lithosphere*, Wiley & Sons, New York, p. 1521 - 1554.

SCHWARTZ, F.W., and MUEHLENBACHS, K., 1979, Isotope and ion geochemistry of groundwaters in the Milk River Aquifer, Alberta: *Water Resources Research*, v. 15, p. 259 - 268.

SHEPPARD, S.M.F., 1986, Characterisation and Isotopic variations in Natural Waters, in Valley, J.W., Taylor, Jr., H.P., and O'Neil, J.R., eds., *Stable Isotopes in High Temperature Geological Processes*, *Reviews in Mineralogy*, v. 16, Mineralogical Society of America, p. 165 - 184.

SIMPSON, R.D.H., and WHITLEY, P.K.J., 1981, Geological input to reservoir simulation of the Brent Formation, in Illing, L.V., and Hobson, G.D., eds., *Petroleum Geology of the Continental Shelf of North West Europe*, Heyden & Son, London, p. 310 - 314.

SOMMER, F., 1978, Diagenesis of Jurassic sandstones in the Viking Graben: *Jour. Geol. Soc. London*, v. 135, p. 63 - 68.

TAYLOR, H.P. Jr., 1974, The application of oxygen and hydrogen isotope studies to problems of hydrothermal alteration and ore deposition: *Econ. Geol.* v. 69, p. 843 - 883.

UREY, H.C., 1947, The thermodynamic properties of isotopic substances: *Jour. Chem. Soc.*, p. 582 - 581.

VON GUMBEL, C.W., 1868, *Geognostische Beschreibung des ostbayerischen Grenzgebirges oder des bayerischen und oberpfalzer Waldebirges*, Perthes, Gotha, 968p.

WALTHER, J., 1893-1894, *Einleitung in die Geologie als historische Wissenschaft. Beobachtungen über die Bildung der Gesteine und ihrer organischen Einschlüsse*, Fischer, Kassel, 1144p.

WERNICKE, B., 1985, Uniform - sense normal simple shear of the continental lithosphere: *Canadian Jour. Earth. Sciences*, v. 22, p. 108 - 125.

WHITE, N., and MCKENZIE, D.P., 1988, Formation of the "steer's head"

geometry of sedimentary basins by differential stretching of the crust and mantle: *Geology*, v. 16, p. 250 - 253.

YEH, H., and SAVIN, S.M., 1977, Mechanism of burial metamorphism of argillaceous sediments: 3. O-isotope evidence: *Geol. Soc. America Bull.* v. 88, p. 1321 - 1330.

ZIEGLER, P.A., 1980, Northwest European Basin: geology and hydrocarbon provinces, in, Miall, A.D., ed., *Facts and Principles of World Petroleum Occurrence: Can. Soc. Petrol. Geol., Mem. 6*, p. 672 - 706.

————— 1982a, Faulting and Graben formation in western and central Europe: *Phil. Trans. R. Soc. London, A 305*, p. 113 - 143.

————— 1982b, *Geological Atlas of Western and Central Europe: Shell. Int. Petrol. Maats. B.V., Distributed by Elsevier, Amsterdam, 130p.*

Figure 1.1 : Location of the Brent Province, East Shetland Basin, northern North Sea. (Line A - A', see Fig. 1.3.b)

Figure 1.2 : Location of major oilfields, and principal structures within the Brent Province, East Shetland Basin.

Figure 1.3.a : Structural regime of westerly dipping fault blocks which typify the East Shetland Basin. Hydrocarbons are reservoired in the Brent Group and underlying Statfjord Formation.

Figure 1.3.b : Line of section A -A' (see Fig.1.1), illustrating a cross-sectional view of the North Viking Graben, (after Parsley 1984).

Figure 1.4 : a and b, modified from Rowley & Sahiagan (1986), depicting the cross sectional geometry of lithospheric stretching in extensional basin formation models, as applied to the development of the North Sea graben system. (Crust thickness - 30 km, Mantle Lithosphere thickness - 95 km).

Figures 1.4.a.i./1.4.b.i. : Initial configuration for McKenzie (1978) model of uniform stretching and the Royden & Keen (1980) discontinuous non-uniform (depth dependent) stretching model.

Figure 1.4.a.ii. : Geometry immediately after instantaneous uniform stretching. Arrows indicate direction of syn-stretching vertical movement.

Figure 1.4.b.ii. : Geometry immediately after discontinuous non-uniform stretching. Stretching factors (R) for the crust and mantle lithosphere are independent but uniform.

Figure 1.4.b.iii. : Initial geometry of continuous non-uniform (depth dependent) stretching (Rowley & Sahiagan 1986).

Figure 1.4.b.iv. : Geometry immediately after instantaneous, continuous non-uniform stretching. This geometry results in thinning of the lithosphere beneath the crustal regions, that are less stretched, the crustal uplift caused by asthenospheric upwelling below these regions. This causes stretching factors for the mantle that are less than those for the crust, a relationship opposite to

derived by discontinuous non-uniform stretching models (Royden & Keen 1980).

Figure 1.4.c. : Simple shear model, Wernicke (1985). Normal simple shear of the entire lithosphere is envisaged with dominance at the proximal end.

Figure 1.5 : Jurassic lithostratigraphy in the East Shetland Basin with the Brent Group and its five Formations indicated, after Brown (1984).

Figure 1.6 : The depth defined model for carbonate cements illustrating the characteristic $\delta^{13}\text{C}$ values generated by different processes, after Irwin et al. (1977), modified from Leeder (1982).

Figure 1.7 : Sulphur isotope distribution in nature (modified from Kaplan 1983).

Figure 1.8 : Plot of δD versus $\delta^{18}\text{O}$ for oilfield brines from North America (Clayton et al. 1966, Hitchon & Friedman 1969, Kharaka et al. 1973). SMOW ($\delta\text{D} = 0$, $\delta^{18}\text{O} = 0\%$) is indicated. In each sedimentary basin the $\delta\text{D}/\delta^{18}\text{O}$ of the brines are seen to evolve at varying degrees from the meteoric water line to enriched δD and $\delta^{18}\text{O}$ compositions.

Figure 1.9 : Variation of the $^{87}\text{Sr}/^{86}\text{Sr}$ ratio of marine carbonates in Phanerozoic time. Adapted from data by Burke et al. (1982) and using the timescale of Palmer (1983).

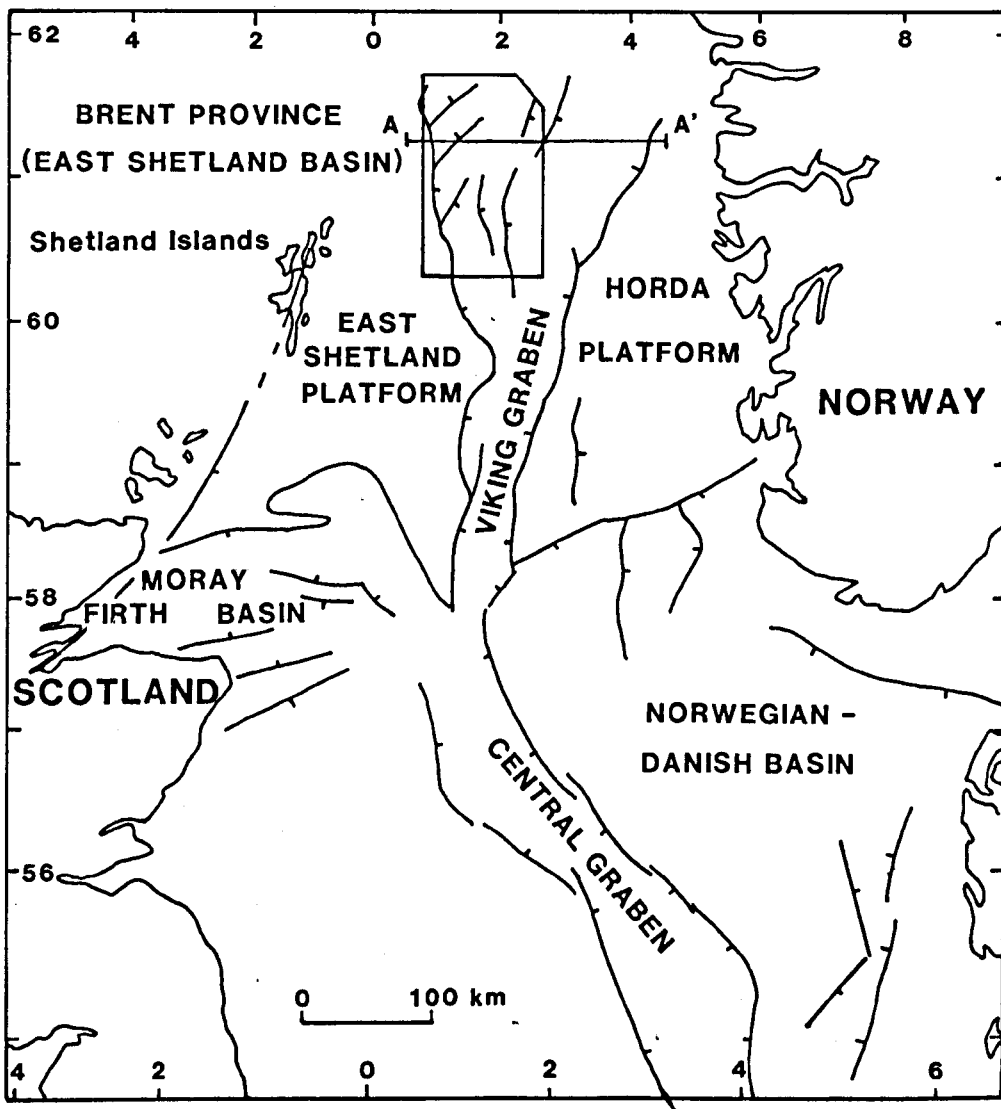


Figure 1.1

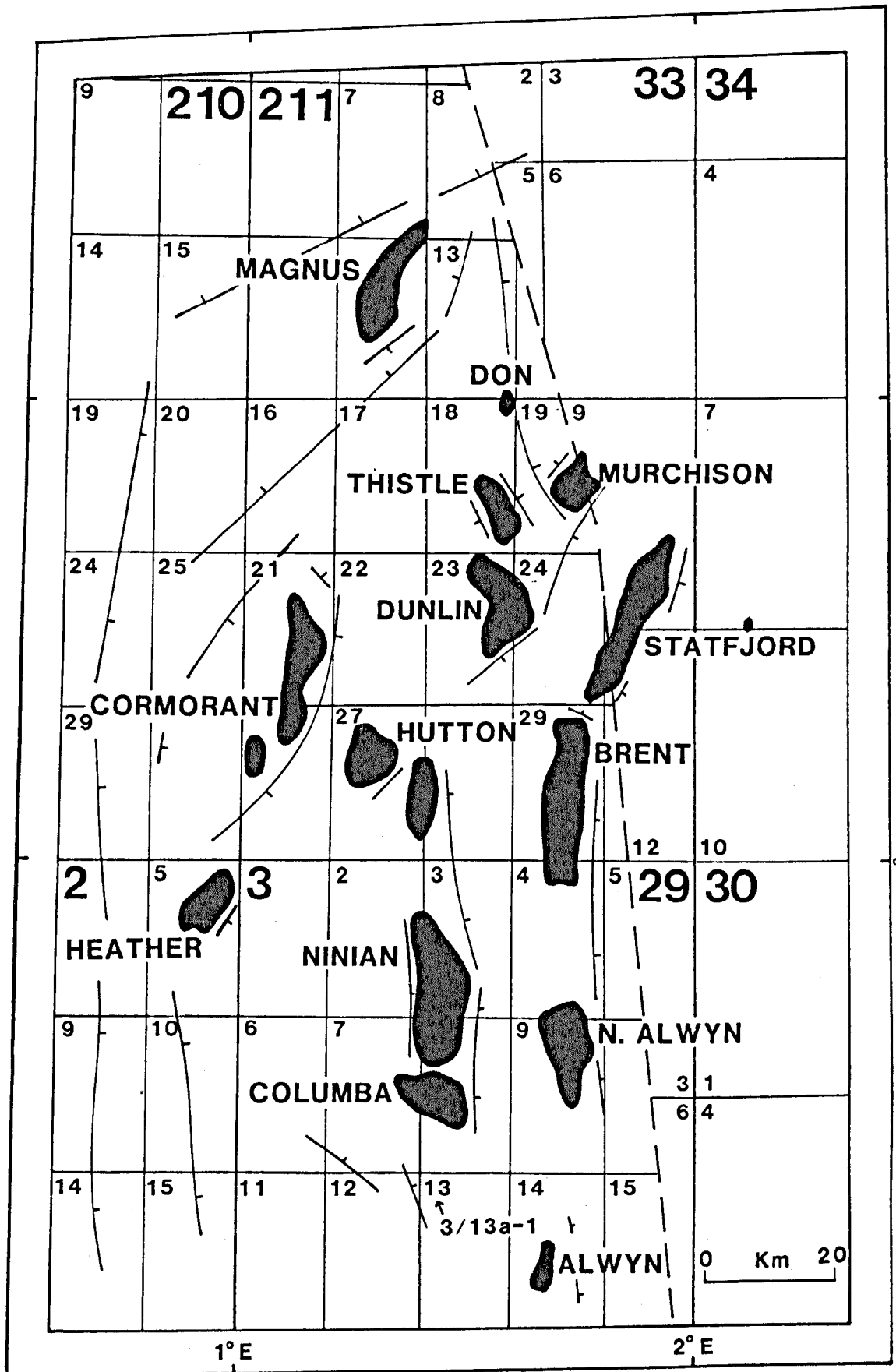


Figure 1.2

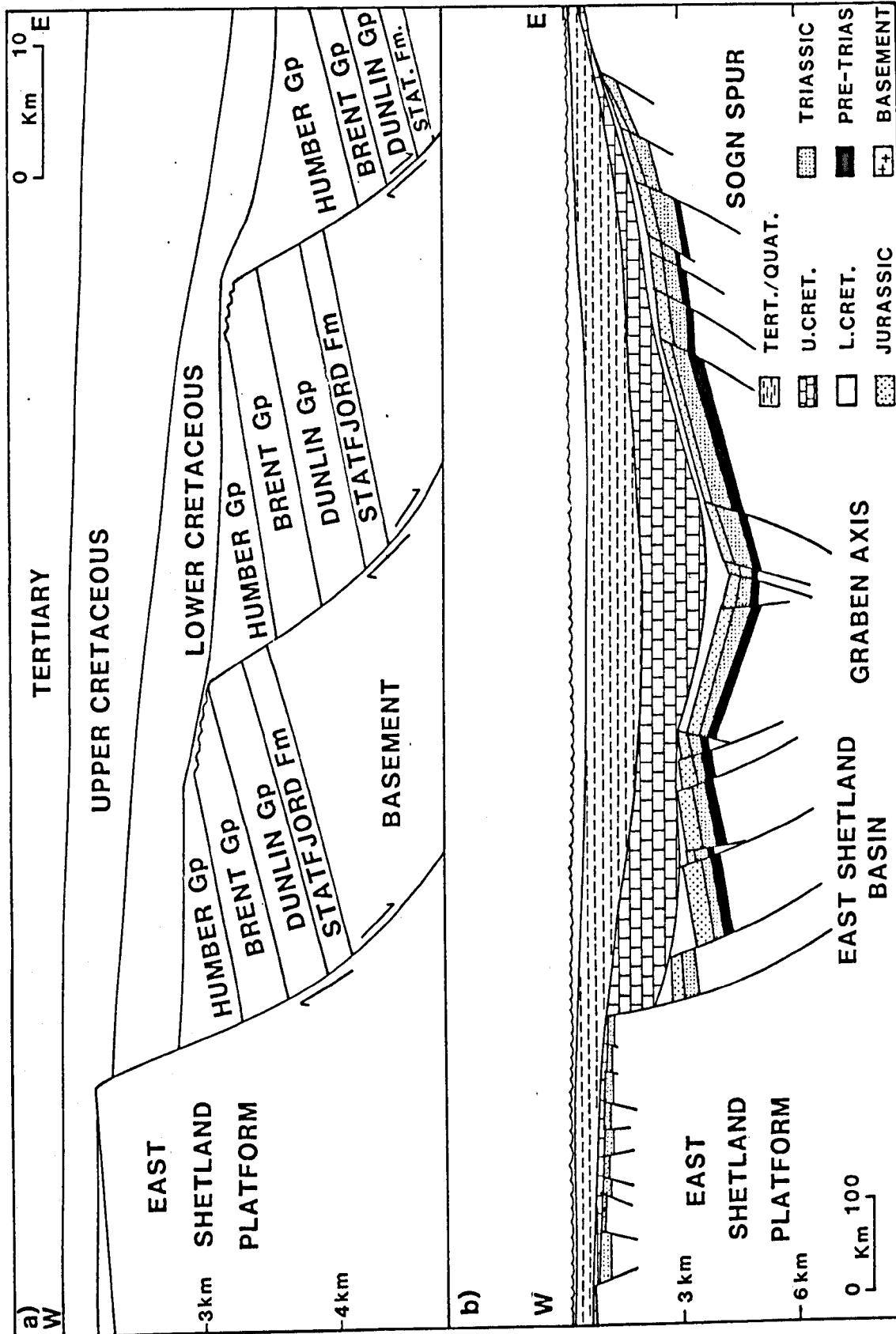
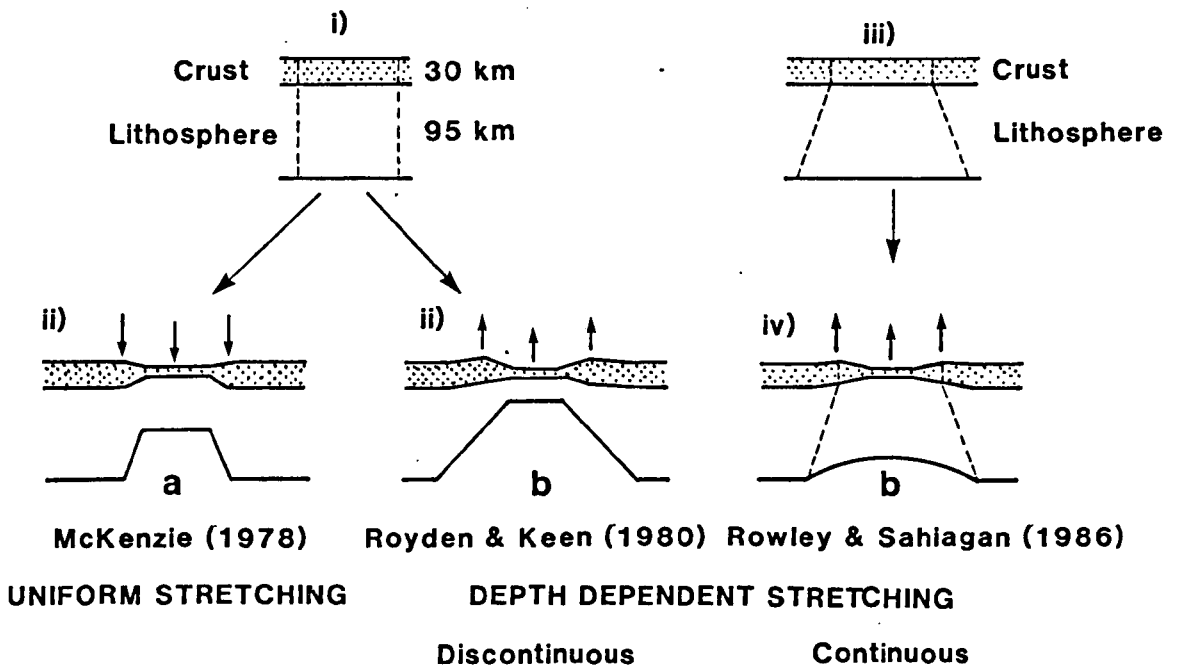


Figure 1.3



C SIMPLE SHEAR MODEL Wernicke 1985

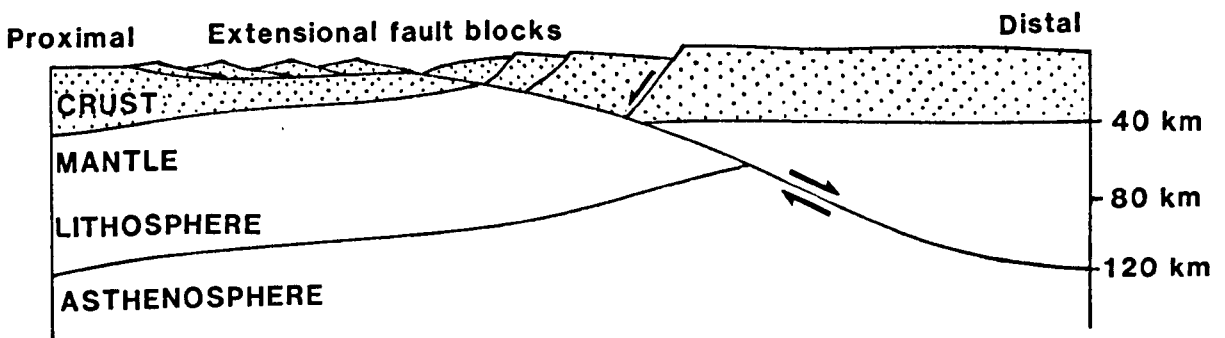


Figure 1.4

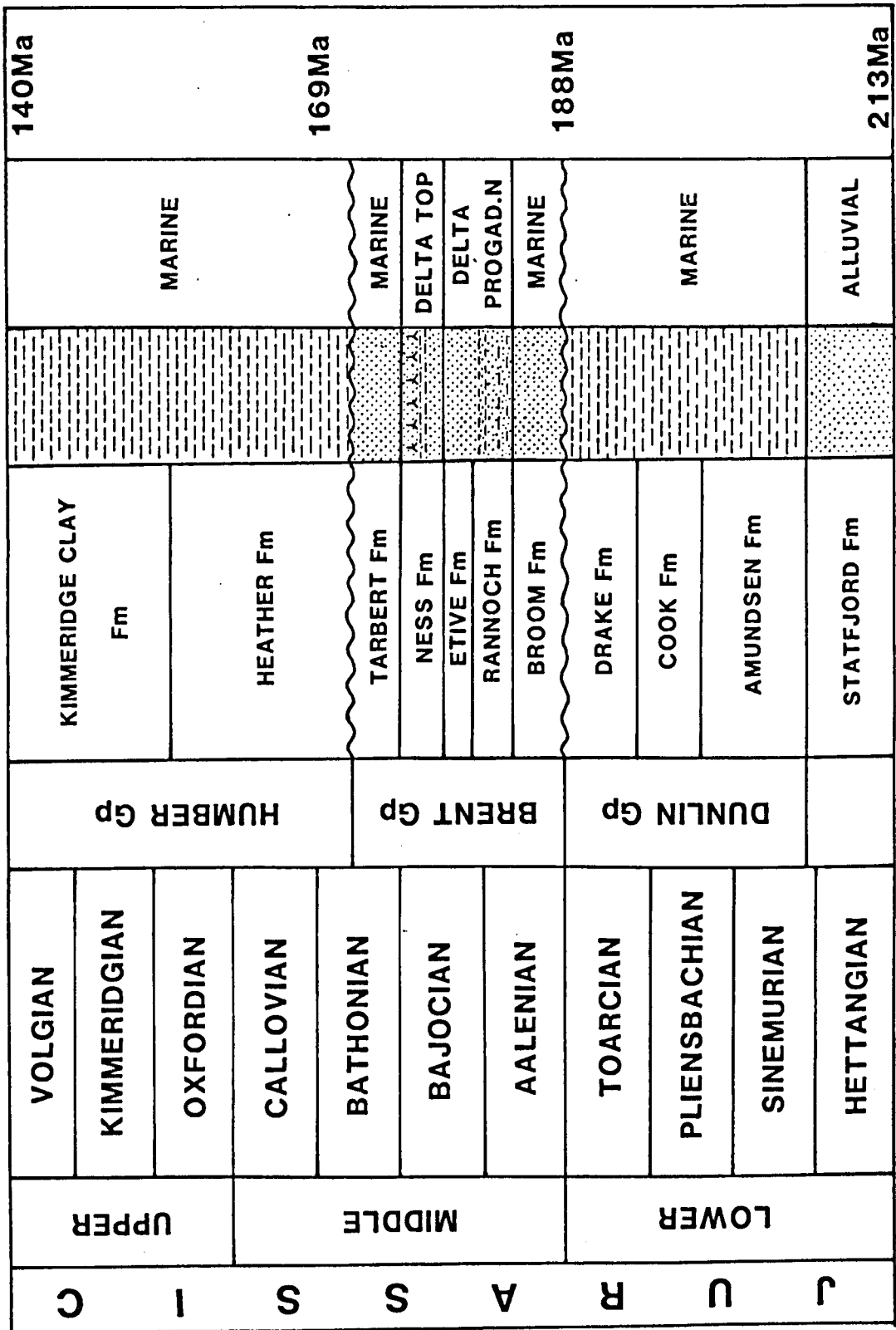
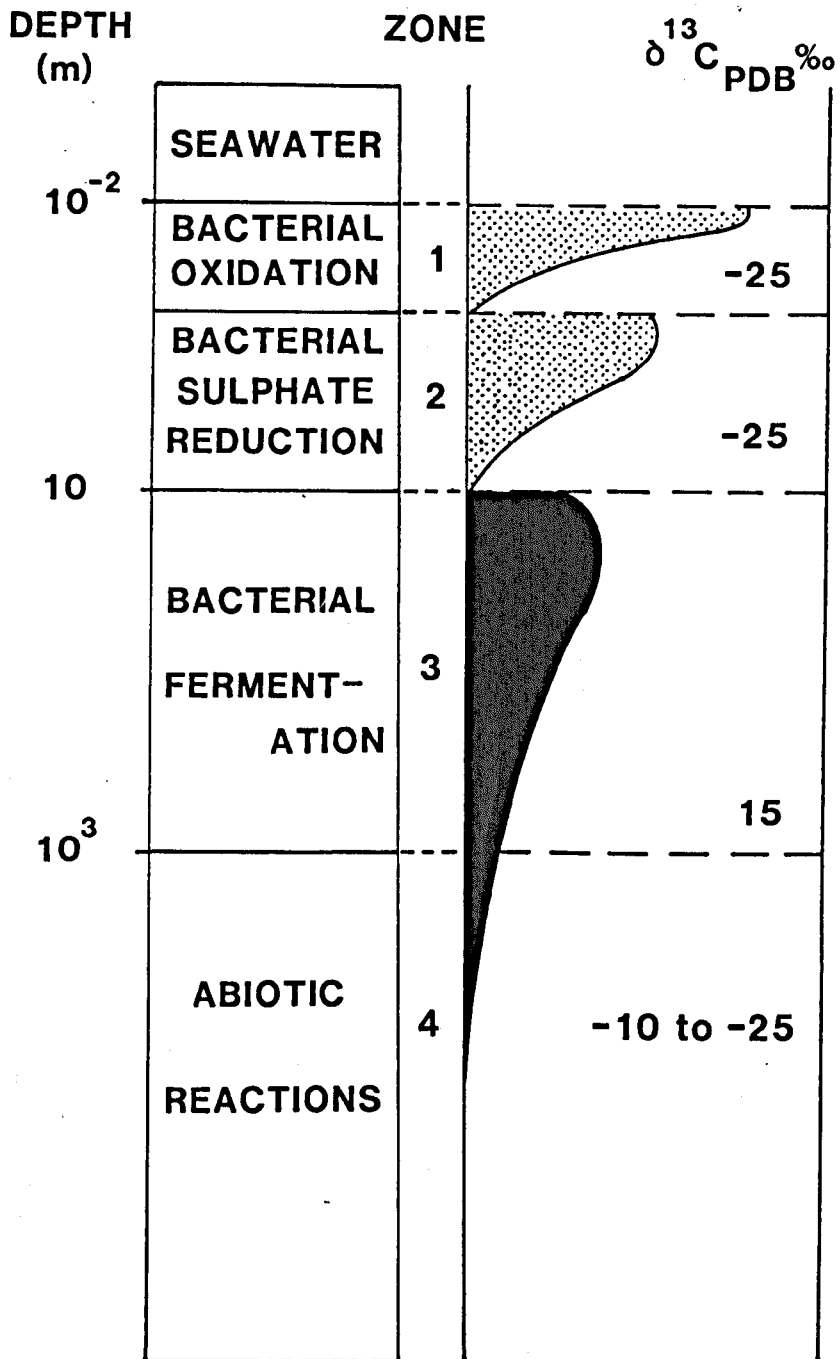


Figure 1.5



ISOTOPICALLY LIGHT CO₂



ISOTOPICALLY HEAVY CO₂

Figure 1.6

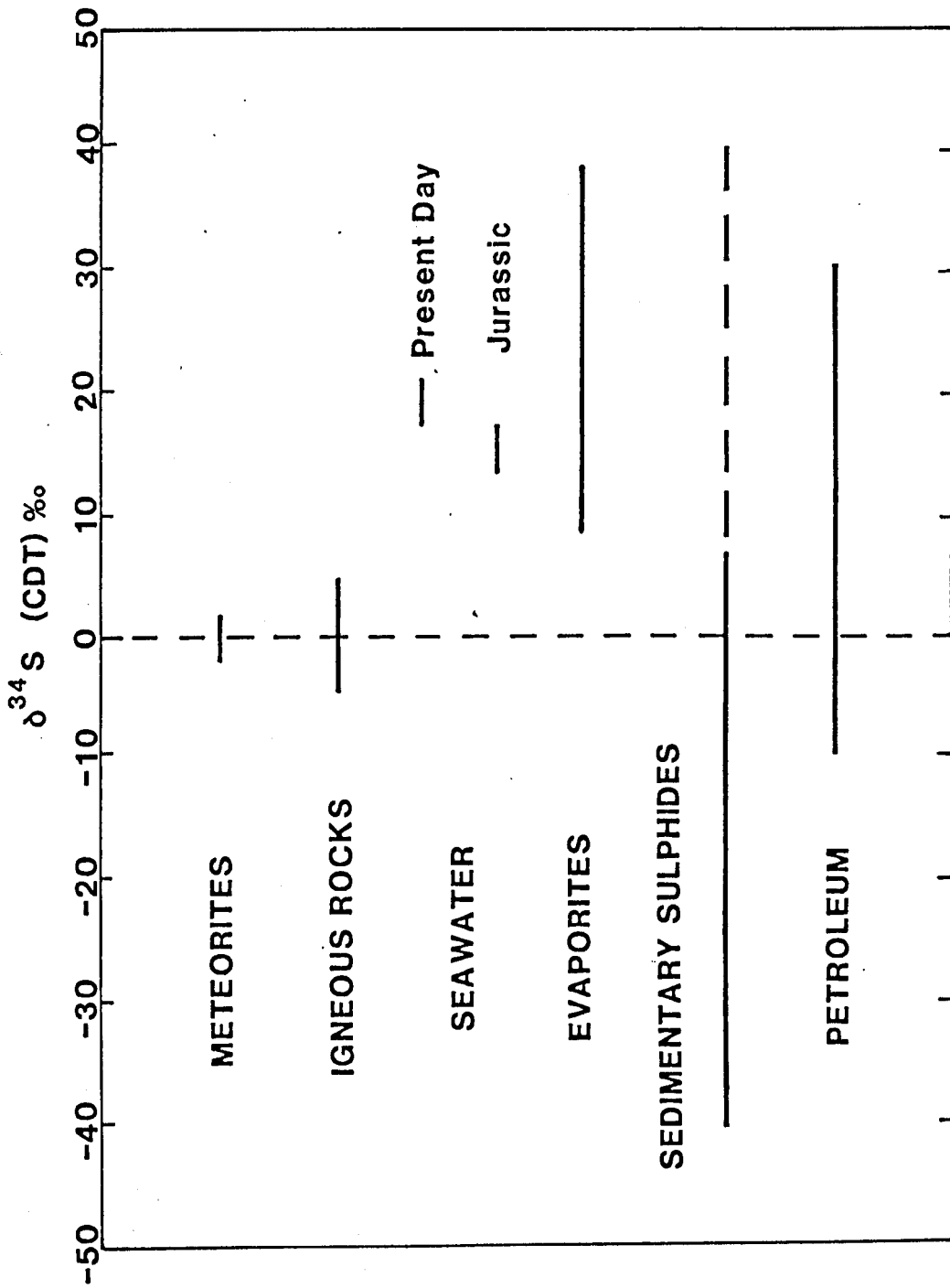


Figure 1.7

SULPHUR ISOTOPE DISTRIBUTION IN NATURE (modified from Kaplan 1983)

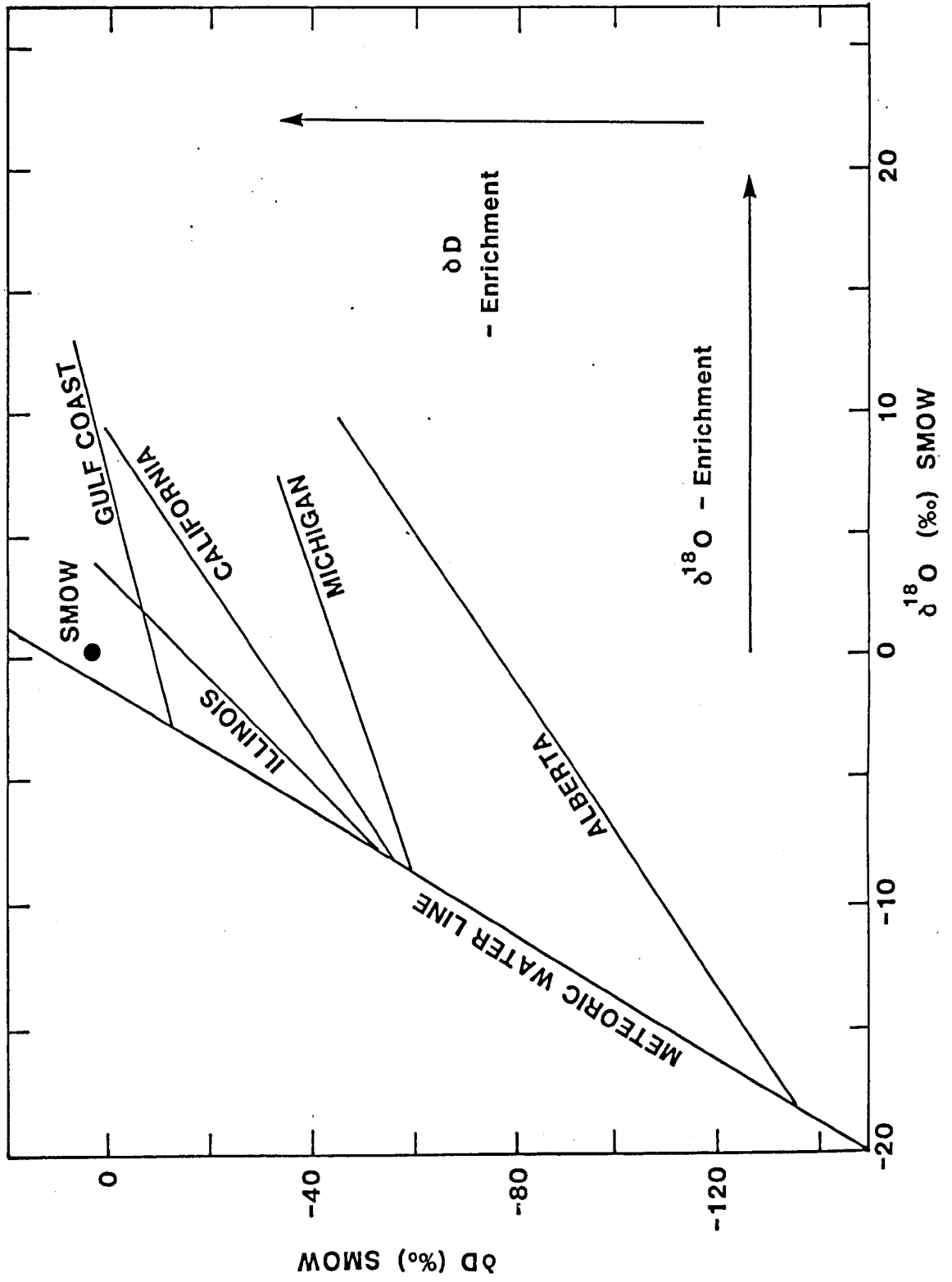


Figure 1.8

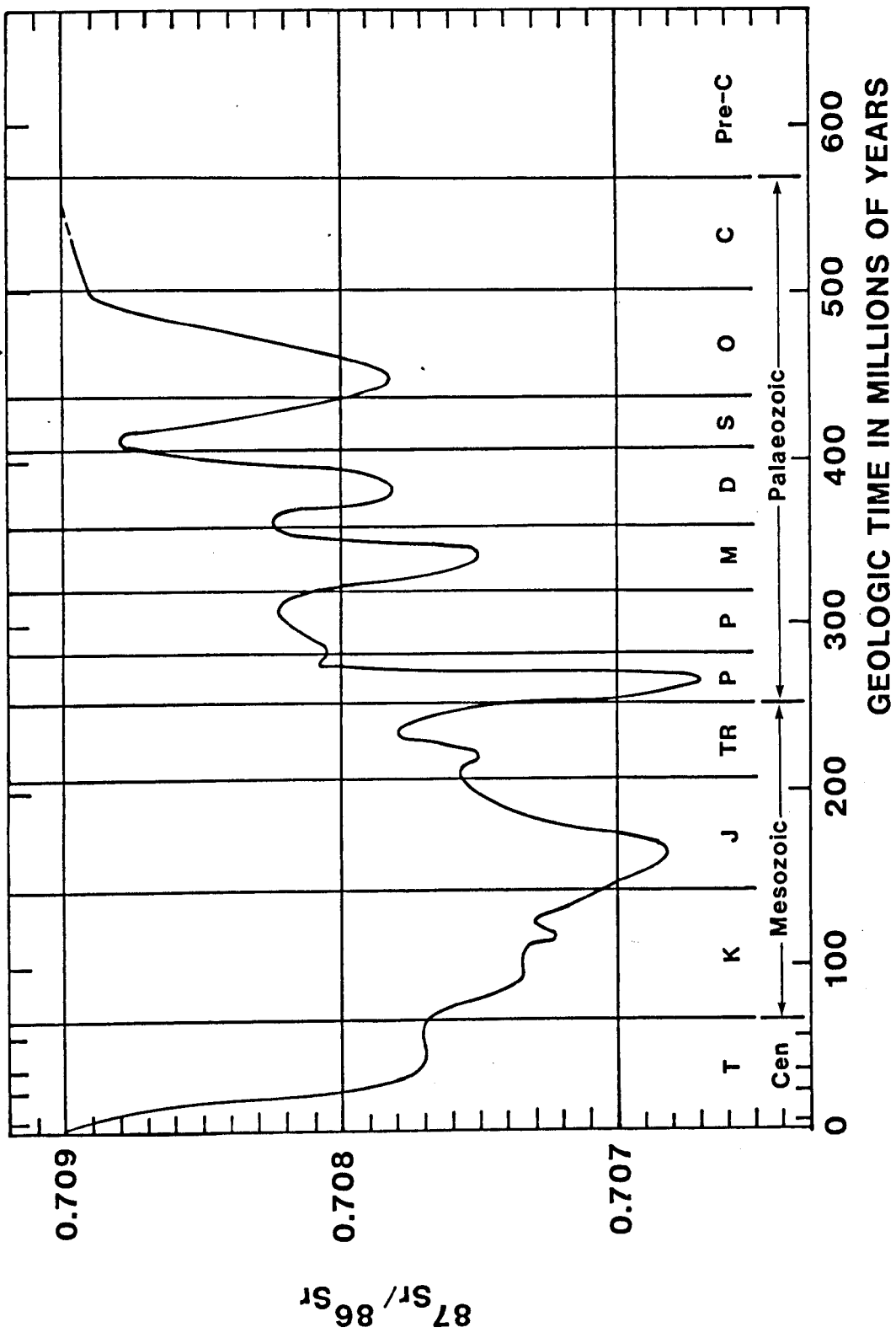


Figure 1.9

CHAPTER 2

2.

OXYGEN ISOTOPIIC ANALYSIS OF DIAGENETIC QUARTZ OVERGROWTHS FROM THE
BRENT SANDS: A COMPARISON OF TWO PREPARATION METHODS.

J.F.BRINT

DEPARTMENT OF APPLIED GEOLOGY,
UNIVERSITY OF STRATHCLYDE,
GLASGOW, G1 1XJ

P.J.HAMILTON

ISOTOPE GEOLOGY UNIT, S.U.R.R.C.,
EAST KILBRIDE, GLASGOW, G75 0QU

R.S.HASZELDINE

DEPARTMENT OF APPLIED GEOLOGY,
UNIVERSITY OF STRATHCLYDE,
GLASGOW, G1 1XJ

A.E.FALLICK

ISOTOPE GEOLOGY UNIT, S.U.R.R.C.,
EAST KILBRIDE, GLASGOW, G75 0QU

Format: Journal of Sedimentary Petrology

Two preparation methods used for determining the $\delta^{18}\text{O}$ of quartz overgrowths are compared from sandstones of the Middle Jurassic Brent Group, Northern North Sea.

Method one uses dilute HF to preferentially attack interfacial materials present between the overgrowth and the detrital core, with subsequent ultrasonic agitation used to break the overgrowths off at the weakened contacts. Size fractionation by sieving should concentrate overgrowths into the smaller grain size separates. However in the Brent sands studied little interfacial material is present between overgrowth and core. Concentration of the diagenetic overgrowths is therefore difficult. This difficulty is compounded by large amounts of detrital quartz in the size fractions as a result of internal fracturing of the grains. The $\delta^{18}\text{O}$ (SMOW) values for the finest size fraction (supposedly overgrowth rich) ranging from 9.0‰ to 13.3‰, are unusually low for diagenetic quartz overgrowths, and result from the high detrital component.

The second method derives the $\delta^{18}\text{O}$ values for the overgrowths by the difference in $\delta^{18}\text{O}$ for the quartz grains plus overgrowths and quartz grains from which the overgrowths have been removed by HF dissolution. The mass balance used requires the overgrowth abundance to be known from point counting. The calculated $\delta^{18}\text{O}$ values obtained are typical for authigenic quartz overgrowths and range from 17.1 to 20.9‰.

Direct isolation of quartz overgrowths for $\delta^{18}\text{O}$ measurement is suitable where interfacial material exists between the detrital grain and the overgrowth. Otherwise preferential HF dissolution of the overgrowths and a $\delta^{18}\text{O}$ mass balance calculation is the preferred method.

Authigenic silica in the form of quartz overgrowths constitutes a common cement in hydrocarbon reservoir sandstones, and its presence may severely reduce porosity and permeability. Oxygen isotopic analysis ($^{18}\text{O}/^{16}\text{O}$) of authigenic quartz overgrowths in sandstones is important as an aid to constraining the thermal and pore fluid conditions of their formation. Until in situ isotopic analysis becomes feasible in a thin section, it is necessary to undertake some physical isolation procedure prior to analysis. As an increasing number of laboratories attempt such techniques in hydrocarbon related projects, it is important to realise the limitations, and a preparation technique suitable for one sandstone may give totally incorrect results if applied to another sandstone. Here, two preparation techniques used in quartz overgrowth ^{18}O determination are compared. Method one being an attempt at direct isolation of the overgrowths by separating them from the detrital cores (Lee & Savin (1985)). Method two being similar to the technique described in Milliken et al. (1981) and Fisher & Land (1986). This indirect measure of the $\delta^{18}\text{O}$ for quartz overgrowths involves $\delta^{18}\text{O}$ analysis of two aliquots one of which consists of the detrital cores and attached overgrowths and the other in which the overgrowths have been dissolved off to leave the detrital cores. The mass balance calculation for the overgrowth $\delta^{18}\text{O}$ requires the percentage abundance of overgrowths and detrital cores to be known in the two aliquots.

The sandstones used in this study are from the Middle Jurassic Brent Group, taken from the Thistle and Murchison oilfields of the U.K. sector of the Northern North Sea (Hallet 1981, Morton and Humphreys 1983, Brown 1984) and are chiefly subarkosic. The Brent Group is considered to be a deltaic sequence (Budding and Inglin 1981), and quartz samples were separated and analysed from fluvial (Ness formation) and tidal (Etive formation) sedimentary facies of the Group (Brown 1984).

To obtain pure quartz samples the sandstone was disaggregated and treated in a solution of 0.3M Na-citrate, 1.0M NaHCO_3 and

sodium dithionite to remove iron oxides. It was then treated in 6% (w/v) hydrogen peroxide to remove organic matter and finally a NaOAc - HOAc solution (buffered to pH = 5) to remove carbonates (Jackson 1979). Each sample was then size separated (<20, 20-50, 50-85, 85-160, 160-250, 250-500 and >500 microns). Under S.E.M examination, the 160-250 micron size fraction was seen to contain the best developed and greatest abundance of quartz overgrowths. Therefore this size fraction was used. Quartz sand was isolated after fusion in NaHSO₄ and removal of feldspars in H₂SiF₆ (Syers et al. 1968). The remaining quartz sand was resieved to ensure that the 160-250 micron size range was maintained. X-ray diffraction analysis confirmed the purity of the quartz samples. This method of quartz isolation is common to both preparation methods. Samples were then prepared either by method one or method two (see below) and analysed for $\delta^{18}\text{O}$ as follows.

Oxygen from the quartz was liberated by reaction with ClF₃ (Borthwick & Harmon 1982) at 650°C for 14 hours, converted to CO₂ over a platinised carbon rod and the gas then analysed on a VG SIRA-10 mass spectrometer. Results were corrected using standard procedures (Craig 1957) and are presented as parts per thousand relative to the SMOW standard in the usual $\delta^{18}\text{O}$ ‰ notation. Reproducibility of results is to within $\pm 0.2\%$, and during the course of the experiments, a value for NBS-28 of $9.6 \pm 0.2\%$ was obtained.

2.4

METHOD ONE - TECHNIQUE AND PREPARATION

This technique which is intended to separate quartz overgrowths from detrital grains is essentially the same as that described by Lee & Savin (1985). This allows the direct isolation of overgrowths and hence a direct measurement of the authigenic quartz. The quartz sand samples used by Lee and Savin (1985) were from the Permian Rotliegendes of the Southern North sea, the Cretaceous Muddy sandstone, Powder River basin and an undisclosed source. These samples had well developed dust rims and overgrowths. This same technique has been applied to a number of sandstone samples at the Isotope Geology Unit, East Kilbride but with variable success. This method was attempted on bulk quartz separates from sandstones of the Middle Jurassic Brent Group. These quartz samples have a poorly developed, or no dust rim between the detrital grain and the

authigenic overgrowth (Fig.2.1). In most samples fluid inclusions delineate the boundary between the overgrowth and the detrital grain.

After X-ray diffraction analysis had confirmed that a pure quartz separate had been obtained each sample was then etched in dilute HF (8%) for between 14 hours to one/two days depending on the sample. The overgrowths were then broken off using a Soniprep ultrasonic disintegrator (5 mins.). As reported by Lee and Savin (1985), etching times to enable quartz overgrowths to break off vary from sample to sample and must be determined for each case. Each quartz sample was then sieved into four size fractions: 30-53, 53-85, 85-160 and 160-250 microns, the overgrowths being concentrated into the finer size fractions. The morphology of the quartz in the four size fractions was checked by S.E.M and then analysed for the oxygen isotopic composition (Borthwick and Harmon 1982, after Clayton and Mayeda 1963).

2.5 METHOD ONE - RESULTS AND DISCUSSION

Initially, seven quartz separates (see Table 2.1,(set one)) each of two grams, were etched in 8% HF and ultrasonically agitated repeatedly in order to split off the quartz overgrowths. Repeated etchings were necessary as the quartz overgrowths did not easily detach, as evidenced by S.E.M checks (Fig.2.2) made between these etching periods. Table One indicates the number of repetitions made per sample in order to detach overgrowths from the detrital grains. Finally, S.E.M checks on the fine fractions showed many successfully split euhedral overgrowths (30-53 microns), see figure 2.3, but also other angular fragments of indeterminate origin (Fig.2.4).

The oxygen isotope analyses show no significant increase in $\delta^{18}\text{O}$ from coarse to fine fractions in set one (Table 2.1). This is contrary to the trend noted by Lee and Savin (1985) for marked increases in $\delta^{18}\text{O}$ from the coarse to fine fractions. The values reported by Lee and Savin (1985) of between 19 to 22‰ for the fine fractions, are typical for diagenetic quartz overgrowths in sandstones (Milliken et al. 1981, Fisher and Land 1986, Longstaffe and Ayalon 1986, Blatt 1987 and McBride et al. 1987).

The mean value for set one of this study is +11.6‰ (SMOW) for the 30-53 micron fraction and +11.7‰ (SMOW) for the 160-250 micron fraction (Table 2.1). Consideration of the results obtained in this

first sample set suggested that the repeated etching/ultrasonic agitation treatment had caused internal splitting of the detrital quartz grains, resulting in significant detrital contributions in all of the size fractions, and hence the similarity in oxygen isotopic compositions for all the size fractions.

It seemed possible that using a larger initial mass of quartz and less ultrasonic agitation would generate more meaningful results. Thus, 20 grams of quartz starting material was used for the six samples of set two (Table 2.2). Only one etching/ultrasonic agitation treatment was made so as to eliminate the shattering effects of repeated treatments. The samples being etched in 8% HF for 14 hours and ultrasonically agitated for 5 minutes. S.E.M morphology checks on the split size fractions showed successfully separated overgrowths and other angular fragments similar to that observed in Set One (see Figs. 2.3 and 2.4). The oxygen isotopic analyses (Table 2.2) again showed no significant increase from the coarse to fine fractions. The mean value for the 30-53 micron fraction is +11.7‰ and +11.8‰ for the 160-250 micron fraction (Table 2.2). This similarity is again attributed to internal shattering of detrital quartz grains causing them to occur in all four size fractions of each sample.

Finally, a third set of three samples using 150 grams of quartz starting material was attempted. The preparation technique omitted the fusion with NaHSO_4 (Syers 1968), because of the quantity involved (12:1 ratio of NaHSO_4 to sample). This obviously has a consequence for the purity of the samples, though XRD checks still indicated pure quartz samples. As in Set Two (see Table 2.2) only one etching/ultrasonic agitation treatment was made. S.E.M morphology checks again showed separated overgrowths but also other angular fragments similar to that observed in the previous experiments. Table 2.3 presents the data. The mean oxygen isotopic value for the 30-53 micron fraction is +10.0‰ and for the 160-250 micron fraction +11.4‰. Once again the expected increase in oxygen isotopic values from coarse to fine fractions was not observed. Again indicating a high detrital component in all size fractions.

2.6

METHOD ONE - CONCLUSIONS

Three separate attempts were made to effect the isolation of quartz overgrowths and failed to generate pure overgrowths in the

finer fractions. It is considered that this failure is due to the lack of interfacial dust material at the overgrowth-detrital grain boundary (Fig.2.1). Consequently the HF etching during successive treatments helps weaken internal fractures in the quartz grains (polycrystalline grains in particular, comprise up to 14% in the sands studied). With ultrasonic agitation, the fracturing is not confined to overgrowth-detrital grain boundaries, so the detrital cores are split into a range of sizes. Each oxygen isotopic composition (Tables 2.1 - 2.3) represents a value for a detrital quartz and overgrowth mixture. Figure 2.5 presents the difference between a schematic trend similar to that found by Lee & Savin (1985) where successful overgrowth isolation occurred, and a trend from this study using sample 9116' (from Table 2.1) as a representative example, showing the unsuccessful isolation of overgrowths.

Blatt (1987) gives an average $\delta^{18}\text{O}$ value of quartz in sandstone, from published data of +11‰. The values for all the size fractions in this study are very similar to this average, a further indication that the separated fractions are a mixture of authigenic and detrital quartz.

2.7

METHOD TWO - TECHNIQUE AND PREPARATION

As the quartz overgrowth oxygen isotopic values were anomalously low compared to those reported by other workers (e.g. Milliken et al.1981, Fisher and Land 1986, Longstaffe and Ayalon 1986, Blatt 1987, McBride et al.1987). It was decided to obtain the values by another preparation method modified from that described in Milliken et al.(1981) and Fisher and Land (1986).

Once pure quartz samples had been obtained (five grams initially prepared for each sample), thin sections were made of the grains. These were point counted (300 counts per slide), to determine the proportion of overgrowth. An aliquot of each quartz sample was analysed for oxygen isotopic composition with the remainder being leached in concentrated HF to remove the overgrowths (Milliken et al. 1981, Fisher & Land 1986). Subsequent checks using S.E.M and thin sections were made to ensure complete removal of the overgrowths. The oxygen isotopic composition of the quartz cores was then measured. The oxygen isotopic composition of the quartz overgrowths was calculated by mass balance (Table 2.4).

The $\delta^{18}\text{O}$ composition for the total sample i.e.(quartz plus overgrowths) for each one ranges from +11.9 to +12.8‰ (SMOW). These are consistently higher than their respective $\delta^{18}\text{O}$ values for the detrital cores (total range +10.3 to +11.8‰ SMOW), see Table 2.4. The overgrowth percentages from each section gave an overall range from 14 to 18%. This allowed the mass balance calculation (Table 2.4) to derive $\delta^{18}\text{O}$ values for the quartz overgrowths of between +17.1 to +20.9‰ SMOW. These values are typical for authigenic quartz cements in sandstones.

Fisher and Land(1986) recognised that interpretation of oxygen isotopic data for quartz cement is complicated by certain factors. With reference to this method, the factors which may complicate the results in method two are (1) the $\delta^{18}\text{O}$ detrital quartz variation, up to 2 per mil ; (2) some quartz overgrowths may be inherited from earlier sedimentary cycles; (3) calculation of the oxygen isotopic composition of quartz overgrowths requires an extrapolation from the values of the core and core plus overgrowth to the value of the overgrowth and (4) Cathode luminescent zonation within the quartz overgrowth cement of similar Brent sands has been observed (Hogg et al. 1987). These growth zones may have formed over a range of temperatures and from a range of $\delta^{18}\text{O}$ waters. This bulk analytical technique cannot resolve this so the $\delta^{18}\text{O}$ value for the overgrowths is an average one. These calculated $\delta^{18}\text{O}$ values for the quartz cement are estimated to be accurate to within $\pm 2\%$ based on the reproducibility of oxygen isotopic analyses to within $\pm 0.2\%$ and a point counting error of 2% for 300 counts of samples having approximately 15% cement (Table 1; Folk 1974, p155).

Method one is not subject to all of these factors. If overgrowths had been successfully concentrated and a direct $\delta^{18}\text{O}$ analysis accomplished only factors 2 (inherited quartz overgrowths) and 4 (cathodoluminescence zonation) would have been applicable.

As this technique involves dissolution of the overgrowths and use of a mass balance calculation the problem of successful separation of overgrowths from the detrital cores is avoided. Rather

the problem lies in the indirect nature of obtaining the $\delta^{18}\text{O}$ value for the overgrowth. But allowing for the greater inherent errors, $\delta^{18}\text{O}$ values are attainable (+17.1 to +20.9) and credible by this method.

2.10

FINAL REMARKS

In this comparison of two preparation methods, method one (Lee & Savin 1985) is suitable for quartz overgrowth isolation when there is sufficient, distinct interfacial material separating the overgrowth from the detrital grain. However when this method is applied to Brent fluvial and tidal sandstones where the quartz overgrowths have minor or no interfacial material, the etching/ultrasonic agitation process attacks internal fractures or planes of weakness in the quartz grains as well as overgrowth - detrital grain boundaries (Fig.1.6). This renders detrital quartz into all the size fractions, and gives low $\delta^{18}\text{O}$ values throughout, thus limiting its applicability.

An alternative preparation method had to be used to obtain the isotopic composition of the cement. This method, which dissolves off the overgrowths and uses a mass balance calculation to attain the $\delta^{18}\text{O}$ composition has a much greater error ($\pm 2\%$) than the direct measurement of isolated overgrowths developed by Lee & Savin (1985). However, until the advent of in situ measurement of quartz overgrowths in a thin section, this method is the most accurate for overgrowths of this nature.

The authors would like to thank the technical staff and in particular Terry Donnelly at the Isotope Geology Unit, S.U.R.R.C, East Kilbride for their help throughout, and to Dr.G.A Blackburn of Britoil for the use of the S.E.M. We are grateful to Britoil and the Hydrocarbons unit of B.G.S. for access to core. Discussions with Andrew Robinson and Christine Bloodworth (British Petroleum) and Dr. Lynton Land were most helpful. J.F.B acknowledges receipt of a N.E.R.C grant.No. GT4/85/GS/97. P.J.H is supported by the Royal Society of Edinburgh Fellowship scheme. The Isotope Geology Unit is supported by the N.E.R.C and the Scottish Universities.

- BLATT, H., 1987, Oxygen isotopes and the origin of quartz: *Jour. Sed. Petrology*, v. 57, p. 373-377.
- BORTHWICK, J., and HARMON., R. S., 1982, A note regarding ClF_3 as an alternative to BrF_5 for oxygen isotope analysis: *Geochim. Cosmochim. Acta*, v. 46, p. 1665-1668.
- BROWN, S., 1984, Jurassic: In Glennie, K. W., ed. *Introduction to the Petroleum Geology of the North Sea*, Blackwell Scientific Publications, p. 103-131.
- BUDDING, M. C., and INGLIN, H. F., 1981, A reservoir geological model of the Brent sands in Southern Cormorant, in Illing, L.V., and Hobson, G.D., eds. *Petroleum Geology of the Continental Shelf of North West Europe*, Heyden & Son, London, p. 326-334,
- CLAYTON, R. N., and MAYEDA, T. K., 1963, The use of bromine pentafluoride in the extraction of oxygen from oxides and silicates for isotopic analysis: *Geochim. Cosmochim. Acta*, v. 27, p. 43-52.
- CRAIG, H., 1957, Isotopic standards for carbon and oxygen and correction factors for mass spectrometric analysis of carbon dioxide: *Geochim. Cosmochim. Acta*, v. 12, p. 133-149.
- FISHER, R. S., 1982, Diagenetic history of Eocene Wilcox sandstones and associated formation waters, South-Central Texas: Ph.D. dissertation, Univ. of Texas at Austin, 185 p.
- FISHER, R. S., and LAND, L. S., 1986, Diagenetic history of Eocene Wilcox sandstones, South-Central Texas: *Geochim. Cosmochim. Acta*, v. 50, p. 551-561.
- FOLK, R. L., 1974, *Petrology of Sedimentary Rocks*: Hemphill Book Store, Austin, Texas, 174 p.
- HALLETT, D., 1981, Refinement of the geological model of the Thistle field, in Illing, L.V., and Hobson, G.D., eds., *Petroleum Geology of the Continental Shelf of North West Europe*, Heyden & Son, London, p. 315-325.
- HOGG, A. J. C., JOURDAN, A., SELLIER, E., and PEARSON, M.J., 1987, Cathodoluminescence of Quartz cements in Brent Group sandstones,

South Alwyn, Northern North Sea: Publications of the Department of Geology and Mineralogy, University of Aberdeen, 26th Annual Meeting of the British Sedimentology Research Group, December 19-22, Abstract No. 60.

JACKSON, M. L., 1979, Soil Chemical Analyses- Advanced Course 2nd ed: Published by the author: Madison, Wis.53705, 895 p.

LEE, M., and SAVIN, S. M., 1985, Isolation of diagenetic overgrowths on sand grains for oxygen isotopic analysis: *Geochim. Cosmochim. Acta*, v. 49, p. 497-501.

LONGSTAFFE, F. J., and AYALON, A., 1986, Oxygen isotope studies of diagenesis in clastic rocks from the Viking and Belly River formations, Alberta: *Terra Cognita*, v. 6, p. 109.

McBRIDE, E. F., LAND, L. S., and MACK, L. E., 1987, Diagenesis of eolian and fluvial feldspathic sandstones, Norphlet formation (Upper Jurassic), Rankin County, Mississippi, and Mobile County, Alabama: *Am. Assoc. Petroleum Geologists Bull.*, v. 71, p. 1019-1034.

MILLIKEN, K. L., LAND, L. S., and LOUCKS, R. G., 1981, History of burial diagenesis determined from isotopic geochemistry, Frio formation, Brazoria County, Texas: *Am. Assoc. Petroleum Geologists Bull.*, v. 65, p. 1397-1413.

MORTON, A. C., and HUMPHREYS, B., 1983, The Petrology of the Middle Jurassic sandstones from the Murchison field, North Sea: *Jour. Petrol. Geology*, v. 5, p. 245-260.

SYERS, J. K., CHAPMAN, S. L., JACKSON, M. L., REX, R. W., and CLAYTON, R. N., 1968, Quartz isolation from rocks, sediments and soils for determination of oxygen isotopic composition: *Geochim. Cosmochim. Acta*, v. 32, p. 1022-1025.

Fig. 2.1 - Quartz overgrowth with poorly developed dust rim, Ness Formation, 211/18-A30ST, 9116 feet subsea, (2778 metres subsea). Field of view - 0.6mm.

Fig. 2.2 - Quartz overgrowths still attached to detrital grains after one etching/agitation period. Etching of the overgrowth by HF is evident. Ness Formation. 211/18-A30ST, 9223 feet subsea, (2811 metres subsea). Scale bar 200 microns.

Fig. 2.3 - Successfully split quartz overgrowth, Ness Formation, 211/18-A30ST, 9116 feet subsea, (2778 metres subsea). Scale bar 50 microns.

Fig. 2.4 - Angular fragment, probably of detrital origin, in the 30 - 53 micron size fraction. Ness Formation, 211/18-A30ST, 9116 feet subsea, (2778 metres subsea). Scale bar 50 microns.

Fig. 2.5 - $\delta^{18}\text{O}$ vs. particle size showing a) a schematic trend in $\delta^{18}\text{O}$ caused by the successful concentration of overgrowths in the finer size fractions (as found by Lee & Savin 1985) and b) using sample 9116', (2778 m), (211/18-A30ST), to illustrate the trend of low $\delta^{18}\text{O}$ values caused by unsuccessful concentration of overgrowths in this study. Detrital grains occurring in all size fractions.

Fig. 2.6 - Sketch diagram of internal fracturing of quartz grains causing a detrital component to occur in all size fractions.

Table 2.1 : Set 1 - $\delta^{18}\text{O}$ values for separated quartz size fractions

Table 2.2 : Set 2 - $\delta^{18}\text{O}$ values for separated quartz size fractions

Table 2.3 : Set 3 - $\delta^{18}\text{O}$ values for separated quartz size fractions

Table 2.4 : Oxygen isotopic compositions of quartz overgrowths calculated from the mass balance equation.

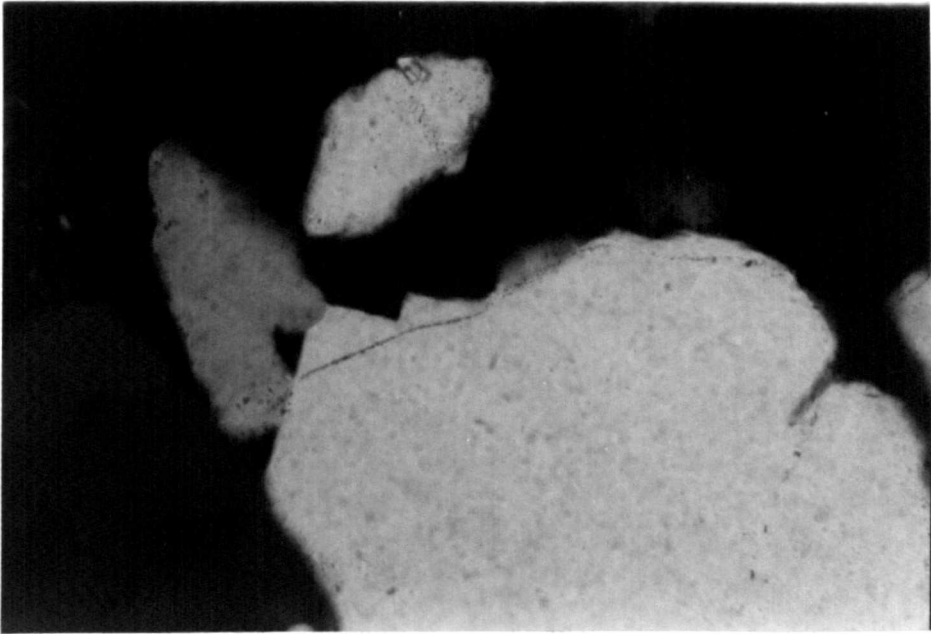


Figure 2.1

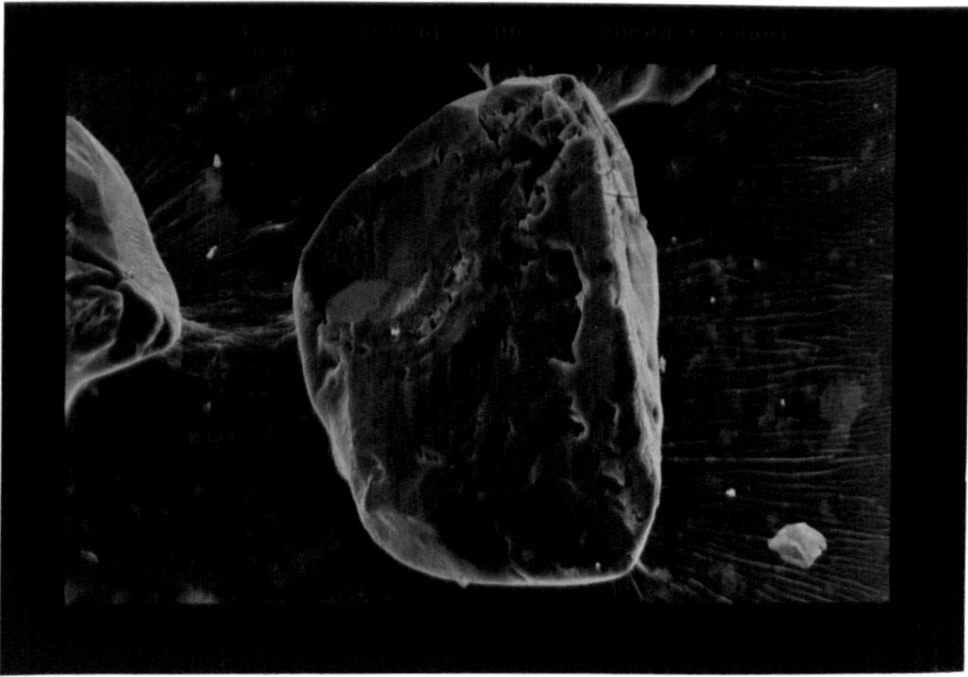


Figure 2.2

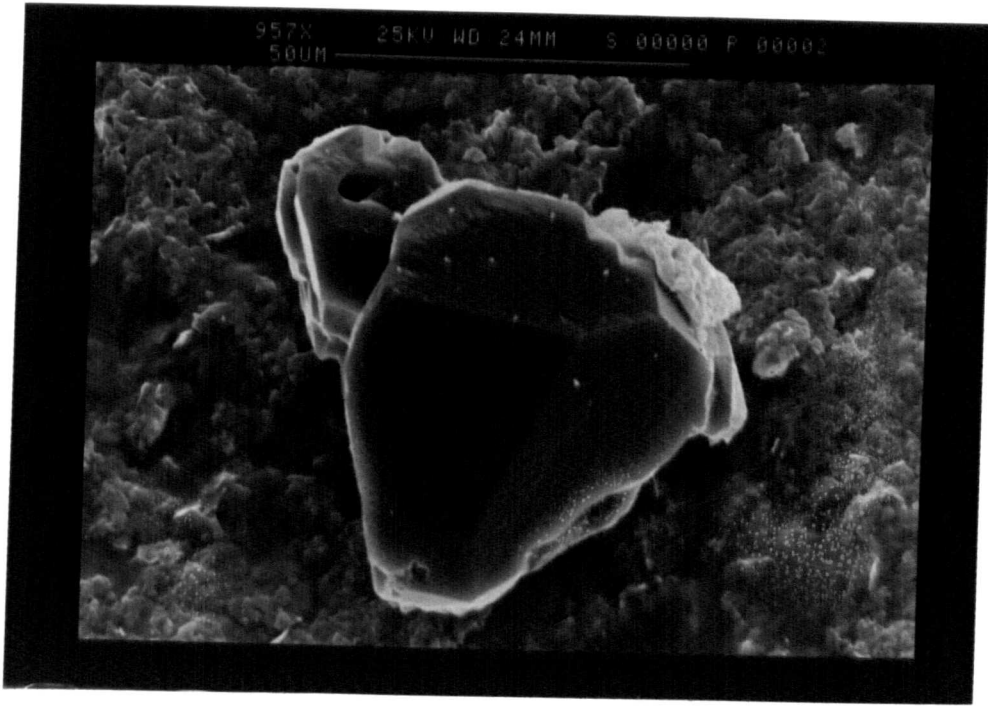


Figure 2.3

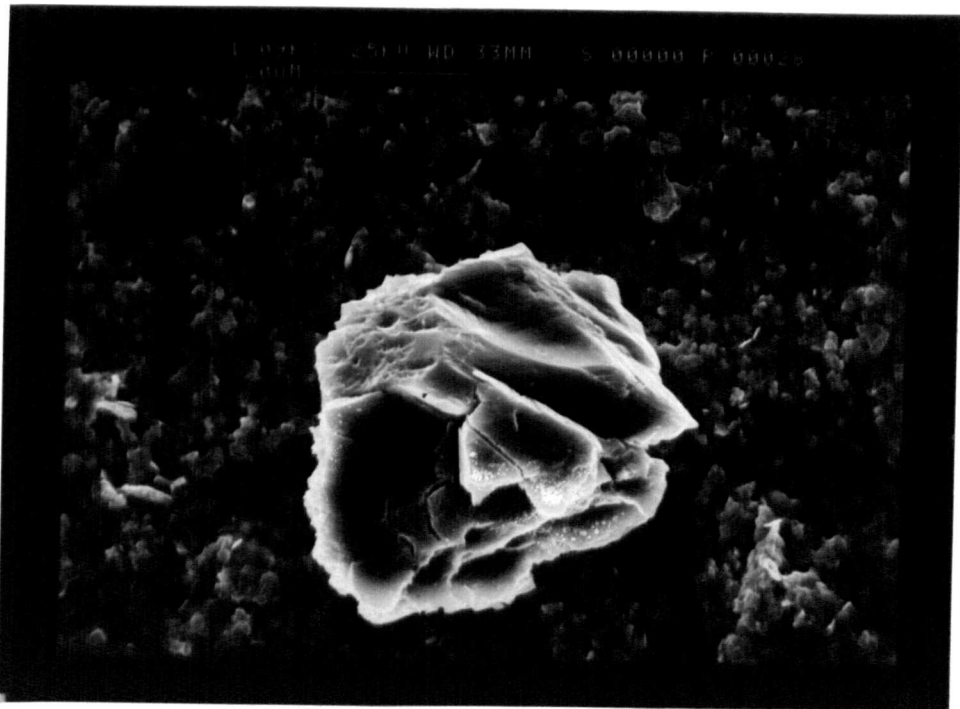


Figure 2.4

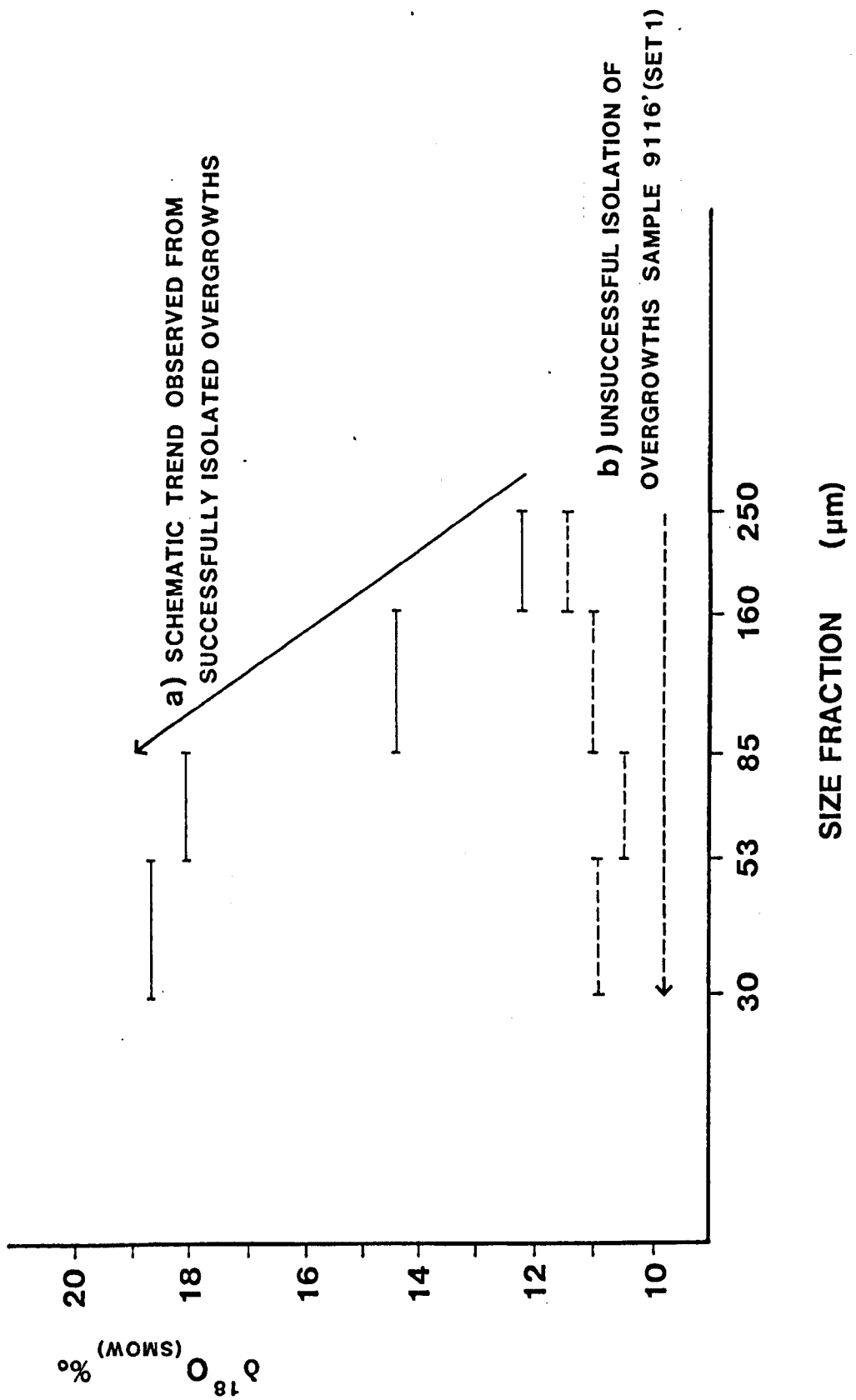


Figure 2.5

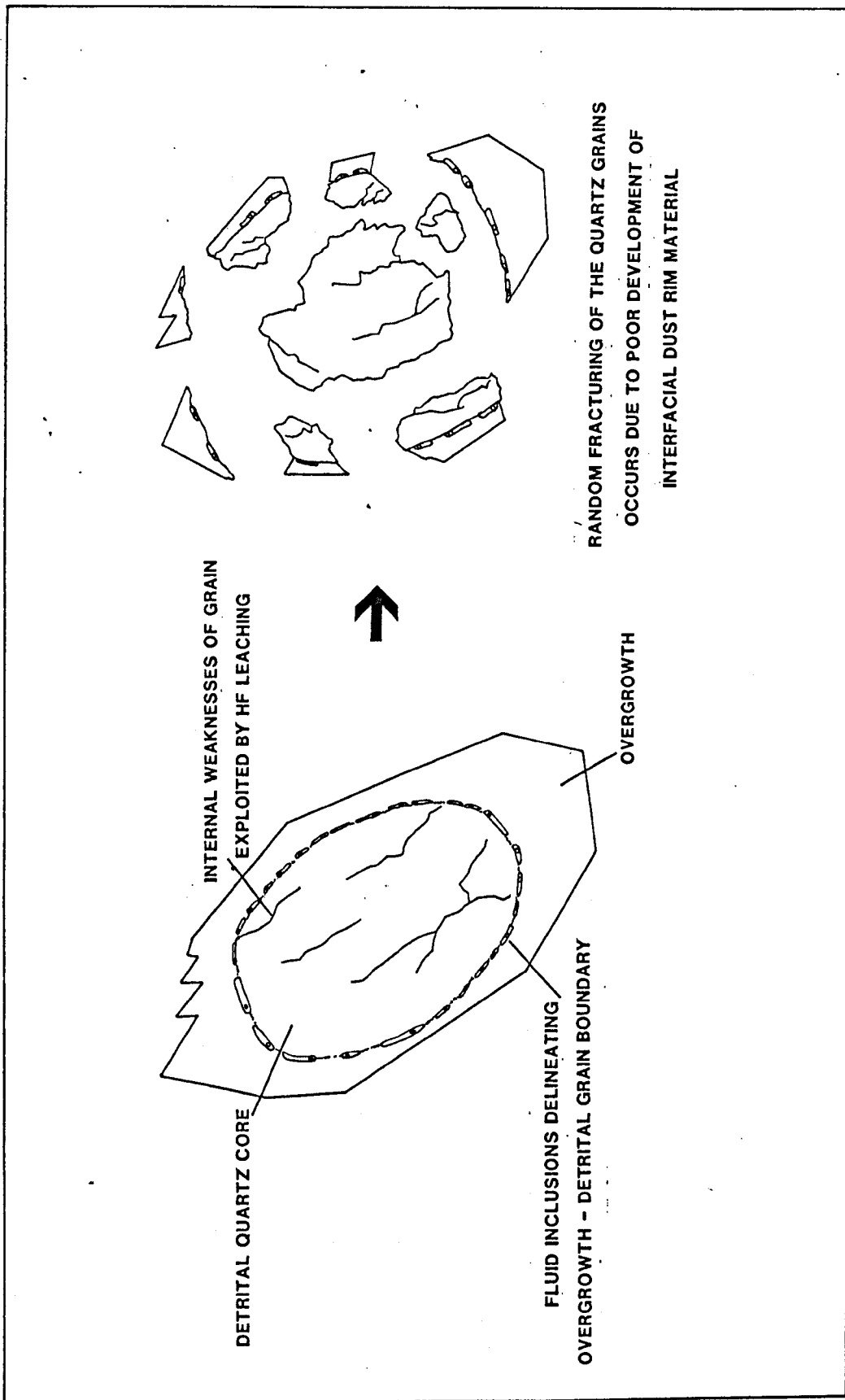


Figure 2.6

TABLE 2.1: SET 1 $-\delta^{18}\text{O}$ VALUES FOR SEPARATED QUARTZ SIZE FRACTIONS

SAMPLE	DEPTH TVD.SS (FT) (M)	FORMATION	NO. OF ETCHING/ AGITATION TREATMENTS	TOTAL HOURS IN 8% HF	SIZE FRACTIONS (microns)			
					30-53 $\delta^{18}\text{O}$	53-85 $\delta^{18}\text{O}$	85-160 $\delta^{18}\text{O}$	160-250 $\delta^{18}\text{O}$
WELL: 211/18-A30ST (THISTLE)								
9116	2778	NESS	2	32	+10.9	+10.5	+11.0	+11.5
9156	2791	NESS	3	48	+10.5	+11.7	+11.9	+11.7
9223	2811	ETIVE	3	48	+10.9	+11.1	+11.8	+12.0
9246	2818	ETIVE	3	48	+11.8	+11.4	+10.8	+11.4
9278	2828	ETIVE	2	32	+11.9	+11.4	+11.5	+11.9
WELL: 211/19-3 (MURCHISON)								
9942	3030	NESS	3	48	+12.2	+11.5	+11.9	+12.5
10188	3105	NESS	3	48	+11.5	+10.8	+11.7	+12.3

TABLE 2.2: SET 2 $-\delta^{18}\text{O}$ VALUES FOR SEPARATED QUARTZ SIZE FRACTIONS

			SIZE FRACTIONS (microns)			
			30-53	53-85	85-160	160-250
			$\delta^{18}\text{O}$	$\delta^{18}\text{O}$	$\delta^{18}\text{O}$	$\delta^{18}\text{O}$
SAMPLE						
WELL: 211/18-A30ST						
DEPTH	TVD.SS	FORMATION				
(FT)	(M)					
9116	2778	NESS	+13.2	+11.1	+11.2	+12.5
9156	2791	NESS	+13.3	+12.1	+11.8	+12.6
WELL: 211/19-3						
9942	3030	NESS	+11.9	+11.4	+11.9	+12.6
10188	3105	NESS	+11.2	+11.8	+11.4	+12.1
10300	3139	ETIVE	+10.9	+11.0	+11.4	+12.0
10331	3148	ETIVE	+11.4	+11.5	+11.4	+12.0

(Only one etching/agitation treatment made, with a total of 14 hours in 8% HF)

TABLE 2.3: SET 3 $\delta^{18}\text{O}$ VALUES FOR SEPARATED QUARTZ SIZE FRACTIONS

			SIZE FRACTIONS (microns)			
			30-53	53-85	85-160	160-250
			$\delta^{18}\text{O}$	$\delta^{18}\text{O}$	$\delta^{18}\text{O}$	$\delta^{18}\text{O}$
SAMPLE						
WELL: 211/18-A45						
DEPTH	TVD.SS	FORMATION				
(FT)	(M)					
8624	2628	ETIVE	+11.8	+11.8	+11.0	+11.7
8631	2631	ETIVE	+9.1	+9.6	+10.9	+10.1
8651	2637	ETIVE	+9.0	+8.2	+12.4	+12.4

(Only one etching/agitation treatment made, with a total of 14 hours in 8% HF)

TABLE 2.4: OXYGEN ISOTOPIC COMPOSITIONS OF QUARTZ OVERGROWTHS CALCULATED FROM THE MASS BALANCE EQUATION:-

$$\delta^{18}\text{O}_T = \delta^{18}\text{O}_C \cdot X_C + \delta^{18}\text{O}_{OG} \cdot X_{OG}$$

WELL:211/18-A30ST

DEPTH (FT)	9116	9156	9223	9246	9278
TVD.SS (M)	2778	2791	2811	2818	2828
$\delta^{18}\text{O}_T$	+12.2	+12.8	+11.9	+12.2	+12.8
$\delta^{18}\text{O}_C$	+10.3	+11.6	+10.6	+11.4	+11.8
%OG	18.0	16.4	16.0	14.0	17.0
$\delta^{18}\text{O}_{OG}$	+20.9	+19.3	+18.8	+17.1	+17.4

T = Total Sample (Quartz + overgrowths)

C = Detrital Core

OG = Overgrowth

X = Mole Fraction

(From Fisher 1982)

CHAPTER 3

3. ISOTOPE DIAGENESIS AND PALAEOFLUID MOVEMENT IN THE BRENT
SANDSTONES, NORTHERN NORTH SEA.

J.F. BRINT

DEPARTMENT OF APPLIED GEOLOGY,
UNIVERSITY OF STRATHCLYDE,
GLASGOW, G1 1XJ

R.S. HASZELDINE

DEPARTMENT OF APPLIED GEOLOGY,
UNIVERSITY OF STRATHCLYDE,
GLASGOW, G1 1XJ

P.J. HAMILTON

ISOTOPE GEOLOGY UNIT, S.U.R.R.C.,
EAST KILBRIDE, GLASGOW, G75 0QU

A.E.FALLICK

ISOTOPE GEOLOGY UNIT, S.U.R.R.C.,
EAST KILBRIDE, GLASGOW, G1 1XJ

S. BROWN

BRITISH GEOLOGICAL SURVEY,
19 GRANGE TERRACE,
EDINBURGH, EH9 2LF

Format: Bulletin of the American Association
of Petroleum Geologists.

The deltaic sandstones of the Middle Jurassic Brent Group show a sequence of diagenetic minerals of kaolinite - Fe,Ca carbonates - quartz overgrowths - Fe,Mg carbonates - illite. Most secondary porosity formed early in burial but was infilled by early kaolinite, but did continue to develop during burial. The quantity of diagenetic minerals in the micaceous Rannoch Formation is low due to its low permeability. By contrast, the quantities of diagenetic cements in the porous and permeable Etive, Ness and Tarbert Formations are larger, up to 18% of the rock. This implies movement of fluid during diagenesis. Early silicate and carbonate cements formed at burial depths down to ≈ 1 km, in an open flow system dominated by meteoric water ($\delta^{18}\text{O} = -7\text{‰}$). Deeper "late" cements formed in a progressively more closed hydrological system, and show a gradual isotopic evolution away from meteoric water to coincide with the present day porewater composition in the Brent of $\delta^{18}\text{O} = +2\text{‰}$ and $\delta\text{D} = -24\text{‰}$ (SMOW). Fluid inclusion microthermometry on quartz overgrowths and $\delta^{18}\text{O}$ values for quartz overgrowths and latest ankerite indicate that these cements grew from dominantly fresh porewaters between 73° and 131°C at 1.8 to 2.3km burial. This requires either a geothermal gradient of $70^\circ\text{C}/\text{km}$ at 58 Ma, or our preferred hypothesis of pulsed migrations of warm fluid from deeper in the basin.

The study of diagenesis is an aid to understanding and characterising hydrocarbon reservoirs. Diagenesis encompasses the physical and chemical changes that occur to a sandstone. These involve physical compaction, the precipitation of authigenic minerals (porosity and permeability destruction) and the dissolution of framework grains and authigenic minerals (porosity and permeability enhancement). In order to predict the degree of sandstone diagenesis, and hence reservoir quality, it is essential to understand the processes which have controlled diagenesis, their volumetric importance, geographical extent and timing throughout the history of the basin.

Previous studies on the Brent sandstones have been restricted either to single wells (Blanche & Whittaker 1978, Hancock & Taylor 1978, Sommer 1978, Bjorlykke et al. 1979, Bjorlykke & Brendsdal 1986) or to small study areas (Blackbourn 1984, Malley et al. 1986, Thomas 1986, Hamilton et al. 1987, Jourdan et al. 1987, Glassman et al. 1989 in press).

In this study an examination of the 3-dimensional distribution of diagenetic minerals in the Brent Group is presented using groups of wells over a significantly wider area within the East Shetland Basin. A multidisciplinary approach was used combining structural information, burial history and poroperm data with standard petrographic techniques, fluid inclusion microthermometry and stable and radiogenic isotopes. The combination of these techniques enables greater understanding of the diagenetic modifications which occurred to sandstones.

The aims of this paper are to establish a diagenetic sequence in a typical Brent sandstone over a 3500 km² area, to relate it to the reservoir quality, and model the fluid movement and pathways, the temperature and the timing of mineral cementation in relation to basin history. In studying the areal extent of mineral cements, the simplified sequence of kaolinite -Fe, Ca carbonates-quartz overgrowths-illite is observed throughout. Variation in volume of cement varies geographically with greater proportions of mineral cements, particularly quartz overgrowths and illite in the south of the basin. In the sandstones studied the permeable Tarbert, Ness and

Etive Formations contained over twice as much authigenic cement than the less permeable Rannoch Formation. The early phases of siderite, calcite and kaolinite precipitated in a porewater that had a strong meteoric component. With burial continuing through the Cretaceous, the porewater became trapped and evolved isotopically with kaolinite, pyrite, ankerite, quartz overgrowths and illite precipitating at higher temperatures (fluid inclusions in quartz overgrowths give $T_h = 73-131^\circ\text{C}$). The quartz overgrowths and illite severely reduced porosity and permeability at the end Cretaceous, prior to peak oil migration.

The Middle Jurassic Brent sandstones studied are taken from the Rannoch, Etive, Ness and Tarbert Formations of the Thistle, Murchison and Dunlin oilfields and well 3/13a-1 in the East Shetland Basin, northern North Sea (Fig.3.1). Core material was supplied by the British Geological Survey and Britoil plc.

3.3

GEOLOGICAL SETTING

The Thistle (211/18 and 211/19), Murchison (211/19 and 33/9) and Dunlin (211/23 and 211/24) oilfields and well 3/13a-1 (Fig.3.2) are all located in the East Shetland Basin which is situated on the western margin of the Northern Viking Graben approximately 150 kilometres northeast of the Shetland Islands in the Northern North Sea (Fig.3.1).

3.3.1 STRUCTURE

The East Shetland Basin is a fault bounded, block faulted terrace on the western flank of the N. Viking Graben (Fig.3.1), and is related to the development of a major graben system which was probably initiated in the Permian (Glennie 1984). Badley et al. (1988) have recognised two rifting episodes in the Northern Viking Graben, 1) ?Late Permian-Early Triassic and 2) Bathonian-Ryazanian. The first episode involved extension about a N-S axis with thermal subsidence occurring in the Triassic-Middle Jurassic. During the second rifting episode a NE-SW fault trend (Caledonian) was reactivated in the area. At Middle Jurassic level, the East Shetland Basin had developed as a series of fault terraces consisting of tilted fault blocks which dominantly dip to the west. Badley et al.

(1988) indicate that the cessation of rotation of these fault bounded blocks was in the Ryazanian, and hence the termination of this rifting phase. Post rift thermal subsidence saw the graben fill with Cretaceous, Tertiary and Quaternary marine sediments (Fig.3.3) up to four kilometres thick in the East Shetland Basin and six kilometres in the Graben axis. Two major subparallel fault terraces with N-S and NE-SW trends dominate the basin (Fig.3.2). The westerly terrace controls the location of the Ninian, Hutton, Dunlin and Murchison oilfields, that to the east having the Brent and Statfjord oilfields (Fig.3.2). Hallet (1981) points out that many of the faults in the East Shetland Basin were synsedimentary during deposition of the Middle Jurassic Brent delta.

3.3.2 STRATIGRAPHY AND FACIES

Continental Upper Triassic sediments are overlain by NE-prograding non-marine alluvial fan sandstones of the Statfjord Formation (Rhaetian-Sinemurian), (Fig.3.4), Kirk (1980), Chauvin & Valachi (1981). These are conformably overlain by marine Dunlin Group shales of Lower Jurassic age. The Brent Group overlies the Dunlin Group, in places unconformably (Fig.3.4). It is a sand dominated deltaic sequence (Bowen 1975, Budding & Inglin 1981, Simpson & Whitley 1981, Brown 1986, Brown et al. 1987, Richards et al. 1988) of Aalenian to Bathonian age, which is in turn overlain by the marine shales of the Middle-Upper Jurassic Heather Formation and Oxfordian-Kimmeridgian age Kimmeridge Clay Formation, which constitutes the Upper Jurassic (Fig.3.4). The boundary between the Brent Group and the Heather Formation is an unconformity and at the crests of the tilted fault blocks erosion has cut down to Aalenian level within the Brent Group.

Deegan & Scull (1977) divided the Brent Group into five units - Broom, Rannoch, Etive, Ness and Tarbert (Fig.3.4). The Broom Formation (Kirk 1980, Budding & Inglin 1981, Eynon 1981) is typically a medium-coarse grained sandstone locally associated with bioturbated and argillaceous sandstones. Brown et al. 1987, concluded that due to the lithological character, distribution, thickness variations (1-23 metres) and the presence of low energy, marine offshore transition muds separating the Broom from the overlying Rannoch Formation over most of the area, together suggest that the Broom Formation

represents a genetically distinct depositional system from the remainder of the Brent Group. The micaceous sandstones of the Rannoch Formation (Hodson 1975) are considered to be a shallow marine delta front or shoreface deposit shaped by storm influences (Richards & Brown 1986). The basal Rannoch Formation consists of parallel laminated heterolithic beds (bioturbated in places) overlain by laminated and hummocky cross stratified micaceous (very fine - fine grained) sandstones, (Richards & Brown 1986). To the north, the basal Rannoch Formation occurs as a mudstone with thin interbedded mica rich sandstones. Bioturbation is common in the mudstone and lower sandstone intervals. The Rannoch Formation is a unit which has an erosive or gradational boundary with the overlying thick, commonly structureless sandstones of the Etive Formation. The Rannoch-Etive Formations may be in excess of 100 metres thick. The Etive sandstones are typically medium grained with localised thin basal coarse lag deposits and at the top, rootlet zones (Brown et al. 1987). The Etive Formation forms a near continuous unit across the basin and has been interpreted as a barrier bar complex (Budding & Inglin 1981) as mouth bar sands (Albright et al. 1980) and as distributary channel sands (Parry et al. 1981). Brown et al. (1987) consider that the lateral continuity of the Etive and underlying Rannoch Formation and the presence of superjacent marine and brackish salinity muds of the Ness Formation tend to favour the first hypothesis. The sandstones are mica poor, generally well sorted and fine-medium grained. The overlying Ness Formation has been interpreted as a back barrier delta plain consisting of interbedded sandstones, siltstones and mudstones (which have both upwards coarsening and fining grain size trends) and coals (Brown et al. 1987), Formation thickness may exceed 90 metres. Finally the Tarbert Formation records a marine transgression over the abandoned progradational deltaic sediments, locally with a sharp erosive boundary. In places it is composed of vertically stacked, upward coarsening units, which may be bioturbated. The sandstones also exhibit hummocky cross stratification and storm/fairweather couplets similar to that seen in the Rannoch Formation (Brown et al. 1987). The Tarbert Formation is commonly thin or absent due to erosion on tilted fault block crests.

3.3.3 RESERVOIR CONNECTEDNESS

The Brent Group of the East Shetland Basin preserves a group of laterally uniform depositional facies over a wide area which prograded from the southwest (Richards et al.1988) and which has no major facies variation between fields. Therefore, diagenesis of each facies in individual fields can be directly compared. The three-dimensional distribution of facies will have influenced flow of water through the basin during diagenesis. The Rannoch Formation should have good lateral connectivity due to the wide uniform shoreface facies. However vertical connectivity will be poor due to the extensive horizontally deposited layers of impermeable micas and clay. Etive Formation sandstones are coarser grained and contain less mica and clay. The Formation is laterally uniform across the basin and facilitates good connectedness both horizontally and vertically. Connectivity between channel sandstones within the Ness Formation is poor due to the extensive formation of poorly permeable fine grained sediments of the interbedded lacustrine and levee facies. However fault controlled zones of channel sandstones within the muds may have allowed three-dimensional connectedness to be maintained over geological timescales, rather than oil production timescales. The transgressive nature of the Tarbert sandstones should prove to have good connectivity over a wide area, although it tends to be variable. Therefore it is expected that the flow of fluid through the Brent sandstones will be controlled by depositional geometries and the poroperm quality of the Formations, there being no major facies variation between fields. The relationship of diagenesis to porosity and permeability is illustrated in Fig. 3.5, using well 211/18-A33. Porosity is high in all formations but permeability is severely reduced in the Rannoch. The high permeabilities maintained in Etive. Ness and Tarbert facilitate a greater opportunity for fluid flow and hence the precipitation of more diagenetic cements than in the Rannoch. This is borne out not only in 211/18-A33 but also using average values for all sandstones studied from the Thistle, Dunlin and Murchison oilfields,(Fig.3.5, Table 3.1). Well 3/13a-1 in the south of the basin has suffered more extreme diagenesis but still shows the general trend of greater diagenetic cementation in the Etive, Ness and Tarbert Formations (Table 3.1).

3.3.4 RESERVOIR CONDITIONS

The Brent Group oil reservoirs consist of sub-unconformity and fault seal traps at the uptilted edge of the fault blocks (Fig.3.3). The top seal is either Upper Jurassic or Lower Cretaceous shales. The Kimmeridge Clay Formation is the generally accepted principal hydrocarbon source (Goff 1983). The Brent Group in the wells studied occurs at depths of 8,624 to 12,459 feet TVD subsea (2.63 to 3.79 kms). The thickness of the Brent sequence in the wells studied varies from 100 to 175 metres. Porosities average 17%, with a maximum of 30%, whilst permeabilities average 200mD with a maximum of 6000mD in the fields studied (Nadir & Hay 1978, Engelstad 1987). Reservoir temperatures in the Brent sequence range from 85 to 107 C (Thistle), 110 C in the Murchison oilfield (Engelstad 1987) and 115 C in the Greater Alwyn area. Initial reservoir pressures have an average of 400 bar from logs for the Thistle field, 458 bar from logs for the Dunlin field, and 444 bar in Murchison (Engelstad 1987). Lithostatic and hydrostatic pressures at a depth of 2.7 kms (Thistle) are 688 and 265 bar respectively, at 3.0 kms (Dunlin) are 765 and 294 bar, and at 2.9 kms (Murchison) 739 and 284 bar. This indicates that at the present day the reservoirs are overpressured.

3.4 ANALYTICAL TECHNIQUES

3.4.1 PETROGRAPHY

Elucidation of textural relationships and the cement stratigraphy was undertaken using optical microscopy on porosity impregnated (blue-dyed epoxy) thin sections, scanning electron microscopy on a Cambridge Instruments Stereoscan 100 coupled with a Link Energy Dispersive Analysis System, and cathodoluminescence using a Technosyn cold cathode luminescence 8200 mk II unit.

3.4.2 FLUID INCLUSION MICROTHERMOMETRY

Measurements were made on a Linkam TH 600 heating/freezing stage (Shepherd 1981) used in conjunction with a Leitz-Dialux 20-EB binocular microscope fitted with a long working distance condenser lens at magnifications up to x1250. Wafers were doubly polished 40-100 microns thick prepared by the method of Crosbie (1981).

Homogenisation temperatures, salinities and eutectic measurements were made on fluid inclusions in quartz overgrowths.

3.4.3 X-RAY DIFFRACTION

Oriented sample mounts were prepared by sedimentation onto glass slides. The air dried samples were analysed on a Philip 3 kw diffractometer using Fe-filtered Co-K α radiation, with 0.5° divergence, antiscatter slits and a 0.1 micron receiving slit (for clays) and 1° divergence, antiscatter slits and a 0.1 micron receiving slit (for whole rock).

3.4.4 ISOTOPIC ANALYSES

Isotopic analyses were made on authigenic quartz overgrowths, kaolinite, illite, calcite, siderite and ankerite. Procedures for sample preparation are given in Appendix One. Appendix Two presents the methods employed for obtaining $\delta^{18}\text{O}$, δD and $\delta^{13}\text{C}$ analyses.

The oxygen data for silicates are presented in the usual δ notation, with the results being corrected using standard procedures (Craig 1957) and are given as parts per thousand relative to the SMOW standard in the $\delta^{18}\text{O}$ ‰ notation. Reproducibility of results is to within $\pm 0.2\%$, and during the course of the analyses a value for NBS-28 of $9.6 \pm 0.2\%$ was obtained. For carbonates the oxygen and carbon data are also presented in the usual notation and corrected using the standard procedures (Craig 1957) presented as parts per thousand relative to the PDB standard. Oxygen values were subsequently calculated to the SMOW standard. Furthermore, the oxygen isotopic analyses for the siderite and ankerite had corrections made to the fractionation factor (α) for the reaction temperatures employed; siderite (100°C): 1.00881 and ankerite (100°C): 1.00901, Rosenbaum & Sheppard (1986). Reproducibility of results is to within $\pm 0.2\%$ and a value for NBS-20 during the course of analyses gave $\delta^{18}\text{O}_{\text{SMOW}} = +26.5 \pm 0.2\%$ and $\delta^{13}\text{C}_{\text{PDB}} = -1.2 \pm 0.1\%$.

Hydrogen isotopic analyses (δD) on kaolinite and illite were corrected relative to SMOW in the usual δ notation, and are presented as parts per thousand relative to the SMOW standard. Reproducibility of results is to within $\pm 2\%$. Values for a laboratory kaolinite standard gave $\delta\text{D} = -55 \pm 2\%$. (This standard has been calibrated

using NBS-30 biotite for which $\delta D = -64\%$ in the laboratory at S.U.R.R.C., East Kilbride.

Appendix Three gives procedures for K/Ar dating of an illite sample. Analysis was made on a pure 0.1 micron size sample, which was confirmed $\approx 98\%$ pure by X-ray diffraction.

3.4.5 CORE SAMPLING

Typical sandstones from major sandbodies in each of the Formations were sampled from groups of wells. The number of sample points varied with the thickness of each sandbody, usually samples were taken at the centre and near the top and the base (the thicker the sandstone, the more samples taken). Major sandbodies in the Rannoch, Etive, Ness and Tarbert Formations were sampled.

3.5 PETROGRAPHY

Sampling and examination of typical sandbodies allowed differences and similarities in the framework grains and diagenetic cements to be observed and hence related to porosity and permeability.

3.5.1 FRAMEWORK GRAINS

The seventy six sandstone samples studied are dominantly subarkosic with a limited number of quartz arenites (Table 3.1, Fig.3.6). Rannoch sandstones are subarkosic in the Thistle, Dunlin and Murchison oilfields but are quartz arenites in well 3/13a-1 (Fig.3.6). The Etive, Ness and Tarbert sandstones have subtle variations which indicate that Ness sandstones plot towards the quartz arenite field compared to Etive sandstones. Tarbert sandstones have a greater proportion of rock fragments (Fig.3.6).

Quartz is recognised in both monocrystalline and polycrystalline forms. The monocrystalline quartz is usually unstrained and constitutes 11.2 to 60% of the framework grains. Polycrystalline grains comprise 1.6 to 44% of the framework. Feldspar occurs as K-Feldspar and plagioclase. K-Feldspar comprises up to 11.4% of the framework, whilst plagioclase constitutes at most 1.4%. The K-feldspar is predominantly orthoclase and may occur totally dissolved through to fresh. Perthites and microcline are present to a

lesser degree showing preferential dissolution of lamellae. Plagioclase is relatively fresh and has an albitic composition. Rock fragments comprise up to 2.6% of the framework, with metamorphic fragments (quartz -muscovite schist, metaquartzite and meta-argillites) the most abundant. Igneous rock fragments of volcanic origin and sedimentary rock fragments of claystone constitute the remainder. Muscovite and biotite occur sporadically throughout the sequence but tend to be concentrated in the Rannoch Formation (maximum of 12.5 and 9.0% respectively, see Table 3.1). A detrital matrix is evident in the Rannoch sandstones studied, and in the Murchison wells which have a silt size quartz matrix, and 3/13a-1 which has detrital clay in places, otherwise the Brent sandstones generally free of a detrital matrix.

The depositional mineralogy and sorting has affected the general porosity and permeability of the sandstones. The Rannoch formation has increased concentrations of mica present relative to the other Formations (Table 3.1). Permeability in these sandstones is very poor (Fig.3.7), particularly vertically due to the alignment of these micas. Porosity is not as severely affected (up to 27%, see Fig.3.7). The massive sandstones of the Etive Formation are very "clean" with average porosities of 24%, with a maximum of 30% and permeabilities which average 1100mD, with a maximum of 6000mD. Ness sandstones which have local concentrations of mica, have maintained average porosities of 22% with a maximum of 27% and permeabilities which average 1000mD with a maximum of 3500mD. Tarbert sandstones contain bedded mica which has caused restrictions on permeabilities compared to Etive and Ness (Fig.3.7) and are akin to the Rannoch sandstones in their porosity and permeability characteristics.

3.6 DIAGENESIS

The diagenetic sequence of the Brent sandstones (Fig.3.8) was elucidated using thin section petrography and S.E.M studies to deduce the cement stratigraphy. The sequence is consistent throughout the area studied but with varying cement volume, i.e. illite development is considerably poorer in the northern part of the basin (Thistle, Dunlin, Murchison area) than that observed in well 3/13a-1 (Table 3.1) or in the area surrounding this well (Jourdan et al.1987). The

diagenetic sequence is considered in two sections, 1) Early and 2) Late (burial) cements. Early diagenetic cements are those which precipitated when high porosities existed shortly after deposition (Fig.3.8). The last of these being calcite cementation which has minus cement porosities which average 40% and a maximum of 52%. The late diagenetic cements are those which precipitated as the Brent sequence underwent burial and compaction.

3.6.1. EARLY DIAGENETIC CEMENTS

3.6.1.a. QUARTZ OVERGROWTHS I

Within the calcite cemented zones of the sandstones, thinly developed quartz overgrowths occur on detrital quartz grains. This early silicification event is a minor cement (1%) and the size of the overgrowths is difficult to estimate as no dust rim is evident between the overgrowth and the detrital grain.

3.6.1.b. SIDERITE

Siderite predates the main phase of calcite cementation, occurring as discrete rhombs (av. size 10 microns) which coalesce (Fig.3.9.a) along biotite-rich lamellae. The siderite forms at the sites of altering biotites and may be seen forcing the biotite flakes apart as it grows (Bjorlykke & Brendsdal 1986, Boles 1982). Along the biotite rich lamellae the siderite occupies up to 8% locally, and 2% of the rock overall. The siderite is concentrated in the Rannoch, Ness and Tarbert Formations.

3.6.1.c. PYRITE

Early pyrite is dominantly framboidal, with minor cubic development, of average size 5 microns and occurs in trace amounts <1%. It forms at the sites of degrading biotites and within the calcite concretions.

3.6.1.d. K-FELDSPAR OVERGROWTHS

These overgrowths precipitate prior to calcite concretion cementation and probably continue with diagenesis. The size of the overgrowths varies from 2-10 microns and under cathodoluminescence are light blue. They do not constitute a volumetrically important cement (<1%).

3.6.1.e. KAOLINITE I

Early kaolinite morphology exists as 1) a replacement of mica and feldspar and 2) a pore filling vermiform structure, (a third, burial related blocky morphology of late kaolinite is discussed later). The first two morphologies began forming prior to calcite cementation (Fig.3.9.b) and continued to do so in carbonate free sandstones throughout early diagenesis. The alteration of K-feldspar and mica, particularly muscovite, is very common and is seen to varying degrees, i.e. from complete kaolinisation to the incipient degradation of muscovite edges which then splay out (Blanche & Whitaker 1978, Hancock & Taylor 1978, Bjorlykke et al. 1979, Bjorlykke et al. 1986, Jourdan et al. 1987). The "snake-like" vermiform growth of kaolinite is a major porosity occluder and can form long (<100 microns) trains consisting of individual plates of kaolinite (Fig.3.9.c), the individual plates range from 2 to 20 microns across. Hurst & Irwin (1982) indicate that this type of kaolinite morphology is formed by transport controlled processes i.e. fluid flow. The kaolinite occupies an average 10% of the rock and a maximum of 21%.

3.6.1.f. CALCITE CONCRETIONS

Several areas within the Rannoch, Ness and Tarbert have zones tightly cemented by calcite which totally fills pore space and are interpreted as concretions. Individual concretions range from 0.9 to 3.0 metres thick. The cement (cf. Fig.3.8) post dates the initiation of quartz overgrowths I, siderite, pyrite, K-feldspar overgrowths and early kaolinite formation, and forms a useful marker in the textural diagenetic sequence. The evidence for early calcite cementation is firstly the lack of framework grain to grain contacts (Fig.3.9.a,b) and secondly the original porosity filled by calcite has an average of 40%, with a maximum of 52% (cf. Table 3.1). The cement is poikilotopic, the average crystal size is 0.5 to 1 mm. The calcite concretions show changes at the margins to slightly ferroan calcite and ankerite (see later), suggesting that carbonate growth continued during burial.

3.6.1.g. EARLY DIAGENETIC DISSOLUTION

The early calcite cementation has preserved the dissolution

features caused in early diagenesis.

1)Mica: As discussed earlier, biotite alters to siderite and pyrite. The muscovite to kaolinite alteration also starts prior to calcite cementation, generating microporosity at an early stage.

2)K-feldspar: Dissolved feldspars are sites for kaolinite growth prior to calcite cementation. Preferential dissolution of perthite lamellae is observed.

3)Ferromagnesian minerals are severely degraded in early diagenesis.

Overall the effects of this early dissolution on porosity and permeability are negated by the formation of kaolinite and siderite at the dissolution sites.

3.6.2. LATE (BURIAL) DIAGENETIC CEMENTS

3.6.2.a. KAOLINITE II

This kaolinite occurs as small booklets, average length 20 microns (Fig.3.9.d) as opposed to the early vermiform morphology. In well 3/13a-1 the individual plates of kaolinite display a blocky nature. This "burial" kaolinite occurs as a pore filling cement and is found in all formations. In Thistle, Dunlin and Murchison the individual plates are not as blocky but are generally smaller (<5 microns). Where developed, this kaolinite may constitute up to 10% of the rock and it is cogenetic with the development of late quartz overgrowths (II). The blocky booklets are typical of slow, diffusive formation processes compared to the larger vermiform kaolinite I which is characteristic of rapid transport controlled formation processes (Hurst & Irwin 1982).

3.6.2.b. ANATASE

Titanium oxides in the form of anatase are developed to varying degrees in different sequences. The anatase occurs as pore filling tetragonal crystals (average size 50 microns), Figure 3.9.e, which may show growth zonation under S.E.M and are syn/post kaolinite and pre quartz overgrowth II. The anatase is often seen growing around biotite and is particularly prevalent in 211/19-6 (Murchison). It constitutes <2% of the rock and is found in all formations.

3.6.2.c. PYRITE

Pyrite is scattered throughout the samples studied. It is dominantly a late diagenetic cement (cf. pyrite early diagenesis) with cubic and octahedral forms which may coalesce as a pore filling sulphide cement (cf. wells 211/19-3 and -6, Fig.3.9.f). Pyrite growth predates quartz overgrowths II and overall constitutes <2% of the rock.

3.6.2.d. QUARTZ OVERGROWTHS II

This main phase of quartz cementation precipitated during burial diagenesis with overgrowths which range from 30-60 microns and show growth zonation under S.E.M. The boundary between the overgrowth and detrital grain is usually a line of fluid inclusions. These euhedral, well developed overgrowths (Fig.3.9.g) are more intensely developed in the south of the basin (3/13a-1, average 7.7%, maximum 11.6%, Table 3.1) compared to those in Thistle, Dunlin and Murchison (average 4.7%, maximum 9.4%, Table 3.1) in the North. This episode of silicification is post early diagenetic cements and pyrite, and syn/post kaolinite II, pre/syn illite (Fig.3.8). Overall the quartz overgrowths are preferentially developed in the Tarbert, Ness and Etive Formations compared to the Rannoch. Silicification also occurs in fractures associated with faults at this time (211/18-A45).

3.6.2.e. LATE CARBONATES: DOLOMITE, SIDERITE, CALCITE, ANKERITE

Minor amounts of these minerals occur late in the sequence. Individual euhedral rhombs of dolomite range between 75-90 microns and are very fresh in comparison to siderite rhombs (average size 40-60 microns) which appear oxidised and have a deep brown colour.

Calcite occurs with a ragged appearance compared to the above. Under cathodoluminescence the calcite is non-luminescent indicating a ferroan character. The ankerite surrounds one of the early calcite concretions in well 211/23-4 with the crystal size similar to that in the calcite (0.5-1.0 mm). The ankerite occupies 17-22% of the pore space. Overall these late carbonates occupy <1% of the rock. Siderite appears to be preferentially developed in the Ness Formation and the proximity of the muds in this Formation may explain the supply of the iron.

3.6.2.f. ILLITE

The illite has a filamental morphology (Fig.3.9.h) which extends out into pore space. However, the samples were not critical point dried (Cocker 1984) so the present morphology may not be as pore filling/permeability reducing as one may expect. This filamentous illite may attain lengths of up to 20 microns. The filaments tend to wrap round themselves so developing alveolar structures (Fig.3.9.i). Illite is best developed throughout the Brent section in the south of the basin compared to the northern area where good illite development is restricted to the Rannoch Formation. Illitisation of kaolinite is readily observable with the thin filaments growing out from the altering kaolinite, so post dating it. Illite is cogenetic with the later stages of quartz overgrowths (Fig.3.9.i). Illite occupies <1% of the Rannoch Formation in the Thistle, Dunlin and Murchison area in comparison to that in well 3/13a-1 where illite occupies an average 10% and a maximum of 18.5% (Table 3.1).

3.6.2.g. LATE DIAGENETIC DISSOLUTION

Secondary porosity development during burial diagenesis constitutes on average 2% and at a maximum 4% of the total porosity. Framework grain dissolution probably occurred throughout burial but may be constrained definitely to post pyrite. K-feldspar alteration is the dominant manifestation of the dissolution.

3.7

RESERVOIR QUALITY

The Brent sandstones have maintained very high porosities and permeabilities (cf. Fig.3.7), with the Etive Formation retaining the best poroperm characteristics compared to the Ness, Tarbert and Rannoch.

Pre cement porosities of all samples range from 22 to 48% (average = 33.4%) with a few exceptions, see later. Assuming a depositional sand porosity of 48% (Berg,1986) the average porosity loss is 16.6% by all compactional processes in the sandstones studied. This is due to packing readjustments within the sandstones causing tighter packing during the initial burial and the continued compaction on burial, and any pressure solution.

The cement distribution in Thistle, Dunlin and Murchison evaluated by point counting, indicates that the Rannoch has less kaolinite (average 6.4%) and quartz overgrowth (average 2.7%) than Tarbert (av.13.5%, 6.1%), Ness (av.11.2%, 5.5%), and Etive (av.10.0%, 4.2%) but more illite. Overall Tarbert has an average of 18.6% (kaol.+qtz o/g+ill.), Ness 16.7%, Etive 14.9% and Rannoch 9.0% of authigenic cements. Reservoir quality was severely reduced in the calcite concretions from early diagenesis.

3.8 POROSITY DEVELOPMENT

The dominant type of porosity in the Brent sandstones has been discussed by several authors (Selley 1978, Bjorlykke et al. 1979, Schmidt & MacDonald 1981, Bjorlykke & Brendsdal 1986). Schmidt & MacDonald (1981) considered the Brent an example of sandstone reservoirs with considerable secondary porosity. Their interpretation was that the Brent sandstones were cemented by carbonate throughout, and subsequent dissolution gave the present high porosities. Bjorlykke & Brendsdal (1986) however suggest that a late stage leaching event is only of minor importance in producing secondary porosity and that petrographic evidence supports leaching being early. They suggest that dissolution was due to early flushing of meteoric pore water and that the pore water in late diagenesis was buffered with respect to carbonate. Bjorlykke (1980) cites calculations that insufficient CO₂ would be released during burial to cause large scale leaching. Selley (1978) states that the primary porosity has been preserved by the development of abnormal pore pressures and additionally by the palaeoflow of meteoric water descending through the sequence during Tarbert deposition (end middle Jurassic) and at the end Upper Jurassic (Sommer 1978).

In this study the dominant secondary porosity development is considered to have occurred during early diagenesis with mica and K-feldspar degradation. The dissolution of these grains did not enhance porosity greatly as the grains were replaced by vermicular kaolinite. The late stage of secondary porosity development contributed on average 2%, and a maximum of 4% porosity to the rock during burial diagenesis. Features like etch pits and embayments are not observed in the authigenic cements (i.e. quartz overgrowths) under S.E.M. on a wide scale. When secondary porosity is observed it

is manifested as embayments, oversized pores and occasional enlarged porethroats (Kantorowicz & Burley 1986). Therefore the opinions of Bjorlykke & Brendsdal (1986) are considered more in agreement with the petrographic evidence observed here.

3.9 PRESSURE SOLUTION

Throughout the sequence tightly cemented mm thick zones may be found, particularly where there are concentrations of detrital clay and degrading ferromagnesian minerals. This suggests a local supply or nucleation- controlled diagenetic mineral growth in these areas. Overall pressure solution is not a major feature of the sandstones in Thistle, Dunlin and Murchison studied. However in well 3/13a-1 stylolites are clearly evident in core. Although these cemented zones occur in all Formations the Rannoch has a more severe grain packing arrangement than Etive, Ness and Tarbert due to being finer grained, the high mica presence, ductile grain dissolution and dominance of concavo-convex contacts (Fig.3.9.j). The Rannoch Formation may thus be a local source of silica. An attempt was made via thin section examination to quantify the amount of silica required to cement up the sandstone. The scheme of Sibley & Blatt (1976) was followed to determine whether import or export of silica was required, and the volume lost at ductile grain resistant grain contacts. Point counting using a standard petrographic microscope assessed the percentage of quartz overgrowths and to quantify silica loss, all types of grain contact were considered during counting as a site of pressure solution, and hence a maximum estimate for pressure solution. Figure 3.10 presents a crossplot of quartz cement against volume of detrital grains lost by pressure solution. This shows that the vast majority of sandstones on a thin section scale require silica to be imported. Rannoch sandstones are net exporters of silica, as suggested above, along with a number of tightly compacted zones within the other Formations. This silica may then have been a local source of silica for the cements found in the Formations. The maximum volume lost by grain pressure solution was 6.5% whilst the volume lost by ductile grain deformation was minor, <2%. Pressure solution of quartz and other silicates in the Brent sandstones as a whole, would appear not to be the sole source of diagenetic silica.

3.10 CLOSED OR OPEN DIAGENESIS

Present porosity and permeability in the Rannoch Formation is between 10-20% and 50-1000 mD. Vertical permeability is lower due to the presence of mica along bedding laminae, so restricting porewater flow both today and during diagenesis. As stated above the Rannoch is finer grained than the other Formations and has compacted tightly with the presence of mica allowing ductile grain deformation and pressure solution. The Rannoch would appear to have cemented in a semi-closed/closed system (isochemical diagenesis).

This is in contrast to the fluid flow scenario envisaged as an explanation for the "cleaner" clay free Etive, Ness and Tarbert Formations. Figures 3.5 and 3.6 illustrate the point that the Etive, Ness and Tarbert Formations have better porosity and permeability characteristics than the Rannoch, so indicating that fluid flows more easily through these Formations. This allowed the precipitation of kaolinite, and quartz overgrowths, in greater quantities in Etive, Ness and Tarbert. The more open style to the cementation of the Etive, Ness and Tarbert is in contrast to the stagnant, diffusive conditions of the Rannoch.

3.11 FLUID INCLUSION DATA: QUARTZ OVERGROWTHS

Fluid inclusion studies on quartz overgrowths which precipitated late in the diagenetic sequence (Fig.3.8) give information on the salinity and composition of the diagenetic fluid and also estimates of the temperature of entrapment. Only primary two phase aqueous liquid-vapour fluid inclusions were observed (Roedder 1984) with most of them occurring at the boundary between the detrital grain and the overgrowth. The vast majority of inclusions are <5 microns in diameter and proved too small to observe phase changes. Larger inclusions (up to 15 microns) were scarce but did facilitate measurement of the homogenisation temperature (T_h), the minimum temperature of entrapment. It is assumed that these inclusions which occur in cements in an oilfield are CH_4 saturated (Hanor 1980). Hence T_h is equivalent to the true trapping temperature T_t at which the quartz overgrowths formed (Roedder 1984) and so no pressure correction need be applied (see discussion).

Two other types of microthermometric measurement were made when optical resolution was sufficient for the phase changes in the inclusion to be observed. The inclusion was supercooled (-100°C) to freeze it, and its melting behaviour observed during warming. The temperature of first melting of ice (T_e) gives an indication of the salt system (NaCl, KCl, MgCl) of the aqueous fluid contained in the inclusion and represents the eutectic melting point for the system (Crawford 1981). The temperature at which the remaining ice melts (T_m) gives an indication of the total salinity of the fluid trapped in the inclusion. In total 102 two phase aqueous liquid-vapour (LV) inclusions were measured from the Thistle, Murchison oilfields and well 3/13a-1 for the homogenisation temperatures (T_h). From these, 13 T_e and 18 T_m values were measured. Inclusions in overgrowths from the Dunlin oilfield were too small for analysis.

3.11.1. THISTLE OILFIELD

Temperatures of homogenisation (T_h) were measured (61 values) from wells 211/18-A30, -A30ST, -A31 and -A45. Samples were taken from typical sandstones in the Etive and Ness. The range in T_h is from 72.4 to 121.6°C (Fig.11a) with modes at 82.5 , 92.5 , 107.5 and 117.5°C . The present day depth range over which analysis was conducted is 8624 - 9246 feet TVD.

The freezing data obtained for the Thistle field are given in figures 3.12.a,b. The eutectic temperatures (T_e) of the inclusions range from -53.4 to -14.4°C (Fig.3.12.a). This implies a multicomponent salt system dominated by NaCl (Crawford 1981).

The final melting temperatures (T_m) are given in Fig.3.12.b and show a range between -5.6 and -1.9°C . The calculated salinity values (Potter 1977) for the T_m values range from 8.6 to 3.2 wt.% eq. NaCl.

3.11.2. MURCHISON OILFIELD

Twenty homogenisation temperatures were obtained from one depth (10500 feet TVD) in well 211/19-6. The range is between 84.2 and 122.4°C with a mode at 97.5°C (Fig.3.11.b).

The freezing data obtained for this depth are given in figures

3.12.a, b. Only three T_e values were obtained; -22.3, -22.7 and -35.0°C, and imply a MgCl₂-NaCl, KCl-NaCl salt system (Crawford 1981).

The final melting of ice (T_m) values range between -2.0 and -3.4°C (Fig.3.12.a). Calculated salinities (Potter 1977) indicate relatively low salinity waters (3.4 to 6.6 wt% eq. NaCl).

3.11.3. WELL 3/13a-1

Homogenisation temperatures (T_h) from twenty one inclusions at three depths in this well (12207, 12267, 12283 feet TVD) range from 93.6 to 131.1°C with a mode at 97.5°C (Fig.3.11.c).

The freezing data obtained for 3/13a-1 are given in figures 3.12.a and 3.12.b. T_e measurements range between -13.5 and -36.2 C. The values imply a salt system composed of KCl, KCl-NaCl and MgCl₂-NaCl.

The T_m values (Fig.3.12.a) of -1.1 to -1.9°C, indicate low salinity inclusions (1.9 to 3.2 wt% eq. NaCl).

3.11.4 DISCUSSION

Homogenisation temperatures for all inclusions are combined and given in Fig.3.14. This combined T_h histogram exhibits three main population modes at the intervals 80-85, 90-95, 105-110°C. Normally, workers in metamorphic rocks and ore deposits would apply a pressure correction to the T_h values so as to ascertain the true trapping temperature of the inclusions and hence the temperature at which the quartz overgrowths formed. However this has been omitted after consideration that the inclusions from an oilfield basin may have dissolved methane present (Hanor 1980). Hanor (1980) discusses in detail the potential effect on the PVT properties of fluid inclusions that dissolved methane in sedimentary brines may have. He points out that subsurface sedimentary waters which have associated hydrocarbon accumulations contain significant concentrations of dissolved methane (Jones 1976, Price 1976, Randolph 1977, Wallace et al 1979). The presence of methane complicates the interpretation of inclusion behaviour and could yield erroneously high estimates for trapping temperatures when a pressure correction is made (Hanor 1980). The effect of methane on T_m values is negligible. However it can be difficult to distinguish between CH₄ hydrate melting

and ice melting and this may cause problems in estimating the salinity of an inclusion.

The overall range for the homogenisation temperatures is 72.4 - 131.1°C (Fig.3.13) and this broad range can be seen in several wells. The homogenisation data for Thistle and Murchison is quite similar whilst well 3/13a-1 has a higher homogenisation temperature interval than the above (Fig.3.11). This well is located in the southern part of the basin (Fig.3.2). Microthermometric studies in the Alwyn area by Malley et al.(1986) have similar homogenisation temperatures with modes at 82.5 , 92.5 and 107.5°C.

Only a limited number of salinity measurements were possible, giving a broad range from 1.9 to 8.4 wt% eq. NaCl (Fig.3.14). The major mode for the salinity of inclusions is 3-4 wt% eq. NaCl. Fig.3.15 is a cross plot of homogenisation temperature and salinity and suggests the presence of two fluids, one of low salinity (1-4 wt% eq. NaCl) and the other more saline of 5-8.6 wt% eq. NaCl. The low salinity fluid is recognised throughout studies of the quartz overgrowths (Malley et al. 1986, Jourdan et al. 1987, Glassman et al. 1989 in press) and would appear to be the dominant fluid present whilst quartz overgrowths precipitated. This is compatible with the present day pore water salinities which are between 1.4-4.0 wt% eq. NaCl (Selley 1978, Engelstad 1987). However explanation of the group of higher salinity inclusions is problematic (Fig.3.15), (a similar such group was noted by Malley et al.(1986) in the Alwyn area). The higher salinities are associated with most negative T_e values (Fig.3.15) which indicates a Ca, Mg dominated salt system for these inclusions. These highest salinities are found in the Thistle field in wells 211/18-A30, and -A30ST. In the underlying Triassic and Lower Jurassic in wells 211/18-1, -3 and -4A the composite logs show the presence of anhydrite cemented zones. It is possible that these localised, hot, dense anhydritic fluids may have moved up through the sequence, possibly using the faults which cut through the Brent sequence. However it must be pointed out that measurements were made without the facility of a UV attachment so hydrocarbon rich inclusions would not be detected. Other studies of fluid inclusions in quartz overgrowths in the Brent show the presence of hydrocarbon rich inclusions (Malley et al. 1986, Jourdan et al. 1987, Glassman et al. 1989 in press, Cocker et al. 1989 in press). The lower

temperature inclusions in these studies were found to be hydrocarbon rich ($\approx 70-90$ C). If the inclusions are hydrocarbon rich then the salinity values become inaccurate. So the high salinities found in this study must be interpreted with this in mind, and independent UV analyses on a separate microscope indicated that $<5\%$ of the inclusions were hydrocarbon rich.

The presence of hydrocarbon rich inclusions indicates that quartz overgrowth precipitation was contemporaneous with oil generation and migration in the basin. Therefore quartz overgrowth precipitation took place in a dominantly low salinity pore fluid and at temperatures which as we shall see later are far hotter than expected for a normal geothermal gradient for the depth of burial at the time of precipitation.

3.12

OXYGEN ISOTOPIC STUDIES

$\delta^{18}\text{O}$ analysis of a diagenetic mineral may be used to ascertain the $\delta^{18}\text{O}$ of the water from which it precipitated and also the temperature at which formation of the mineral occurred (Fig.3.16). These parameters are related by the oxygen isotopic fractionation equation ($1000 \ln \alpha_{\text{mineral-water}} = A(10^6/T^2) - B$, where A and B are specific to mineral water pairs). Experimentally derived oxygen isotope fractionation factors for individual mineral water pairs ($\alpha_{\text{mineral-water}}$) are used for this purpose. At temperatures for normal sedimentary environments most minerals do not experience significant isotopic exchange with the porefluids, only where dissolution and reprecipitation occurs is there the possibility of changes in the oxygen isotopes (Yeh & Savin 1976,1977, Eslinger & Yeh 1981). Therefore the oxygen isotope compositions of diagenetic minerals should be a record of the conditions at their formation.

Several diagenetic cements were separated from disaggregated sandstone (Appendix 1) and $\delta^{18}\text{O}$ analyses conducted (see below). Using the $\delta^{18}\text{O}_{\text{mineral}} - \delta^{18}\text{O}_{\text{water}} - \text{temperature}$ relationship (Fig.3.16) it is intended to illustrate that the $\delta^{18}\text{O}$ composition during the basin history.

3.12.1. SIDERITE

The siderite is texturally early (Fig.3.8), forming prior to

calcite concretion cementation. Samples from the Tarbert and Ness Formations (Appendix 2) have $\delta^{18}\text{O}$ values between +19.9 and +24.4‰ (Fig.3.17.a, Table 2). $\delta^{13}\text{C}$ values range between -0.1 and -10.4‰ PDB, these are discussed elsewhere.

3.12.2. KAOLINITE

The kaolinite is texturally early (Fig.3.8) and petrography suggests that it continues to form into late diagenesis (i.e. cogenetic with quartz overgrowths, Fig.3.8.d). Kaolinite occurs in all of the Brent Formations and has $\delta^{18}\text{O}$ (SMOW) values ranging from +14.7 to +18.3‰ (Fig.3.17.b, Table 3.2). It was not possible to separate the vermiform kaolinite I from the blocky kaolinite II, but thin section examination indicated that the greater the proportion of vermicular kaolinite (Fig.3.9.c), the higher the value, and conversely the later booklet morphology of kaolinite II was associated with the lower values. No distinct populations were observed. The purest size separate (2-5 microns) was analysed in each case.

3.12.3. CALCITE

The calcite occurs as a texturally early cement (Fig.3.9.a) in tightly cemented concretions in Rannoch, Ness and Tarbert Formations enclosing vermiform kaolinite and siderite. The poikilotopic calcite was sampled from the Ness and Tarbert Formations and has $\delta^{18}\text{O}$ values between +17.8 and +20.4‰ (Fig.3.17.c, Table 3.2). $\delta^{13}\text{C}$ values range from -11.4 to +2.2‰ PDB, and are discussed elsewhere.

3.12.4. ANKERITE

The ankerite is associated with replacement and rimming of one of the calcite cemented concretions and has $\delta^{18}\text{O}$ values between +19.1 and +22.9‰ (SMOW), (Fig.3.17.d, Table 3.2) and $\delta^{13}\text{C}$ values of -7.6 and -4.1‰ PDB, which are discussed elsewhere.

3.12.5. QUARTZ OVERGROWTHS

This major burial porosity reducing cement (Fig.3.8) has a fairly restricted range in $\delta^{18}\text{O}$ values of between +17.1 and +22.3‰ (SMOW), (Fig.3.17.e, Table 3.2). Silica diagenesis appears to show no grain size dependence in these sandstones.

3.12.6. ILLITE

As discussed earlier, the illite is a late cement co-genetic with the latest stages of quartz cementation (Fig.3.9.i). $\delta^{18}\text{O}$ values for <0.1 micron fractions give a range between +13.1 and +14.2‰ (Fig.3.17.f, Table 3.2).

Finally, all the minimum and maximum $\delta^{18}\text{O}$ mineral cement curves are combined and presented in Figs.3.18.a,b.

3.13

DISCUSSION OF OXYGEN ISOTOPES

By combining the oxygen isotope data and the petrographic studies it is possible to elucidate the changes that have occurred in the oxygen isotope composition of the porefluid during diagenesis of the Brent sandstones. To construct this pore fluid evolution pathway, the minimum and maximum $\delta^{18}\text{O}$ mineral curves for all minerals are superimposed and an evolution pathway constructed through the curves which allows for all possible temperatures and $\delta^{18}\text{O}$ porewater compositions for each diagenetic mineral (c.f. Longstaffe 1987). This pathway must also be in concert with the diagenetic sequence and geological evolution of the East Shetland Basin, the site of the Brent Province.

The $\delta^{18}\text{O}$ porefluid pathway may be further constrained by using other independent factors which are available:

1) Present day formation fluids in the Brent Province have $\delta^{18}\text{O}$ values of between +1 and +2‰ (BP pers comm. Columba field), and of 0‰ from the Heather field (Glassman et al 1989 in press). Formation fluids with $\delta^{18}\text{O}$ of +2.5 to +3.5‰ from the Hild field, a Brent type play in the Norwegian sector are reported by Lonoy et al.(1986). Uncorrected bottom hole temperatures of between 85 and 107 C are recorded in Thistle well log completion reports. The average temperature of the Murchison oilfield is 110°C (Engelstad 1987), and Jourdan et al (1987) report temperatures of 115°C in the Alwyn area.

2) Homogenisation temperatures (T_h) for fluid inclusions in the quartz overgrowths range from 72.4 to 131.1°C. These may be used as an independent temperature control in the isotopic fractionation equations.

3) Initial depositional pore fluids in the Brent are

considered to be meteoric (Hancock & Taylor 1978, Sommer 1978, Bjorlykke et al 1979, Bjorlykke 1984, Bjorlykke & Brendsdal 1986, Hamilton et al 1987, Jourdan et al 1987). $\delta^{18}\text{O}$ values for the meteoric water have been suggested as -6‰ in the Middle Jurassic (Hamilton et al 1987). Also by extrapolation between the estimates for Devonian meteoric waters (-5‰, Fallick et al 1985) and that for Eocene (-12‰, Taylor & Forester 1971) for Northern Britain, Jurassic meteoric water would be -7‰. As will be shown later, using δD analysis the $\delta^{18}\text{O}$ value for Jurassic meteoric water is calculated at -7‰ (Fig.3.20).

So by using these independent constraints a $\delta^{18}\text{O}$ porefluid evolution path may be constructed and a likely present day end point plotted. Ayalon & Longstaffe (1988) point out some uncertainties with this approach must be borne in mind:-

- 1) The potential isotopic re-equilibration of diagenetic minerals e.g. calcite recrystallisation.

- 2) The mineral curves generated from the isotopic fractionation equations (Fig.3.17) are subject to the experimentally derived understanding of the fractionation factor at low temperatures for mineral - water pairs.

- 3) The purity of the samples after all the mineral separation techniques.

The oxygen isotope studies are considered in two parts - 1) early and 2) late diagenesis below.

3.13.1 EARLY DIAGENESIS

Meteoric porewater has been considered a major factor during early diagenesis in the Brent sands. It has been proposed that the deltaic, marginal marine setting of the Brent allowed meteoric water to penetrate into the sands during deposition. Sommer (1978) also suggests that meteoric influx also occurred during the end Jurassic uplift when a low-lying topography is thought to have emerged above sea-level to produce the sub-Cretaceous unconformity seen on a number of the Brent structural blocks (Fig.3.3). The diagenetic mineral assemblage itself indicates the presence of low pH fluids i.e. formation of siderite and kaolinite. Hamilton et al (1987) used O and C isotopes to show that the early calcite cement was precipitated at

low temperatures (25 - 50°C) from a pore fluid of $\delta^{18}\text{O}_{\text{water}} = -6\text{‰}$. Calcite $\delta^{13}\text{C}$ and $\delta^{18}\text{O}$ data from this study is very similar to that reported by Hamilton et al (1987) and petrographic study shows calcite to be an early cement (Fig.3.8).

If Jurassic seawater ($\delta^{18}\text{O} = -1.2\text{‰}$) is considered to be the original porefluid then isotopically calculated formation temperatures would be rather high and diverse (Siderite 40°C, Kaolinite 65°C, Calcite 68°C, Fig.17) which equates to burial depths of 1 - 1.8 kms, assuming a geothermal gradient of 35°C/km. By contrast assuming a meteoric ($\delta^{18}\text{O}_{\text{water}} = -7\text{‰}$) porefluid gives formation temperatures of 1) siderite 14-34°C, 2) kaolinite 26°C, continuing through diagenesis and 3) calcite 32-47°C, Fig.3.17). Assuming a geothermal gradient of 35°C/km, this equates to depths of formation of 0.5-1.3 kms which is in accord with the petrographic sequence of cements (Fig.3.8) and their formation at shallow depths. D/H ratios of clays (see below) also supports formation from a meteoric derived fluid. The degree of oxygen isotope shift during this early diagenetic regime is difficult to assess (Fig.3.19.a). It is likely that the isotopic composition of the porefluid remained barely changed from its depositional (-7‰) value. Only when burial diagenesis started and water:rock ratios became <1 and the system became more closed did the oxygen isotope composition of the porefluid start to change markedly.

3.13.2 BURIAL DIAGENESIS

At the onset of the Cretaceous the Brent sequence began its major burial phase and the associated diagenetic changes with it. Kaolinite continued to precipitate during this time and by the late Cretaceous/Early Tertiary quartz overgrowth cementation had started with $\delta^{18}\text{O}$ values from +22.3 to +17.1‰. With the minimum homogenisation temperature of 72.4°C from fluid inclusions in the overgrowths, the oxygen isotope composition of the porefluid would be -2.4‰ (Fig.3.19.b). Ankerite formation commenced during early diagenesis ($\approx 50^\circ\text{C}$, +22.9‰) and continued to form during the precipitation of quartz overgrowth II, at temperatures up to $\approx 102^\circ\text{C}$ (Fig.3.19.b). The least positive $\delta^{18}\text{O}$ values of kaolinite, and the entire illite $\delta^{18}\text{O}$ field of values show an overlap with the

quartz cement implying possible co-precipitation of kaolinite-quartz and quartz-illite. This is supported by the co-genetic textural diagenetic relationships observed (Fig.3.8,3.9.i).

At this deeper stage of burial, water/rock ratios would have decreased as compaction ensued. Under these conditions, the $\delta^{18}\text{O}$ of the porefluid will become gradually buffered by the rock and so the porefluid is more liable to evolve as the new cements precipitate and framework grains continue to dissolve. Reported present day formation water $\delta^{18}\text{O}$ compositions are between 0 and +2‰ in the East Shetland Basin and bottom hole temperatures between 85 and 115°C. These can act as a guide to the present day end point of the pathway during burial diagenesis. It is quite straight forward to "make" the porewater evolution path reach these final conditions (Fig.3.19.b), but this leaves the problem of explaining the large field of quartz overgrowths and much of the ankerite which from fluid inclusion measurements on the quartz overgrowths precipitated at considerably hotter temperatures ($T_{\text{Hmax}} = 131.1^\circ\text{C}$) than the present day formation conditions. This may be explained by two extreme hypotheses :-

1) By envisaging a "closed" water system (Fig.3.19.b). In this case, the water and rock remain in equilibrium whilst the rock is heated over a several million year timespan. Quartz and ankerite precipitate during the pathway for the rock to reach its maximum temperature of 131.1°C and least positive $\delta^{18}\text{O}$ quartz value of +17.1‰. The sandstone must then cool to present day temperatures with the porewater curve evolving through the isotopically permitted fields for the quartz, illite, ankerite and kaolinite growth (Fig.3.19.b). No additional porefluid is required and the minerals grow in equilibrium with hot porefluid. A problem with this hypothesis is why illite should only grow during retrograde cooling, and not in the same temperature range in prograde heating as no illite with $\delta^{18}\text{O}$ compositions of +11 to +9‰ are measured, and illite is texturally observed to extensively post date quartz rather than predate it. However if it can be shown that different areas have quartz overgrowths with differing temperatures which depended on their subsidence depths at the time of quartz overgrowth formation, then this gradual heating hypothesis will be strengthened. Fluid inclusion temperature values for quartz overgrowth formation are

similar across the basin, (i.e. this study, Malley et al. 1986, Jourdan et al 1987, Cocker et al. 1989, Glassman et al. 1989). However individual fields illustrate different temperature modes (Fig. 11); Murchison - 92°C, Thistle - 82°C and 3/13a-1 - 107°C. This demonstrates a temperature variability as the burial depth during quartz cementation was similar at ≈ 2 km in the basin. This observation appears to go against a stratified temperature gradient.

2) By envisaging a closed system porewater which was periodically open to influxes of hot fluid, or subjected to rapid short duration heating events (Fig.3.19.c). In this hypothesis, the reservoir fluids would continue to evolve towards their present day conditions in equilibrium with kaolinite and illite. Superimposed on this, brief temperature excursions are required (shown by arrows, Fig.3.19.c). These pulses account for the highest fluid inclusion temperatures and lowest $\delta^{18}\text{O}$ quartz overgrowth and ankerite values. The reservoir would cool back towards an equilibrium thermal condition after each heat pulse. Such pulses could be induced by fault movements occurring in the basin to accommodate the increase in sediment deposition in the Early Tertiary due to rejuvenation of the East Shetland Platform (Fig.3.1) which was supplying the sediment. The hot fluids used the faults to ascend into the reservoirs with subsequent quartz precipitation. This model is supported by the occurrence of illite post dating most quartz cement, and the fluid inclusion evidence for several temperature modes of formation (Malley et al (1986), Jourdan et al (1987)). In Figure 3.13 the modes may represent three heat excursions in the areas studied. As already stated, well 211/18-A45 has quartz cemented fractures further suggestive, of fault assisted fluid movement. This second hypothesis is considered as the more feasible scenario at this time.

3.14

HYDROGEN ISOTOPE STUDIES

Deuterium/hydrogen (D/H) analyses of hydroxyl hydrogen in kaolinite and illite may be used to characterise the origin of the porewater from which the minerals precipitated. According to Liu & Epstein (1980) at low temperatures $\delta D_{\text{kaolinite-water}}$ has only a small temperature dependence and so the dominant influence on δD of kaolinite is the δD of the water. Thus the D/H values may be used

to determine the nature of the porewater i.e. meteoric, seawater etc. Hydrogen isotope fractionation over the temperature interval 0-120°C (Yeh (1980)), is appropriate for <0.1 micron size illite. This allows the calculation of water values from which the illite formed (see discussion). Kaolinite and illite samples were separated for this purpose.

3.14.1. KAOLINITE

3.14.1.a. Results

Kaolinite δD data for Thistle, Murchison, Dunlin and well 3/13a-1 are presented in Table 3.3. Pure kaolinite separates in the 2-5 microns range fall between D of -48 and -68‰ (SMOW), (Table 3.3). One value of -51‰ (SMOW) was obtained for a pure 5-10 microns size separate. There is no systematic variation with present day depth or with sandstone Formation.

3.14.1.b. Discussion

As stated above, Liu & Epstein (1980) attempted to determine the value for the fractionation factor for the kaolinite - water system at temperatures below 400°C and found that at isotopic equilibrium between the reacted kaolinite and water, the D of the kaolinite may be expressed as

$$\delta D_{\text{Kaolinite}} = \delta D_{\text{water}} + 10^3 \ln \alpha.$$

By using this relationship over the temperature range during which kaolinite precipitated in the Brent sandstones it is possible to gain an indication of the δD of the porefluid and so its origin. Fig.9 in Liu & Epstein (1980) illustrates this relationship. An average value of -20‰ for the fractionation has been used in the calculation of the δD of the porewater from the measured δD of the mineral, in preference to individual calculations due to the relatively poorly constrained nature of the fractionation at these temperatures. The overall range in δD for kaolinite is -48 to -68‰ (SMOW), therefore using a water-kaolinite fractionation of -20‰ :-

$$\delta D_{\text{water}} = \delta D_{\text{kaolinite}} - (-20),$$

So, the water values for kaolinite are between -28 and

-48‰(SMOW). These values suggest a component of meteoric water in the porefluid. This is in accord with $\delta^{18}\text{O}$ water values for kaolinite which themselves suggest formation from a water of meteoric derivation (Fig.3.17.b).

3.14.2. ILLITE

3.14.2.a. Results

Illite δD values from well 3/13a-1 and 211/19-4 (Murchison) are given in Table 3.3. The pure illite separates (<0.1 microns) range from $\delta\text{D} = -55$ to -61 ‰(SMOW).

3.14.2.b. Discussion

As with the kaolinite, the objective was to obtain the signature of the porefluid from which the illite precipitated. Yeh (1980) calculates and discusses the hydrogen isotope fractionation in <0.1 micron clays. Yeh points out that the hydrogen $\alpha_{\text{clay-water}}$ is a function of the octahedral cation chemistry of the clays (Suzuoki & Epstein 1976, Kulla 1979). Since the octahedral compositions of the illite and montmorillonite are similar (Hower & Mowatt (1966), Helgeson & Mackenzie (1970), Perry (1971)) then either the hydrogen $\alpha_{\text{illite-water}}$ or $\alpha_{\text{montmorillonite-water}}$ may be used to represent the $\alpha_{\text{clay mineral}}$ of the <0.1 micron fractions. Yeh gives the temperature dependence of $\alpha_{\text{clay-water}}$ between 0 and 120°C as

$$1000 \ln \alpha_{\text{montmorillonite-water}} = -19.6 \cdot 10^3 / T + 25.$$

So knowing the $\delta\text{D}_{\text{illite}}$, temperature of formation (K), the hydrogen isotope composition of water co-existing in equilibrium with that illite may be calculated.

With δD illite values between -55 and -61‰(SMOW), Table 3.3, the equilibrium isotopic water compositions are -30 to -36‰ for a temperature of 107°C. This temperature was selected as the uppermost mode of the fluid inclusions in the quartz overgrowths, which are cogenetic with the latest stages of formation with the illite. The overall error in the water values using 82°C (lowermost fluid inclusion mode) and 131°C (T_{H} maximum) is ≈ 2 ‰. These δD values are depleted relative to present day seawater ($\delta\text{D} = 0$ ‰, $\delta^{18}\text{O} = -1.2$ ‰(SMOW)), and also suggest a meteoric water component. Fallick

et al.(1985) report δD values for Devonian meteoric water in Central Scotland of -30‰ , whilst Forester & Taylor (1977) report a δD of -85‰ for Tertiary water on the west coast of Scotland. Hogg et al.(1987) reports depleted values (-33 to -50‰) for illites from the Alwyn field (see Fig.3.1).

3.14.3. INTERPRETATION OF δD ANALYSES

The diagenetic sequence (Fig.3.8) shows that kaolinite is texturally early and continues to precipitate throughout diagenesis, whilst illite is a late burial cement. Calculated formation temperatures from oxygen isotopes mirror the order of the diagenetic cements (Fig.3.19.a,b), yet the δD analyses are not significantly different. The computed water values for kaolinite and illite are presented on Fig.3.20, a δD - $\delta^{18}O$ plot. $\delta^{18}O$ water values calculated for kaolinite (-7 to -2.4 (this latter value is a least positive value for the water composition from which kaolinite formed, using the cogenetic relationship with quartz overgrowths)), (Fig.3.19.c), and δD values calculated for kaolinite (-48 to -28) constrain a boxed area close to the meteoric water line of Craig (1961). Kaolinite is considered to have formed at least during the earliest stages of quartz overgrowth cementation. The stippled area on Fig.3.20 indicates the possible oxygen water compositions over which the kaolinite precipitated. Illite precipitated from water of δD between -30 and -36‰ and is petrographically observed as cogenetic with the latest stages of quartz overgrowth authigenesis. The water $\delta^{18}O$ composition during these late diagenetic events is $+1$ to $+2\text{‰}$, for illite mineral values of $+13.1$ to $+14.2\text{‰}$, ($T=107^\circ\text{C}$, from fluid inclusions in quartz overgrowths). The illite $\delta D/\delta^{18}O$ water compositions are plotted on Fig.3.20. Present day isotopic water compositions in the reservoir of $\delta^{18}O= 0$ to $+2\text{‰}$ and $\delta D= -24$ to -27‰ provide a useful end point to this isotopic trend away from the meteoric water line (Fig.3.20). It illustrates a considerable enrichment of the $\delta^{18}O$ water composition during diagenesis (-7 to $+2\text{‰}$) but a much lesser shift in the δD values (-48 to -28‰). Explanation of this requires consideration of the Water/Rock ratio in terms of the weights of oxygen and hydrogen. For oxygen the Water/Rock ratio is low and so isotopic exchange is readily achieved,

causing the marked isotope shift observed. For hydrogen the Water/Rock ratio is high and consequently the isotopic shift would be less pronounced, as is noted (Fig.3.20).

In summary, using computed water values from diagenetic minerals an isotopic trend for the porewaters of the Brent sandstones is observed ($\delta^{18}\text{O} = -7$ to $+2\%$), (Fig.3.20). This involves a system whereby the water evolves towards more positive isotopic values away from the meteoric water line, a trend that is observed in other sedimentary basins (Fig.3.21).

3.15

K/Ar Illite Dating

One pure (0.1 micron fraction) illite sample has been dated from the Rannoch Formation of the Murchison oilfield, well 211/19-4 (10202' TVD). Appendix three describes the methods employed for analysis. In the Thistle and Dunlin oilfields it was not possible to separate enough pure illite for dating, the illite occurring in quantities of <1% (total rock) in the Rannoch Formation, none being observed in the overlying Formations. The <0.1 micron fraction separated gave an early Tertiary age for illite growth at 58Ma. This age is similar to more extensive studies on illite dating on the Brent sandstones. Sommer (1975) reports an age of 45Ma, Hamilton et al (1987) on illite from the Rannoch Formation, Thistle field report ages between 60-46Ma. In the Alwyn area (Fig.3.2), Jourdan et al.(1987) found that illite grew between 75-35Ma, Hogg et al.(1987) report ages between 45-35Ma and Thomas (1986) of 62-28Ma.

Dating of illite provides another constraint on the timing of diagenetic events in the basin. Illite has a cogenetic textural relationship with the latest stages of quartz overgrowth cementation (Fig.3.8). By combining the fluid inclusion temperatures, the $\delta^{18}\text{O}$ of quartz overgrowths and illite, δD illite with K/Ar dating a unique fix can be established on the reservoir temperature, porefluid composition at 58Ma in the early Tertiary. The illite is the last diagenetic mineral phase observed and so the date is taken as the cessation of diagenesis due to fill of this reservoir sandstone in Murchison by significant oil migration. Illite formation in well 3/13a-1 occurs in all Brent Formations. As already stated dates for illite formation in this Alwyn area range from 75-28 Ma,

and have facilitated detailed modelling of oil fill of the reservoirs (Jourdan et al.(1987)).

Consequently the lack of illite in the Etive, Ness and Tarbert and lower quantities of illite in the Rannoch Formation in the Thistle, Murchison and Dunlin wells studied compared to the Alwyn area, may be due to fill of the reservoirs with oil before illite had the opportunity to form in large quantities (similarly, quartz overgrowths have a greater abundance in the Alwyn area in comparison to the Thistle, Murchison and Dunlin oilfields).

3.16

SYNTHESIS

By combining the previous individual studies it is possible to build up an overall scenario for diagenesis in the Brent sandstones.

3.16.1. EARLY DIAGENESIS

The early diagenetic environment was influenced by a meteoric dominated porewater which flushed through the Brent Group (Fig.3.22). Initial compaction in the Rannoch Formation limited lateral and especially vertical fluid flow through the sandstone in comparison to the overlying Etive, Ness and Tarbert Formations. Early cementation saw widespread kaolinite development with carbonate cemented horizons developed particularly in the Rannoch and Tarbert Formations, less so in the Ness and none in the Etive. Formation of these carbonate cemented horizons restricted permeability and hence vertical diagenetic flow in these areas of the reservoir. Isotopic evidence requires that meteoric water was the dominant fluid at this time with a $\delta^{18}\text{O} = -7\%$ and $\delta\text{D} = -48\%$ (SMOW) in the Middle Jurassic. Pre-calcite concretion cements also indicate a freshwater acidic fluid which allowed the widespread development of vermicular kaolinite along with feldspar and mica dissolution. Siderite predates the concretionary calcite (Fig.3.8) where reducing conditions were prevalent, the siderite forming at sites of degrading biotites. Strontium analyses of the siderite and calcite (0.711, Hamilton et al.(1987), when considered with the $\delta^{13}\text{C}$ and $\delta^{18}\text{O}$ values indicate a continued supply of meteoric groundwater flow, not marine. Under these conditions, siderite (14°C), kaolinite (26°C) and calcite (32°C) precipitated at low temperatures alongwith dissolution of mica

and feldspar. Minor amounts of K-feldspar overgrowths and pyrite were precipitated at this stage. The dissolution of the mica and feldspar was a possible source for the kaolinite and other early silicate cements.

3.16.2. BURIAL DIAGENESIS

As stated earlier, the burial diagenetic cements formed from the early Cretaceous onwards. Kaolinite continued to precipitate in the sandstones through burial diagenesis and became a more blocky, booklet shape (Fig.3.9.d). These later forms were cogenetic with quartz overgrowths whose lowest fluid inclusion precipitation temperature of 72.4°C occurred from a porewater with a $\delta^{18}\text{O}$ of -2.4‰ (quartz overgrowth $\delta^{18}\text{O}$ = +22.3‰). At this time some calcite cemented concretions were being altered to a more ferroan and ankeritic compositions. Late siderite, dolomite and ferroan calcite precipitated contemporaneously. The quartz overgrowth precipitation events had a wide fluid inclusion temperature range (Fig.3.13). These can be dated as Late Cretaceous to early Tertiary, as 58Ma illite is cogenetic with the latest stages of quartz overgrowth development in this study. The presence of hydrocarbons in the quartz fluid inclusions also indicates that at this time, oil generation and migration was occurring in the basin.

During illite and silica cementation and the latest stages of ankerite growth, the Brent Group was buried at a maximum depth of 2.3km (decompacted value, see Fig.3.26). The maximum fluid inclusion temperature (which gives a measure of the palaeoreservoir temperature) is 131.1°C. Assuming a geothermal gradient of 35°C/km (present day North sea) and a 10°C surface temperature then the burial temperature at the early Tertiary would be 10 + 80°C (2.3km burial depth) = 90°C for the reservoir. Therefore the fluid inclusion temperatures are up to 40°C higher than that expected.

Thermal modelling of well 211/18-8, Thistle oilfield was kindly undertaken by N. Wilson, B.P. Pet. Dev. to help understand this temperature excursion. The program considered the lithologies present in the well section, their thicknesses and heat conductivity/flow parameters. A basal heat flow of 50 mW/m² was assumed. Fig. 3.27 presents the thermal model with time for the well section, but like the foregoing simplistic calculation, it predicts a

temperature (68°C) which considerably less than that indicated for the reservoir from fluid inclusions. The data suggests that the quartz overgrowths, illite, latest ankerite and minor late kaolinite II precipitated from a hot, dominantly freshwater (Figs. 3.13, 3.14) porefluid which may have come up from depth in the basin. This would suggest that either 1), a major influx of hot fluid occurred at this time or 2) an extremely high geothermal gradient existed ($\approx 70^{\circ}\text{C}/\text{km}$), (Fig. 3.25). Either way, the reservoir has since cooled down to the present day temperatures ($85\text{-}115^{\circ}\text{C}$).

1) Evidence for fluid influx - Carstens & Finstad (1981) state that present day high interval geothermal gradients ($>35\text{ C}/\text{km}$) measured in the Jurassic sequence of the East Shetland Basin cannot be explained by the thermal properties of the rocks, and indicate that the fault block structures and their faults are allowing the upward migration of warm fluids from deeper in the basin. Analogy with a present day rift graben suggests that such upward fluid flow may be more important during rifting. Present day geothermal gradients in the Landau 2 borehole (2063m deep), on the western flank of the actively subsiding Rhine Graben are $77^{\circ}\text{C}/\text{km}$ (Doebel et al. 1974). The present high geothermal gradient started 15Ma ago (i.e. short lived), at the onset of Rhine Graben taphrogenesis. The high values observed are thought by Doebel et al. (1974) to be the result of thermal waters rising through the fault system. This present day scenario is here considered as an actualistic comparison for the Brent which underwent a short lived temperature excursion during rapid basin subsidence in the Early Tertiary.

Alternatively, the reservoir temperature was affected by 2) - an extremely high conductive geothermal gradient. This would appear unlikely as interval geothermal gradients of $15\text{ - }40^{\circ}\text{C}/\text{km}$, show the overlying Cretaceous to be thermally conductive (Carstens & Finstad 1981). At 58 Ma these sediments were $\approx 1.8\text{ km}$ thick and so still requires an interval gradient in the Jurassic ($\approx 0.4\text{ km}$ thick) of $\approx 150^{\circ}\text{C}/\text{km}$, to account for the fluid inclusion temperatures of 130 C measured. This argument would require either thinning of the crust or intrusions into the crust in the East Shetland Basin at this time. At present the highest measured geothermal gradients are $100^{\circ}\text{C}/\text{km}$, in the overpressured zones of Gulf Coast sediments (Jones & Wallace 1974).

Crustal thinning at the Palaeocene (65 Ma) does however appear attractive to a conductive geothermal gradient model. To account for the maximum fluid inclusion temperatures (131°C), a geothermal gradient of $70^{\circ}\text{C}/\text{km}$ inferred - this requires the thickness of the crust to be halved to 15 km, implying a stretching factor of $R = 2$, (McKenzie 1978) in the Palaeocene. A crustal thickness of 15 km was calculated from seismic reflection and refraction profiles across the North Sea (Barton et al. 1984, Beach 1986). However, the $R = 2$ factor ignores pre-Palaeocene thinning.

Other factors however go against this conductive heating hypothesis:-

a) For a $R = 2$, evidence of faulting in the Palaeocene is expected, but it is not observed on seismic lines (Parsley 1984). Therefore pure shear of the crust is required. This however is problematic, Beach (1986) suggested that faults can be traced through the entire crust, from regional reflection seismic, to explain the basin development by a Wernicke (1985) simple shear model, although McGeary et al. (1987) do not recognise fault-plane reflections that can be traced from the surface into the mantle. Fault traces recognised by McGeary et al. (1987) are considered to flatten or merge into horizontal reflections in the lower crust.

b) For a $R = 2$ at 65 Ma, 3.5 km of thermal subsidence is expected (McKenzie 1978) plus that from initial fault subsidence. This implies a present day basin subsidence of > 4 km. However even in the deepest parts of the Central Graben (Quadrant 22, U.K. sector), the Palaeocene thickness is calculated at only 3.5 km (from isopach data, Day et al. 1981). In the Viking Graben east of the East Shetland Basin the Tertiary sediments are only 2.2 km thick.

c) For a $R = 2$ at 65 Ma, the crustal thinning gives higher heat flow followed by exponential decay. The subsequent heat flow today should be 1-2 HFU ($\approx 50\text{mW}/\text{m}^2$), McKenzie (1978). In the Central Graben (Quadrant 22) the present day heat flow is in fact higher at 60-90 mW/m^2 (Andrews-Speed & Oxburgh 1984). This then requires the inference of a present day heat flow/rifting event being initiated. In the Oseberg field (Norwegian Sector - Brent play), Dahl et al. (1987) recognise an increase in heat flow at the present day and also in the Eocene, with rapid decrease in the heat flow between times. This suggests that heat flow changes rapidly with time, a

factor that is more compatible with fluid influxes than conductive heating and cooling.

d) Illite with $\delta^{18}\text{O}$ compositions (+13.1 to +14.2 ‰) precipitated at 58 Ma in waters of $\delta^{18}\text{O} = 0$ to +2‰ at temperatures around 100–110°C, and at a maximum of 120°C (Fig. 3.19.c). Quartz overgrowths precipitated at temperatures up to 130°C at 60–65 Ma. Therefore by 58 Ma, the reservoir temperature had cooled by 20–25°C within 5 – 10 million years. McKenzie (1978, Fig.2) predicts that heat flow (and hence temperature) is constant for the first 15 million years if $R = 2$ for a thermal event. Therefore it is unlikely that the temperature loss was by conductive decay, but was rapid by the cessation of fluid flow.

The idea of a high conductive geothermal gradient appears superficially attractive but geodynamically problematic.

The $\delta^{18}\text{O}$ of the porewater had by this time become more positive (0 to +2‰) due to the decrease in water/rock ratios (<1) and continuing oxygen isotope exchange during diagenetic mineral growth. The chemistry of the porewater was also altering with the development of illite which forms in more alkaline conditions (in comparison to the acidic porewater conditions prevalent during early diagenetic kaolinite precipitation. Present day formation water pH is between 7.1 and 8 (Selley (1978), B.P. pers com) in support of this.

Fig.3.24 illustrates a radical alteration for the Brent sandstones during burial diagenesis from an open meteoric circulation which dominated early diagenesis to a semi/closed system whereby warm fluids precipitated the major porosity and permeability reducers, quartz overgrowths and illite. The source of the cements is difficult to assess. Pressure solution of quartz is not a major feature in the studied sections and so it is not possible to derive enough quartz locally in the sandy Formations to cement the sandstones (Fig.3.9). Distant sources for the quartz cement cannot be ruled out. Although it is uncertain if "distant" = Rannoch Formation, surrounding overlying Heather and underlying Dunlin mudrocks, or deeper pre-Triassic sediments..

The heat excursion at the early Tertiary is problematic. No major rifting event in the East Shetland Basin has been recorded. However, from the Palaeocene increased subsidence occurred, shown by deepening of water from Maastrichtian chalk to a deep clastic basin.

At the same time, uplift of the East Shetland Platform sourced submarine fan sands from the east (Fig.3.1) (Lovell 1984), with associated fault movement in the basin to accommodate this and relative elevation of the East Shetland Platform (Wheatley et al.1987). It may be that the associated fault movement in the basin allowed fluid movement up the faults and through sandstone aquifers from depth up into Brent sandstones of hydrocarbon rich and silica rich solutions. Also at this time, igneous activity on the western seaboard of Scotland from 60 - 50 Ma (Emeleus 1983) was occurring with a major phase of opening of the Atlantic ocean. Although a general tensional regime may have been affecting this area of northwest Europe, it is difficult to show any causal relationship between the heat excursion in the Brent Province and this igneous activity, the nearest centres are >50kms distant (Duindam & Van Hoorn 1987). Figure 3.24 illustrates the burial diagenetic scenario during quartz and illite authigenesis. The hot silica rich, oil-prone fluids ascending from depth which are required for quartz cementation are not necessary for illite authigenesis. Fig.3.25 illustrates the previous points during early and late (burial) diagenesis. After this event, hydrocarbons continued to fill the reservoirs and arrest diagenesis in the Brent Group as it cooled back to its present day temperature conditions (Fig.3.19.c).

3.17

CONCLUSIONS

- 1) The Brent sandstone diagenetic sequence may be simplified to kaolinite - Fe,Ca carbonates - quartz overgrowths - Fe,Mg carbonates - illite.
- 2) The good poroperm characteristics and the 3-D connectivity of Etive, Ness and Tarbert sandstone aquifers permitted diagenesis to be controlled by a fluid flow. By contrast, the highly micaceous and relatively finer grained Rannoch sandstones have good porosities but very poor permeabilities due to burial compaction and carbonate cementation. This caused dramatic losses in the reservoir quality during diagenesis and so restricted any significant later diagenesis occurring due to restrictions on fluid flow.
- 3) Isotopic studies indicate that early diagenesis occurred in an open system flow of dominantly meteoric porewater ($\delta^{18}\text{O} = -7\text{‰}$).

Early diagenetic cements of widespread vermicular kaolinite and (in the Rannoch, Ness and Tarbert), siderite and calcite began to form at 14°C (siderite), 26°C (kaolinite) and 32°C (calcite).

4) Progressive burial of the sequence by Lower Cretaceous sediments eventually sealed the Brent from the meteoric "head".

5) Kaolinite authigenesis which continued during burial changed to a booklet form, with individual plates becoming blocky.

6) Quartz overgrowth cementation occurred by the end Cretaceous ($T_{\min} = 72.4^{\circ}\text{C}$) in an evolved porewater of $\delta^{18}\text{O} = -2.4\text{‰}$ to $+1\text{‰}$. Precipitation continued to temperatures of 131.1°C. Fluid inclusion measurements indicate formation in an abnormally warm, dominantly low salinity (1-5 wt.% eq. NaCl) water.

7) Illite precipitation is cogenetic with the latest stages of quartz overgrowth cementation at 58Ma. Illite precipitation took place in an alkaline porewater (pH = 7.1 to 8) in comparison to the acidic porewater envisaged during early diagenesis. The system is thought to become semi/closed at this time, on the scale of the Brent Group, with respect to illite. Total closure is not possible due to oil migration from the structurally deeper Kimmeridge Clay Formation.

8) Reservoir temperatures reached 131.1°C (fluid inclusions in quartz overgrowths) which are in excess of a normal geothermal gradient in the early Tertiary. Proximity of faults and their silicification (211/18-A45) may have allowed open system fluid movement from deeper (hotter) in the basin up into the sandstones carrying oil and as a possible source of silica for cementation.

9) After the heat excursion the reservoir cooled back to its present day temperature (85-115°C). The calculated oxygen and hydrogen isotope values, from the mineral cements, indicate a porewater of $\delta^{18}\text{O} = +1$ to $+2\text{‰}$ (SMOW), $\delta\text{D} = -31$ to -36‰ (SMOW). This is in accord with the present day formation water data available, $\delta^{18}\text{O} = 0$ to $+2\text{‰}$, $\delta\text{D} = -24$ to -27‰ (SMOW).

10) The oxygen isotope trend in the authigenic minerals of the Brent sandstones shows a porewater evolution from -7‰ to $+2\text{‰}$ (SMOW) during burial and diagenesis.

The authors would like to thank the technical staff and in particular Terry Donnelly, at the Isotope Geology Unit, S.U.R.R.C., East Kilbride for their assistance throughout, to Dr. G.A. Blackburn of Britoil for access to the S.E.M., and to Dick Sutherland for his help at the B.G.S. core store. We are grateful to A. Robinson and N. Wilson of British Petroleum for information on formation waters and thermal modelling. J.F.B. acknowledges receipt of a NERC grant No. GT4/85/GS/97. P.J.H is supported by the Royal Society of Edinburgh Fellowship Scheme and S. Brown publishes with permission of the Director of the British Geological Survey (NERC). The Isotope Geology Unit is supported by the NERC and the Scottish Universities.

Albright, W. A., W. L. Turner, and K.R. Williamson, 1980, Ninian Field, U.K. Sector, North Sea, in M. T. Halbouty, ed., Giant Oil and Gas Fields of the Decade 1968-1978: AAPG Memoir 30, p.173-193.

Andrews-Speed, C.P., E.R. Oxburgh, and B.A. Cooper, 1984, Temperatures and Depth-Dependent Heat Flow in Western North Sea: AAPG Bulletin, v. 68, p.1764-1781.

Ayalon, A., and F.J. Longstaffe, 1988, Oxygen isotope studies of diagenesis and pore-water evolution in the Western Canada sedimentary basin: Evidence from the Upper Cretaceous Basal Belly River sandstone, Alberta: Journal of Sedimentary Petrology, v.58, p.483-505.

Badley, M.E., J.D. Price, C. Rembach Dahl, and T. Agdestein, 1988, The structural evolution of the northern Viking Graben and its bearing upon extensional modes of basin formation: Journal of the Geological Society of London, v.145, p.455-472.

Barton, P., D. Matthews, J.Hall and M. Warner, 1984, Moho beneath the North Sea compared on normal incidence and wide-angle seismic records: Nature, v. 308, p. 55-56.

Beach, A., 1986, A deep seismic reflection profile across the northern North Sea: Nature, v.323, p. 53-55.

Berg, R.R., 1986, Reservoir Sandstones, Prentice-Hall, New Jersey, 481p.

Bjorlykke, K., and A. Brendsdal, 1986, Diagenesis of the Brent sandstone in the Statfjord field, North Sea, in D. L. Gautier, ed., Roles of Organic Matter in Sediment Diagenesis, SEPM Special Publication 38, p.157-167.

Bjorlykke, K., A. Elverhoy, and A.O. Malm, 1979, Diagenesis in Mesozoic sandstones from Spitsbergen and the North Sea - a comparison: Geologische Rundschau, v.68, p.1152-1171.

Blackbourn, G.A., 1984, Diagenetic history and reservoir quality of a Brent sand sequence: Clay Minerals, v.19, p.377-389.

Blanche, J. B. and J. H. McD. Whitaker, 1978, Diagenesis of part of the Brent Sand Formation (Middle Jurassic) of the northern North Sea Basin: *Journal of the Geological Society of London*, v.135, p.73-82.

Boles, J. R., 1982, Active albitization of plagioclase, Gulf Coast Tertiary: *American Journal of Science*, v.282, p. 165-180.

Borthwick, J., and Harmon, R. S., 1982, A note regarding ClF_3 as an alternative to BrF_5 for oxygen isotope analysis: *Geochimica et Cosmochimica Acta*, v. 46, p.1665-1668.

Bowen, J.M., 1975, The Brent Oilfield, in A.W. Woodland, ed., *Petroleum and the Continental Shelf of North-West Europe*, v.1: Geology, Applied Science Publishers, Barking, p.353-362.

Brown, S., 1986, Jurassic, in, K.W. Glennie, ed., *Introduction to the Petroleum Geology of the North Sea*, 2nd ed., Blackwell Scientific Publications, London, p.133-159.

Brown, S., P.C. Richards, and A.R. Thomson, 1987, Patterns in the deposition of the Brent Group (Middle Jurassic) UK North Sea, in J. Brooks and K.W. Glennie, eds., *Petroleum Geology of North West Europe*, Graham & Trotman, London, p.899-913.

Budding, M. C., and H. F. Inglin, 1981, A reservoir geological model of the Brent sands in southern Cormorant, in L. V. Illing and G. D. Hobson, eds., *Petroleum Geology of the Continental Shelf of North West Europe*, Heyden & Son, London, p. 326-334.

Burley, S. D., and J. D. Kantorowicz, 1986, Thin section and S.E.M textural criteria for the recognition of cement - dissolution porosity in sandstones: *Sedimentology*, v. 33, p. 587-604.

Carstens, H., and Finstad, K.G., 1981, Geothermal Gradients of the Northern North Sea Basin, 59-62°N, in, Illing, L.V., and Hobson, G.D., eds., *Petroleum Geology of the Continental Shelf of North-West Europe*, Heyden & Sons, London, p. 152-161.

Chauvin, A.L., and L.Z. Valachi, 1980, Sedimentology of the Brent and Statfjord Formations of Statfjord Field, in *The Sedimentation of the North Sea Reservoir Rocks*, Geilo, Norwegian Petroleum Society, p.16/1-17.

Clayton, R.N. and T.K. Mayeda, 1963, The use of bromine pentafluoride in the extraction of oxygen from oxides and silicates for isotopic analysis: *Geochimica et Cosmochimica Acta*, v.27, p.43-52.

Craig, H., 1957, Isotopic standards for carbon and oxygen and correction factors for mass-spectrometric analysis of carbon dioxide: *Geochimica et Cosmochimica Acta*, v.12, p.133-149.

Craig, H., 1961, Isotopic variations in meteoric waters: *Science*, v. 133, p.1702-1703.

Crawford, M.L., 1981, Phase equilibria in aqueous fluid inclusions, in *Short Course in Fluid Inclusions: Applications to Petrology*, L.S. Hollister and M.L. Crawford, eds., Mineralogical Association of Canada, p. 75-100.

Crosbie, T., 1981, Polished wafer preparation for fluid inclusion and other studies: *Transactions of the Institute of Mining and Metallurgy*, v.90, B82-83.

Dahl, B., E. Nysaether, G.C. Speers and A. Yukler, 1987, Oseberg area - integrated basin modelling, in J. Brooks and K.W. Glennie, eds., *Petroleum Geology of North West Europe*, Graham & Trotman, London, p. 1029-1938.

Day, G.A., B.A. Cooper, C. Andersen, W.F.J. Burgers, H.C. Ronnevik and H. Schoneich, 1981, Regional Seismic Structure Maps of the North Sea, in L.V. Illing and G.D. Hobson, eds., *Petroleum Geology of the Continental Shelf of North West Europe*, Heyden & Son, London, p. 76-84.

De'Ath, N. G. and S. F. Schuyleman, 1981, The geology of the Magnus oilfield, in L. V. Illing and G. D. Hobson, eds., *Petroleum Geology of the Continental Shelf of North West Europe*, Heyden & Son, London, p. 342-351.

Deegan, C. E., and B. J. Scull, 1977, A standard lithostratigraphic nomenclature for the Central and Northern North Sea: Report of the Institute of Geological Sciences. 77/25, pp.36.

Doebel, F., Heling, D., Homann, W., Karweil, J., Teichmuller, M., and Welte, D., 1974, Diagenesis of Tertiary clayey sediments and included dispersed organic matter in relation to geothermics in the Upper

Rhine Graben, in, Illies, J.H., & Fuchs, K., eds., Approaches to Taphrogenesis, Schweizerbart'sche Verlagsbuchhandlung, Stuttgart, p. 192-207.

Duindam, P., and B. van Hoorn, 1987, Structural evolution of the West Shetland continental margin, in J. Brooks and K.W. Glennie, eds., Petroleum Geology of North West Europe, Graham & Trotman, London, p.765-773.

Dutton, L.S., and L.S. Land, 1985, Meteoric burial diagenesis of Pennsylvanian arkosic sandstones, southwestern Anadarko Basin, Texas, Geological Society of America, Memoir 151, p. 355 - 366.

Emeleus, C.H., 1983, Tertiary Igneous Activity, in G.Y. Craig, ed. Geology of Scotland, Scottish Academic Press, p. 357-397.

Engelstad, N., 1987, Murchison, in A.M. Spencer, ed., Geology of the Norwegian Oil and Gas Fields, Graham & Trotman, London, p.295-305.

Eslinger, E.V., 1971, Mineralogy and oxygen isotope ratios of hydrothermal and low-grade metamorphic argillaceous rocks (unpubl. Ph.D. dissert.): Cleveland, Ohio, Case Western Reserve University, 205p.

Eslinger, E.V. and H. Yeh, 1981, Mineralogy, $^{18}\text{O}/^{16}\text{O}$ and D/H ratios of clay rich sediments from Deep Sea Drilling Project site 180, Aleutian Trench: Clays and Clay Minerals, v.29, p.309-315.

Eynon, G., 1981, Basin development and sedimentation in the Middle Jurassic of the northern North Sea, in L.V. Illing and G.D. Hobson, eds., Petroleum Geology of the Continental Shelf of North-West Europe, Heyden & Son, London, p.196-204.

Fallick, A.E., J. Jocelyn, T. Donnelly, M. Guy, and C. Behan, 1985, Origin of agates in volcanic rocks from Scotland: Nature, v.313, p.672-674.

Fisher, R.S., 1982, Diagenetic history of Eocene Wilcox sandstones and associated formation waters, South-Central Texas, Ph.D. dissertation, University of Texas at Austin, 185 p.

Forester, R.W., and H.P. Taylor, Jr., 1977, $^{18}\text{O}/^{16}\text{O}$, D/H, and $^{13}\text{C}/^{12}\text{C}$ studies of the Tertiary igneous complex of Skye,

- Scotland: American Journal of Science, v. 277, p.136-177.
- Friedman, I., and J.R. O'Neil, 1977, Compilation of stable isotope fractionation factors of geochemical interest, in M. Fleischer, ed., Data of Geochemistry (6th ed.): United States Geological Survey Professional Paper 440-KK, 12p. + figures.
- Glassman, J.R., P.D. Lundegard, R.A. Clark, B.K. Penny, and I.D. Collins, 1989, Geochemical evidence for the history of diagenesis and fluid migration: Brent sandstone, Heather Field, North Sea: Clay Minerals in press.
- Glennie, K.W., 1986, Early Permian - Rotliegend, in K.W. Glennie, ed., Introduction to the Petroleum Geology of the North Sea, 2nd ed., p.63-85.
- Goff, J. C., 1983, Hydrocarbon generation and migration from Jurassic source rocks in the East Shetland Basin and Viking Graben of the northern North Sea: Journal of the Geological Society of London, v.140, p. 445-474.
- Hallett, D., 1981, Refinement of the geological model of the Thistle field, in L. V. Illing and G. D. Hobson, eds., Petroleum Geology of the Continental Shelf of North West Europe, Heyden & Son, London, p. 315-325.
- Hamilton, P.J., A.E. Fallick, R.M. Macintyre, and S. Elliott, 1987, Isotopic tracing of the provenance and diagenesis of Lower Brent Group sands, North Sea, in J. Brooks and K.W. Glennie, eds., Petroleum Geology of North West Europe, Graham & Trotman, London, p.939-949.
- Hancock, N. J., and A. M. Taylor, 1978, Clay mineral diagenesis and oil migration in the Middle Jurassic Brent sand Formation: Journal of the Geological Society of London, v.135, p.69-72.
- Hanor, J. S., 1980, Dissolved methane in sedimentary brines: Potential effect on the PVT properties of fluid inclusions: Economic Geology, v.75, p.603-609.
- Harland, W.B., A.V. Cox, P.G. Llewellyn, C.A.G. Pickton, A.G. Smith and R. Walters, 1982, A Geologic Time Scale: Cambridge University Press, Cambridge, 127p.

- Helgeson, H.C., and F.T. Mackenzie, 1970, Silicate-seawater equilibria in the ocean system: *Deep-Sea Research*, v.17, p.877-892.
- Hodson, G. M., 1975, Some aspects of the geology of the Middle Jurassic in the Northern North sea with particular reference to electro-physical logs, in *Jurassic Northern North Sea Symposium*, Stavanger, Norw. Petrol. Soc., p.16/1-39.
- Hogg, A.J.C., M.J. Pearson, A.E. Fallick, P.J. Hamilton, and R.M. Macintyre, 1987, Clay mineral and isotope evidence for controls on reservoir properties of Brent Group sandstones, British North Sea: *Terra Cognita*, v.7, p.342.
- Hollister, L. S., 1981, Mineralogical Association of Canada, Short course in fluid inclusions: *Applications to Petrology* v.6, p.1-12.
- Hower, J., and T.C. Mowatt, 1966, The mineralogy of illites and mixed layer illite/montmorillonites: *American Mineralogist*, v.51, p.825-854.
- Hurst, A., and H. Irwin, 1982, Geological modelling of clay diagenesis in sandstones: *Clay Minerals*, v.17, p.5-22.
- Jackson, M.L., 1979, *Soil Chemical Analysis - Advanced Course* (2nd ed.): Madison, WI., published by the author, 895p.
- Jones, P.H., 1976, Natural gas resources of the geopressured zones in the northern Gulf of Mexico basin, in *Natural gas from unconventional geologic sources*, National Research Council, National Academy of Sciences, p.17-33.
- Jourdan, A., M. Thomas, O. Brevart, P. Robson, F. Sommer, and M. Sullivan, 1987, Diagenesis as the control of the Brent sandstone reservoir properties in the Greater Alwyn area (East Shetland Basin), in J. Brooks and K.W. Glennie, eds., *Petroleum Geology of North West Europe*, Graham & Trotman, London, p.951-961.
- Kirk, R.H., 1980, Statfjord Field: a North Sea giant, in M.T. Halbouty, ed., *Giant oil and Gas Fields of the Decade: 1968-1978*: AAPG Memoir 30, p.95-116.
- Kulla, J.B., 1979, Oxygen and hydrogen fractionation factors determined in experimental clay-water systems, Ph.D. Dissertation,

University of Illinois.

Land, L.S., and S.P. Dutton, 1978, Cementation of a Pennsylvanian deltaic sandstone: isotopic data: *Journal of Sedimentary Petrology*, v.48, p.1167-1176.

Liu, K., and Epstein, S., 1984, The hydrogen isotope fractionation between kaolinite and water: *Isotope Geoscience*, v.2, p.335-350.

Longstaffe, F. J., 1986, Oxygen isotope studies of diagenesis in the basal Belly River sandstone, Pembina I-Pool, Alberta: *Journal of Sedimentary Petrology*, v.56, p.78-88.

Longstaffe, F.J., 1987, Stable isotope studies of diagenetic processes, in T.K. Kyser, ed., *Stable Isotope Geochemistry of Low Temperature Fluids: Mineralogical Association of Canada Short Course No. 13*, p.187-257.

Lonoy, A., J. Akselsen, and K. Ronning, 1986, Diagenesis of a deeply buried sandstone reservoir: Hild field, Northern North Sea: *Clay Minerals*, v.21, p.497-511.

Lovell, J.P.B., 1984, Cenozoic, in Glennie, K.W., ed., *Introduction to the Petroleum Geology of the North Sea*, Blackwell Scientific Publications, London, p. 179-196.

Malley, P., A. Jourdan, and F. Weber, 1986, Etude des inclusions fluides dans les nourrisages siliceux des gres reservoirs de Mer du Nord: une nouvelle lecture possible de l'histoire diagenetique du Brent de la region d'Alwyn: *Comptes Rendus de L'Academie des Sciences*, Paris, v.302, p.653-658.

Matsuhisa, Y., J. R. Goldsmith, and R. N. Clayton, 1979, Oxygen isotopic fractionation in the system quartz-albite-anorthite-water: *Geochimica et Cosmochimica Acta*, v.43, p.1131-1140.

Milliken, K.L., L.S. Land, and R.G. Loucks, 1981, History of burial diagenesis determined from isotopic geochemistry, Frio Formation, Brazoria County, Texas: *AAPG Bulletin*, v.65, p.1397-1413.

Nadir, F.T., and J.T.C. Hay, 1978, Geological and reservoir modelling of the Thistle field, in *Proceedings of the European Offshore Petroleum Conference*, London. The Society of Petroleum Engineers

(U.K.) Ltd., v.II, p.233-242.

O'Neil, J.R., R.N. Clayton, and T.K. Mayeda, 1969, Oxygen isotope fractionation in divalent metal carbonates: *Journal of Chemical Physics*, v.51, p.5547-5558.

Parry, C.C., P.H.J. Whitley, and R.D.H. Simpson, 1981, Integration of palynological and sedimentological methods in facies analysis of the Brent Formation, in L.V. Illing and G.D. Hobson, eds., *Petroleum Geology of the Continental Shelf of North-West Europe*, Heyden & Son, London, p.205-215.

Perry, E.A., 1971, Silicate-seawater equilibria in the ocean system: A discussion: *Deep-Sea Research*, v.18, p.921-924.

Price, L.C., 1976, Aqueous solubility of petroleum as applied to its origin and migration: *AAPG Bulletin*, v.60, p.213-244.

Randolph, P.L., 1977, Natural gas content of geopressed aquifers, in the Proceedings of the 3rd Geopressed-Geothermal Energy Conference, Univ. S.W. Louisiana, v.1, p.23-46.

Richards, P.C., S. Brown, J.M. Dean, and R. Anderton, 1988, A new palaeogeographic reconstruction for the Middle Jurassic of the northern North Sea: *Journal of the Geological Society of London*, v.145, p.883-885.

Richards, P.C., and S. Brown, 1986, Shoreface storm deposits in the Rannoch Formation (Middle Jurassic), North West Hutton oilfield: *Scottish Journal of Geology*, v.22, p.367-375.

Roedder, E., 1984, Fluid Inclusions, *Reviews in Mineralogy* v.12, Mineralogical Society of America, 646p.

Rosenbaum, J., and S.M.F. Sheppard, 1986, An isotopic study of siderites, dolomites and ankerites at high temperatures: *Geochimica et Cosmochimica Acta*, v.50, p.1147-1150.

Schmidt, V., and D.A. McDonald, 1979, The role of secondary porosity in the course of sandstone diagenesis: *SEPM Special Publication* 26, p.157-207.

Sclater, J.G., and Christie, P.A.F., 1980, Continental stretching: An explanation of the Post-Mid-Cretaceous subsidence of the Central

North Sea Basin: *Journal of Geophysical Research* v.85, p.3711-3739.

Selley, R.C., 1978, Porosity gradients in North Sea oil-bearing sandstones: *Journal of the Geological Society of London*, v.135, p.119-132.

Sibley, D.F., and H. Blatt, 1976, Intergranular pressure solution and cementation of the Tuscarora orthoquartzite: *Journal of Sedimentary Petrology*, v.46, p.881-896.

Simpson, R.D.H., and P.K.J. Whitley, 1981, Geological input to reservoir simulation of the Brent Formation, in, L.V. Illing and G.D. Hobson, eds., *Petroleum Geology of the Continental Shelf of North West Europe*, Heyden & Son London, p.310-314.

Sommer, F., 1975, Histoire diagenetique d'une serie greseuse de mer du Nord: Datation de l'introduction des hydrocarbures: *Revue de l'institut Francais du Petrole*, v.30, p.729-746.

Sommer, F., 1978, Diagenesis of Jurassic sandstones in the Viking Graben: *Journal of the Geological Society of London*, v.135, p.63-67.

Suzuoki, R., and S. Epstein, 1976, Hydrogen isotope fractionation between OH - bearing minerals and water: *Geochimica et Cosmochimica Acta*, v.40, p.1229-1240.

Syers, J.K., S.L. Chapman, M.L. Jackson, R.W. Rex, and R.N. Clayton, 1968, Quartz isolation from rocks, sediments and soils for determination of oxygen isotopes: *Geochimica et Cosmochimica Acta*, v.32, p.1022-1025.

Thomas, M., 1986, Diagenetic sequences and K/Ar dating in Jurassic sandstones, Central Viking Graben: Effects on reservoir properties: *Clay Minerals*, v.21, p.695-710.

Wallace, R.H., Jr., T.F. Kraemer, R.E. Taylor, and J.B. Wesselman, 1979, Assessment of geopressured-geothermal resources in the Northern Gulf of Mexico basin, in L.J.P. Muffler, ed., *Assessment of geothermal resources of the United States-1978*, United States Geological Survey Circular 790, p.132-155.

Wheatley, T.J., D. Biggins, J. Buckingham, and N.H. Holloway, 1987,

The geology and exploration of the Transitional Shelf, an area to the west of the Viking Graben, in J. Brooks and K.W. Glennie, eds., Petroleum Geology of North West Europe, Graham & Trotman, London, p.979-989.

Yeh, H., 1980, D/H ratios and late-stage dehydration of shales during burial: *Geochimica et Cosmochimica Acta*, v.44, p.341-352.

Yeh, H., and S.M. Savin, 1976, The extent of oxygen isotope exchange between clay minerals and seawater: *Geochimica et Cosmochimica Acta*, v.40, p.743-748.

—————, 1977, Mechanism of burial metamorphism of argillaceous sediments, 3. Oxygen isotope evidence: *Geological Society of America Bulletin*, v.88, p.1321-1330.

Figure 3.1 : Location of the Brent Province, (East Shetland Basin), northern North Sea, (Line of section, see Fig 3.3.b).

Figure 3.2 : Location of the study areas within the East Shetland Basin; Thistle, Murchison and Dunlin oilfields and well 3/13a-1.

Figure 3.3.a : Structural regime in the East Shetland Basin, characterised by tilted fault blocks at Jurassic level.

Figure 3.3.b : Line A - A' (see Fig.1), displaying the overall structural regime across the North Viking Graben (after Parsley 1984).

Figure 3.4 : Jurassic stratigraphy and facies in the East Shetland Basin containing the Brent Group, (Timescale of Harland et al. 1982).

Figure 3.5 : Fluid flow control on diagenesis: Using well 211/18-A33 (Thistle), as a representative example shows higher poroperm in the Brent sandstones of the Etive, Ness and Tarbert Formations compared to the Rannoch. This should allow greater palaeofluid flow these Formations (thicker arrows represent greater fluid flow). This is reflected in the higher proportions of diagenetic cements in the former Formations of well 211/18- A33 (ref. to Table 3.1, point count data). This trend is also observed in all Brent sandstones studied (Table 3.1).

Figure 3.6 : Quartz - Feldspar - Rock Fragment plot for all samples from Table 3.1. Classification after Pettijohn (1975), modified from Dott (1964). Total number of samples 76, 500 point counts in each case.

Figure 3.7 : Porosity versus permeability plot for the Brent Group reservoir sandstones. Data from conventional core analyses (B.G.S files) n = 67.

Figure 3.8 : Paragenesis of diagenetic minerals in the Brent sandstones studied.

Figure 3.9.a : Photomicrograph of siderite (Sid) patches which formed prior to calcite (Cal) cementation, (Field of view - 2.5 mm), 8882'

(2707.1m), Tarbert Formation, 211/23-3, Dunlin oilfield.

Figure 3.9.b : Photomicrograph of early diagenetic kaolinite (Kaol) displaying a vermiform habit (Verm.) and also as an alteration product of muscovite (Musc - Kaol), (field of view - 1.25mm), 8885' (2708m), Tarbert Formation, 211/23-3, Dunlin oilfield.

Figure 3.9.c : S.E.M photomicrograph of porefilling vermicular kaolinite, displaying a "snake-like" form, (scale bar - 100 microns), 9116' (2778m), Ness Formation, 211/18 - A30ST, Thistle oilfield.

Figure 3.9.d : S.E.M photomicrograph of porefilling late diagenetic, blocky kaolinite, (scale bar - 50 microns), 12207' (3720m), Tarbert Formation, 3/13a-1.

Figure 3.9.e : S.E.M photomicrograph of porefilling anatase (TiO_2), (scale bar - 50 microns), 10590' (3228m), Ness Formation, 211/19-6, Murchison oilfield.

Figure 3.9.f : Photomicrograph of pore filling pyrite, also pre-dating secondary porosity, (field of view - 1.5mm), 10500' (3200m), Ness Formation, 211/19-6, Murchison oilfield.

Figure 3.9.g : S.E.M photomicrograph of euhedral quartz overgrowths, (scale bar - 50 microns), 12207' (3720m), Tarbert Formation, 3/13a-1.

Figure 3.9.h : S.E.M photomicrograph of porefilling filamental illite, (scale bar - 50 microns), 12433' (3789m), Rannoch Formation, 3/13a-1.

Figure 3.9.i : S.E.M photomicrograph of filamental illite predating quartz overgrowth. Illite displaying an alveolar texture (individual illite "hairs" wrapping in on themselves). Scale bar - 5 microns, 12459' (3797m), 3/13a-1.

Figure 3.9.j : Photomicrograph of a highly compacted zone within the Rannoch Formation. Such zones may act as a local source of silica. Field of view - 2.5mm, 9514' (2900m), 211/23-2, Dunlin oilfield.

Figure 3.10 : Crossplot of quartz cement versus volume of detrital grains lost by pressure solution: The line divides samples for which volume loss by pressure solution exceeds volume of quartz cement (net

silica exported), from samples for which volume of quartz cement exceeds volume lost by pressure solution (net silica imported). The crossplot indicates that the majority of Rannoch sandstones are net silica exporters along with a minor number of Etive and Ness sandstones. The vast majority of Etive, Ness and Tarbert require silica import for to account for all quartz cement.

Figure 3.11.a : Histogram of homogenisation temperatures from fluid inclusions in quartz overgrowths II, Thistle oilfield.

Figure 3.11.b : Histogram of homogenisation temperatures from fluid inclusions in quartz overgrowths II, Murchison oilfield, 211/19-6, 10500' TVD.SS.

Figure 3.11.c : Histogram of homogenisation temperatures from fluid inclusions in quartz overgrowths II, well 3/13a-1.

Figure 3.12.a : Histogram of the eutectic temperatures from fluid inclusions in quartz overgrowth II, Thistle, Murchison and well 3/13a-1, n = 13.

Figure 3.12.b : Histogram of final melting temperature of ice from fluid inclusions in quartz overgrowth II, Thistle, Murchison and well 3/13a-1, n = 18.

Figure 3.13 : Histogram of all homogenisation temperatures from fluid incusions in quartz overgrowths, n = 102. Three modes are recognised at 80-85°C, 90-95°C and 105-110°C.

Figure 3.14 : Histogram of total calculated salinities from final teperatures of ice melting. Salinities calculated from inclusions in well 3/13a-1 have the lowest values (1-4 wt.% eq. NaCl), i.e. less than seawater. Whilst Murchison values range from 3-6 wt.% eq. NaCl, and those from Thistle have the highest calculated salinities, the range of which extends from 3-9 wt.% eq. NaCl, n = 18.

Figure 3.15 : Plot of homogenisation temperature versus salinity displays two distinct groups of fluids - 1) low salinity (1-4 wt.% eq. NaCl) and 2) high salinity (5.5-8.6 wt.% eq. NaCl).

Figure 3.16 : $\delta^{18}\text{O}_{\text{porewater}}$, $\delta^{18}\text{O}_{\text{mineral}}$ and temperature relationship.

Figure 3.17.a : Maximum and minimum $\delta^{18}\text{O}$ curves for siderite -

$1000 \cdot \ln \alpha_{\text{Siderite-Water}} = 2.78 \cdot 10^6 \cdot T^{-2} - 2.89$, Friedman & O'Neil (1977), after O'Neil (1969).

Figure 3.17.b : Maximum and minimum $\delta^{18}\text{O}$ curves for kaolinite -

$1000 \cdot \ln \alpha_{\text{Kaolinite-Water}} = 2.5 \cdot 10^6 \cdot T^{-2} - 2.87$, Land & Dutton (1978), Eslinger (1971).

Figure 3.17.c : Maximum and minimum $\delta^{18}\text{O}$ curves for calcite -

$1000 \cdot \ln \alpha_{\text{Calcite-Water}} = 2.78 \cdot 10^6 \cdot T^{-2} - 2.89$, Friedman & O'Neil (1977), after O'Neil (1969).

Figure 3.17.d : Maximum and minimum $\delta^{18}\text{O}$ curves for ankerite -

$1000 \cdot \ln \alpha_{\text{Ankerite-Water}} = 2.78 \cdot 10^6 \cdot T^{-2} + 0.32$, Dutton & Land (1985).

Figure 3.17.e : Maximum and minimum $\delta^{18}\text{O}$ curves for quartz overgrowths -

$1000 \cdot \ln \alpha_{\text{Quartz-Water}} = 3.34 \cdot 10^6 \cdot T^{-2} - 3.31$, Matsuhisa et al. (1979)

Figure 3.17.f : Maximum and minimum $\delta^{18}\text{O}$ curves for illite -

$1000 \cdot \ln \alpha_{\text{Illite-Water}} = 2.43 \cdot 10^6 \cdot T^{-2} - 4.82$, Eslinger & Savin (1973), Yeh & Savin (1977).

Figure 3.18 : $\delta^{18}\text{O}$ values of formation water versus temperature ($^{\circ}\text{C}$) for diagenetic siderite, ankerite, quartz overgrowth and illite from the Brent sandstone. The top diagram illustrates the curves for the minimum values, the lower diagram for the maximum values.

Figure 3.19.a : Model for the oxygen isotope evolution of the porewater during early diagenesis in the Brent sandstones which was determined using the paragenetic sequence (Fig.3.8), and the $\delta^{18}\text{O}$ values of the diagenetic minerals.

Figure 3.19.b : Model for the continued oxygen isotope evolution of the porewater with burial diagenesis of the Brent sandstones.

Figure 3.19.c : Model for the continued oxygen isotope evolution of the porewater with burial of the Brent sandstones, with the

temperature excursions illustrated which occurred prior to the reservoir cooling back to present day conditions.

Figure 3.20 : δD versus $\delta^{18}O$ water composition plot calculated from diagenetic minerals in the Brent sandstones. The meteoric water line (MWL) is taken from Craig (1961):- an isotopic evolution trend for both hydrogen and oxygen is observed, which is compatible with the paragenetic sequence (Fig. 3.8), from more to less negative D values, and from negative to positive $\delta^{18}O$ values during early to burial diagenesis.

Figure 3.21 : Plot of δD versus $\delta^{18}O$ for oilfield brines from North America (Clayton et al.1966, Hitchon & Friedman 1969, Kharaka et al.1973) with that for the Brent using waters calculated from diagenetic minerals (Fig.3.20) following a similar trend to the other sedimentary basins.

Figure 3.22 : Scenario envisaged for early diagenesis - meteoric water influx into the subsurface during Brent deposition and influencing diagenetic processes. The inset illustrates possible meteoric water influx at the end Cimmerian when some fault blocks may have been subaerally exposed, (Sommer 1978).

Figure 3.23 : Thermal model of the burial history of the Brent sandstone, in well 211/28-8, Thistle oilfield, illustrating the expected temperature of 68C for the Brent reservoir at 58 Ma.

Figure 3.24 : Burial diagenetic scenario during quartz and illite authigenesis: During the Cretaceous/Early Tertiary, quartz overgrowths and late ankerite precipitated at temperatures in excess of the expected burial temperature. This probably reflects the migration of hot fluids from deeper in the basin. Isotopic studies suggest that illite did not form (see inset) from the hot fluids

Figure 3.25 : Burial curve on structure for Thistle, Murchison and Dunlin oilfields (from present day rock thicknesses, and decompacted thicknesses - Sclater & Christie 1980), assimilating the $\delta^{18}O$ and the δD changes during burial with diagenetic cements and events, and their relationship to burial depth.

Table 3.1 : Point count data for all Brent sandstones studied (n = 76).

Figure 3.2 : $\delta^{18}\text{O}$ data for kaolinite, quartz overgrowths and illite. $\delta^{13}\text{C}$ and $\delta^{18}\text{O}$ for siderite, calcite and ankerite.

Table 3.3 : δD data for kaolinite and illite.

Appendix 1: Isotopic preparation methods

Appendix 2: Isotopic analysis

Appendix 3: K/Ar dating

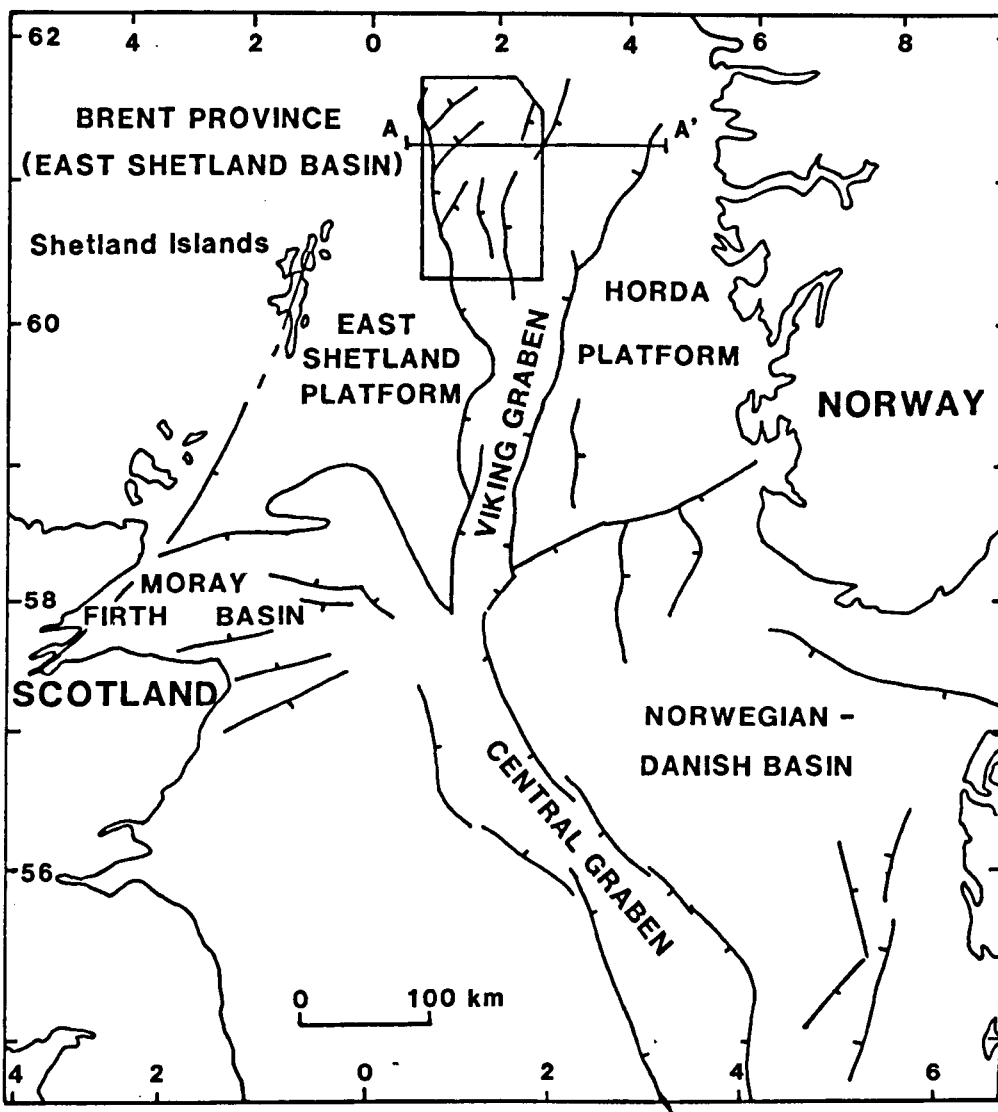


Figure 3.1

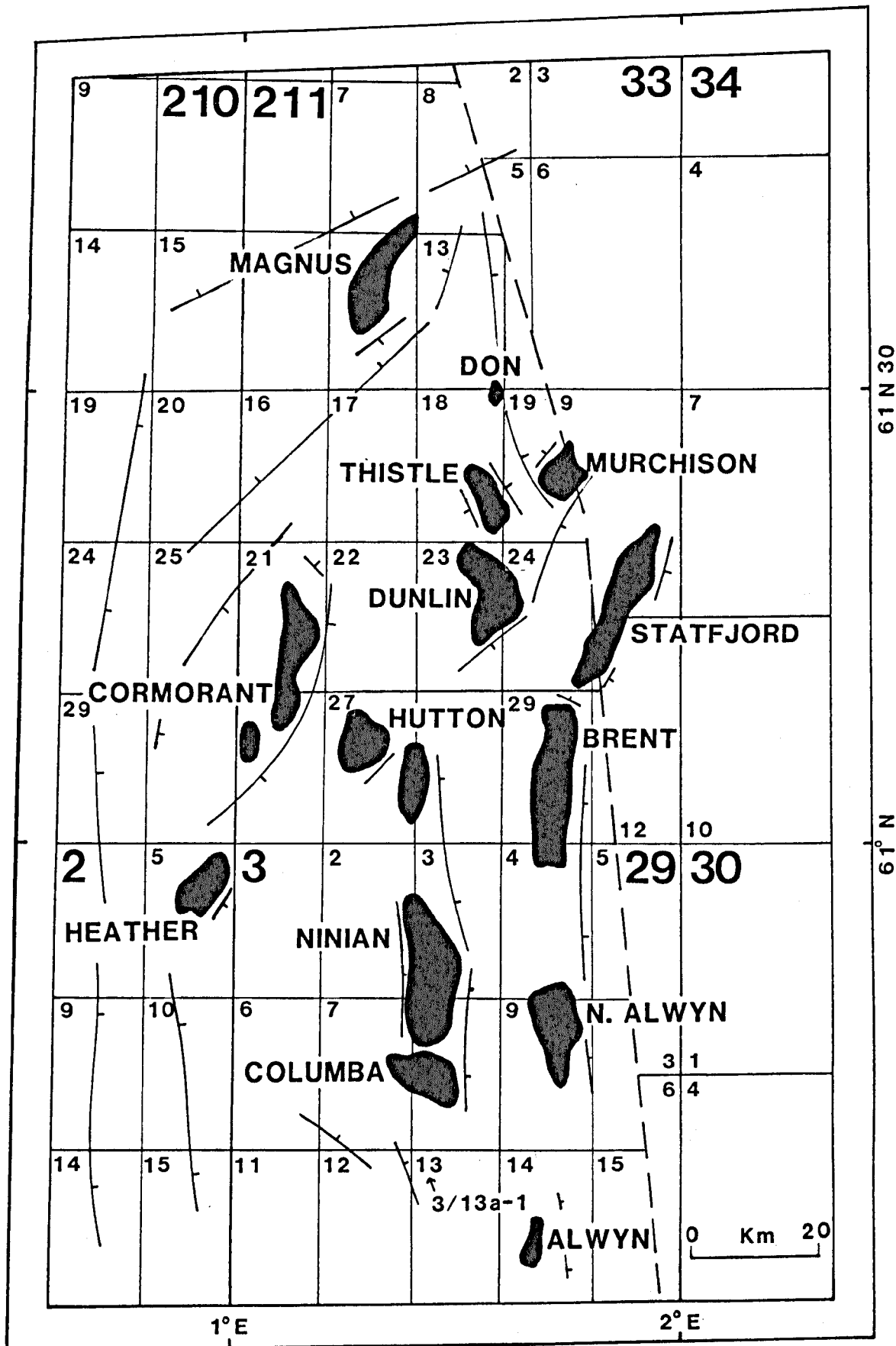


Figure 3.2

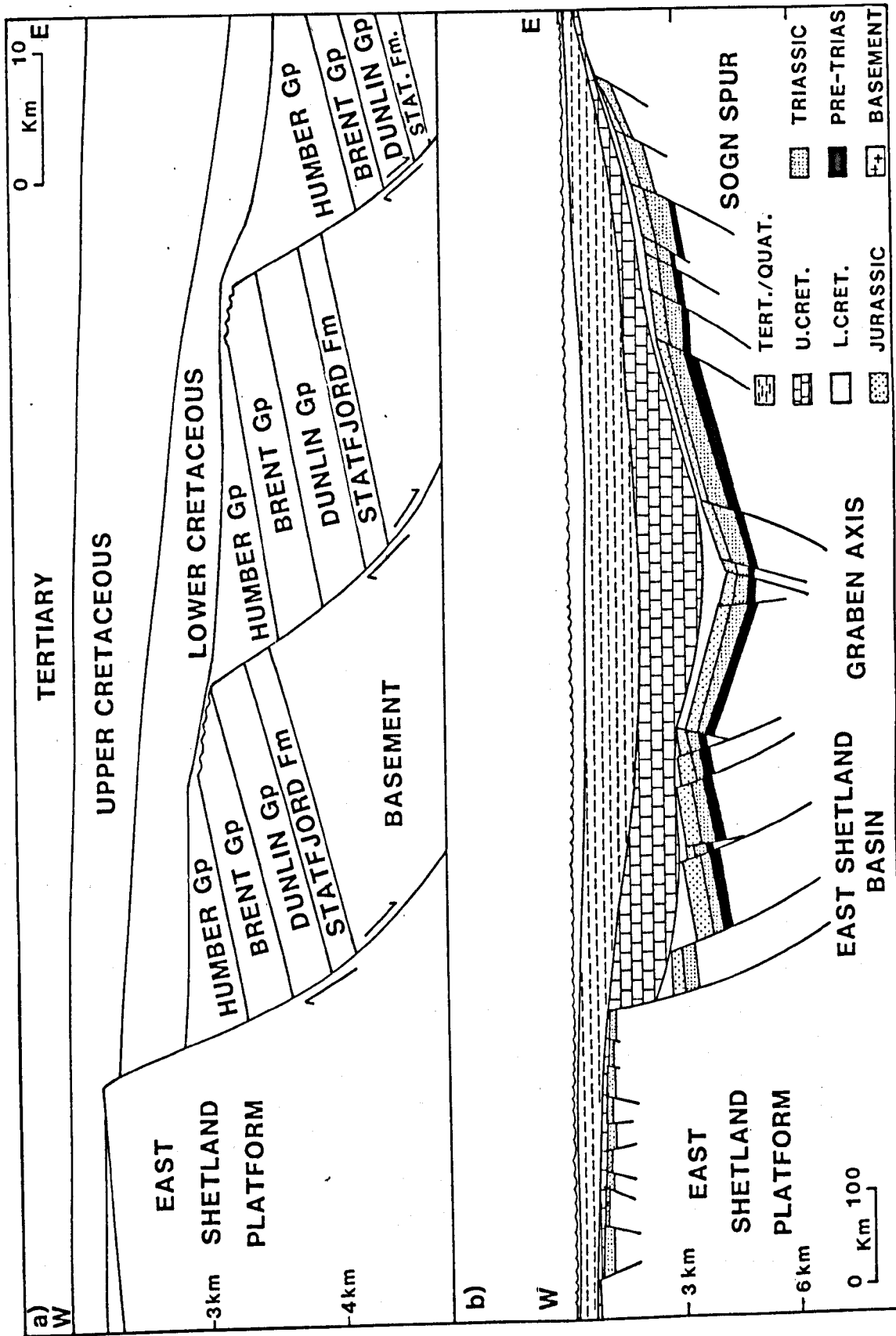


Figure 3.3

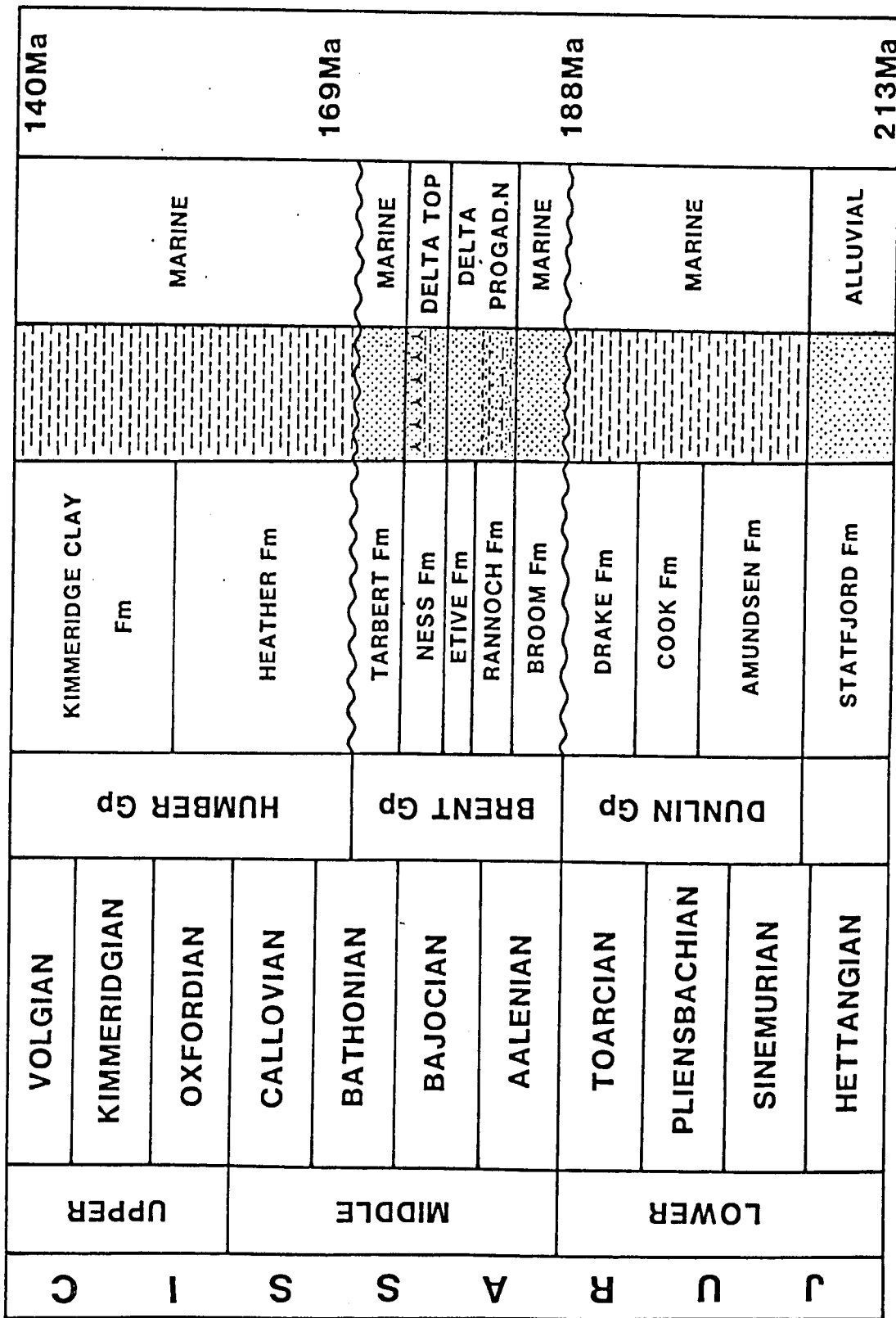


Figure 3.4

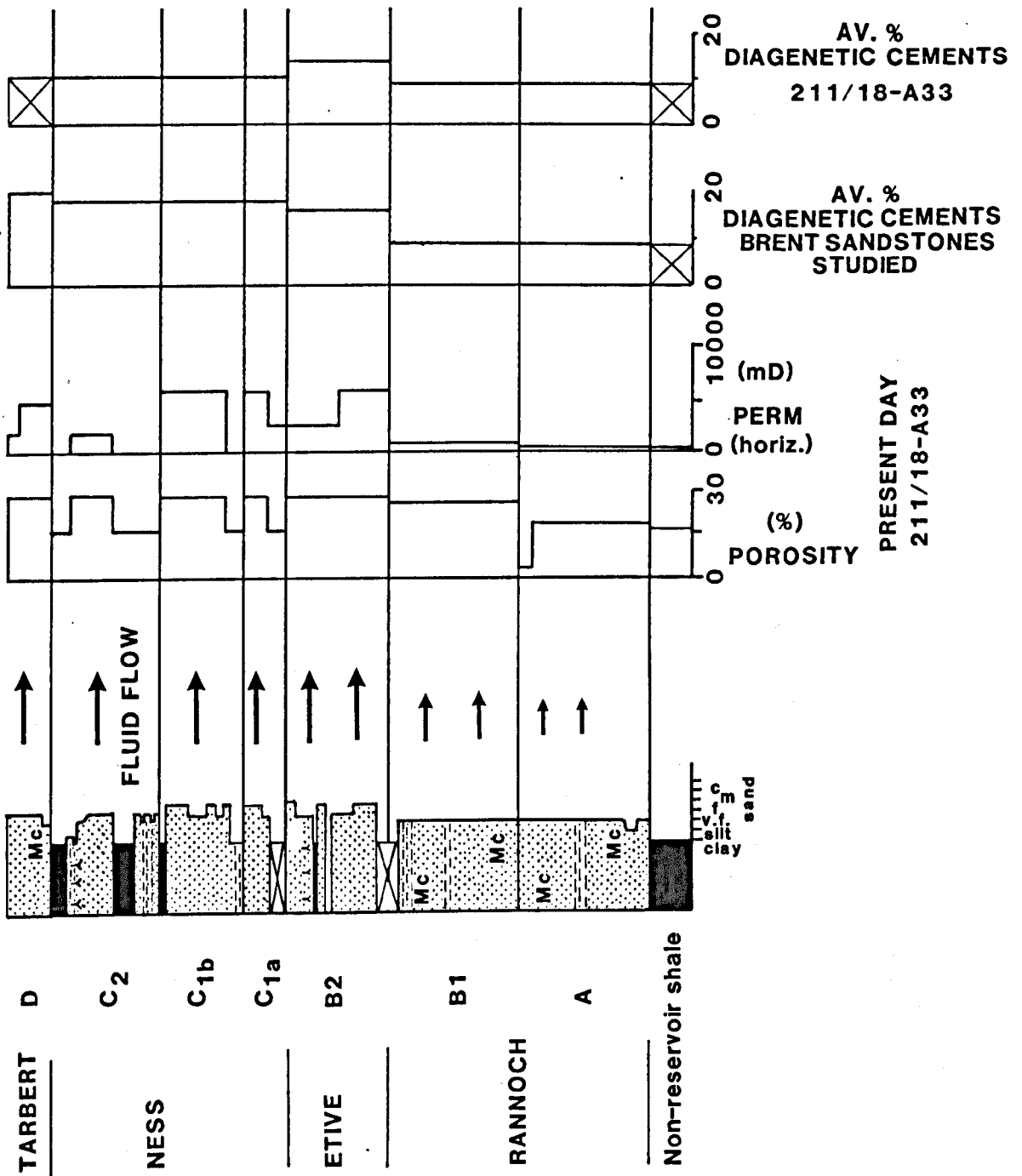


Figure 3.5

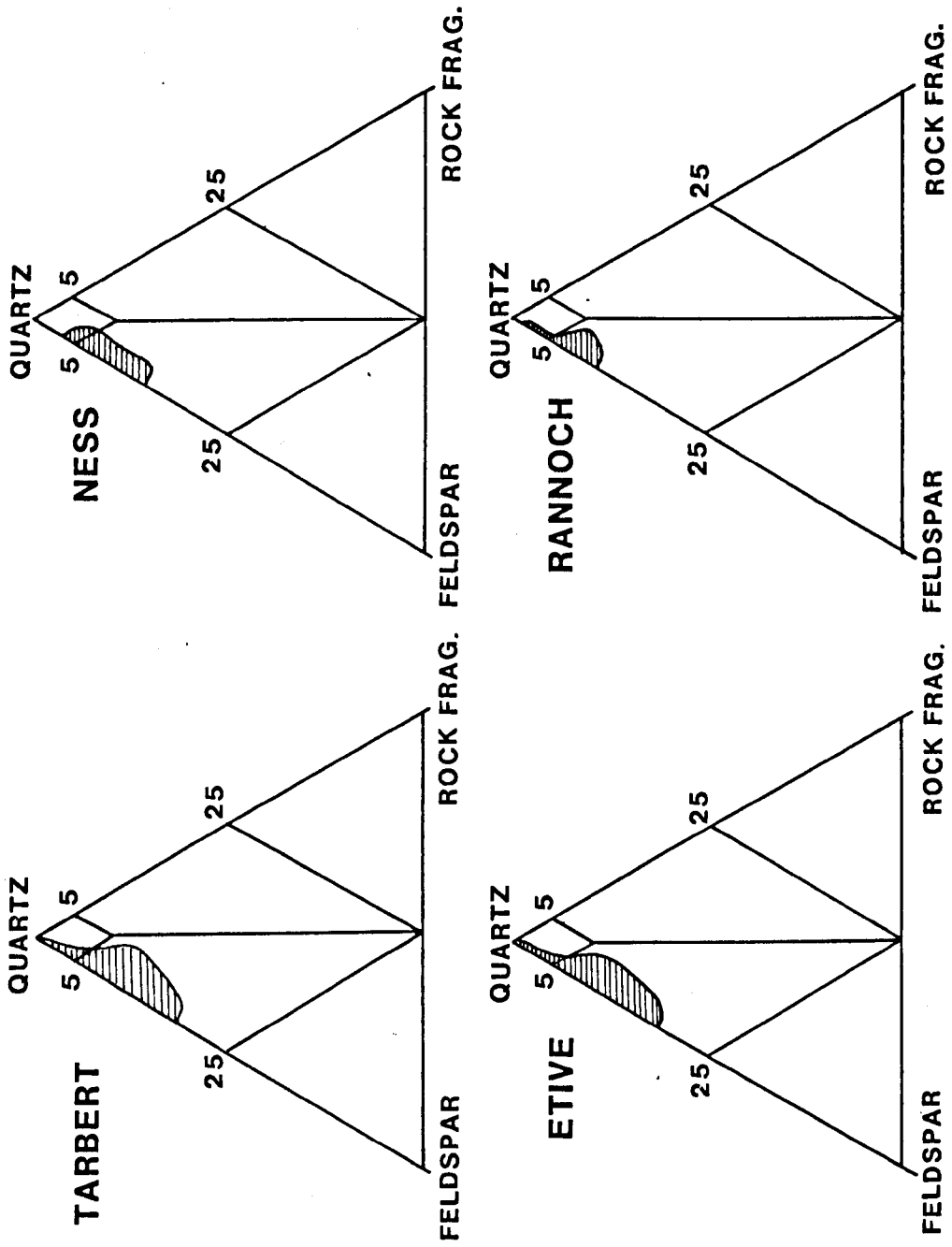


Figure 3.6

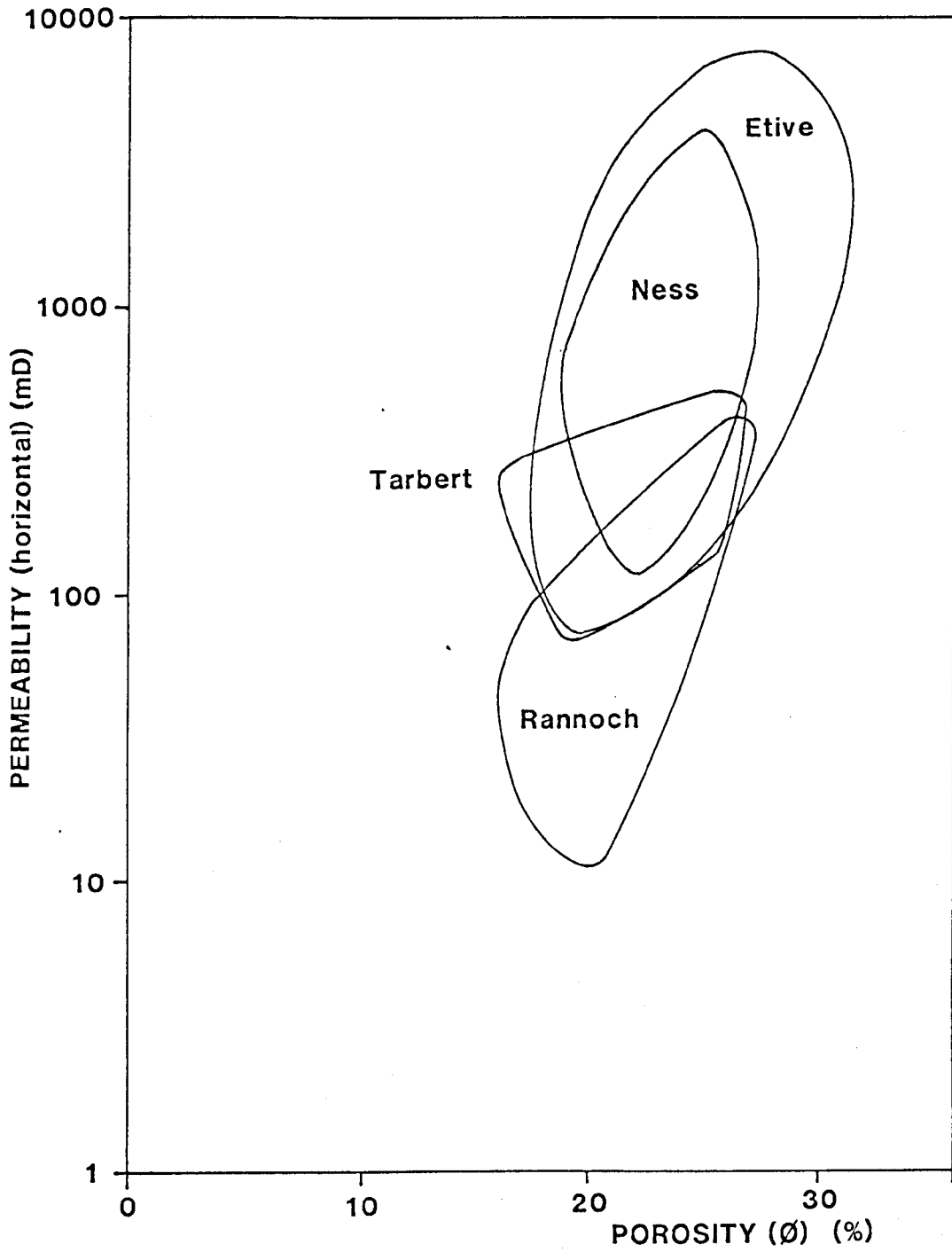


Figure 3.7

TIME →

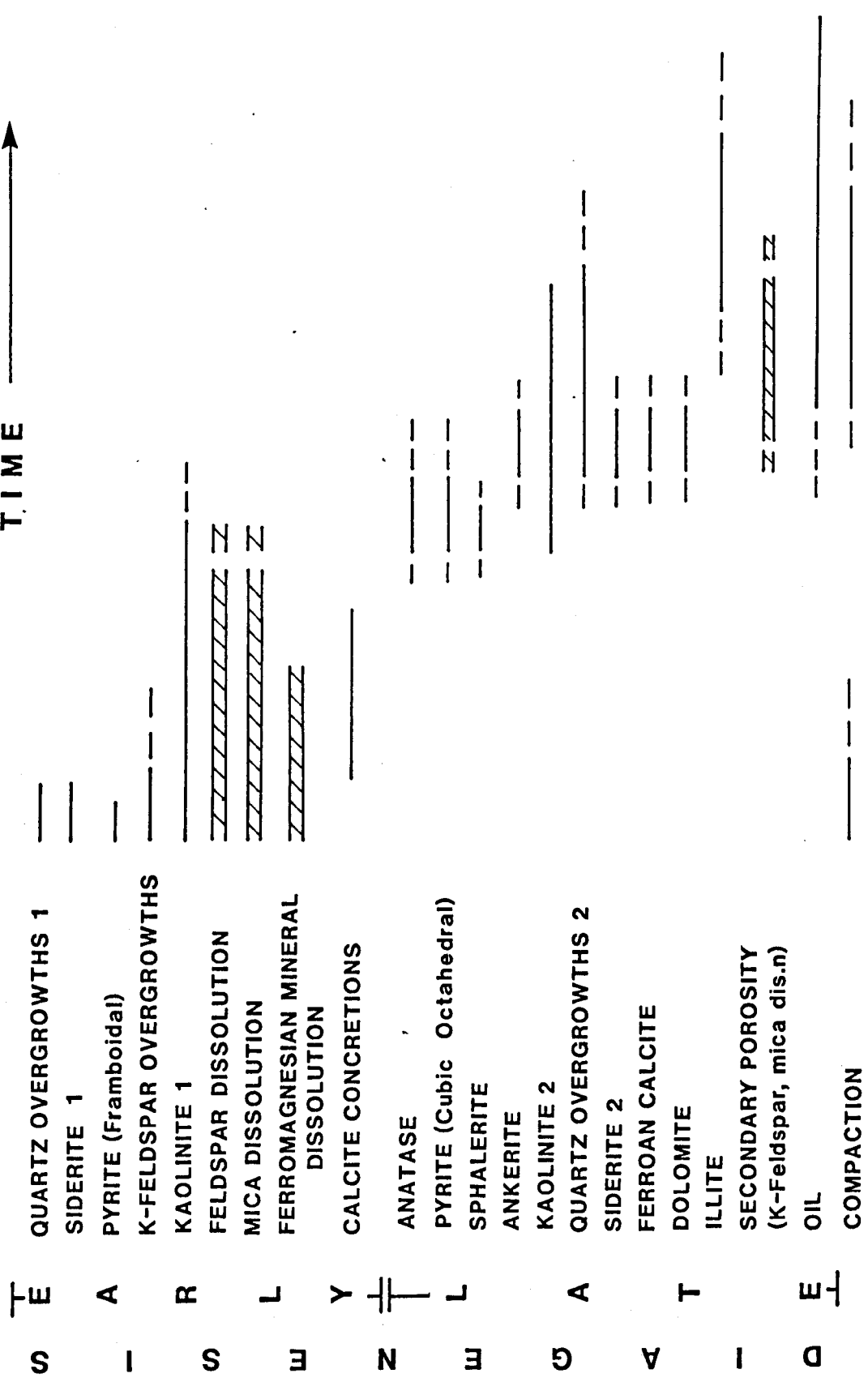


Figure 3.8

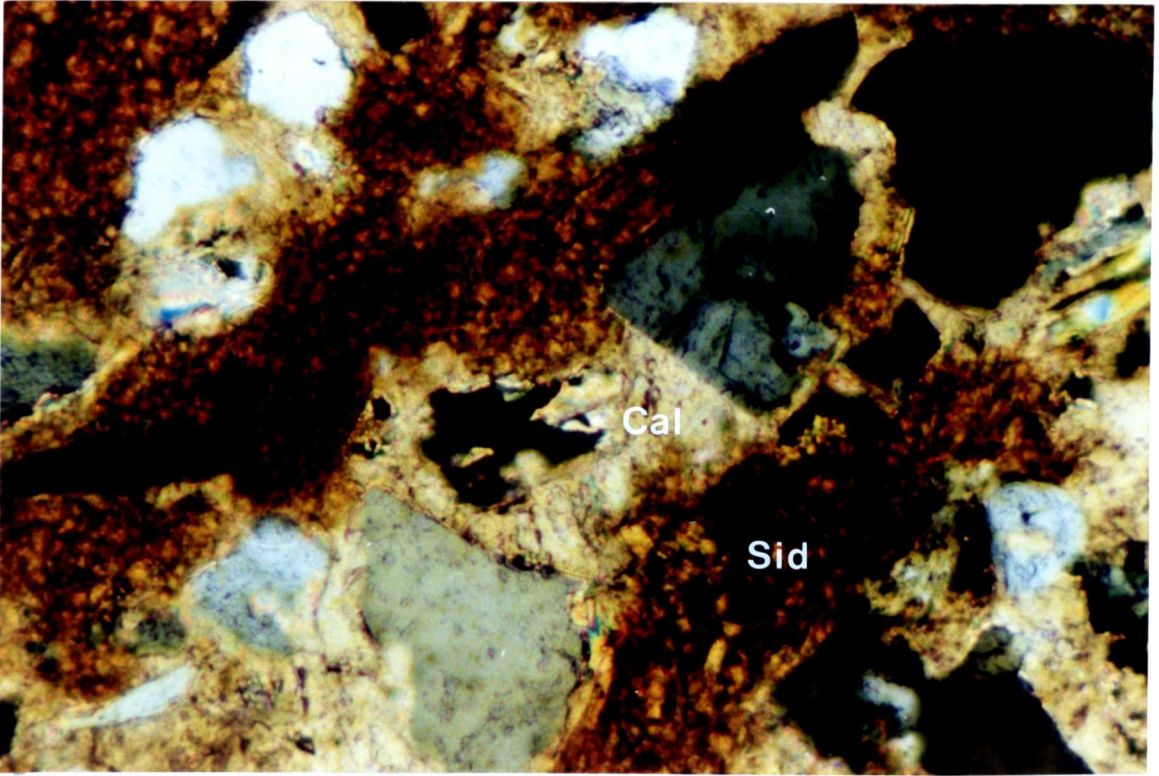


Figure 3.9.a

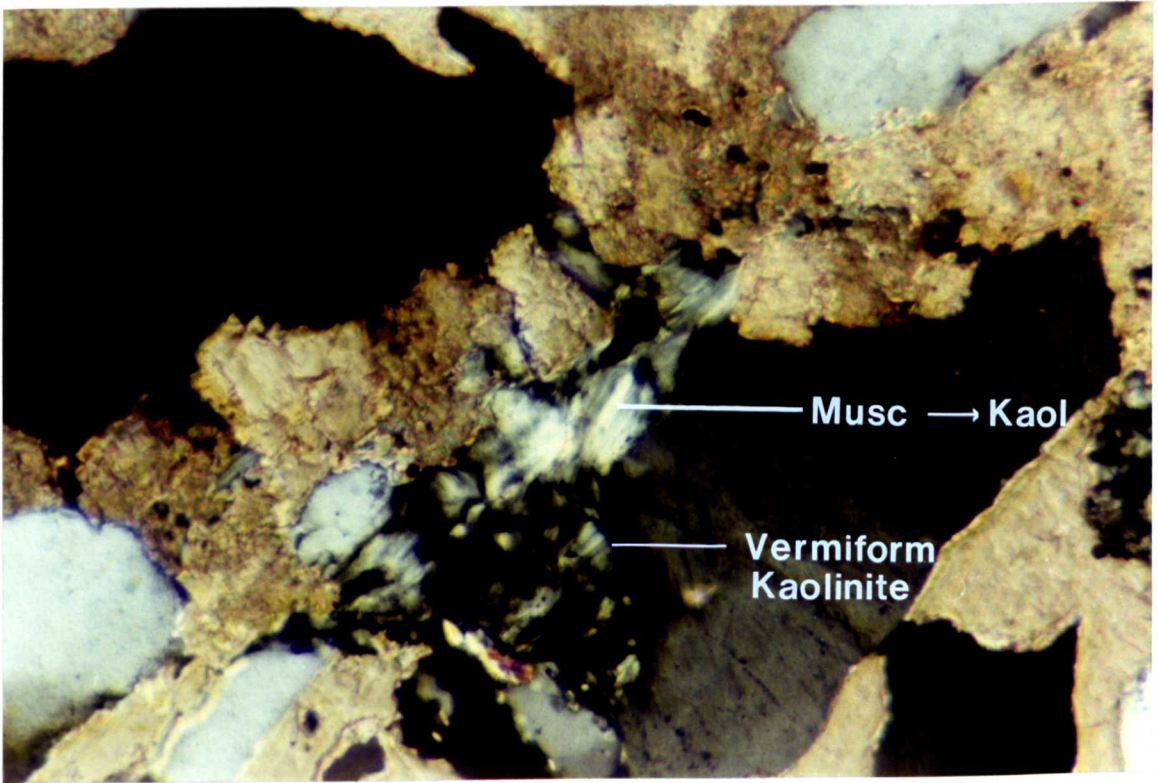


Figure 3.9.b

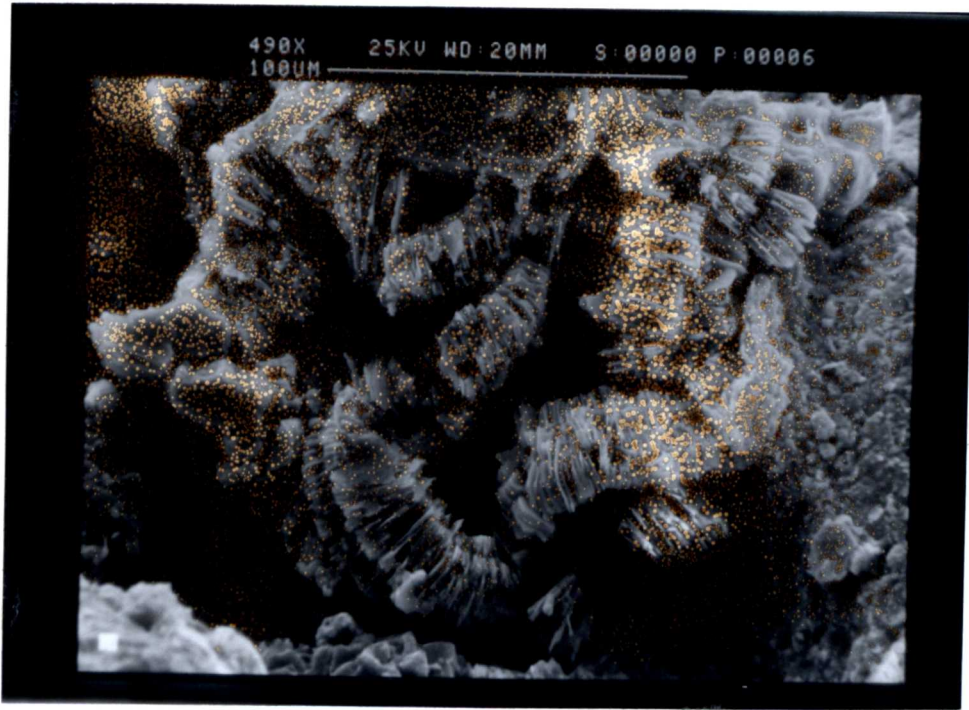


Figure 3.9.c



Figure 3.9.d

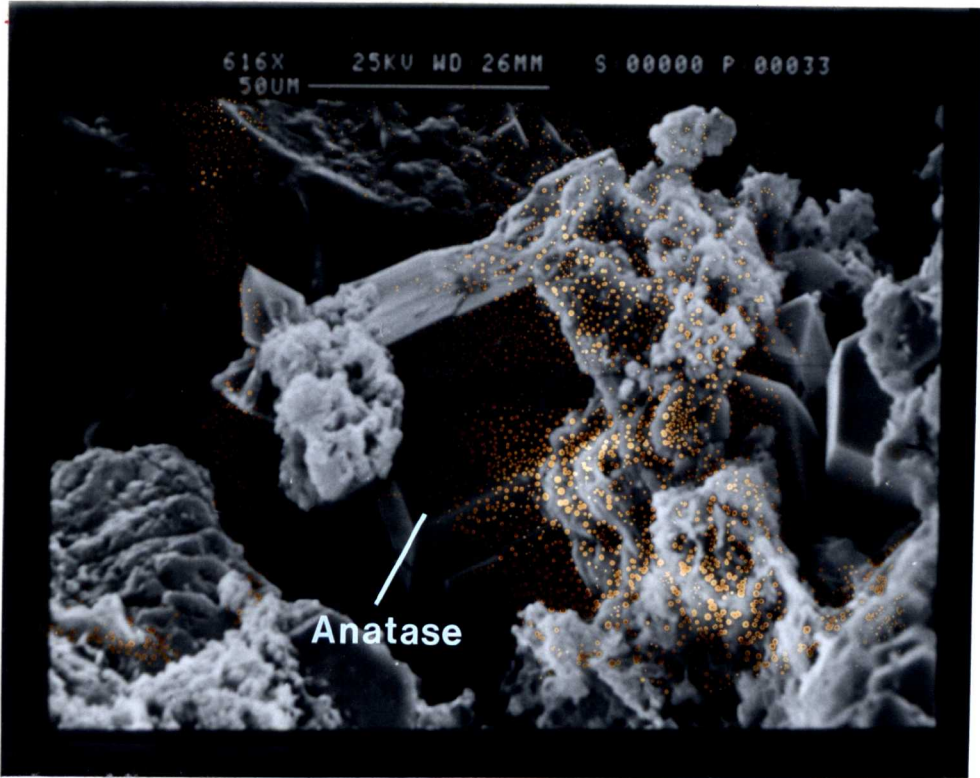


Figure 3.9.e

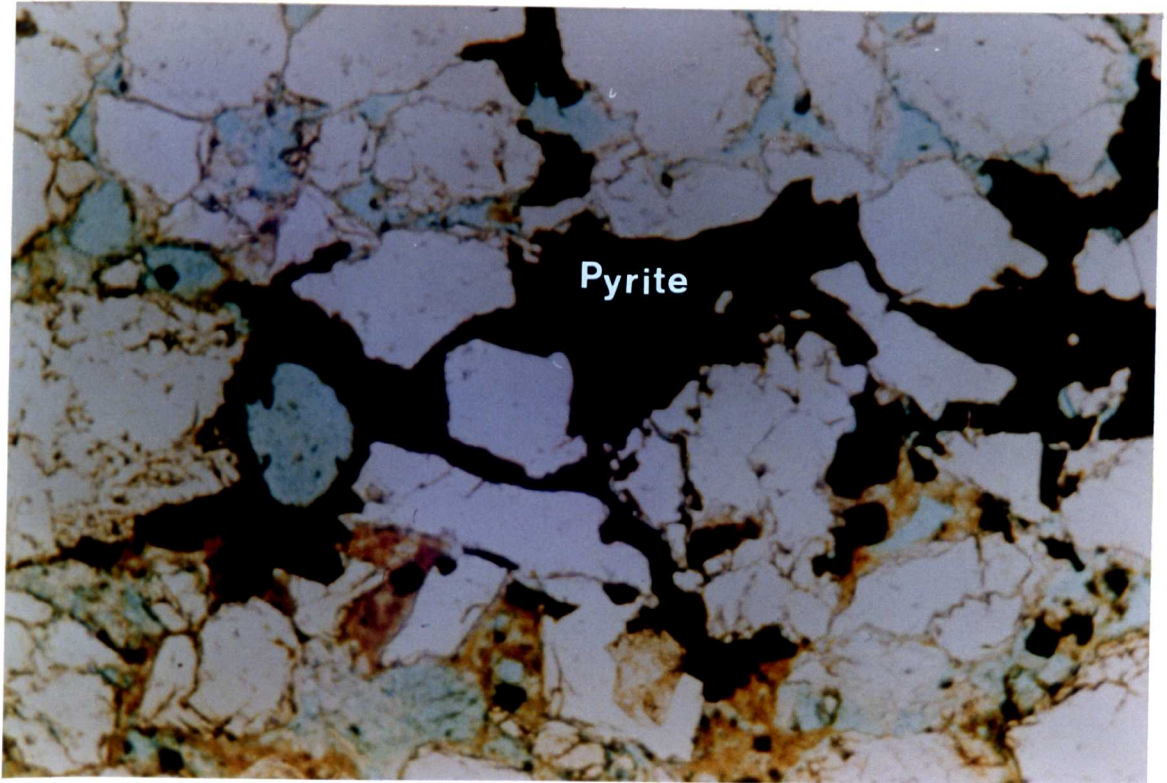


Figure 3.9.f

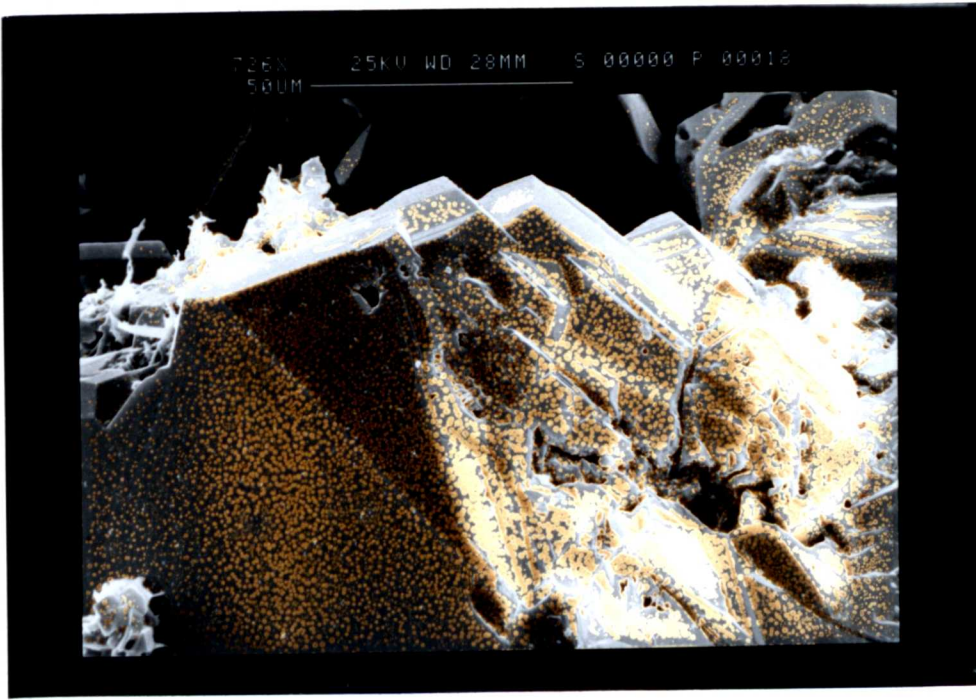


Figure 3.9.g

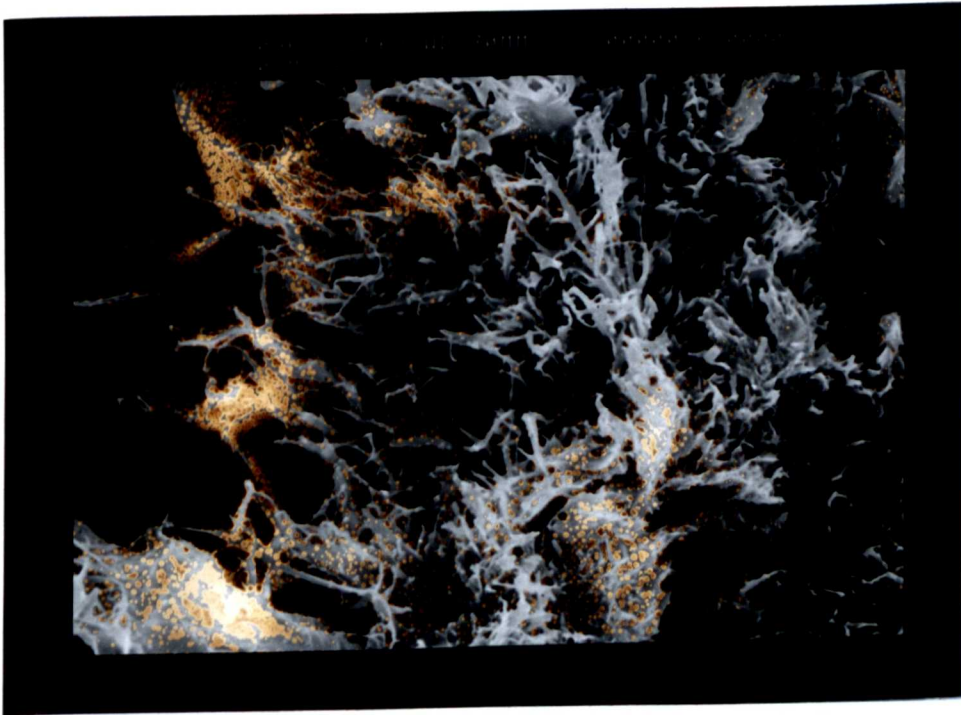


Figure 3.9.h



Figure 3.9.i

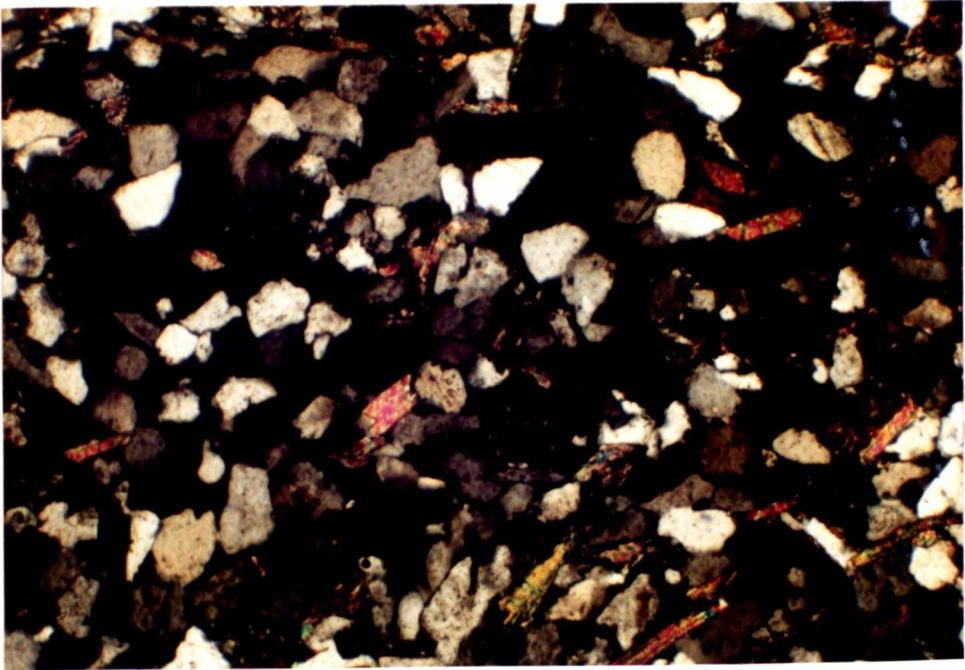


Figure 3.9.j

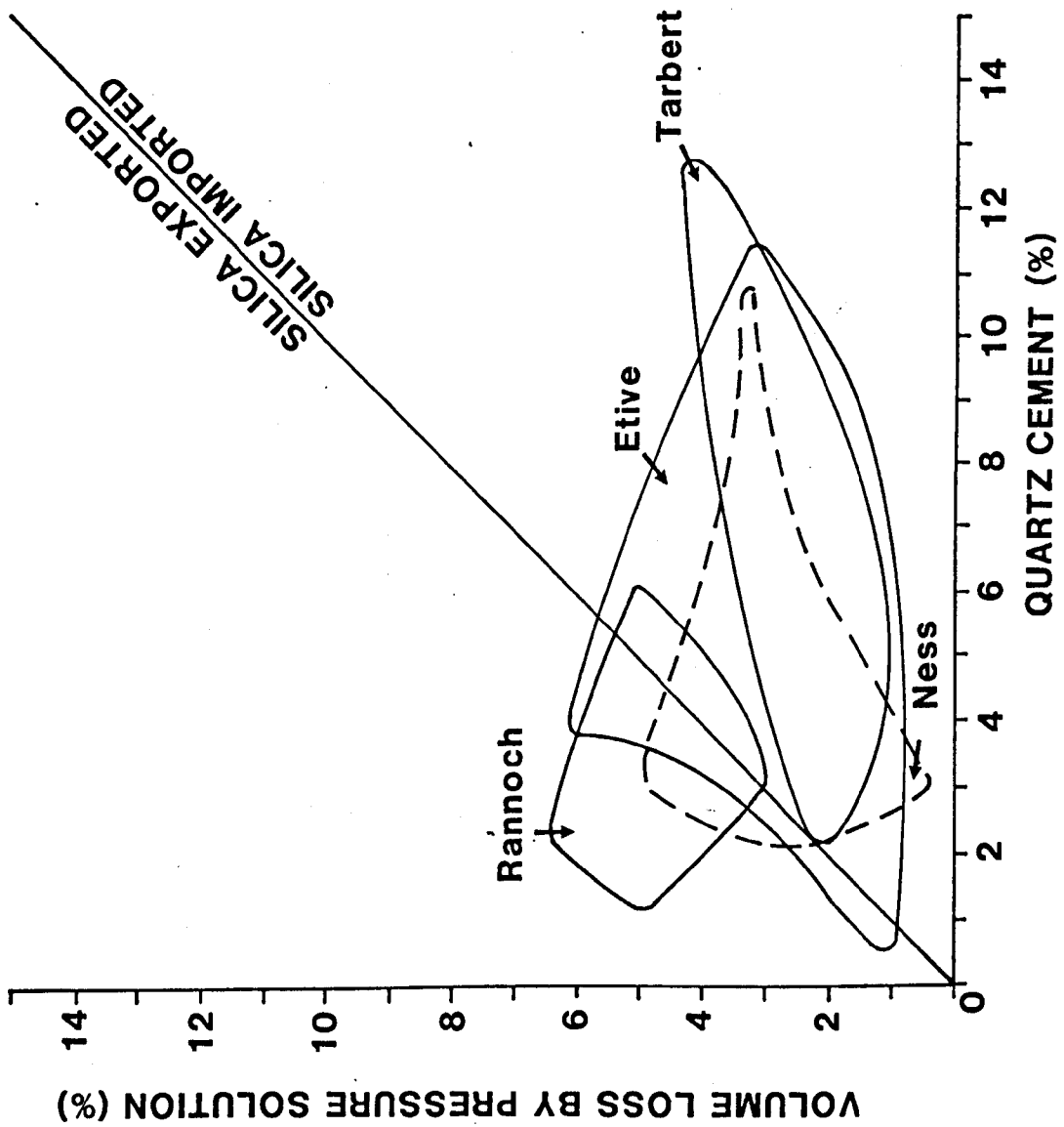
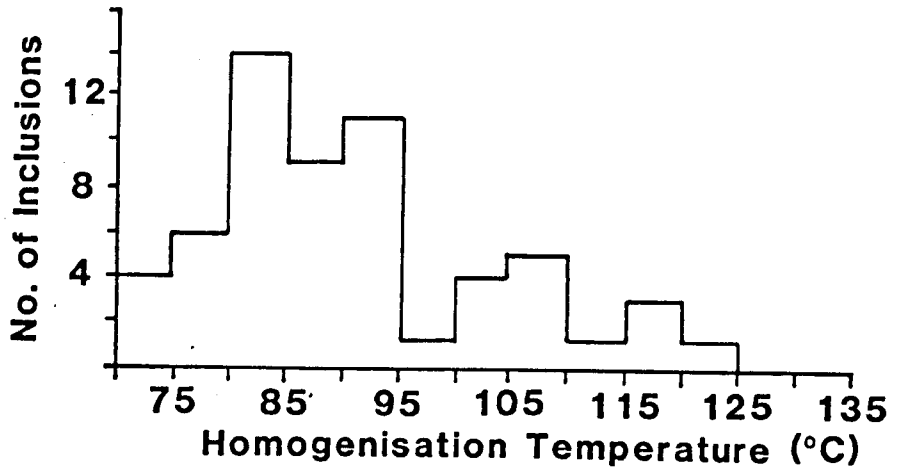
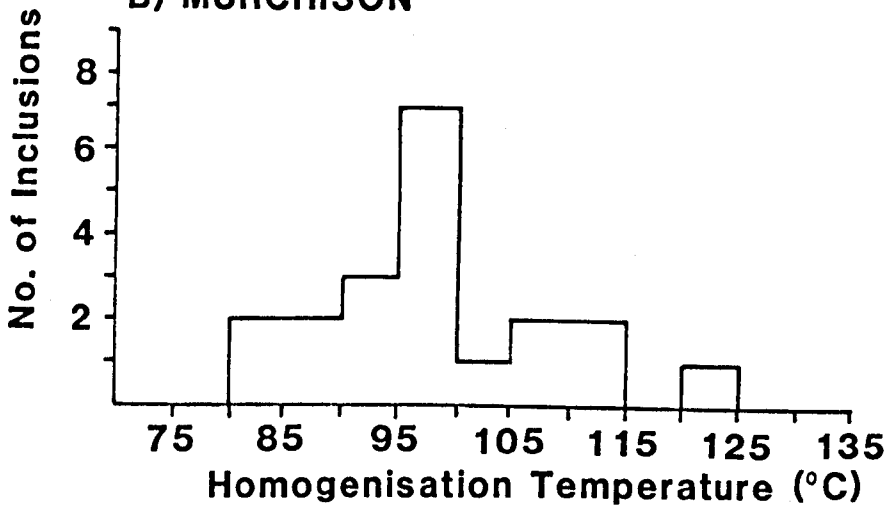


Figure 3.10

A) THISTLE



B) MURCHISON



C) WELL 3/13a-1

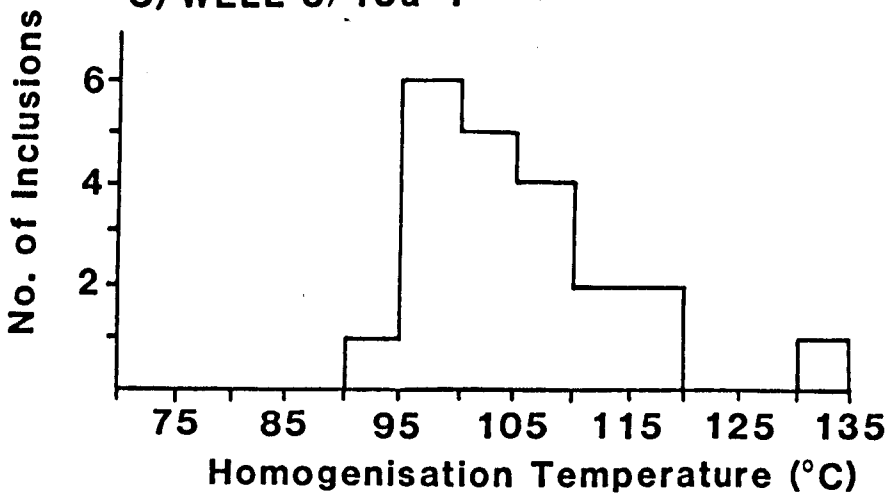
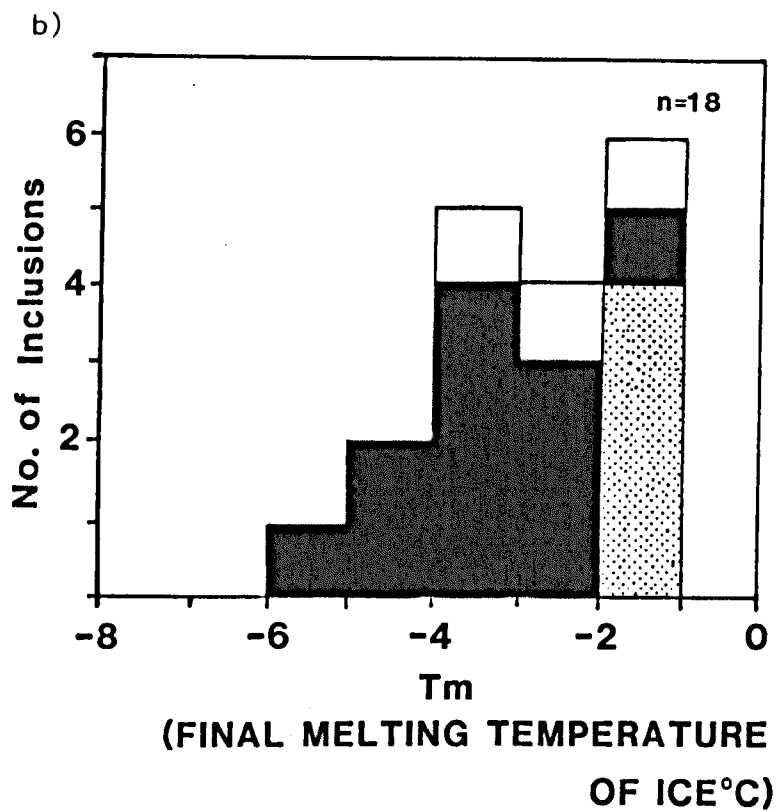
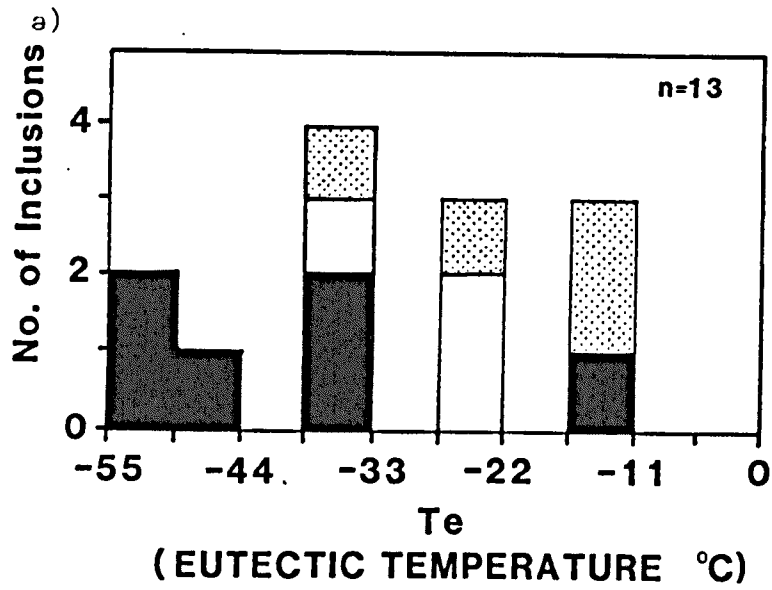


Figure 3.11



Thistle
 Murchison
 3/13a-1

Figure 3.12

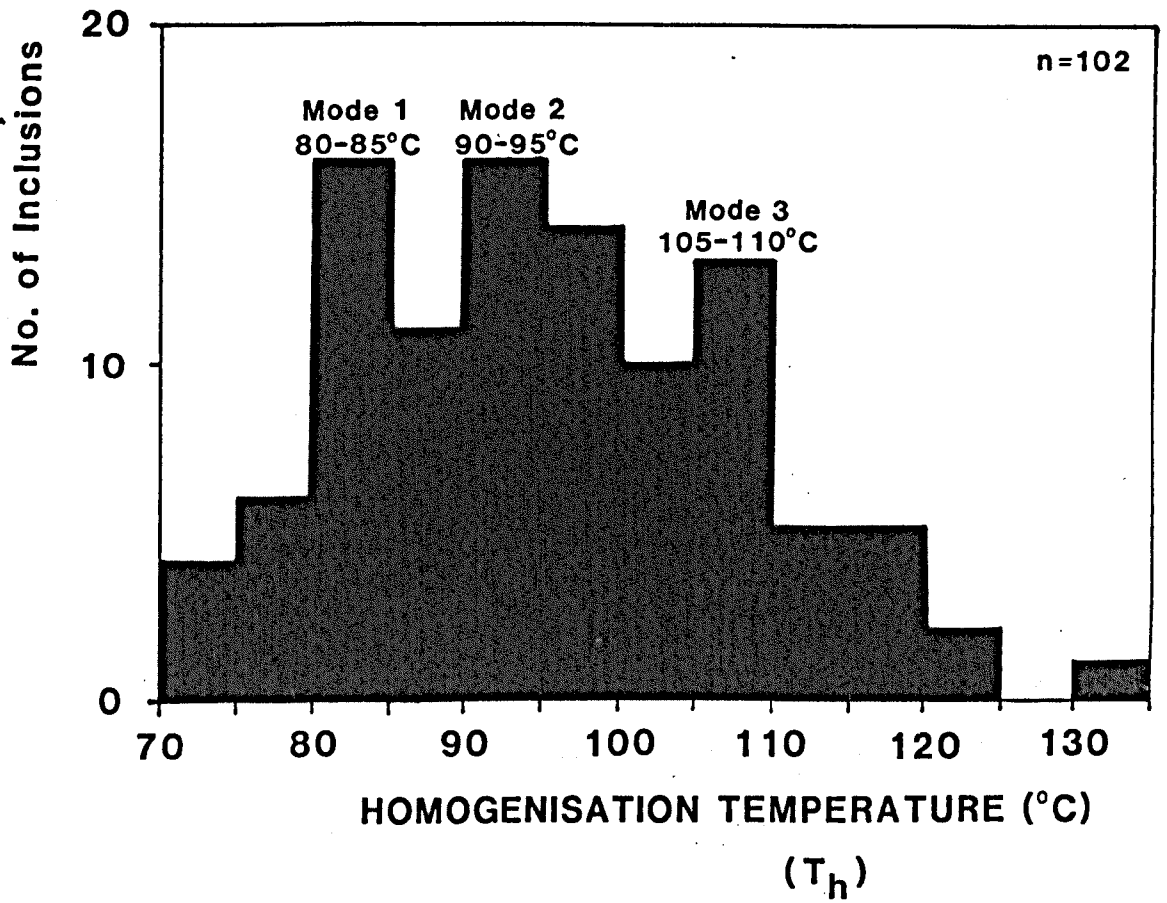


Figure 3.13

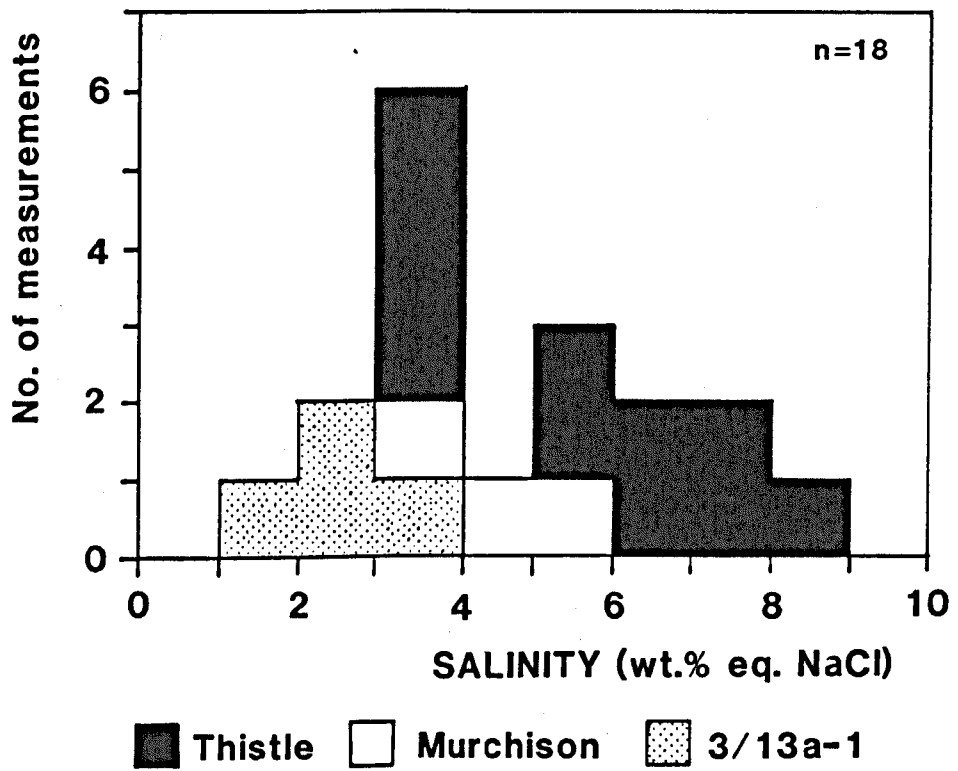


Figure 3.14

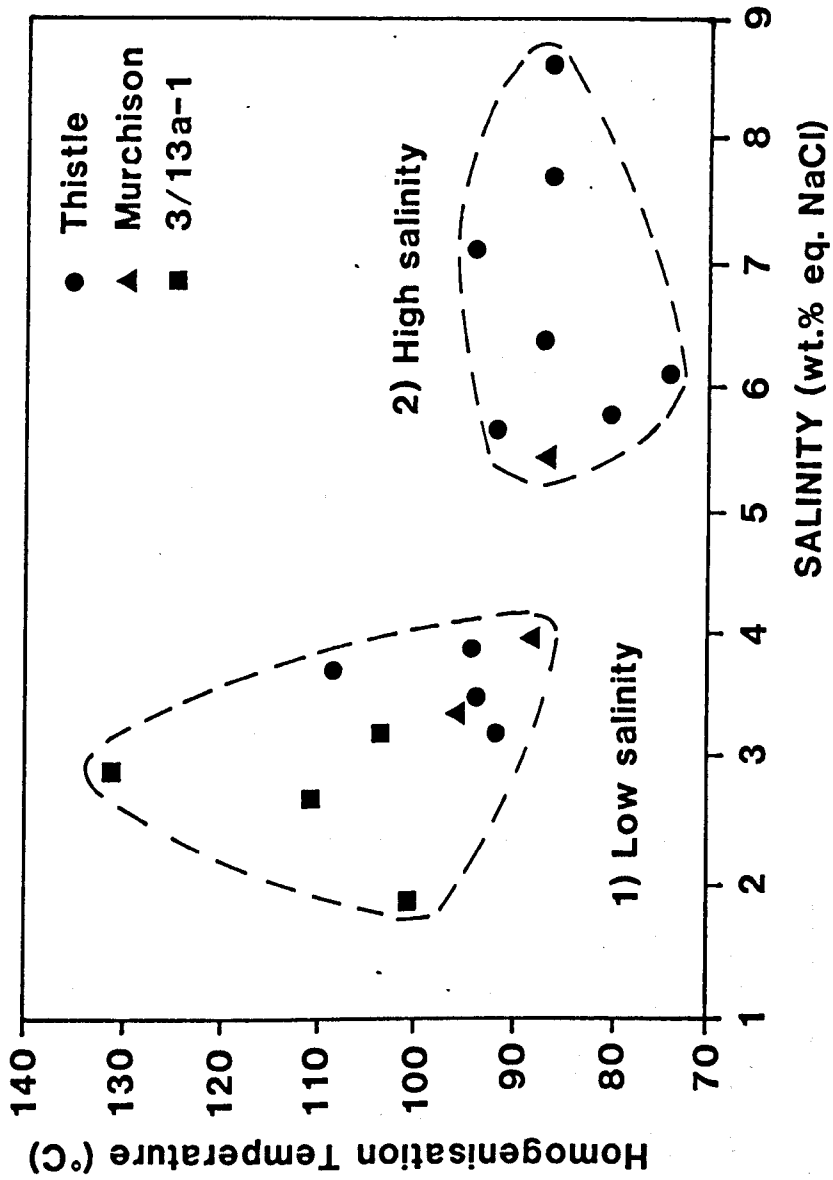


Figure 3.15

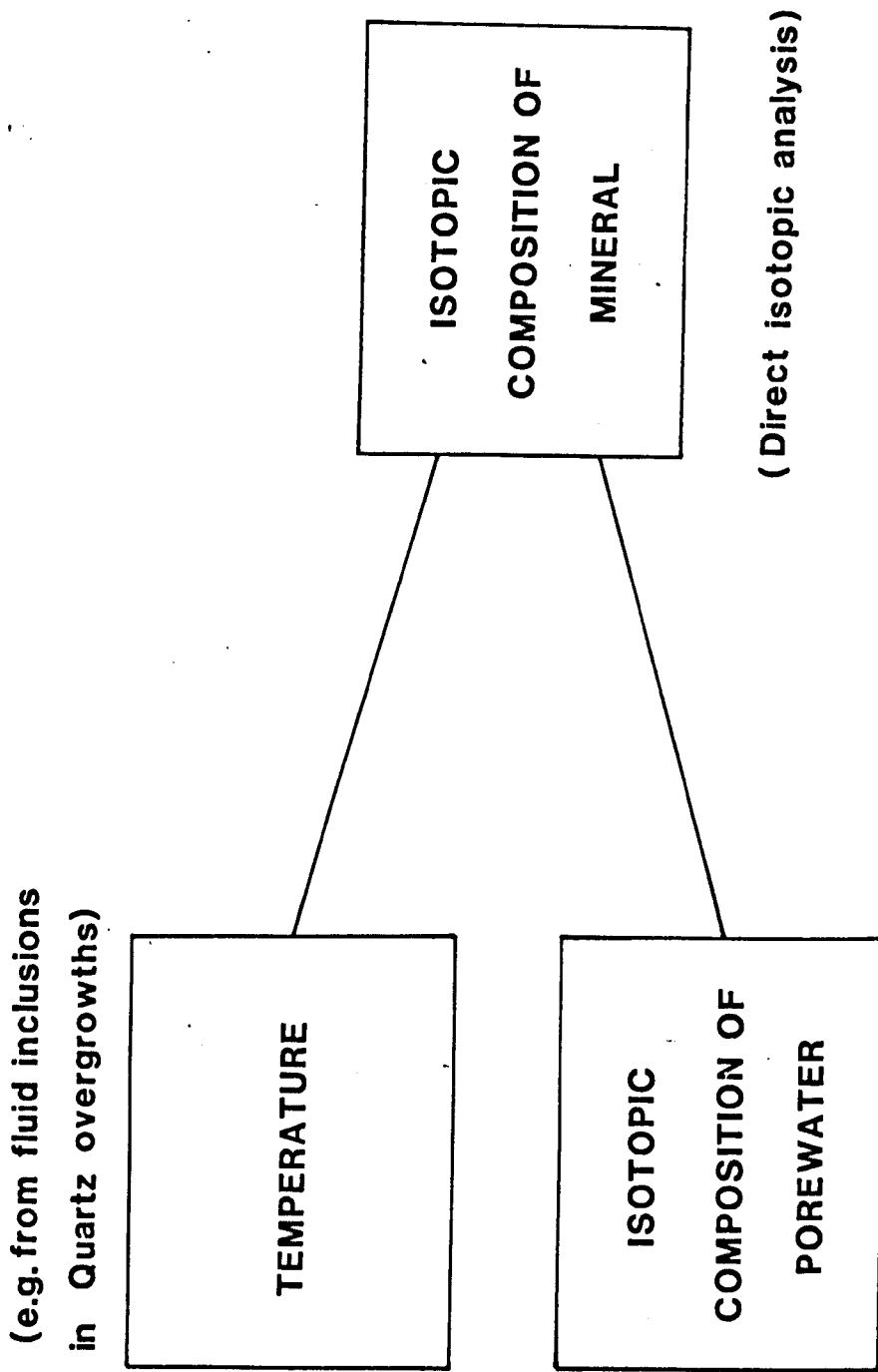


Figure 3.16

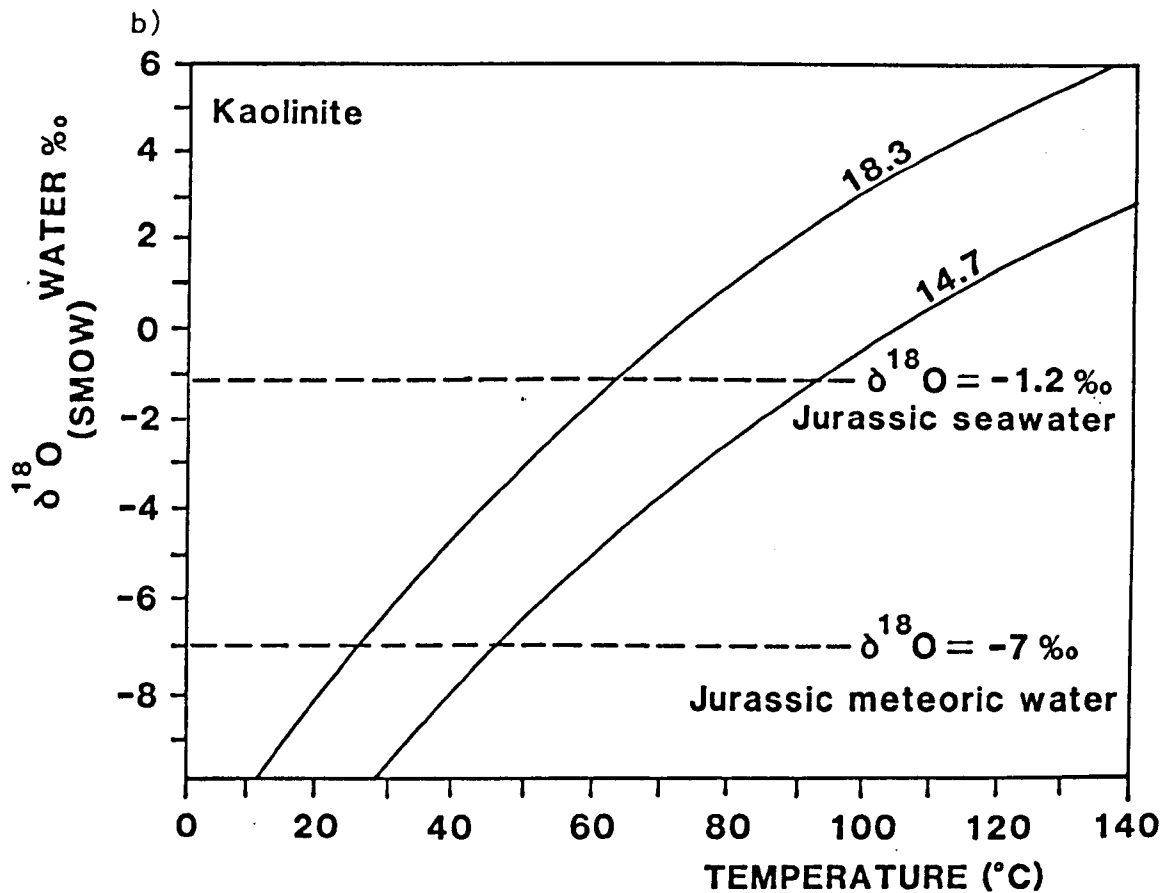
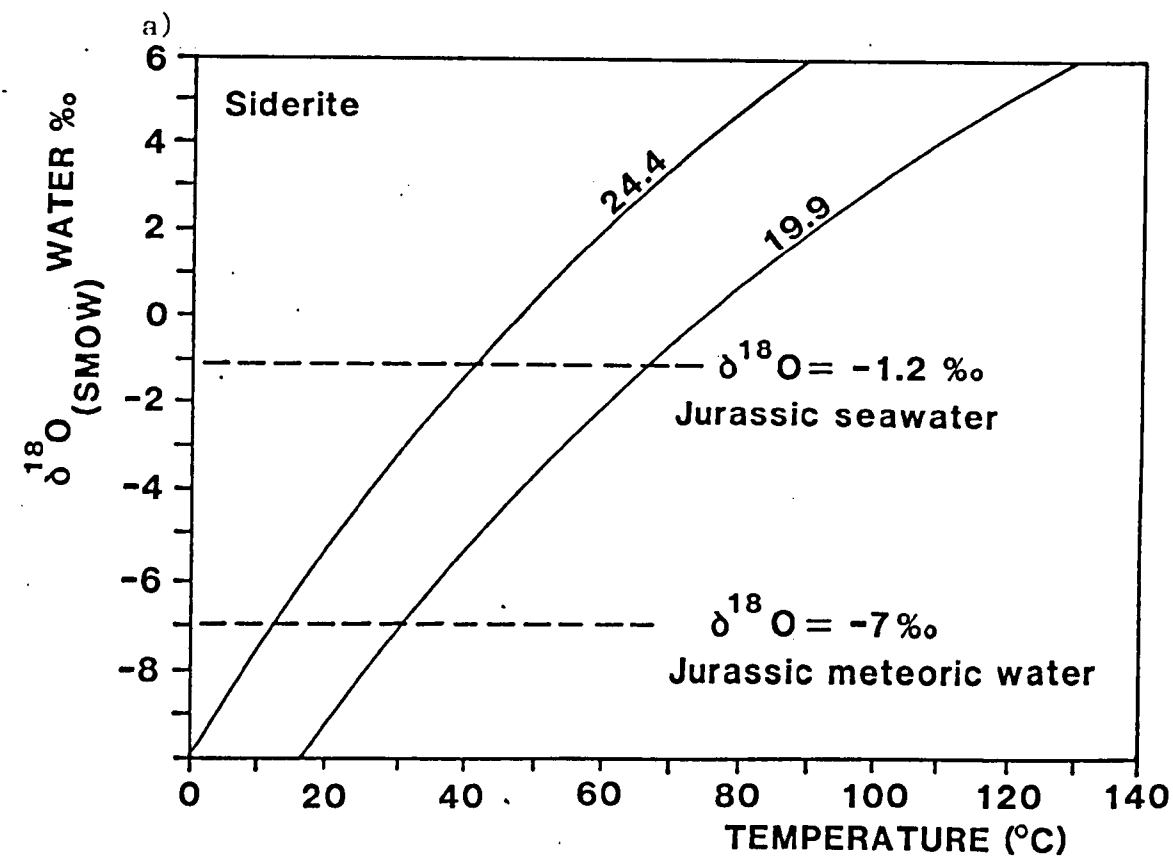


Figure 3.17

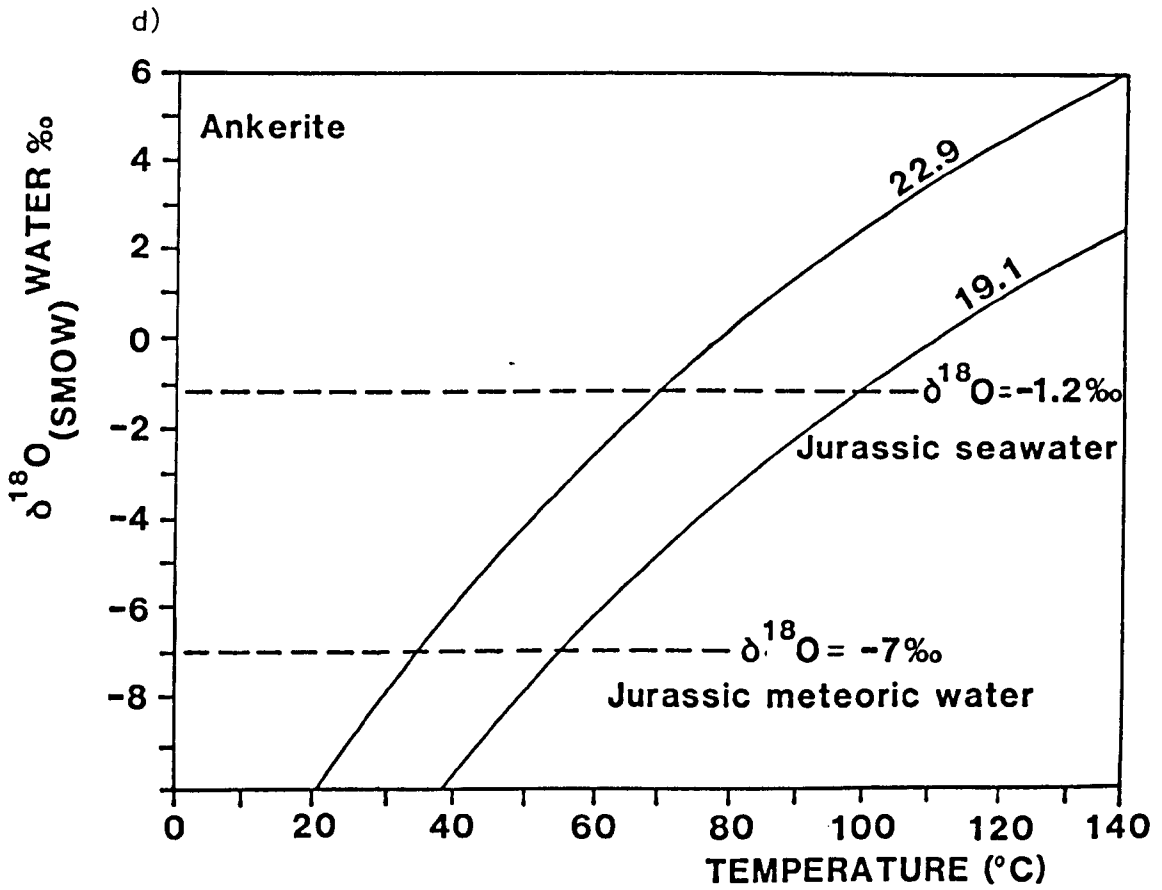
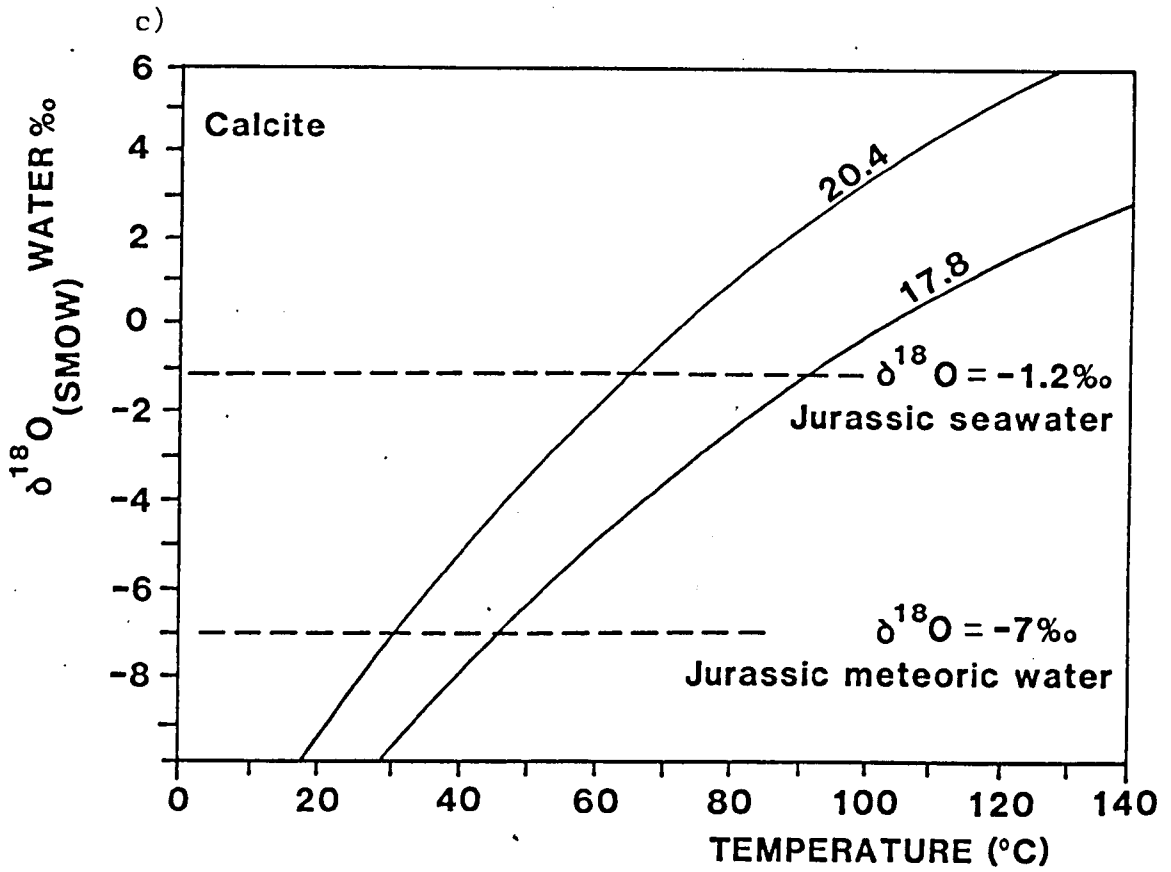


Figure 3.17

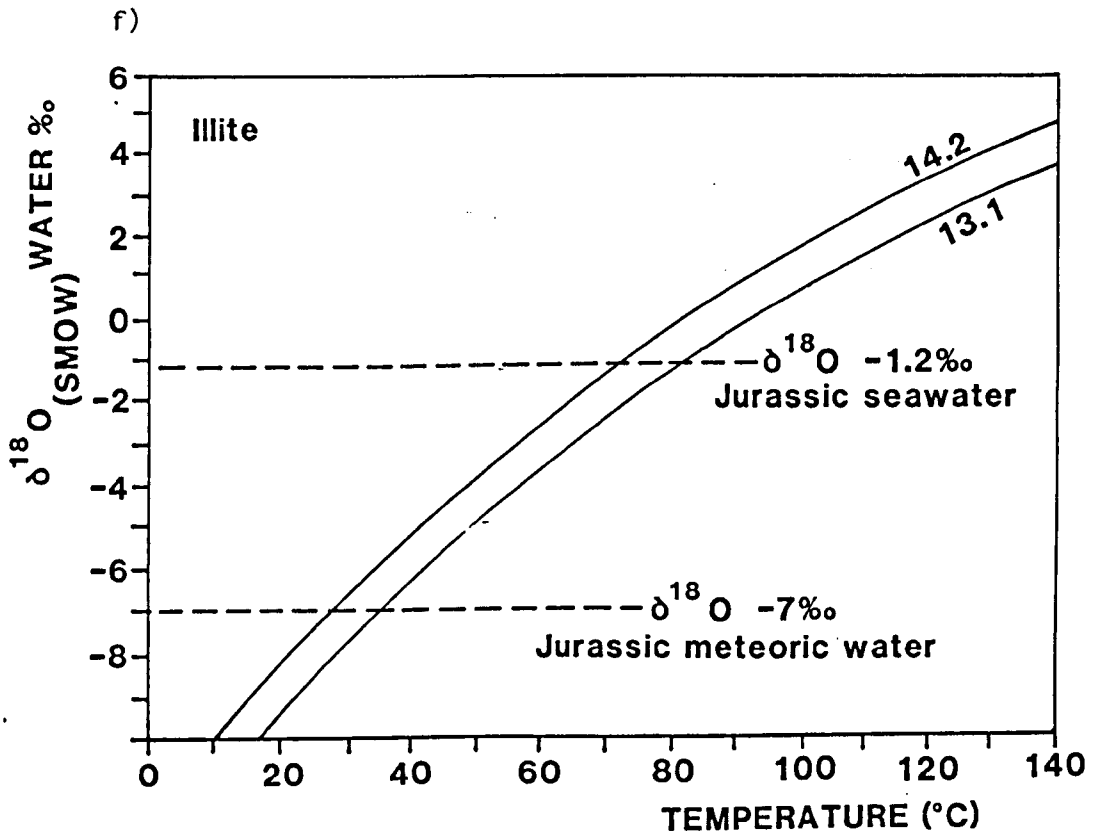
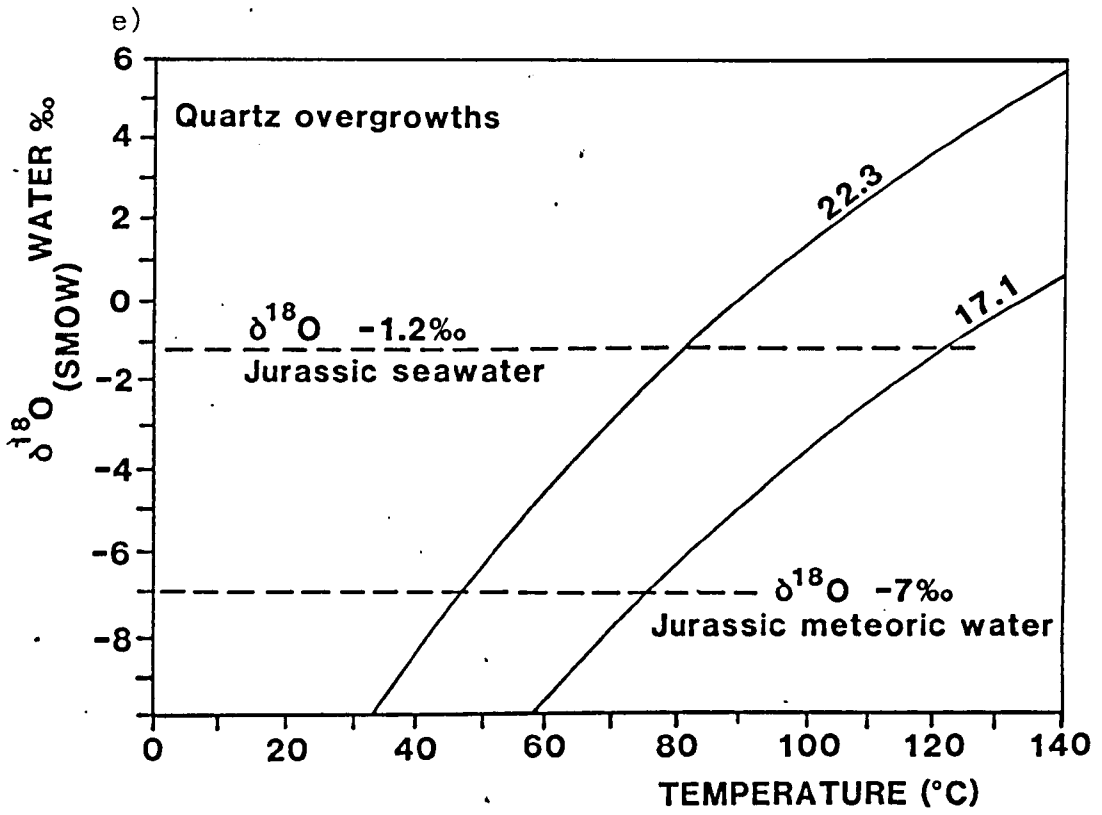


Figure 3.17

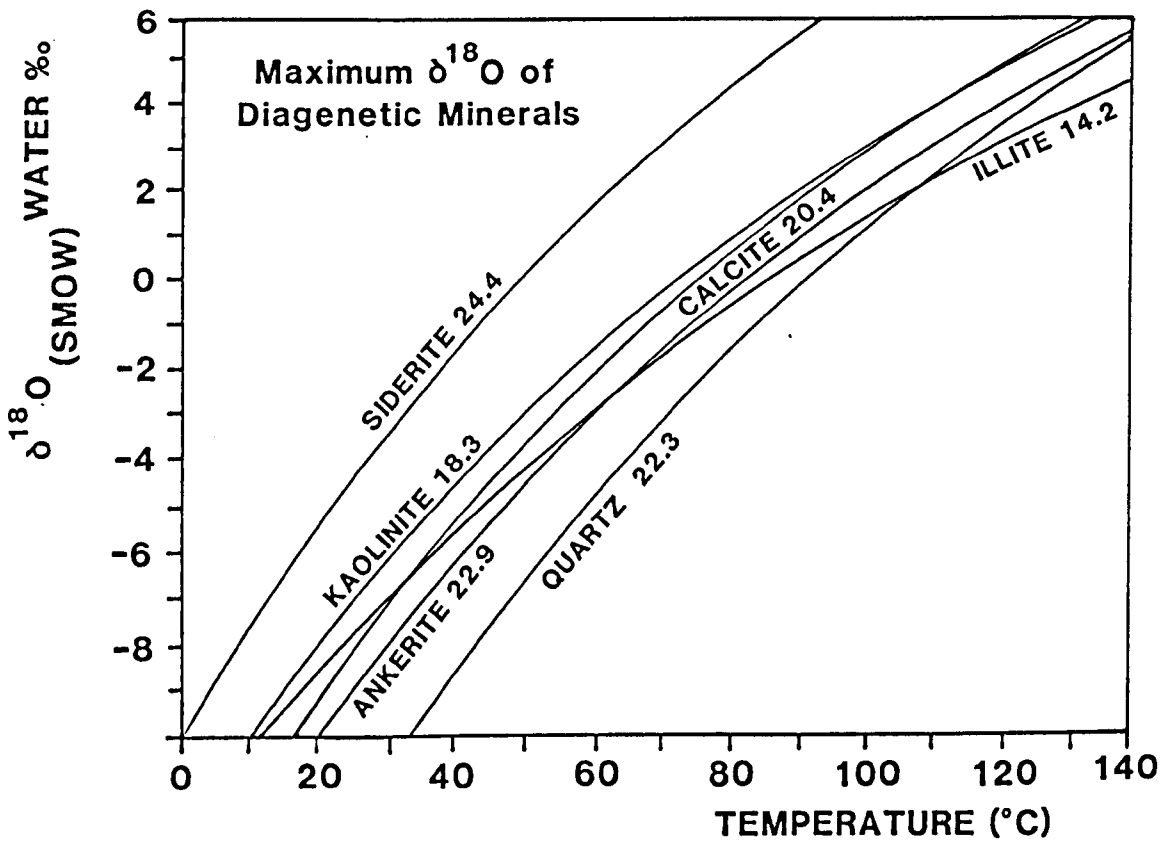
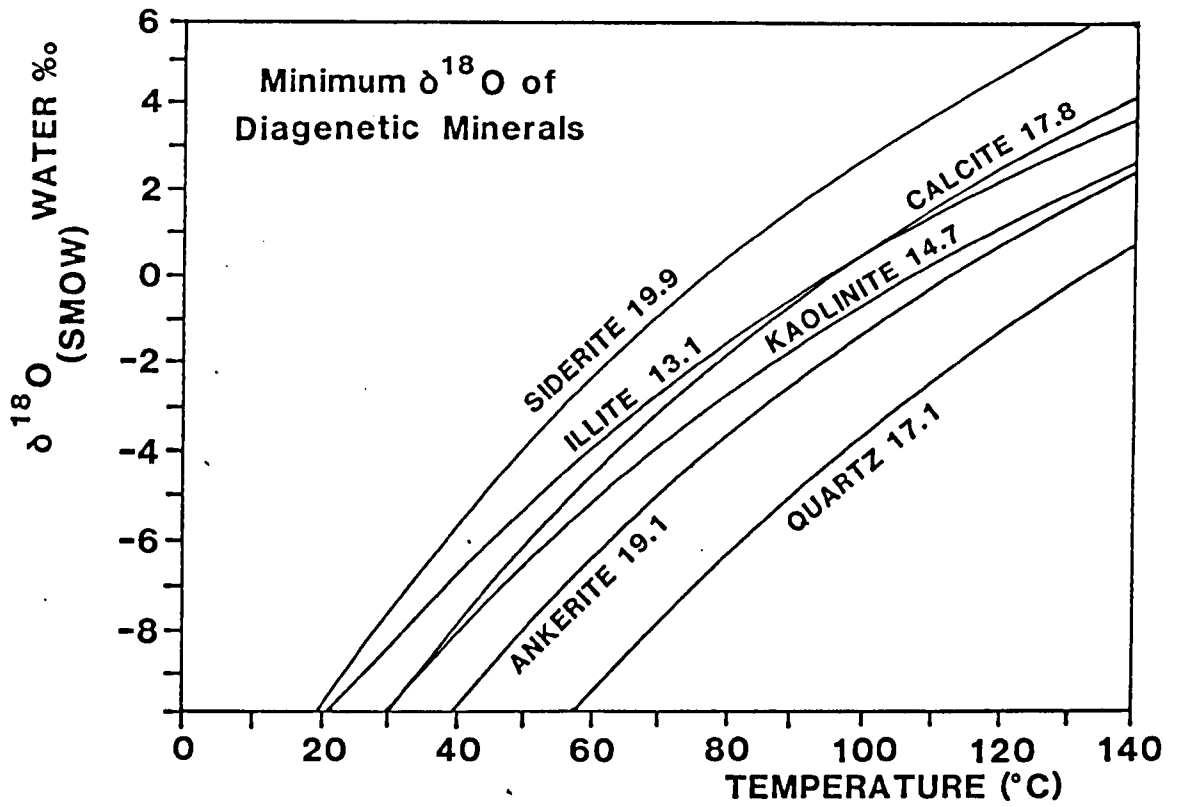


Figure 3.18

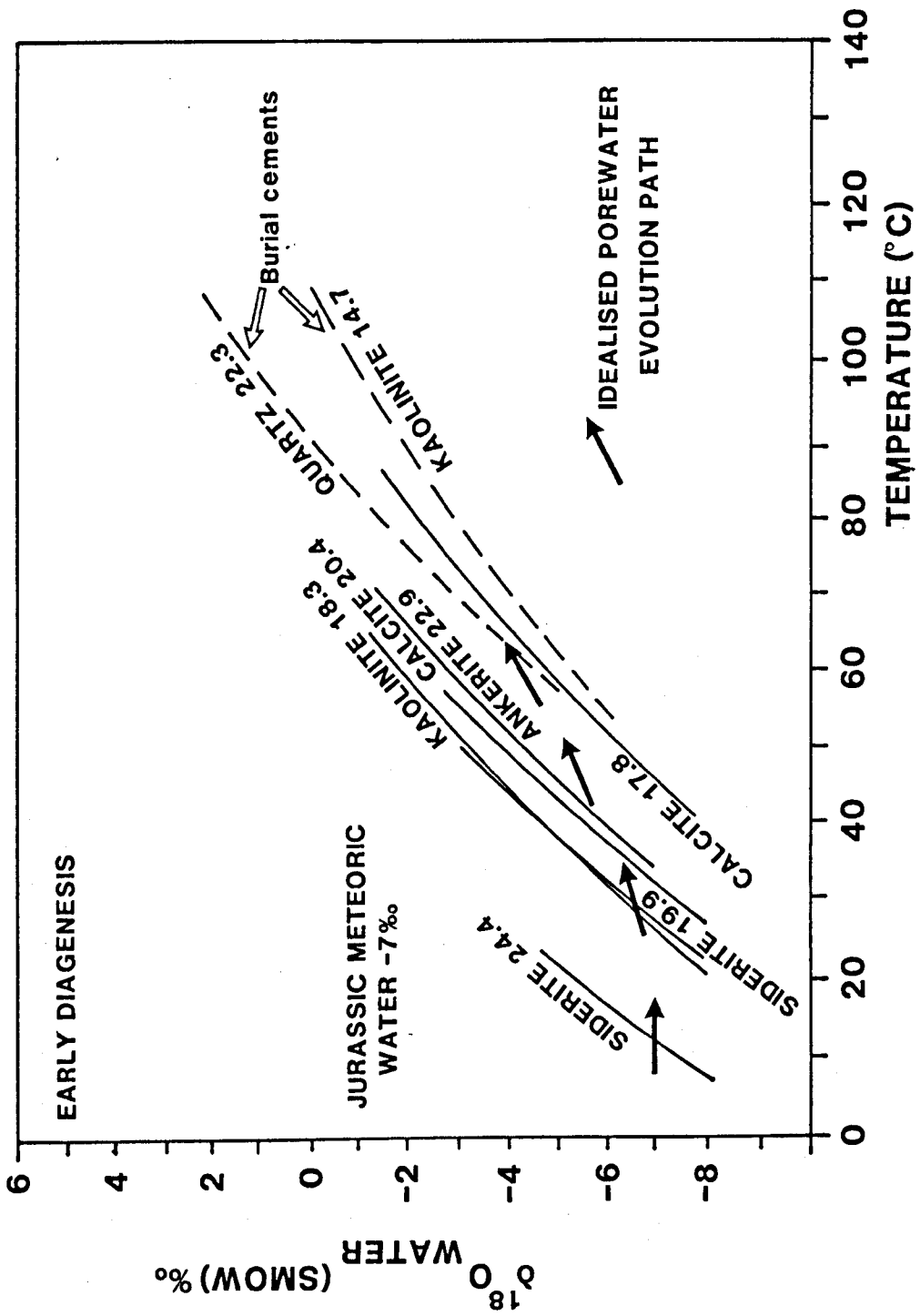


Figure 3.19.a

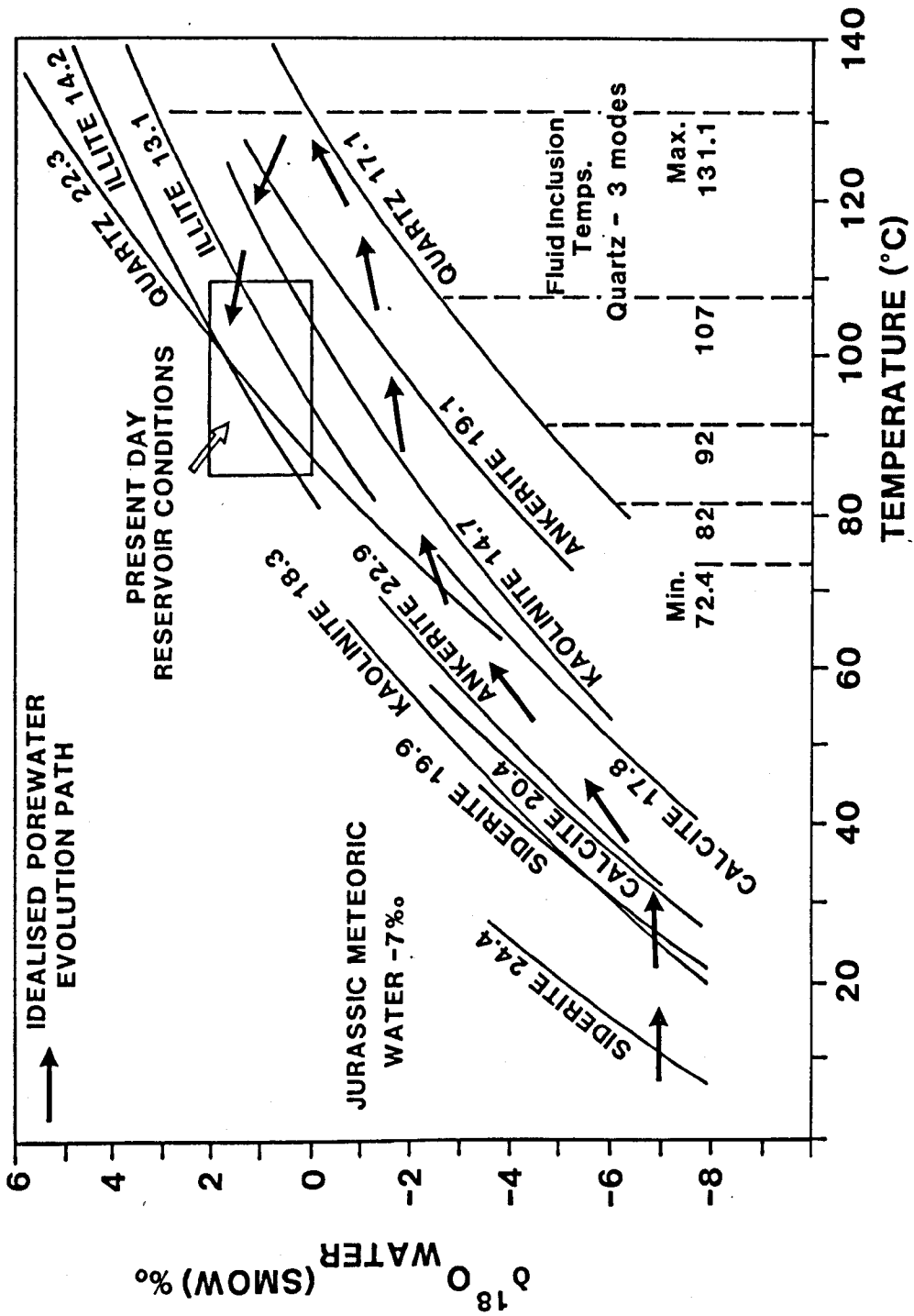


Figure 3.19.b

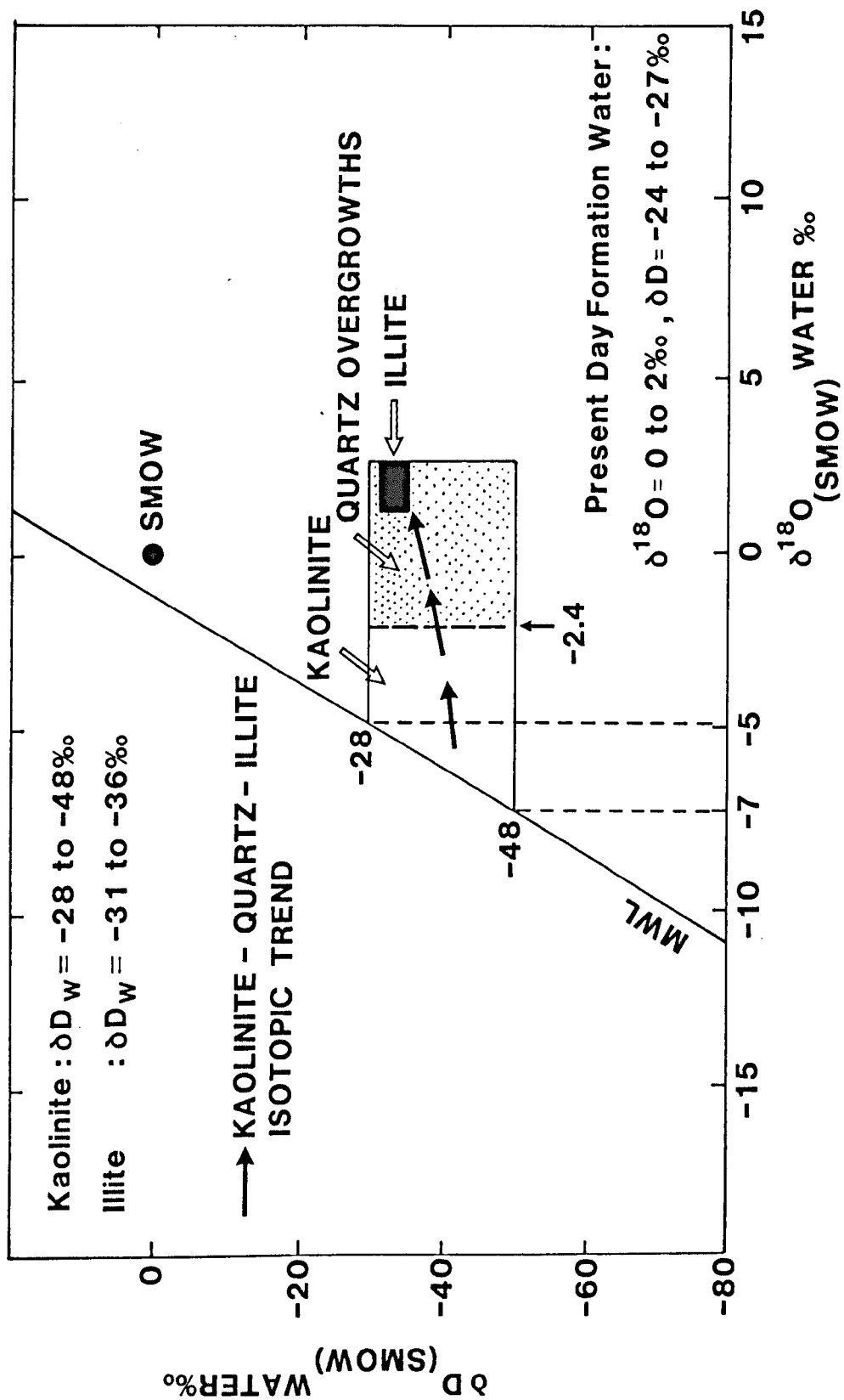


Figure 3.20

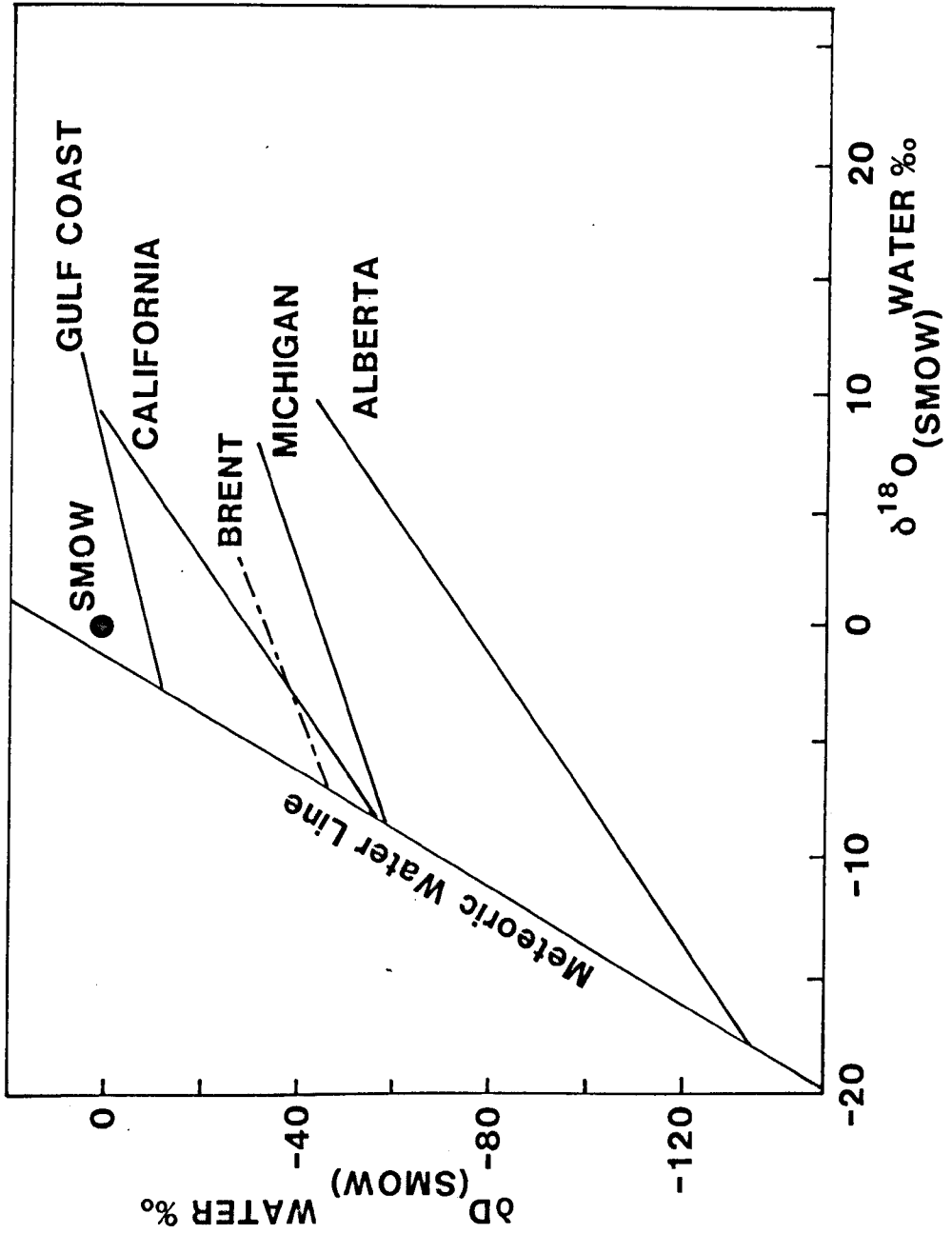


Figure 3.21

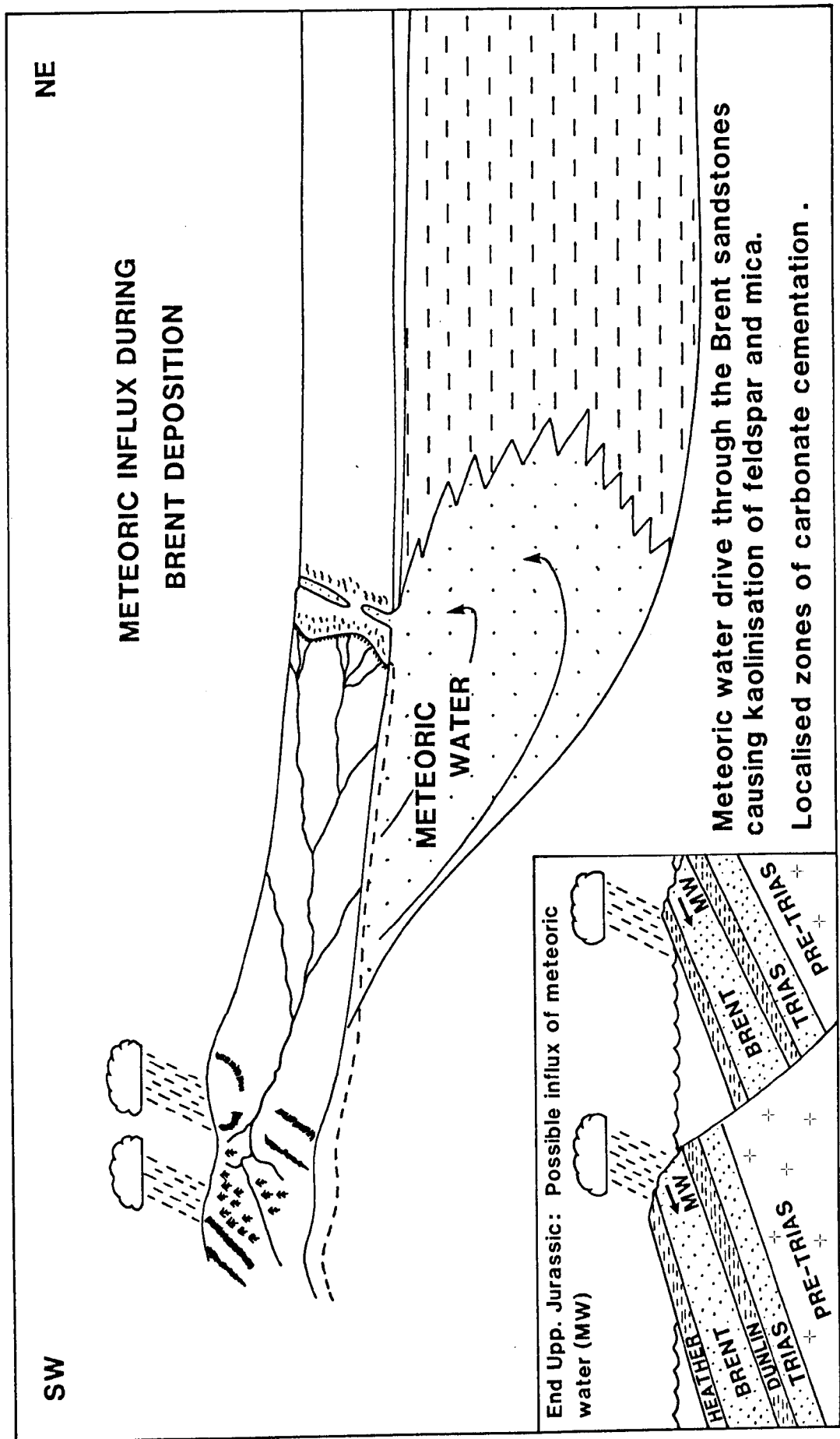


Figure 3.22

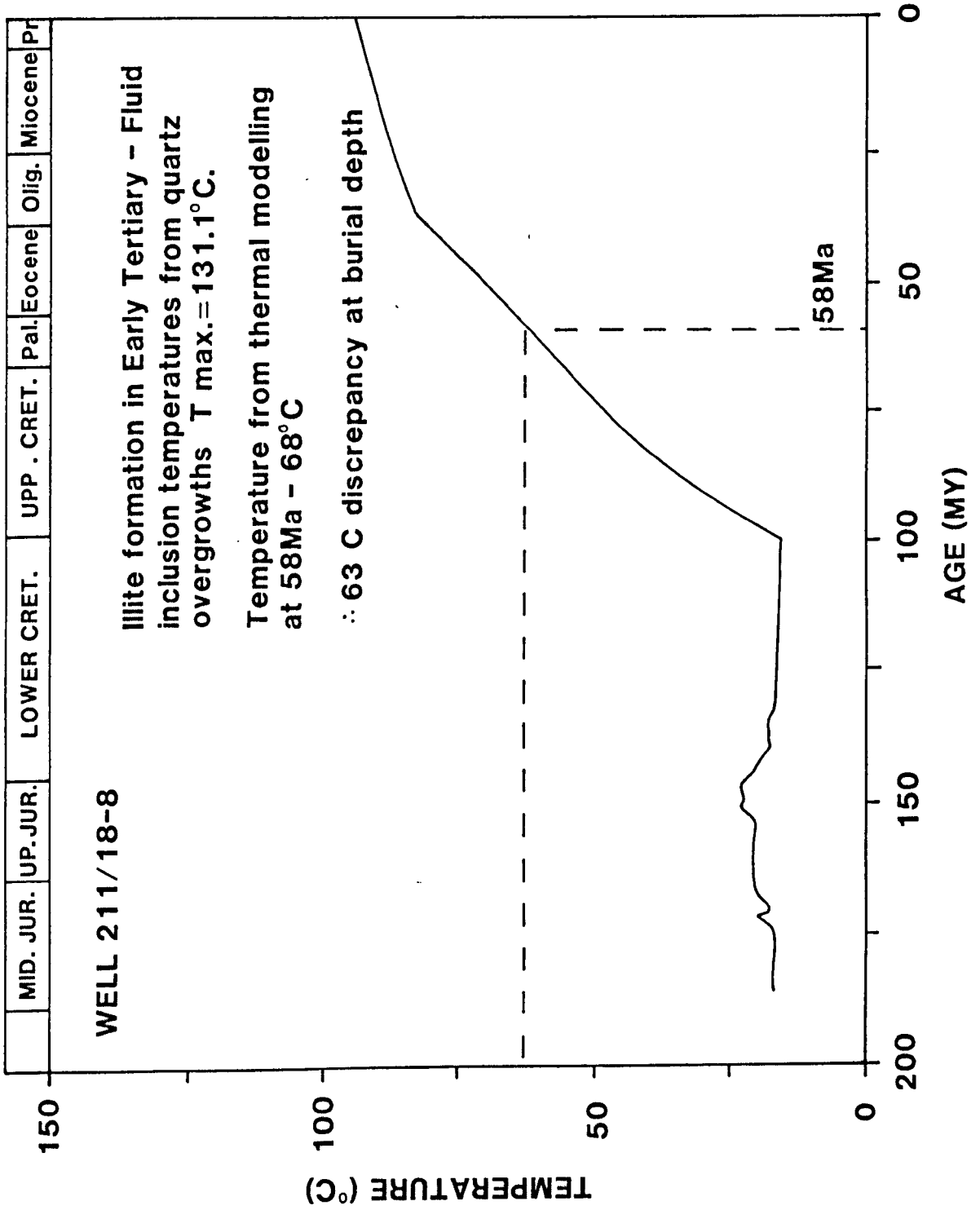


Figure 3.23

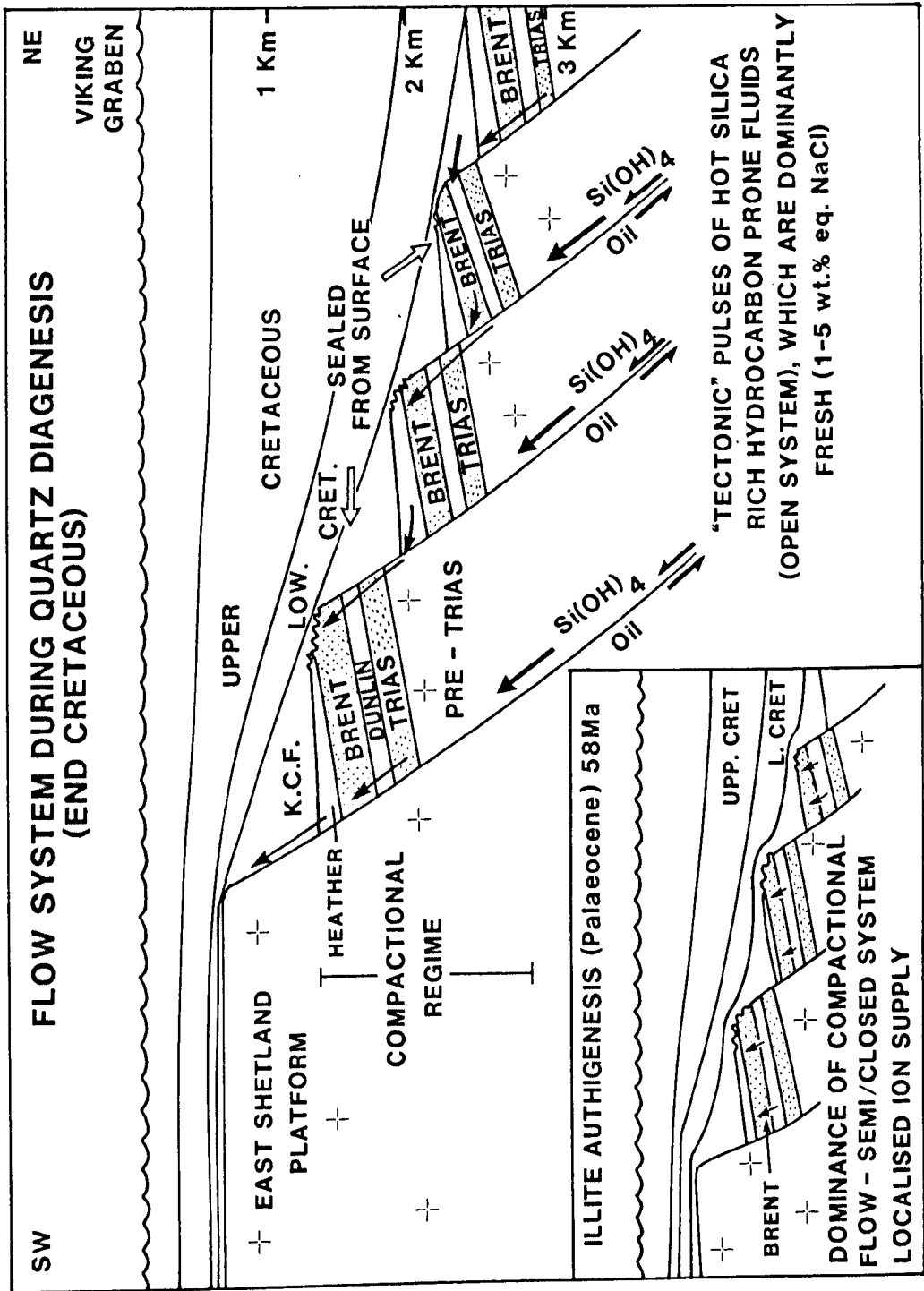


Figure 3.24

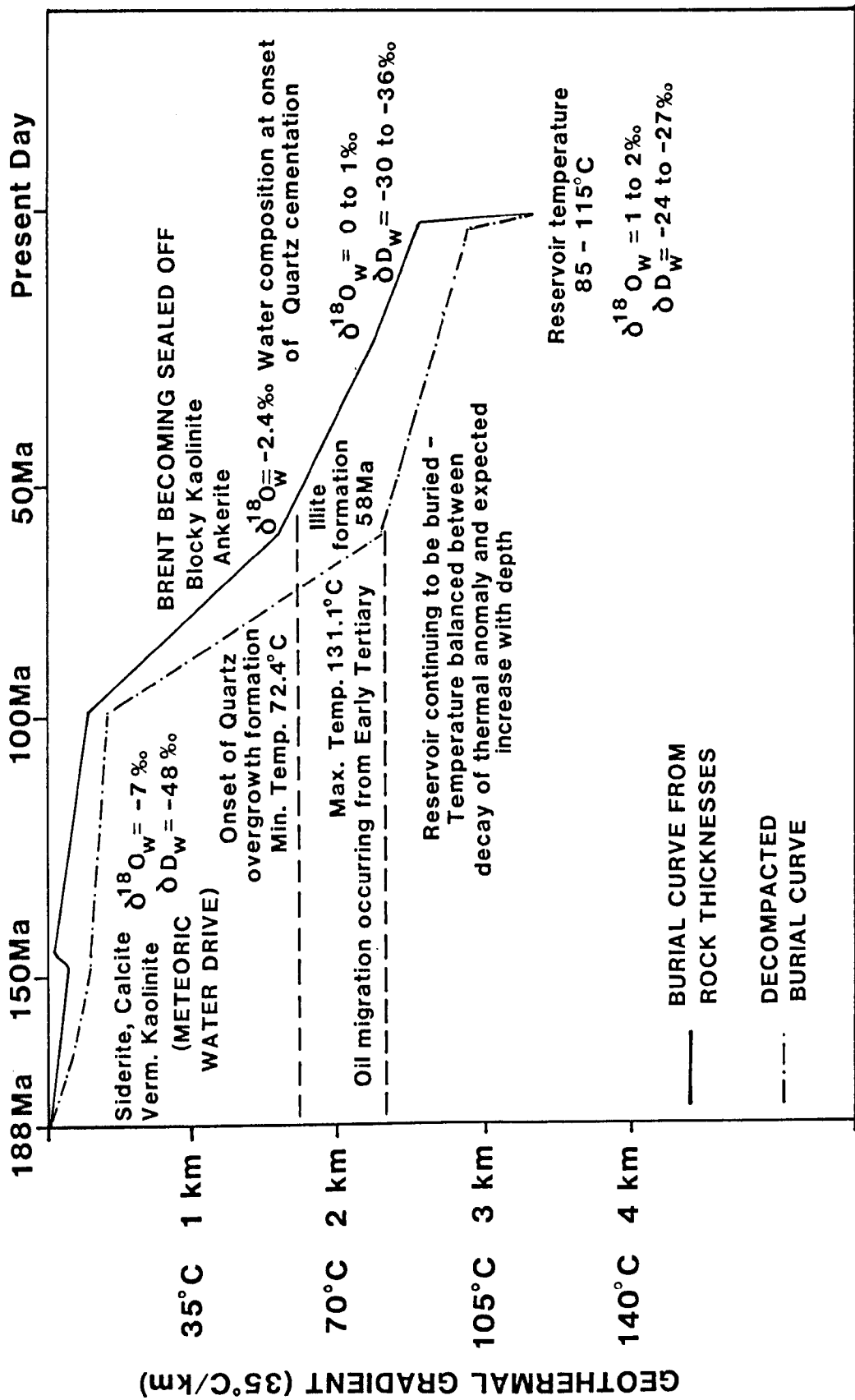


Figure 3.25

TABLE 1: POINT COUNT DATA FOR THE BRENT SANDSTONES STUDIED

WELL	FORMATION	DEPTH (FT)	DEPTH (M)	Av. G.S.	RND.	SPHER.	SORT.	QTZ	PQTZ	KFSP	PLAG	M.R.F	S.R.F	I.R.F	MUSC	BIOT	DET. MATRIX	CLAY	OPAQUES	CARB MAT.	QTZ OG.	KAOL.	ILLITE	CAL.	DOL.	SID.	ANK.	K-FSP OG.	PYR	SPHAL	POROSITY
THISTLE																															
211/18-A30ST	NESS	9116	2778	0.3	A-SR	M-H	POOR	42.0	10.0	4.4	0.6	-	-	-	-	-	1.2	-	-	-	8.2	16.3	-	-	-	2.8	-	tr	0.4	-	14.1
	NESS	9154	2790	0.1	SA-SR	M-H	WELL	50.7	1.6	7.2	0.6	-	-	-	0.8	-	2.6	-	-	-	7.4	12.3	-	-	-	-	-	-	0.6	-	16.2
	NESS	9156	2791	0.2	SA-SR	MOD	WELL	52.1	4.2	8.7	-	-	-	-	-	-	-	-	-	-	7.2	3.0	-	-	-	-	-	-	-	-	24.8
	ETIVE	9223	2811	0.3	SA-SR	L-M	MOD	44.2	13.6	6.2	-	-	-	-	-	-	-	-	-	-	6.0	9.8	-	-	-	-	-	-	-	-	19.6
	ETIVE	9246	2818	0.4	A-SA	MOD	MOD	44.8	17.2	7.8	-	-	-	-	-	-	-	1.8	-	-	-	5.4	6.2	-	-	-	-	-	-	-	16.8
	ETIVE	9278	2828	0.4	SA-SR	M-H	POOR	41.5	23.2	8.8	-	-	-	-	-	2.7	-	1.2	0.6	-	3.6	3.4	-	-	-	-	-	-	-	-	15.0
211/18-A30	RANNOCH	9351	2850	0.1	SA-SR	HIGH	WELL	54.2	7.8	4.1	-	-	-	-	-	-	1.0	0.4	-	-	3.2	5.6	-	-	-	-	-	-	-	-	23.7
	ETIVE	9164	2793	0.4	SR	HIGH	WELL	32.6	27.4	7.2	0.4	1.4	-	-	-	-	-	-	-	-	4.8	7.8	0.2	0.6	-	-	-	-	-	-	17.8
	ETIVE	9187	2800	0.5	SR	HIGH	WELL	31.8	28.4	6.2	0.4	2.2	0.2	-	0.2	0.2	-	-	-	5.4	6.4	0.1	0.8	-	-	-	-	0.4	-	-	16.4
211/18-A31	ETIVE	9227	2812	0.3	SA-SR	M-H	MOD	33.2	30.0	7.6	0.6	1.2	0.2	0.2	1.4	0.4	-	-	-	-	5.8	4.2	-	0.4	-	0.2	-	-	-	-	14.8
	NESS	8994	2741	0.4	SR-SA	M-W	WELL	48.6	10.2	7.0	0.6	2.8	-	-	0.8	-	-	-	-	-	4.6	14.8	-	-	-	0.2	-	-	0.2	-	10.2
	ETIVE	9042	2756	0.4	SR-R	MOD	M-W	50.2	12.4	4.4	-	1.4	-	-	0.4	-	-	-	-	-	5.4	7.8	-	0.6	-	-	-	-	-	-	17.4
211/18-A45	ETIVE	9072	2765	0.3	SA-SR	M-H	MOD	45.8	14.0	5.6	0.6	1.4	-	-	0.6	0.2	-	-	-	-	3.4	15.8	-	-	-	0.6	-	-	0.8	-	11.2
	ETIVE	9081	2768	0.2	SR	L-M	MOD	49.3	4.3	4.7	0.3	1.3	0.3	0.3	0.4	0.7	-	-	-	-	4.7	11.4	-	-	-	0.7	-	-	-	-	21.6
	ETIVE	8624	2628	0.1	SA-SR	HIGH	WELL	43.8	2.8	5.4	0.6	1.0	-	-	0.4	1.6	-	-	-	-	9.4	11.8	-	0.4	-	0.8	-	-	0.6	-	21.4
	ETIVE	8629	2630	0.3	SA-R	HIGH	MOD	52.4	10.0	3.4	0.4	0.2	-	-	-	-	-	-	-	-	3.6	5.2	-	0.2	-	0.2	-	-	-	-	24.4
	ETIVE	8631	2631	0.4	SA-SR	M-H	POOR	49.2	2.2	3.2	0.2	1.0	-	-	0.8	0.2	-	-	-	0.4	1.8	14.4	1.2	3.6	-	0.6	-	-	1.2	-	20.0
211/18-A33	ETIVE	8643	2634	0.4	SA-SR	M-H	POOR	51.6	7.0	3.8	-	1.2	-	-	-	-	-	-	-	-	4.8	3.6	-	0.4	-	-	-	0.4	-	27.4	
	ETIVE	8651	2637	0.3	A-SA	MOD	MOD	40.4	13.0	6.6	-	0.6	-	-	2.2	-	0.2	-	-	-	5.8	8.8	-	0.4	-	3.2	-	-	0.6	-	18.2
	NESS	8919	2718	0.5	SA-SR	MOD	WELL	49.0	15.0	7.0	0.7	1.7	-	-	-	-	0.3	-	-	-	5.0	3.0	-	0.3	-	-	-	-	-	-	18.0
	ETIVE	8985	2738	0.4	SA-SR	HIGH	WELL	39.3	24.0	6.7	-	3.0	-	-	0.7	-	-	-	-	-	5.3	6.7	-	-	-	-	-	-	-	-	14.3
	ETIVE	8999	2743	0.3	A-SA	MOD	HIGH	35.6	21.0	8.3	1.3	4.0	-	-	1.7	-	0.7	-	-	-	3.7	10.7	-	-	-	-	-	-	-	-	13.0
RANNOCH	9105	2775	0.1	SA-SR	L-M	HIGH	58.0	8.0	6.3	0.3	2.7	-	-	4.3	1.0	-	-	-	-	1.0	4.0	-	0.7	-	2.0	-	-	0.7	-	10.7	
RANNOCH	9122	2780	0.1	SA-SR	L-M	HIGH	50.3	7.7	4.0	0.7	1.7	-	-	11.1	6.6	-	-	-	-	1.0	5.7	-	1.7	-	2.7	-	-	1.0	-	6.0	

WELL	FORMATION	DEPTH (FT)	TVD (M)	Av. G.S.	RND.	SPHER.	SORT.	QTZ	PQTZ	K-FSP	PLAG	M.R.F	S.R.F.	I.R.F	MUSC	BIOT	NET. CLAY MATRIX	OPAQUES	CARB. MAT.	QTZ OG.	KAOL.	ILLITE	CAL.	DOL.	SID.	ANK.	K-FSP OG.	PYR	SPHAL	POROSITY	
MURCHISON																															
211/19-3	NESS	10155	3095	0.5	SR-R	M-H	WELL	39.0	24.6	3.6	0.6	0.6	-	-	-	0.4	-	-	-	3.8	17.2	-	0.8	-	0.8	-	tr	1.6	0.6	4.4	
	NESS	10188	3105	0.3	SR	M-H	MOD	47.6	18.4	3.4	-	0.8	-	-	-	-	0.6	-	-	3.0	17.8	-	0.6	-	0.2	-	-	0.6	-	7.0	
	ETIVE	10300	3139	0.3	SA-SR	L-M	WELL	55.0	11.2	4.6	0.2	0.2	-	0.2	1.4	-	-	-	-	2.6	14.0	-	1.6	-	-	-	tr	-	-	9.0	
	ETIVE	10331	3148	0.2	SA-SR	MOD	MOD	39.2	24.8	7.0	0.4	1.0	0.2	-	1.4	-	0.2	-	-	2.4	14.6	-	0.4	-	-	-	-	-	-	8.4	
211/19-4	NESS	9884	3012	0.3	A-SA	L-M	MOD	60.0	6.0	3.7	-	1.3	-	-	2.0	-	1.7	-	-	6.0	4.3	-	0.7	-	0.3	-	-	-	-	14.0	
	NESS	9922	3024	0.4	SR-R	HIGH	M-W	56.2	12.2	4.2	-	0.6	-	-	-	-	0.8	-	0.2	5.0	4.4	-	0.2	-	-	-	-	-	-	16.2	
	NESS	9967	3038	0.3	SR	M-H	POOR	48.7	12.7	8.3	-	1.3	-	-	1.0	-	2.0	-	-	3.3	7.3	-	-	-	-	-	-	-	-	15.4	
	ETIVE	9993	3048	0.3	A-SA	MOD	MOD	52.0	7.0	4.3	1.0	1.3	-	-	-	-	-	-	-	5.0	11.4	-	1.7	-	-	-	-	1.0	-	15.3	
	ETIVE	10027	3056	0.3	SA-SR	MOD	MOD	59.3	8.7	1.7	-	-	-	-	0.7	-	3.0	-	-	3.3	10.6	-	0.7	-	0.7	-	-	-	-	10.6	
	ETIVE	10059	3065	0.3	SR	L-M	WELL	42.6	20.4	7.6	0.2	1.0	0.4	-	1.2	-	3.8	-	0.2	1.4	14.4	-	-	-	-	-	tr	-	-	6.6	
	RANNOCH	10072	3069	0.1	A-SA	L-M	MOD	58.3	6.7	3.7	0.7	0.7	-	-	10.0	5.3	0.7	-	-	2.7	3.2	-	2.7	-	2.3	-	-	-	-	3.0	
	RANNOCH	10107	3080	0.1	SA-SR	MOD	MOD	61.3	5.0	4.3	0.7	0.3	-	-	8.3	7.0	-	-	-	0.7	3.3	-	4.7	-	1.7	-	-	-	-	2.3	
	RANNOCH	10202	3109	0.1	SA	MOD	MOD	59.3	4.3	4.4	0.7	1.7	-	-	5.7	1.6	-	-	-	2.5	9.4	1.7	1.3	-	0.7	-	-	0.7	-	6.0	
211/19-6	NESS	10458	3187	0.3	SA-SR	M-H	MOD	57.8	2.6	8.6	-	0.4	-	-	0.4	-	3.2	-	-	3.2	9.8	-	-	-	-	-	-	0.8	0.8	12.4	
	NESS	10500	3200	0.2	SA-SR	MOD	WELL	51.6	5.8	5.4	0.2	-	-	-	0.4	-	0.2	-	-	4.4	4.8	-	0.6	-	-	-	-	0.6	0.6	25.0	
	NESS	10550	3215	0.2	A-SA	L-M	POOR	48.2	11.2	8.2	-	0.2	-	-	2.8	-	0.8	-	-	1.2	8.0	-	0.2	-	-	-	-	5.8	2.4	11.0	
	NESS	10590	3228	0.2	A-SA	L-M	MOD	54.6	4.6	7.4	0.2	0.4	-	-	0.4	-	1.4	-	-	2.0	12.6	-	0.2	-	-	-	-	1.4	-	14.8	
	ETIVE	10622	3237	0.3	SA-SR	MOD	POOR	57.8	5.6	6.4	0.2	-	-	-	0.4	-	0.4	-	-	1.6	13.3	-	0.2	-	0.2	-	-	0.2	-	13.7	
	ETIVE	10638	3242	0.4	A-SA	L-M	MOD	59.9	6.6	5.2	0.4	-	-	-	0.8	-	0.6	-	-	0.8	11.4	-	0.6	-	-	-	-	0.4	-	11.3	
3/13a-1	TARBERT	12207	3720	0.4	SA-R	MOD	MOD	42.3	12.5	2.8	-	-	-	-	2.3	0.2	0.8	0.2	0.6	11.6	16.3	-	-	-	-	-	-	-	-	10.4	
	NESS	12243	3731	0.3	A-SR	M-H	POOR	46.4	9.9	1.7	0.2	-	-	-	1.7	-	3.2	-	1.0	10.7	16.7	0.2	-	-	-	-	-	0.2	-	8.3	
	NESS	12267	3739	0.3	SA-SR	M-H	MOD	54.7	8.8	0.8	-	-	-	-	0.4	-	-	-	0.4	10.2	8.4	6.3	-	-	-	-	-	0.2	-	9.7	
	NESS	12403	3780	0.5	SA-SR	MOD	P-M	19.4	35.0	2.3	-	-	-	-	1.3	-	1.7	-	2.3	9.3	16.2	6.3	-	-	-	-	-	-	-	6.2	
	ETIVE	12419	3785	0.2	A-SR	MOD	P-M	34.0	25.7	1.0	-	-	-	-	3.0	-	-	0.2	0.2	7.0	6.5	14.5	-	-	-	-	-	0.6	-	4.5	
	RANNOCH	12433	3789	0.2	SA-SR	MOD	M-W	36.7	22.5	1.5	-	-	-	-	8.5	4.0	-	-	0.2	0.2	3.6	2.7	12.0	-	-	-	-	0.2	-	6.8	
	RANNOCH	12444	3792	0.2	SA	L-M	M-W	26.5	21.0	1.2	-	-	-	-	9.3	8.6	-	-	-	4.8	10.6	14.8	-	0.2	-	-	-	0.4	-	2.6	
	RANNOCH	12459	3797	0.1	A-SA	L-M	M-W	34.0	17.6	2.8	-	-	-	-	7.9	3.6	-	-	0.2	4.7	12.0	8.5	-	1.2	4.3	-	-	0.4	-	2.8	

WELL	FORMATION	DEPTH	TVD	Av. G.S.	RND.	SPHER.	SORT.	QTZ	PQTZ	K-FSP	PLAG	M.R.F	S.R.F.	I.R.F	MUSC	BIOT	DET. CLAY MATRIX	OPAQUES	CARB. MAT.	QTZ OG.	KAOL.	ILLITE	CAL.	DOL.	SID.	ANK.	K-FSP OG.	PYR	SPHAL	POROSITY
211/23-2	ETIVE	9434	2875	0.5	SR	M-H	M-W	55.7	8.0	8.0	-	1.7	-	-	-	-	-	-	-	2.0	12.3	-	0.7	-	-	-	tr	-	-	11.6
	ETIVE	9449	2880	0.5	SA-SR	L-M	MOD	48.0	11.0	11.0	0.3	1.3	-	-	1.0	-	0.3	-	-	5.7	10.0	-	1.7	-	-	-	-	0.3	-	9.3
	ETIVE	9464	2884	0.5	SA-SR	MOD	POOR	36.6	23.0	11.4	0.2	1.2	-	-	1.2	-	-	-	-	1.8	16.6	0.8	1.6	-	-	-	-	1.0	-	4.6
211/23-3	RANNOCH	9514	2900	0.1	SA	L-M	MOD	46.4	9.6	6.4	0.4	0.2	0.2	-	9.4	2.4	-	-	-	3.0	7.2	0.6	0.2	-	3.6	-	-	0.8	-	9.6
	TARBERT	8881	2707	0.5	SA-SR	MOD	MOD	40.0	11.4	9.3	0.7	1.3	-	-	1.0	0.7	-	-	0.3	5.0	10.0	-	3.7	-	-	-	tr	-	-	13.6
	TARBERT	8882	2707.1	0.4	A-SA	MOD	MOD	21.4	25.6	5.4	0.6	2.6	-	-	2.2	-	-	-	0.2	-	3.0	-	36.4	-	2.6	-	tr	-	-	-
	TARBERT	8883.5	2707.6	0.5	SA-SR	L-M	P-M	22.0	25.0	4.2	0.2	2.4	-	-	0.8	-	-	-	0.6	-	2.6	-	41.8	-	0.4	-	tr	-	-	-
211/23-4	TARBERT	8885	2708	1.0	SA-SR	LOW	POOR	11.2	44.0	6.0	-	2.6	-	-	0.2	-	-	-	0.4	-	1.6	-	33.6	-	0.4	-	tr	-	-	-
	TARBERT	8895	2711	0.5	SA-SR	MOD	MOD	44.7	6.7	7.6	1.0	-	-	-	-	-	-	-	-	5.7	9.0	-	4.6	-	-	-	-	0.7	-	20.0
	TARBERT	9048	2757	0.2	SA-SR	MOD	MOD	46.3	9.3	3.7	-	1.0	-	-	0.3	-	-	-	-	5.4	16.0	-	0.3	-	-	-	-	1.0	-	16.7
	TARBERT	9060	2761	0.3	A-SA	L-M	M-W	50.4	6.0	3.6	0.4	1.6	-	-	0.8	-	-	0.4	-	6.8	10.4	-	4.8	-	-	-	tr	0.8	-	14.0
	TARBERT	9073	2765	0.4	A-SA	MOD	MOD	53.2	10.8	5.2	0.4	2.0	-	-	2.8	-	-	-	-	4.8	8.8	-	0.8	-	0.4	-	tr	0.4	-	10.4
	TARBERT	9079	2767.1	0.2	A-SA	L-M	MOD	37.1	10.3	4.4	1.0	4.0	-	-	5.0	1.3	-	-	-	-	7.6	-	tr	-	7.1	21.7	tr	0.3	-	-
	TARBERT	9081	2767.7	0.3	A-SA	L-M	P-M	26.2	10.6	3.2	0.2	-	-	-	3.0	1.0	-	-	-	-	4.6	-	47.0	-	3.8	tr	tr	0.4	-	-
	TARBERT	9084	2768.7	0.2	A-SA	MOD	P-M	39.0	15.2	7.6	0.2	1.6	-	-	5.0	0.6	-	-	-	-	11.2	-	tr	-	2.3	17.2	tr	0.1	-	-
	TARBERT	9088	2770	0.6	SA-SR	M-W	POOR	32.7	26.6	4.7	-	2.7	-	-	2.7	-	-	-	-	2.7	16.0	-	-	-	-	-	-	0.3	-	11.6
	NESS	9258	2822	0.7	A-SA	MOD	POOR	37.3	16.7	7.7	0.3	-	-	-	1.0	-	-	-	-	7.7	21.0	-	1.3	-	-	-	-	-	-	-
NESS	9276	2827.2	0.4	A-SA	MOD	POOR	39.2	8.8	3.4	0.6	1.2	-	-	2.8	3.0	-	-	-	-	0.8	-	37.8	-	1.4	tr	tr	1.0	-	-	
NESS	9278	2827.8	0.3	SA-SR	L-M	MOD	33.4	17.0	3.4	0.6	0.2	-	0.4	1.4	2.0	-	-	-	-	4.8	-	34.2	-	1.8	-	tr	0.6	-	-	
NESS	9282	2829	0.4	SA	L-M	POOR	30.6	17.0	2.6	0.6	1.2	-	-	-	-	-	-	0.6	-	1.2	-	45.2	-	1.0	-	tr	-	-	-	
NESS	9282	2829	0.2	A-SA	L-M	M-W	21.8	4.2	0.8	0.2	0.4	-	-	5.4	9.0	-	-	-	-	1.8	-	39.8	-	16.0	-	tr	0.4	-	-	
NESS	9285	2829.9	0.1	A-SA	MOD	WELL	24.2	7.4	0.8	0.6	0.4	-	-	8.8	8.0	-	-	-	-	4.0	-	32.8	-	12.4	tr	tr	0.6	-	-	
NESS	9288	2831	0.1	SA-SR	HIGH	WELL	43.3	10.3	5.0	-	-	-	-	4.3	-	-	-	-	4.7	17.7	-	6.7	-	0.3	-	-	1.0	-	5.3	
NESS	9312	2838	0.3	SA-SR	HIGH	WELL	50.3	9.0	4.0	0.7	-	-	-	6.3	3.0	-	-	-	4.0	13.7	-	-	-	-	-	-	1.0	-	8.0	

Av. G.S. - Average grain size (millimetres),
RND. - Rounding:
A - Angular, SA - Subangular,
SR - Subrounded, R - Rounded.
SPHER. - Sphericity: Low, Moderate, High.
SORT. - Sorting: Poor, Moderate, Well.

QTZ - Quartz,
PQTZ - Polycrystalline quartz,
K-FSP - K-Feldspar overgrowths,
PLAG - Plagioclase,
M.R.F - Metamorphic Rock Fragments,
S.R.F - Sedimentary Rock Fragments,
I.R.F - Igneous Rock Fragments,

MUSC - Muscovite,
BIOT - Biotite
DET. CLAY MATRIX - Detrital Clay Matrix,
CARB. MAT. - Carbonaceous Material,
QTZ OG - Quartz overgrowths,
KAOL. - Kaolinite,
CAL. - Calcite,
SID. - Siderite,
ANK. - Ankerite,
PYR. - Pyrite,
SPHAL. - Sphalerite.

TABLE 2: ISOTOPIC RESULTS

 $\delta^{18}\text{O}$ ANALYSES ON KAOLINITE (2-5 microns)

WELL	FORMATION	DEPTH TVD		$\delta^{18}\text{O}$ (SMOW, ‰)
		(FT)	(M)	
THISTLE				
211/18-A45	ETIVE	8624'	2628	+16.9
	ETIVE	8629'	2630	+16.0
	ETIVE	8631'	2631	+16.0
	ETIVE	8643'	2634	+16.9
	ETIVE	8651'	2637	+17.7
211/18-A30	ETIVE	9164'	2793	+16.2
	ETIVE	9187'	2800	+16.1
	ETIVE	9227'	2812	+15.7
211/18-A31	ETIVE	8994'	2741	+15.8
	ETIVE	9042'	2756	+15.8
	ETIVE	9072'	2765	+16.9
	ETIVE	9081'	2768	+15.1
MURCHISON				
211/19-4	NESS	9884'	3012	+17.1
	NESS	9967'	3038	+18.3
	ETIVE	9993'	3048	+17.0
	ETIVE	10027'	3056	+16.7
211/19-6	NESS	10458'	3187	+14.7
	NESS	10590'	3228	+14.9
DUNLIN				
211/23-2	ETIVE	9434'	2875	+15.6
	ETIVE	9449'	2880	+16.1
	ETIVE	9464'	2884	+16.7
211/23-3	TARBERT	8895'	2711	+15.8

TABLE TWO (cont.):

WELL	FORMATION	DEPTH TVD. SS		$\delta^{18}\text{O}$ (SMOW, ‰)
		(FT)	(M)	
211/23-4	TARBERT	9048'	2757	+16.5
	TARBERT	9060'	2761	+17.2
	TARBERT	9073'	2765	+16.7
	NESS	9288'	2831	+18.3
	NESS	9312'	2838	+17.2
WELL 3/13A-1	TARBERT	12207'	3720	+15.7

(Reproducibility for $\delta^{18}\text{O}$ is $\pm 0.2\%$ for each sample, mass spectrometer in run precision $\pm 0.05\%$, (2σ), for all samples.)

TABLE 2 (cont.): CARBONATE $\delta^{18}\text{O}$ AND $\delta^{13}\text{C}$ DATA, DUNLIN FIELD

WELL	FORMATION	DEPTH TVD. SS (FT) (M)	$\delta^{18}\text{O}$ (SMOW, ‰)	$\delta^{13}\text{C}$ (PDB, ‰)	
211/23-3	TARBERT	8882' 2707.1	+20.4	+2.1	CALCITE
	TARBERT	8882' 2707.1	+21.9	-0.1	SIDERITE
	TARBERT	8885' 2708.0	+20.5	+1.8	CALCITE
211/23-4	TARBERT	9079' 2767.1	+22.9	-4.1	ANKERITE
	TARBERT	9079' 2767.1	+24.5	-4.6	SIDERITE
	TARBERT	9081' 2767.7	+19.4	-7.3	CALCITE
	TARBERT	9081' 2767.7	+24.0	-4.6	SIDERITE
	TARBERT	9081' 2767.7	+21.6	-5.5	ANKERITE
	TARBERT	9084' 2768.7	+19.1	-7.6	ANKERITE
	NESS	9276' 2827.2	+17.8	-9.4	CALCITE
NESS	9276' 2827.2	+19.9	-5.9	SIDERITE	
NESS	9278' 2827.8	+18.1	-8.1	CALCITE	
NESS	9282' 2829.0	+19.9	-11.4	CALCITE	
NESS	9282' 2829.0	+20.1	-10.4	SIDERITE	
NESS	9285' 2829.9	+18.8	-10.1	CALCITE	
NESS	9285' 2829.9	+22.1	-6.9	SIDERITE	

(Reproducibility for oxygen $\delta^{18}\text{O}$ is $\pm 0.2\%$, Carbon $\delta^{13}\text{C}$ is $\pm 0.1\%$, 2σ)

TABLE 2 (cont.): $\delta^{18}\text{O}$ ANALYSES ON QUARTZ OVERGROWTHS

WELL	FORMATION	DEPTH	TVD.SS	$\delta^{18}\text{O}$	$\delta^{18}\text{O}$	%	$\delta^{18}\text{O}$	WELL	FORMATION	DEPTH	TVD.SS	$\delta^{18}\text{O}$	$\delta^{18}\text{O}$	%	$\delta^{18}\text{O}$
THISTLE		(FT)	(M)	(SMOW, ‰)	(SMOW, ‰)		(SMOW, ‰)	DUNLIN		(FT)	(M)	(SMOW, ‰)	(SMOW, ‰)	OG	(SMOW, ‰)
211/18-A30ST	NESS	9116'	2778	+12.2	+10.3	18.0	+20.9	211/23-2	ETIVE	9434'	2875	+13.0	+11.0	23.0	+19.4
	NESS	9156'	2791	+12.8	+11.6	16.4	+19.3		ETIVE	9449'	2880	+12.8	+12.3	6.0	+20.6
	ETIVE	9223'	2811	+11.9	+10.6	16.0	+18.8		ETIVE	9464'	2884	+12.0	+11.2	12.0	+17.8
	ETIVE	9246'	2818	+12.2	+11.4	14.0	+17.1								
	ETIVE	9278'	2828	+12.8	+11.9	17.0	+17.4	211/23-3	TARBERT	8895'	2711	+12.6	+12.3	6.0	+17.3
211/18-A45	ETIVE	8624'	2628	+12.1	+11.6	9.0	+17.2	211/23-4	TARBERT	9048'	2757	+13.3	+10.9	21.0	+22.3
	ETIVE	8629'	2630	+13.0	+11.9	14.0	+19.7		TARBERT	9060'	2761	+13.5	+11.7	17.0	+22.3
	ETIVE	8631'	2631	+12.1	+11.9	3.0	+18.6		TARBERT	9073'	2765	+12.1	+9.9	20.0	+20.9
	ETIVE	8643'	2634	+12.2	+11.9	4.0	+19.4		NESS	9288'	2831	+12.9	+10.9	24.5	+19.1
	ETIVE	8651'	2637	+12.2	+11.6	11.0	+17.1		NESS	9312'	2838	+13.1	+11.1	18.0	+22.2
211/18-A30	ETIVE	9164'	2793	+12.6	+12.3	5.0	+18.3	3/13a-1	TARBERT	12207'	3720	+13.6	+12.5	12.0	+21.6
	ETIVE	9187'	2800	+12.0	+11.6	7.0	+17.3		NESS	12243'	3731	+15.1	+14.6	10.0	+19.6
	ETIVE	9081'	2812	+12.6	+11.9	12.0	+17.7		NESS	12267'	3739	+13.9	+11.7	18.0	+20.0
211/18-A31	ETIVE	9042'	2756	+12.9	+12.7	4.0	+17.7		NESS	12403'	3780	+14.2	+12.1	21.0	+22.1
	ETIVE	9072'	2765	+14.3	+12.3	20.0	+22.3		ETIVE	12419'	3785	+15.5	+14.8	14.0	+19.8
	ETIVE	9081'	2768	+14.0	+12.5	18.0	+20.8								
MURCHISON															
211/19-3	NESS	10171'	3010	+13.1	+11.9	14.8	+20.0								
	NESS	10188'	3105	+12.5	+11.5	15.0	+18.2								
	ETIVE	10300'	3139	+12.8	+11.5	21.0	+17.7								
	ETIVE	10331'	3148	+12.8	+11.5	17.0	+19.1								
211/19-4	NESS	9884'	3012	+12.3	+10.8	13.0	+22.3								
	ETIVE	9993'	3048	+12.2	+11.4	9.0	+20.3								
	ETIVE	10027'	3056	+12.1	+10.8	13.0	+20.8								
	ETIVE	10059'	3065	+11.5	+10.9	9.0	+17.6								

(Reproducibility of oxygen $\delta^{18}\text{O}$ is $\pm 0.2\%$, 2σ .)

Oxygen isotopic compositions of quartz overgrowths calculated from the mass balance equation:-

$$\delta^{18}\text{O}_T = \delta^{18}\text{O}_C \cdot X_C + \delta^{18}\text{O}_{OG} \cdot X_{OG}$$

T = Total sample (Quartz core + overgrowths)

C = Detrital Core

OG = Overgrowth

X = Mole Fraction

(From Fisher 1982)

TABLE 2 (cont.): $\delta^{18}\text{O}$ ANALYSES ON ILLITE (<0.1 MICRONS)

WELL	FORMATION	DEPTH (FT)	TVD.SS (M)	$\delta^{18}\text{O}$ (SMOW)
MURCHISON				
211/19-4	RANNOCH	10202'	3109	+14.2
3/13a-1	NESS	12243'	3731	+13.4
	RANNOCH	12433'	3789	+13.4
	RANNOCH	12444'	3792	+13.7
	RANNOCH	12459'	3797	+13.1

(Reproducibility of oxygen $\delta^{18}\text{O}$ is $\pm 0.2\%$, 2σ .)

TABLE 3: δD ANALYSES ON KAOLINITE (2-5 MICRONS) AND ILLITE (<0.1 MICRONS)

KAOLINITE

WELL	FORMATION	DEPTH (FT)	TVD (M)	δD
THISTLE				
211/18-A45	ETIVE	8624'	2628	-48
	ETIVE	8629'	2630	-66
	ETIVE	8631'	2631	-66
	ETIVE	8643'	2634	-54
	ETIVE	8651'	2637	-68
211/18-A30	ETIVE	9187'	2800	-54
		9187'	2800	-51 (5-10 microns)*
	ETIVE	9227'	2812	-68
211/18-A31	ETIVE	8994'	2741	-59
	ETIVE	9042'	2756	-49
	ETIVE	9081'	2768	-55
MURCHISON				
211/19-4	NESS	9884'	3012	-61
	ETIVE	9993'	3048	-58
	ETIVE	10027'	3056	-55
211/19-6	NESS	10458'	3187	-63
DUNLIN				
211/23-2	ETIVE	9434'	2875	-57
	ETIVE	9449'	2880	-54
211/12-3	TARBERT	8895'	2711	-67
211/23-4	TARBERT	9073'	2765	-67
	NESS	9288'	2831	-58
	NESS	9312'	2838	-66

TABLE 3 (cont.): ILLITE

WELL	FORMATION	DEPTH (FT)	TVD.SS (M)	δD (SMOW)
MURCHISON				
211/19-4	RANNOCH	10202'	3109	-60
3/13a-1	RANNOCH	12433'	3789	-61
	RANNOCH	12444'	3793	-56
	RANNOCH	12459'	3797	-55

(Reproducibility of hydrogen δD is $\pm 2\%$, 1σ .)

APPENDIX 1

Preparation methods for the isolation of pure mineral separates for isotopic analyses. The minerals separated are quartz overgrowths, kaolinite, illite, ankerite, siderite and calcite.

METHODOLOGY: QUARTZ-CLAY ISOLATION

- 1) The starting weight of sandstone is dependent on the amount of core available, where possible up to 500 grams was used initially. The sandstone was carefully disaggregated using a jaw crusher and a crown mill. Binocular microscopy was used at regular intervals to ensure that the crushing process was disaggregating the grains rather than smashing them indiscriminantly.
- 2) The disaggregated sandstone was sieved through a 500 micron nylon cloth with the <500 micron fraction kept and used for preparation.
- 3) The sample was treated in a solution of 0.3M Na-citrate, 1.0M NaHCO_3 and sodium dithionite to remove iron oxides. The next stage involved the sample being treated in 6% (w/v) hydrogen peroxide to remove organic matter and finally a NaOAc-HOAc solution (buffered to pH = 5) to remove carbonate (Jackson 1979).
- 4) The sample was then size separated (<20, 20-50, 50-85, 85-160, 160-250, 250-500 and >500 microns).
- 5a) Quartz isolation: The sand size fractions were studied under S.E.M to determine which fraction had the most and best developed overgrowths. This appeared to be the 160-250 microns and so that was the fraction chosen. 5-10 grams of this fraction was fused with NaHSO_4 (to remove hydrous phases) for 2 hours. 3N HCl was used to dissolve the fusion cake, the quartz - feldspar residue was washed in distilled water and dried. The residue was soaked in 30% H_2SiF_6 at a temperature of 5°C for three days to remove feldspars (Syers et al. 1968). The remaining quartz was washed, dried and resieved (160 micron cloth) to ensure that the 160-250 micron size range was maintained. X-ray diffraction was used to confirm that a pure separate had been obtained.

Once this had been done, thin sections were prepared of the

grains. These were point counted (300 counts per slide), to determine the proportion of overgrowth. An aliquot of the quartz sample was analysed for oxygen isotopic composition (see Appendix 2) with the remainder being leached in concentrated HF to remove the overgrowths (Milliken et al.1981, Fisher & Land 1986). Checks using the S.E.M and thin sections were made to ensure complete removal of the overgrowths. The oxygen isotopic composition of the quartz cores was then measured. The oxygen isotopic composition of the quartz overgrowths was calculated by the mass balance (Fisher 1982).

5b) Clay separation: The <20 micron fraction was further size separated by sedimentation to 1-2, 2-5, 5-10 and 10-20 microns. Calgon was added to assist defloculation. The size fractions <0.1, 0.1-0.5 and 0.5-1.0 microns were separated by high speed centrifugation. X-ray diffraction was used to assess sample purity for the isotopic analysis of the kaolinite and illite. Prior to analysis the sample was oxygen plasma ashed in a Polaron Bio-Rad Asher for up to two hours or until no noticeable decrease in weight was observed due to removal of volatile organic matter.

METHODOLOGY: CARBONATE PREPARATION

- 1) The selected carbonate cemented sample was disaggregated using a jaw crusher. It was then sieved using nylon cloth into the <20, 20-50, 50-100, 100-160, 160-250 and >250 microns. The 50-100 micron size fraction was selected for preparation purposes after X-ray diffraction confirmed the presence of the carbonates and as this size fraction is suitable for heavy liquid separation.
- 2) The 50-100 micron size fraction was mixed with 1,1,2,2, tetrabromoethane to facilitate density separation of the carbonate from the silicate framework grains. The carbonate floats in the liquid (each sample having specific settling periods for the best separation results, usually 3-5 hours). This was successful in improving the purity of the carbonate fraction. X-ray diffraction was used to identify the types of carbonate present (i.e. calcite, ankerite and siderite)
- 3) To separate the individual carbonate minerals each sample was put through a Frantz Isodynamic magnetic separator. The separates were checked by XRD to confirm successful separation.
- 4) Prior to isotopic analysis, each sample was oxygen plasma ashed in a Polaron Bio-Rad Asher for up to two hours or until no noticeable decrease in weight was observed due to the removal of organic matter.

OXYGEN ISOTOPIC ANALYSIS:

For the analysis of oxygen in quartz overgrowths, kaolinite and illite reactions were carried out on a silicate fluorination line. 10 mg of sample was loaded into a nickel reaction vessel and reacted with ClF_3 to liberate the oxygen from the minerals (Borthwick & Harmon 1982). For quartz the oxygen was liberated by reaction with ClF_3 at 650°C for 14 hours. Kaolinite is reacted at 600°C for 14 hours. Both quartz and kaolinite undergo a prefluorination treatment with ClF_3 prior to the main 14 hour reaction to remove adsorbed surficial and interlayer water. Illite does not receive this treatment as this reaction with ClF_3 strips out oxygen from within the lattice and hence affects the isotopic value. The liberated oxygen is then converted to CO_2 over a platinised carbon rod and the gas then analysed on a VG Isotopes SIRA-10 mass spectrometer.

HYDROGEN ISOTOPIC ANALYSIS:

Prior to the reaction of the samples of kaolinite and illite on the isotope line, each sample (av. 40 mg) was degassed overnight at 120°C to remove adsorbed surficial and interlayer water.

Each sample was reacted by gradual induction heating to 1200°C in a platinum crucible, with the hydrogen being liberated and collected. Water is also liberated and is passed through a Uranium furnace at 800°C to produce hydrogen. The total hydrogen was collected in a Toepler pump and then analysed on a VG Isotopes Micromass 602 spectrometer.

APPENDIX 3

K/Ar DATING: The K percentage and the Argon value are analysed separately prior to their combination and calculation of an age. The K (%) was determined by flame photometry on 10 mg of the illite. The Argon value is obtained by inductively heating the illite at 1200°C to liberate the argon. Prior to the reaction the sample is degassed overnight at 100°C to remove any adsorbed surficial and interlayer water. 40 mg of sample were used, and the Argon value determined by the usual mass spectrometric techniques.

Sample: 10202', 3109m (TVD SS), 211/19-4, Rannoch Formation.

K (%) = 4.46

% radiogenic Argon = 61.14

Radiogenic Argon 40 = $4.60 \cdot 10^{-10}$ moles/gram

T = 58.5 ± 1.4 Ma.

CHAPTER 4

4.

THE FORMATION AND ORIGIN OF CARBONATE CEMENTED
ZONES IN THE BRENT SANDSTONES OF THE DUNLIN FIELD,
NORTHERN NORTH SEA

J.F. BRINT

DEPARTMENT OF APPLIED GEOLOGY,
UNIVERSITY OF STRATHCLYDE,
75 MONTROSE STREET,
GLASGOW, G1 1XJ

R.S. HASZELDINE

DEPARTMENT OF APPLIED GEOLOGY,
UNIVERSITY OF STRATHCLYDE,
75 MONTROSE STREET,
GLASGOW, G1 1XJ

A.E. FALLICK

ISOTOPE GEOLOGY UNIT,
S.U.R.R.C.,
EAST KILBRIDE,
GLASGOW, G75 0QU

P.J. HAMILTON

ISOTOPE GEOLOGY UNIT,
S.U.R.R.C.,
EAST KILBRIDE,
GLASGOW, G75 0QU

S.BROWN

BRITISH GEOLOGICAL SURVEY,
HYDROCARBONS UNIT,
12 GRANGE TERRACE,
EDINBURGH, EH9 2LF

Format: Journal of Sedimentary Petrology

Carbonate cemented concretion zones, ("doggers"), in the Ness and Tarbert Formations of the Middle Jurassic deltaic Brent sandstones have severely reduced reservoir quality from the earliest stages of diagenesis. Siderite-calcite concretions formed when sediment porosities were on average 40%. Bicarbonate supply was from iron/sulphate reduction of organic matter and the dissolution of shell material. An ankerite rim to one concretion formed between 55 - 102°C at depths of 1.1 - 1.7 km with the bicarbonate supply from a mixture of fermentation and abiotic reactions. Hydrodynamically, the siderite-calcite concretions formed in a flow of dominantly meteoric water which flushed down to 1.1 km from the Mid-Late Jurassic. This reacted with mica detritus to release radiogenic strontium into the siderite (0.7114 - 0.7184). The same water gradually became dominated by high concentrations of strontium with lower $^{87}\text{Sr}/^{86}\text{Sr}$ from aragonitic shell material, and formed a mixing line to high strontium concentration, low $^{87}\text{Sr}/^{86}\text{Sr}$ calcites (≈ 0.711). Concretions first formed siderite around reacting biotite micas and then calcite during early shallow diagenesis in an isotopically open system. The ankerites are Ca rich, with low $^{87}\text{Sr}/^{86}\text{Sr}$ and have replaced and nucleated on earlier concretionary calcite during burial diagenesis. Formation occurred in an isotopically closed system from an evolving meteoric porewater, with an elevated geothermal gradient.

The combination of petrographic and geochemical techniques in the study of carbonate cemented zones in sandstones enables constraints to be placed on the timing, temperature of formation and origin of the porefluid, and dissolved constituents from which the cements precipitated. This gives an insight into changes in trace element and isotopic compositions as the porefluid chemistry evolves during precipitation of the cements. Such an integrated approach of petrography and geochemical techniques has been used in the study of carbonate concretions by several workers (Coleman & Raiswell 1981, Boles et al. 1985, Curtis et al. 1986, Hamilton et al. 1987, Carpenter et al. 1988).

The Middle Jurassic deltaic Brent sandstone Group is a prolific hydrocarbon reservoir in the East Shetland Basin, northern North Sea (Fig.4.1) and is the location of a number of major producing fields. The main reservoir sandstones have maintained very high porosities (up to 30%) and permeabilities (up to 6000mD), (e.g. Blanche & Whitaker 1978, Sommer 1978, Bjorlykke and Brendsdal 1986, Thomas 1986, Jourdan et al. 1987) so permitting major hydrocarbon accumulations. Within the sandstone sequence, carbonate cemented concretion zones, (locally known as "doggers") occlude porosity and permeability. This study has analysed three concretions from the Ness and Tarbert Formations (Fig.4.2) of the Brent Group in the Dunlin oilfield (Fig.4.1) with the aim of making an integrated study of the petrography, microprobe analyses of the chemistry, and C, O and Sr isotope geochemistry of the concretions. Siderite cements started to form at burial depths of a few metres. These developed into calcite concretions under the influence of an open system meteoric fluid flow down to ≈ 1.1 km. The bicarbonate supply was from a mixed source of shell material and oxidation of organic matter during bacterial sulphate reduction. During deeper diagenesis, ankerite rims to concretions grew in a semi-closed system of isotopically evolving meteoric-derived porewater with a high geothermal gradient.

Strontium for siderite and calcite was derived both from the dissolution of carbonate phases, i.e. shell material, and from leaching of detrital mineral phases such as feldspars and micas. Strontium in the ankerite was supplied from both precursor calcite

and silicates in the surrounding mudrocks. One concretion shows an excellent linear correlation of $^{87}\text{Sr}/^{86}\text{Sr}$ versus $1/\text{Sr}$ indicating simple two end member mixing, during siderite formation.

4.3

GEOLOGICAL SETTING

The Middle Jurassic Brent Group is situated in the East Shetland Basin, approximately 150 kms north east of the Shetland Islands, in the northern North Sea (Fig.4.1). The Basin consists of a series of faulted terraces which developed during the Jurassic with the tilted fault blocks dipping dominantly to the west (Fig.4.3). This structure may be related to the development of the complex Viking Graben system which was probably initiated in the Permian (Glennie 1984). In the East Shetland Basin the Lower Jurassic is represented by a non-marine to marginal marine succession (Kirk 1980, Chauvin & Valachi 1981) of sands (Rhaetian-Sinemurian) which are overlain by the marine Dunlin Group shales. The overlying Middle Jurassic Brent Group is a sand dominated deltaic sequence consisting of five Formations (Deegan & Scull 1977):- Broom, Rannoch, Etive, Ness and Tarbert. The Broom Formation has recently been considered a separate fan-delta unit from the remainder of the Group (Richards et al. 1988). The overlying micaceous sandstones of the Rannoch Formation represent storm influenced shallow marine delta front or shoreface deposits (Richards & Brown 1986, Brown et al. 1987). These fine grained Rannoch sandstones grade up into the coarser, massive sandstones of the Etive Formation which is considered to represent subenvironments of a barrier bar complex (Budding & Inglin 1981). The Ness Formation was deposited in a back barrier lagoonal and alluvial environment (Parry et al. 1981) and consists of interbedded sands, silts, shales and coals. The overlying Tarbert Formation sandstones show evidence of storm influence (Brown et al. 1987) and are thought to represent the first stages of the marine transgression that covered the Brent delta (Bowen 1975, Hallet 1981). On the tilted fault block crests the Tarbert is commonly thin or absent due to erosion at end-Brent or end-Upper Jurassic (Sommer 1978). Overlying the Brent succession are the marine shales of the Humber Group (Heather and Kimmeridge Clay Formations, Late-Middle to Upper Jurassic, Fig.2). The boundaries between the Brent Group and the

Heather Formation are locally unconformable, particularly at the crests of many tilted fault blocks. The Jurassic sequence in the East Shetland Basin was subsequently buried by marine Cretaceous and Cenozoic deposits up to 4 kms in places (Parsley 1984).

The samples for this study were taken from two wells in the Dunlin oilfield, 211/23-3, and 211/23-4 (Fig.4.4). The present day burial depths of the concretions are, 1) Concretion A - 8882-8885' (2707.1-2708.0m) true vertical depth (TVD) subsea, 211/23-3, Tarbert Formation; 2) Concretion B - 9079-9084' (2767.1-2768.7m), TVD subsea, 211/23-4, Tarbert Formation; 3) Concretion C - 9276-9285' (2827.2-2829.0m), TVD subsea, 211/23-4, Ness Formation.

4.4 ANALYTICAL TECHNIQUES

4.4.1 PETROGRAPHY

Eleven thin sections from the centre to edge of concretions were examined using standard optical microscopy, and cathodoluminescence on a Technosyn Cold Cathode Luminescence Model 8200 Mk II with a Vickers Instruments microscope attached. Electron probe microanalysis of the carbonates was made on a Jeol Superprobe 733 Electron Probe Microanalyser (JXA-733), all data were normalised to 100 mol% for Ca, Mg, Fe and Mn.

4.4.2 X-RAY DIFFRACTION

Finely ground powders of carbonate were mixed with acetone on a glass slide and analysed using a Philips PW 1120 powder diffractometer with Co filtered Cu K-alpha radiation. Samples were run over the 2θ interval 20-50° with 1° divergence, 0.1° receiver and 1° anti-scatter slits.

4.4.3 STABLE ISOTOPES - MINERAL SEPARATION

Samples were crushed and sieved, with the 50-100 micron fraction being selected for further treatment. X-ray diffraction confirmed the carbonates present. The 50-100 micron fraction was mixed with 1,1,2,2, tetrabromoethane to facilitate density separation of the carbonate phases from the framework grains. After successful improvement in the purity of the carbonates, the carbonate-rich samples were put through a Frantz magnetic separator under

appropriate conditions to separate the calcite, siderite and ankerite. X-ray diffraction was used to confirm that pure separates had been obtained. Each sample was oxygen plasma ashed in a Polaron Bio-Rad Asher for up to two hours or until no noticeable decrease in weight was observed due to the removal of volatile organic matter.

4.4.4 CARBON AND OXYGEN ISOTOPE ANALYSIS PROCEDURES

Calcite samples were reacted overnight at 25°C with phosphoric acid (McCrea 1950). Siderite and ankerite were reacted with phosphoric acid for one hour at 100 C in a sandbath. The evolved CO₂ gas was dried, purified and analysed on a VG Isogas SIRA-10 mass spectrometer. Carbon and oxygen isotope results were corrected using standard procedures (Craig 1957) and are presented in the usual δ notation as parts per thousand relative to PDB. Oxygen analyses are also presented relative to the SMOW standard. As the siderite and ankerite were reacted at 100 C, (a modification of the McCrea (1950) technique of phosphoric acid extraction of CO₂), experimentally determined oxygen isotope fractionation factors presented by Rosenbaum & Sheppard (1986) were used. During the course of analyses a value for the NBS-20 standard of $\delta^{18}\text{O}_{\text{SMOW}} = +26.5 \pm 0.2\%$ and $\delta^{13}\text{C}_{\text{PDB}} = -1.2 \pm 0.1\%$ was obtained.

4.4.5 RADIOGENIC ISOTOPE PROCEDURES

Seven calcite, six siderite and three ankerite samples were analysed for their strontium and rubidium isotope composition. Concentrations of Sr and Rb were single dissolutions of 10 mg aliquots of sample powder. The Rb and Sr were separated by conventional cation exchange chromatography. Rb concentrations were determined by isotope dilution (Moore et al.1973), with the isotopic ratio ($^{87}\text{Rb}/^{85}\text{Rb}$) determined on a VG Micromass 30B mass spectrometer. NBS 987 SrCO₃ gave a value of 0.71028. Sr concentration determinations were also made by isotope dilution in a similar manner. The unspiked isotopic ratio ($^{87}\text{Sr}/^{86}\text{Sr}$) was determined using a VG Isotopes 54E with normalisation to $^{86}\text{Sr}/^{84}\text{Sr} = 0.1194$. NBS-987 SrCO₃ yielded a $^{87}\text{Sr}/^{86}\text{Sr}$ ratio of 0.71027 on this machine.

4.5.1 FRAMEWORK GRAINS

The framework grain petrology of the eleven carbonate cemented sandstones was petrographically investigated. The sandstones are fine to coarse grained, poor to well sorted subarkoses (Fig.4.5, Table 4.1). Quartz observed is dominantly monocrystalline except in 211/23-3 where polycrystalline grains dominate in the coarser grained framework of this concretion. K-feldspar is the dominant feldspar, occurring mostly as orthoclase and minor microcline and perthites. Plagioclase (albite composition) is present in minor amounts (<1.0%). In a quartz-feldspar-rock fragment sandstone classification, total feldspar makes up to 12% of the sandstones (Fig.4.5). Rock fragments constitute up to 4.0% of the framework grains and are dominantly metamorphic (schistose fragments, quartzite). Muscovite occurs in all the sandstones (<8.8%) displaying incipient to complete alteration to kaolinite. Biotite also shows major alteration to siderite and constitutes up to 9% of the framework grains, see Fig.4.5).

4.5.2 DIAGENESIS

Cement stratigraphy and diagenetic textures were elucidated using standard optical microscopy and cathodoluminescence microscopy. Figure 4.6 presents the paragenetic sequence of the Brent sandstones.

4.5.3 PRE-CALCITE CEMENTS

Prior to the main phase of calcite cementation, several non-carbonate cements were precipitated during the earliest stages of diagenesis (see Fig.4.6). Kaolinite forms as an alteration product of muscovite (Fig.4.7.a) and with a pore-filling vermiform morphology (Fig.4.7.b). There is minor development of quartz and K-feldspar overgrowths (Fig.4.7.c). Pyrite has formed at the sites of altering biotites along with siderite (see below).

4.5.4 SIDERITE

The earliest of carbonate phases, siderite occurs as small individual rhombs (average size 10 microns) being seen in patches up to 200 microns across (Fig.4.7.d). These sideritic areas are the sites of original biotites which are now in varying stages of degradation and alteration. The presence of pyrite within a number of the siderite patches is noted, and both biotite/siderite and biotite/siderite/pyrite associations are observed (Fig.4.7.e) (cf. Bjorlykke & Brendsdal 1986). In all concretions the siderite is completely enclosed within the pervasive later calcite cement, and is not observed outwith the concretions. In concretion C, (depth 9282'), the siderite is developed along the biotite rich bedding laminae. In the samples studied, siderite constitutes up to 16% of the sandstones (Table 4.1).

4.5.5 CALCITE

Calcite is the most pervasive of the carbonate cements, and constitutes between 32.8 and 47.0% of the sandstones studied. The calcite cement is dominantly poikilotopic, with crystal sizes ranging from 0.25-2.0 mm, with the detrital grains often displaying a floating grain texture (Fig.4.7.f). The smaller size crystals form an intergranular texture (Fig.4.7.g). Similar features are observed throughout the concretion.

In concretion A (8882' - 8885', 211/23-3, Fig.4.4.a), the poikilotopes are up to 2mm across, with straight contacts. In concretion B (211/23-4, Fig.4.4.b) at 9081', the calcite has a size range between 0.25 and 0.5mm, with the individual crystals having dominantly straight contacts; only a few are microstylotised. In concretion C (9276'-9285', 211/23-4, Fig.4.4.b), the poikilotopic (0.6 - 1.0mm) and intergranular (0.1 - 0.3mm) cements are interlocked with a mixture of straight and microstylotised boundaries. The cement in all three concretions is aggressive in places with the edges of the framework grains showing the effects of dissolution. Both aggressive and non-aggressive cements are petrographically similar. Cathodoluminescence shows that the calcite has a homogeneous dull orange/red colour in all three concretions (Fig.4.7.h) irrespective of grain size or whether the cement is aggressive or not. No growth

zonation is observed.

4.5.6 ANKERITE

Ankerite was observed in concretion B and in trace amounts at the edges of concretion C. In concretion B the centre is calcite with a component of ankerite, whilst the edges of the concretion are of ankerite making up 17.2 (9084') and 21.7% (9079') of the sandstone. The porosity occluded by ankerite at the concretion margin is markedly lower than that occluded by calcite in the other concretions (32.8 to 47%, Table 4.1), and appears to support the idea of continued primary precipitation of ankerite. The ankerite, like the calcite, exists in a range of crystal sizes, up to 0.5mm, and are both intergranular and poikilotopic. Using the microprobe (see later) small patches of calcite were observed in concretion B (9079') amongst the ankerite cement. The ankerite may have in part replaced the calcite (Boles 1982) or could be patches of calcite that is surrounded by ankerite without replacement. Although the ankerite proved to be non-luminescent under cathodoluminescence, the intimate textural association with calcite suggests partial replacement. Kantorowicz (1985) in a study of ankerite growth in the Ninian field reported evidence for ankerite formation at 100 C at the time of oil emplacement. So the ankerite may have precipitated during burial diagenesis, when porosity had decreased, by a combination of calcite replacement and primary precipitation.

4.6

CEMENT-POROSITY RELATIONSHIPS

Total carbonate cement percentages for the sandstones range from 19.5 to 55.8% (Table 4.1), and with the addition of the pre-carbonate mineral cements (cf. Diagenesis section) the minus cement porosities increase to between 30.8 and 58%. It was stated earlier that calcite is aggressive at grain boundaries and several areas show evidence for framework grain dissolution (Fig.4.7.d). Growth of calcite cement during early diagenesis within the high porosity sandstones, caused the grains to be forced apart as the cement precipitated, i.e. expansion of the framework fabric. This would explain why precement values exceed a typical initial porosity of 48% for sandstones soon after deposition (Berg 1986).

However by assuming an initial sandstone porosity value of 48%, an estimate for the compactional effects may be made. All values for cement over 48% are obviously excluded to allow calculation. The sandstone pore space occupied by calcite/siderite cement indicates pre-cement porosities of 34.0 to 46.2% for the samples. The total pre-cement porosity (i.e. inclusion of all pre-calcite cements - kaolinite, pyrite, see Table 4.1) ranges from 35.6 to 47.4% (Table 4.1). So on the assumption of an initial porosity of 48%, compactional effects (i.e. packing readjustments) account for between 0.6 to 12.4% , (mean value, $x = 6.3\%$) of porosity loss prior to calcite cementation, whilst the pre-carbonate cement accounts for between 1.2 to 5.4%, ($x = 2.6\%$). This indicates that cementation by siderite and calcite took place very early in diagenesis at shallow burial depths (see later), so diminishing reservoir quality of the sandstones at a very early stage in the burial history.

The ankerite in concretion B has lower overall pre-cement porosities (36.7 and 30.8%) and increased kaolinite values compared to other samples (Table 4.1). Relative to depositional porosity of 48% at depth 9161', compactional processes have reduced porosity by 11.3%, whilst at depth 9084' compactional processes account for 18.2% prior to ankerite cementation. In view of the higher proportions of kaolinite and the porosity losses due to compaction it is thought that ankerite has precipitated during the later stages of diagenesis.

4.7

SUBSURFACE DEPTH OF GROWTH

Estimation of the burial depth at which the carbonates formed was attempted, assuming that compaction is related directly to the depth of burial, by using empirically derived compaction curves (Baldwin & Butler 1985) and the measured porosity data. For sandstones, Baldwin & Butler (1985) used the following equation to calculate burial depth:-

$$\text{Burial depth (kms)} = 3.7 \ln(0.49/(1-S))$$

where S = solidity and is expressed as $S = 1 - (\text{porosity}(\%)/100)$, Dix & Mullins (1987). Using this equation, the burial depths at which the carbonate cemented concretions formed were calculated (Fig.4.8). These values are however subject to the limitations of the wide range of initial porosities in the sandstones (Pryor 1973, Riecke &

Chilingarian 1974, Baldwin & Butler 1985, Berg 1986), and point counting errors inherent in the analyses (500 counts, 1% error, Folk 1974), but will provide a broad indication of the subsurface depth of growth.

Using total calcite-siderite cement percentages, the calculated subsurface depths of growth of concretions A and C occurred within 1.1 km of the surface, (Fig.4.8), except for depth 8885', concretion A which is calculated at 1.4 km. These are maximum growth depth estimates, but if all the pre-calcite cements are included (these cements having prohibited complete carbonate cementation of the porespace), then concretion A formed within 1.2 km and concretion C within 0.7 km of the surface. These values present a more realistic subsurface growth depth as the total porosity loss due to cements and compactional processes are accounted for. The sample points in the concretions which did not permit calculation suggest formation at very shallow burial depths akin to the shallowest calculated. These calculated formation depths are similar to those estimated by Hamilton et al.(1987) for concretions in the Rannoch Formation of the Brent Group.

Calculation of sandstone burial depth during ankerite precipitation (Concretion B) is difficult to accurately constrain. The calculated burial depth using ankerite percentages alone for 9079' is 3.0kms and for 9084', 3.8kms (Fig.4.8). This is in excess of the present day burial depths of the concretionary horizons yet there is no stratigraphical evidence for uplift within the basin. However, if we calculate burial depth using the pre-ankerite cements too (i.e. siderite, kaolinite, pyrite), this gives ankerite formation depths of 1.1km for 9079' and 1.7km for 9084' (Fig.4.8). These values are considered to be a closer approximation for the burial depth of ankerite formation as the compactional losses and that of porespace occupied by earlier formed cements are still accounted for. So for both siderite/calcite and ankerite formation the depths at which growth occurred were calculated, with the minimum values considered more realistic. The ankerite precipitating at greater depths than the siderite/calcite, a point supported by the petrography.

4.8.1 SIDERITE

The siderite is the earliest of the carbonates and the rhombs display up to three individual zones under backscatter electron microscopy. The backscatter also illustrates the biotite/siderite association, already observed by thin section petrography, with the siderite growing between the laths of biotite which acts as the site for siderite formation (Fig.4.7.d) and as the Fe source.

Siderite rhombs may have two or three individual zones developed. Considering the rhombs with three zones, which are observed in all concretions (Fig.4.9), the innermost zone (I) has Fe+Mn contents of 91.5 to 98.6 mol%, Mg of 0.2 to 4.1 mol% and Ca of 1.2 to 4.4 mol% (Fig.4.10), whilst the middle zone (II) shows a considerable increase in Mg and Ca. Fe+Mn contents range from 57.8 to 66.1 mol%, Mg contents of 19.9 to 27.1 mol% and Ca contents of 10.6 to 22.3 mol%, (Fig.4.10). The outermost zone (III) of these triple zoned siderites indicates a shift back to higher Fe+Mn contents of 72.8 to 82.0 mol%, Mg contents of 12.5 to 24.2 mol% and Ca contents of 2.8 to 11.1 mol% (Fig.4.10).

The siderites with only two zones developed have inner zones with Fe+Mn contents of 62.2 to 69.5 mol%, Mg contents of 19.1 to 25.1 mol% and Ca contents of 8.7 to 16.1 mol% (Fig.4.10). The outer zone has Fe+Mn contents of 71.1 to 79.0 mol%, Mg contents of 11.3 to 16.5 mol% and Ca contents of 9.7 to 12.4 mol% (Fig.4.10).

Several rhombs had well developed inner zones but thinly developed outer zones on which analysis was not possible.

Inspection of Figure 4.10 indicates the relationship of the zonation in the siderites. The composition of the siderites with two zones are similar to the middle and outer zones of the triple zoned siderites. The inner zone of the triple zoned siderites is not recognised in the two zoned siderites. The zonation in the siderite has very irregular boundaries, which is particularly noticeable between the inner and middle zones of the triple zoned siderites (Fig.4.9). This ragged outline is probably due to dissolution of the inner zone prior to precipitation of the middle zone. The marked compositional differences between the two zones (Fig.4.10), suggest increased Ca and Mg in the porewater during formation of the middle

zone. The overall trend observed indicates fluctuations in the relative amounts of Ca, Mg and Fe+Mn in the porewater throughout siderite precipitation.

4.8.2 CALCITE

Calcite mineralogy from the three concretions is very uniform (Fig.4.11), ranging from $\text{Ca}_{98.9}\text{Fe}_{0.9}\text{Mg}_{0.2}$ (mol%) to $\text{Ca}_{92.4}\text{Fe}_{6.2}\text{Mg}_{1.4}$ (mol%): the average composition is $\text{Ca}_{96.3}\text{Fe}_{2.8}\text{Mg}_{0.9}$ (mol%). Under backscatter imagery no evidence for zonation on the calcite was observed (similar to CL observations). This suggests a more uniform porewater chemistry during calcite precipitation.

4.8.3 ANKERITE

Ankerite occurs in concretion B and in trace amounts in concretion C (Table 4.1) with compositions of Ca between 49.2 and 60.0 mol%, Mg contents of 24.3 to 37.5 mol% and Fe+Mn contents of 11.9 to 20.1 mol% (Fig.4.12), the ankerites having a Fe/Mg > 4/1, relative to the ideal ankerite formula $\text{Ca}(\text{Mg.Fe})(\text{CO}_3)_2$. The majority of ankerite analyses at the margins of concretion B have excess calcium to varying degrees except for those analysed from the centre of concretion B (9081'), (Fig.4.12). An excess of calcium has been noted by Deer et al. (1962), Boles (1978) and from the Ninian field, Brent Group, by Kantorowicz (1985). It is possible that the excess calcium comes from the replacement of calcite. In concretion B the replacement of calcite by ankerite has occurred leaving enclaves of calcite within the altered margin. In backscatter imagery the ankerite displays an irregular zonation (Fig.4.13) which has no major compositional differences.

4.9

STABLE ISOTOPES

4.9.1 CARBON - OXYGEN

The $\delta^{18}\text{O}$ value, at equilibrium, when used with the relevant mineral-water fractionation equation, may be related to the temperature of formation and the $\delta^{18}\text{O}$ of the porewater from which the mineral precipitated. Independent knowledge of the temperature or

the $\delta^{18}\text{O}$ of the porewater will permit calculation of one parameter or the other (Longstaffe 1986). $\delta^{13}\text{C}$ in carbonates may be used to indicate the source of the bicarbonate in the porefluid from which the cement precipitated. Depth related processes of organic matter degradation release CO_2 with characteristic carbon isotope signatures. With increasing burial depth these are 1) aerobic oxidation ($\delta^{13}\text{C} = -25\text{‰}$), 2) sulphate reduction ($\delta^{13}\text{C} = -25\text{‰}$), 3) bacterial fermentation ($\delta^{13}\text{C} = +15\text{‰}$) and 4) abiotic thermal processes ($\delta^{13}\text{C} = -20\text{‰}$), see Irwin et al.(1977). Another signature is that of dissolved primary marine carbonate ($\delta^{13}\text{C} = 0\text{‰}$). Intermediate values imply admixtures of sources.

4.9.2 SIDERITE: CARBON VALUES

$\delta^{13}\text{C}$ values for siderite range from -0.1 to -10.3‰ PDB (Fig.4.14). The siderite from concretion A (211/23-3, 8882', Tarbert) is quite distinct (-0.1‰) from the depleted values (-4.6 to -10.4‰ PDB) obtained from concretions B and C in well 211/23-4 (Fig.4.14). The former value is very close to primary marine carbonate; Veizer et al.(1980) report a value for Jurassic marine carbonate of $\delta^{13}\text{C} = +0.48\text{‰}$ PDB. Minor amounts of shell material are present in all of the concretions, and it is possible that the bicarbonate source for this siderite (and this concretion, see calcite $\delta^{13}\text{C}$ values for concretion A) is by dissolution and reprecipitation of Jurassic shell material. The depleted $\delta^{13}\text{C}$ values from concretions B and C are not indicative of an end member bicarbonate source. Siderite in the absence of pyrite precipitates with negative $\delta^{13}\text{C}$ by iron reduction of organic matter (Froelich et al.1979, Maynard 1982, Walker 1984), whilst in association with pyrite the bicarbonate supply is indicative of organic matter degradation by sulphate reduction ($\delta^{13}\text{C} = -25\text{‰}$). Both of these petrographic features are observed in the concretions and indicates a bicarbonate contribution from organic matter degradation by iron/sulphate reduction ($\delta^{13}\text{C} = -25\text{‰}$). The values are mixtures of bicarbonate from shell material ($\delta^{13}\text{C} \approx 0\text{‰}$, Sr data supports this, see later) and that from degradation of organic matter. Assuming this, the contribution from organic derived bicarbonate in the siderites varies from 15 - 42% in these coeval concretions.

4.9.3 SIDERITE: OXYGEN VALUES

$\delta^{18}\text{O}$ values for siderite of -6.1 to -10.5‰PDB, (+24.4 to +19.9‰SMOW) show less overall variation than the carbon values, and no significant variation between concretions. Fig.4.15.a presents siderite precipitation temperatures as a function of the porewater $\delta^{18}\text{O}$. If we assume Jurassic marine water ($\delta^{18}\text{O} = -1.2\text{‰}$) the precipitation temperatures are between 41 to 70°C. By contrast, precipitation temperatures from Jurassic meteoric water ($\delta^{18}\text{O} = -7\text{‰}$) range from 14-33°C.

4.9.4 CALCITE: CARBON VALUES

Calcite $\delta^{13}\text{C}$ values support evidence for two distinct populations (as observed in the siderite). Concretion A has $\delta^{13}\text{C}$ values of +1.8 and +2.1‰PDB, (Fig.4.14), which are only slightly enriched over Jurassic marine carbonate ($\delta^{13}\text{C} = +0.48\text{‰PDB}$), Veizer et al.(1980). As suggested for the siderite in this concretion, the bicarbonate source is by dissolution and reprecipitation of shell material. Although these values may be obtained by mixtures of sulphate reduction and fermentation, the presence of shell material and strontium data (see later) favours the former interpretation. The depleted calcite values in concretions B and C, -6.1 to -10.6‰PDB (Fig.4.14), are considered to reflect a mixture of bicarbonate from shell debris (0%) and by degradation of organic matter by sulphate reduction and/or anaerobic oxidation (-25%). Assuming this, the intermediate calcite values have a contribution from organic derived bicarbonate of between 29-46%.

Subsurface growth depths (Fig.4.8) put concretion formation above or within the fermentation zone (Irwin et al.1977). The bicarbonate contribution from this source is difficult to assess, but factors such as the non-ferroan character of the cement (Curtis 1986, Raiswell 1988), and strontium isotopes (see later) which indicate a strong component of shell material to the calcite, mitigate against its importance.

4.9.5 CALCITE: OXYGEN VALUES

$\delta^{18}\text{O}$ compositions range from -10.6 to -12.6‰PDB (+20.4 to +17.8‰SMOW) so mirroring the features noted from the siderite oxygen

values of a smaller variation in oxygen than carbon which is observed between concretions. Figure 4.15.b presents calcite precipitation temperatures as a function of porewater $\delta^{18}\text{O}$. If we assume Jurassic marine porewater, the precipitation temperature is 68-88°C. For Jurassic meteoric water the precipitation temperature is between 31-45°C. The isotopic temperatures support the petrographic evidence of siderite predating calcite.

4.9.6 POREWATER CONSTRAINTS USING TEXTURAL EVIDENCE

Textural evidence may be used to clarify the type of porefluid present during siderite and calcite formation and to support calculated burial depths. Figure 4.8 shows that growth took place within 1.1 km of the surface. Comparison of the calculated isotopic temperatures with the present day geothermal gradient of 35°C/km for the North Sea helps to distinguish the porewater present at the time of siderite/calcite formation. Referring to Figure 4.8, the siderite/calcite concretions have precipitated (assuming 35C/km) at temperatures < 50°C. This temperature range is not compatible with a meteoric water ($\delta^{18}\text{O} = -7\%$ SMOW), where precipitation of siderite occurred at 14-33°C and calcite at 31-45°C, rather than with marine water $\delta^{18}\text{O} = -1.2\%$ SMOW), which precipitates siderite at 41-70°C and calcite at 68-89°C. The absence of late burial diagenetic cements i.e. quartz overgrowths and illite from the concretions also suggests early formation.

Support for a dominantly meteoric porewater influencing early Brent diagenesis comes from petrographic evidence observed here and by other workers (Sommer 1978, Bjorlykke et al. 1979, Bjorlykke & Brendsdal 1986, Hamilton et al. 1987, Jourdan et al. 1987), e.g. the alteration of muscovite to kaolinite, prior to carbonate cementation. Isotopic evidence from diagenetic silicates confirms this (Brint et al. this vol. Chap.3).

4.9.7 SOURCE OF THE FLUIDS

The most depleted $\delta^{13}\text{C}$ values are found in concretion C (siderite, $\delta^{13}\text{C} = -6.9$ to -10.4% and calcite -8.2 to -11.4% PDB) which is in the non-marine Ness Formation (Fig.4.2) of coaly delta top deposits. This suggests that the organic carbon source has a

major contribution from within the Ness muds and coals. The subsurface passage of meteoric waters through the delta top facies, would permit the oxidation of organic matter and produce CO_2 charged porewaters with characteristically depleted $\delta^{13}\text{C}$ compositions. The porewater is undersaturated with respect to carbonate phases (i.e. shell material) and so dissolution occurs as the flow of water descends through the sediments. With progressive water/rock reactions, the porefluids will become saturated with respect to carbonate resulting in cement precipitation with intermediate values. The Brent sandstone Group is also surrounded by mud dominated sequences i.e. the Dunlin and Humber Group shales (Fig.4.2) which may have added to the organic carbon supply. The contribution from organic carbon decreases in the marine Tarbert facies carbonates due to the increased contribution from marine bicarbonate, so suggesting that in an open system the $\delta^{13}\text{C}$ value is influenced by local facies and porewater flow in the sandstone, even at the same burial depth.

4.9.8 COMPARISON WITH RANNOCH CONCRETIONS

Hamilton et al. (1987), demonstrated that calcite concretions from the Rannoch Formation of the Thistle oilfield, precipitated in a meteoric porewater at temperatures of 32-52°C, ($\delta^{18}\text{O}_{\text{water}} = -6\% \text{SMOW}$). Values for the calcite concretions are $\delta^{13}\text{C} = -0.5$ to $-9.1\% \text{PDB}$, and $\delta^{18}\text{O} = -9.3$ to $-12.8\% \text{PDB}$, and are similar to the results of this study and appear to suggest that the porewater and temperature range during precipitation was homogeneous. Figure 4.14 includes the calcite data from Hamilton et al. (1987).

4.9.9 ANKERITE: CARBON VALUES

The ankerite from concretion B (Fig.4.4.b) has $\delta^{13}\text{C}$ of -4.1 , -5.5 and $-7.6\% \text{PDB}$, (Fig.4.14). These depleted values are again not diagnostic of a particular bicarbonate source. However, the subsurface depth of burial, calculated from minus cement porosity values (Figure 4.8) suggests formation at greater depths of burial than siderite and calcite, at 1.1 and 1.7 km at temperatures of 40-68°C if a geothermal gradient of 35°C/km is assumed. Over this burial depth the processes of fermentation and abiotic reactions

(Irwin et al. 1977) would both contribute to the measured $\delta^{13}\text{C}$ value. Petrography has indicated that ankerite formed partly as a primary precipitate and by replacement of the calcite in the centre of the concretion, so contributions of bicarbonate from the calcite cannot be ignored.

4.9.10 ANKERITE: OXYGEN VALUES

The ankerite has $\delta^{18}\text{O}$ values of -7.6, -9.0 and -11.3‰PDB (+22.9, +21.6 and +19.1‰SMOW), (Fig.4.14, Table 4.2). $\delta^{18}\text{O}$ precipitation temperatures for ankerite are presented as a function of porewater $\delta^{18}\text{O}$ (Fig.4.15.c). For Jurassic marine water ($\delta^{18}\text{O} = -1.2\text{‰SMOW}$), the temperature range is 72-99°C, whilst for Jurassic meteoric water ($\delta^{18}\text{O} = -7\text{‰SMOW}$), ankerite precipitation occurred between 36-55°C. The previous section indicated that formation occurred over a considerable depth range and so leaves the origin of the porewater problematic.

4.9.11 ANKERITE: DISCUSSION

Kantorowicz (1985) states that ankerite formed at burial depths approaching those of the present day, during oil emplacement, at approximately 100 C, assuming a porewater of $\delta^{18}\text{O} = -1.2\text{‰SMOW}$, in the Ninian field, Brent Group. Brint et al.(this vol. Chap.3) indicate that ankerite within the sandstones studied formed between 73 and 102°C, assuming an evolving meteoric porewater of $\delta^{18}\text{O} = -1\text{‰SMOW}$. It is suggested that the ankerite system was semi-closed (in contrast to the early diagenetic open system). Increased rock/water ratios caused isotope exchange reactions which resulted in evolution of the porewater to less negative $\delta^{18}\text{O}$ compositions. The ankerite at depth 9079' ($\delta^{18}\text{O} = +22.9\text{‰SMOW}$) formed first (i.e. having the highest cement porosity value (Table 4.1) and hence forming at the shallowest burial depth (Fig.4.8) of 1.1 km, minimum value). Using the geothermal gradient of 35°C/km this suggests a minimum formation temperature of 39°C for the ankerite. Precipitation of ankerite from Jurassic meteoric water ($\delta^{18}\text{O} = -7\text{‰SMOW}$) indicates formation between 36-55°C, (Fig.4.15.c), so initial ankerite formed in a dominantly meteoric fluid. However the later ankerite (9081', $\delta^{18}\text{O} = +21.6\text{‰}$ and

9084', $\delta^{18}\text{O} = +19.1\text{‰ SMOW}$), formed at increased temperatures from an isotopically evolving porewater (Brint et al. this vol. Chap.3). Precipitation temperatures from a porewater of $\delta^{18}\text{O} = -1\text{‰}$, indicates ankerite precipitation at up to 102°C , (Fig.4.15.c), at a minimum burial depth of 1.7km (Fig.4.8). Brint et al. (this vol. Chap. 3) have constrained the burial depth during the final stages of ankerite development using cogenetic minerals, i.e. quartz overgrowths and illite, at 1.8 - 2.3 km, values very similar to that calculated above. Precipitation temperatures at 1.7 - 2.3 km assuming a 35 C/km geothermal gradient are 65 - 81°C , which are considerably lower than that calculated (102°C). This suggests that the latest ankerite may have grown during a period with an elevated geothermal gradient. Fluid inclusions in cogenetic quartz overgrowths support this (Brint et al. this vol. Chap.3). Also, for growth at 65°C , the porewater would need to be -5‰ (SMOW) which is at variance with the silicate data which indicates formation from a porewater with $\delta^{18}\text{O} = -1$ to $+1\text{‰}$ (Brint et al. this vol. Chap.3).

4.10

STRONTIUM ISOTOPES

Strontium is not measurably isotopically fractionated whilst being assimilated into a solid phase (Veizer 1982). The strontium isotope ratio of the mineral will reflect that of the porewater from which it precipitated. With reference to the carbonate cements studied, there are several possible sources of strontium available (Hamilton et al. 1987);

- 1) Marine porewater
- 2) Meteoric porewater
- 3) Hot formation fluids (at/or derived from depth)
- 4) Fossil carbonate shells
- 5) Local reactive detritus

$^{87}\text{Sr}/^{86}\text{Sr}$ and the strontium concentration were measured on the siderite, calcite and ankerite. $^{87}\text{Rb}/^{85}\text{Rb}$ and rubidium concentrations were measured and age corrections applied where appropriate to the measured $^{87}\text{Sr}/^{86}\text{Sr}$ value to give the true initial value, see Table 4.2, (Faure 1986). Siderite displays a relatively wide range in $^{87}\text{Sr}/^{86}\text{Sr}$ whilst calcite and

ankerite ratios are broadly similar (Table 4.2). Results will enable the characterisation of the strontium source, or sources contributing during carbonate cementation and hence aid in the understanding of the porewater chemistry and its evolution.

4.10.1 SIDERITE

Siderite, which is texturally early, has the highest measured $^{87}\text{Sr}/^{86}\text{Sr}$ ratios of the three carbonate phases (0.7114-0.7277), (Table 4.2). However, high concentrations of rubidium and high $^{87}\text{Rb}/^{86}\text{Sr}$ values (Table 4.2) indicate that these results require recalculation for Rb-Sr decay (Faure 1986). The corrected $^{87}\text{Sr}/^{86}\text{Sr}$ for the siderite are 0.7114-0.7184 (Table 4.2), with strontium concentrations of 74.3 to 661.7 ppm and Rb concentrations of 11.0 to 111.2 ppm (Table 4.2). Oxygen isotope studies have shown that the siderite formed from a dominantly meteoric porefluid, and $^{87}\text{Sr}/^{86}\text{Sr}$ values are considerably more radiogenic than Middle Jurassic marine water (0.707, Burke et al. 1982). Petrographic observations show that the siderite formed at the sites of degrading biotites (Fig.4.7.c), where the siderite rhombs are seen to force apart the individual laths of biotite, whilst muscovite alters to kaolinite (Fig.4.7.a). Radiogenic dates indicate that the provenance of the silicate framework is the Scottish-Norwegian Caledonian orogen (Hamilton et al. 1987) and muscovites from the Rannoch Formation (Fig.4.2) have $^{87}\text{Sr}/^{86}\text{Sr}$ of 0.77685 to 0.93491 (Hamilton et al. 1987). Frost & O'Nions (1985) suggest a bulk value of 0.722 for the Dalradian supergroup within this orogen whilst Faure (1986) reports a value for a sialic component of 0.720 ± 0.005 . So the siderite has the opportunity to incorporate radiogenic strontium from the breakdown of biotite, muscovite and other silicate detritus with high $^{87}\text{Sr}/^{86}\text{Sr}$ values.

Strontium concentrations are variable (74.3 to 661.7 ppm) with higher values associated with lower $^{87}\text{Sr}/^{86}\text{Sr}$ ratios and the lowest Rb concentrations (Table 4.2). This association of high $^{87}\text{Sr}/^{86}\text{Sr}$ with low strontium concentrations is typical of a sialic source (e.g. muscovites from the Rannoch Formation have low strontium concentrations, 33.43 to 47.91 ppm, Hamilton et al. 1987). The mica phases in the Brent may have supplied radiogenic ^{87}Sr

and low strontium concentrations, but are unlikely to account for the high strontium concentrations (up to 661.7 ppm) observed in the two siderites with the least radiogenic $^{87}\text{Sr}/^{86}\text{Sr}$ ratios (0.7114). Therefore an additional source of strontium is required, possibly Jurassic shell material, which has an $^{87}\text{Sr}/^{86}\text{Sr}$ of 0.707 (Jurassic marine water, Burke et al. 1982) and have an extremely high strontium concentration (aragonite shells, av. 7000-9400 ppm, Veizer 1983). So the siderites may have two strontium sources, namely - 1) silicate detritus, (in particular micas) and 2) Jurassic shell material.

4.10.2 CALCITE

Calcite cement has a relatively narrow range in its $^{87}\text{Sr}/^{86}\text{Sr}$ ratio (0.7109-0.7113), and the highest strontium concentrations of the three cements at 555.8 to 2030.4 ppm (Table 4.2). The effects of rubidium are negligible (Table 4.2). As with siderite, calcite has incorporated radiogenic ^{87}Sr , probably from the associated silicate detritus i.e. micas, feldspars, but with $^{87}\text{Sr}/^{86}\text{Sr}$ values that are lower (0.711) and less variable (Fig.4.16.a, Table 4.2). As already indicated, the radiogenic strontium component is incorporated into the carbonates by the leaching of silicate detritus by a dominantly meteoric porewater. However it is unlikely that the high strontium concentrations in the calcite could be obtained by the leaching of silicate detritus (Faure 1986). Fisher & Steuber (1976) note that even small contributions from carbonate beds amongst dominantly silic rock caused an increase in the strontium concentration of the Susquehanna river, so demonstrating that strontium is easily dissolved from carbonates. Consequently, high strontium concentrations in the calcites are feasible from the dissolution of shell material. Veizer (1983) reports strontium concentrations of 7000-9400 ppm in aragonite shells and Kinsman (1969) reports aragonite precipitation from seawater of 8200 ppm. Incorporation of strontium by calcite in varying proportions during formation would explain the high concentrations found (Veizer 1983). Traces of recrystallised fossil shell material are reported from the Brent sequence, (Hamilton et al. 1987, Samways 1986) suggesting that it has dissolved and reprecipitated during early diagenesis. The shell material would have $^{87}\text{Sr}/^{86}\text{Sr}$

similar to Middle Jurassic marine water (0.707) along with high strontium concentrations.

Therefore, calcite $^{87}\text{Sr}/^{86}\text{Sr}$ values are radiogenic due to the contribution from silicate dissolution and have high strontium concentrations from the shell material, suggesting mixing of two strontium components. $^{87}\text{Sr}/^{86}\text{Sr}$ indicate that the strontium composition of the porewater at the time of calcite precipitation had homogenised to an intermediate value (≈ 0.711), with the variation in concentration dependent on the availability of strontium from shell material.

4.10.3 ANKERITE

The ankerite has Rb-Sr corrected $^{87}\text{Sr}/^{86}\text{Sr}$ of 0.7103-0.7113 and strontium concentrations between 332.6 and 678.9 ppm (Table 4.2). The ankerite partly replaces and nucleates on the calcite in the core of concretion B (Fig.4.4). The ankerite at 9081' (core of concretion B) has the highest strontium concentration (678.9 ppm) and a similar $^{87}\text{Sr}/^{86}\text{Sr}$ ratio (0.7113) to the calcites, suggesting a genetic similarity. The ankerite at the margins of concretion B is less radiogenic (0.7103- 0.7109) than all but one of the calcites (9081', 0.7113), and their strontium concentrations are lower (332.6 and 448.1 ppm). Strontium concentrations are probably remnant effects of the shell material which contributed to the calcites. The highest concentration was measured from the core ankerite (678.9 ppm, Table 4.2) and supports the above inference. The ankerite at the margins may reflect a diminished effect from shell material, although input from surrounding shales is also possible. Gallois (1978) reports strontium concentrations of 331 ppm for the Kimmeridge Clay, and Rainey (1987) calculated a value of 247 ppm for the Kimmeridge Clay in the Magnus field.

$^{87}\text{Sr}/^{86}\text{Sr}$ of the ankerites still indicates a component of radiogenic strontium. This could be inherited from the replacement of calcite or alternatively from the leaching of silicate detritus. Textural studies (Fig.4.6) indicate a phase of feldspar dissolution causing secondary porosity development during burial diagenesis. The feldspars would expect to have high $^{87}\text{Sr}/^{86}\text{Sr}$ which cannot explain the strontium values of the ankerite. However if the carbonates recrystallised, strontium is excluded (Veizer 1983), then

the ankerite would have less strontium than calcite and lower $^{87}\text{Sr}/^{86}\text{Sr}$ due to the dominance of shell material. Sullivan (1989) in a study of Rotliegend sandstones (Lower Permian) from the southern North Sea, demonstrated that strontium values in ankerite (0.7109 - 0.7111) and dolomite (0.707 - 0.708) with strontium concentrations between 18 - 100 ppm and 18 - 225 ppm respectively were supplied by the mudrocks and that the $^{87}\text{Sr}/^{86}\text{Sr}$ ratios were coupled with the $\delta^{13}\text{C}$ cement values. The ankerite values (Fig.4.16, Table 4.2) from the Brent approach those from the mudrocks of Sullivan (1989) and may suggest a strontium contribution during burial diagenesis. However no correlation between $\delta^{13}\text{C}$ and $^{87}\text{Sr}/^{86}\text{Sr}$ was noted in this study (Fig. 17), implying that strontium for siderite and calcite did not come from the surrounding mudrocks. With only three data points for ankerite no significant trends are visible.

4.10.4 POSSIBLE TWO COMPONENT MIXING

Consideration of the $^{87}\text{Sr}/^{86}\text{Sr}$ ratios and the strontium concentrations of the carbonates allows assessment of two end member types of strontium source - 1) a high $^{87}\text{Sr}/^{86}\text{Sr}$, low strontium concentration source, i.e. silicate detritus, and 2) a lower $^{87}\text{Sr}/^{86}\text{Sr}$, higher strontium concentration source, i.e. shell material. The siderite displays evidence for the former, whilst the calcite that of the latter (Fig.4.16.a). However the shell material shows a higher $^{87}\text{Sr}/^{86}\text{Sr}$ than Middle Jurassic marine water (0.707) due to the effects of meteoric water leaching radiogenic strontium from micas which consequently raises the composition (av. 0.711).

Faure (1986) demonstrates the systematics of two component mixing for strontium concentrations and $^{87}\text{Sr}/^{86}\text{Sr}$ ratios. It is argued that samples representing mixtures with varying proportions of two components will produce a straight line relationship in a plot of $^{87}\text{Sr}/^{86}\text{Sr}$ versus $1/\text{Sr}$ (concentration). The possibility of two component mixing in the carbonates was investigated and displayed in Figs. 4.16.a and b.

The four siderites from concretion C (Table 4.2) display this relationship most clearly although all three concretions illustrate a similar though less well defined trend. Figure 4.16.b illustrates

that the siderites from concretion C lie on a straight line which ends within the calcite field and so reflects mixing of a high $^{87}\text{Sr}/^{86}\text{Sr}$, low strontium concentration source i.e. micas and feldspars, with the low $^{87}\text{Sr}/^{86}\text{Sr}$, high strontium concentration source, i.e. shell material. Petrography indicates that siderite formed prior to the calcite (Fig.4.6) and so the line demonstrates the increasing influence of the shell material on strontium concentration, and that $^{87}\text{Sr}/^{86}\text{Sr}$ decreased to the homogeneous value during calcite precipitation (Fig.4.16.a,b). So biotite or muscovite degradation influences the siderite formation initially but with the meteoric water continuing to dissolve shell material, the overall $^{87}\text{Sr}/^{86}\text{Sr}$ is lowered and strontium concentrations rise. In concretion B the siderite is dominated by radiogenic strontium from the silicate detritus with low strontium concentrations, whilst the siderite in concretion A exhibits features similar to the calcites (Fig.4.16.a).

The calcites do not exhibit mixing internally but overall the porewater appears to have homogenised, i.e. a balance between the two sources was reached at the termination of siderite authigenesis and the onset of calcite cementation. The ankerites still indicate an input of radiogenic strontium but suggest a different trend with low $^{87}\text{Sr}/^{86}\text{Sr}$ values (0.7103 - 0.7113) and concentrations of 332.6 to 678.9 ppm which may be sourced from recrystallised calcite. A third source of strontium for the ankerites may be the surrounding mudrocks.

4.11

SYNTHESIS

Petrographic studies of the three concretions in wells 211/23-3 and 211/23-4 indicate that carbonate precipitation began with the formation of siderite at the sites of degrading biotites. This was followed by the main cementation phase of calcite. Petrography indicates that siderite and calcite formed during early diagenesis, with sandstone porosities at the time of calcite cementation ranging from 32 to 47%. Grain contacts in these concretions are dominated by floating grain textures, tangential and minor straight contacts. Grain packing and porosity calculations indicate that the concretions formed within 1.1 km of the surface.

Ankerite formation (concretion B) occurred by partial

replacement and nucleation around the calcite core. The ankerite occupies considerably less pore space and calculated burial depths indicate formation at depths between 1.1 and 1.7km. Formation temperatures for the latest stages of ankerite growth indicate an elevated geothermal gradient.

4.11.1 SIDERITE

The siderite precipitated in a variable (Ca and Mg) geochemical environment at very shallow burial depths (Fig. 4.18.a). $\delta^{13}\text{C}$ values for concretions B and C are considerably more depleted (-3.9 to -10.4‰, Table 4.2) than concretion A ($\delta^{13}\text{C} = -0.1‰$) and the $^{87}\text{Sr}/^{86}\text{Sr}$ for the siderites are the most radiogenic of the carbonates (0.7114-0.7184). Each concretion grew during early diagenesis from varying $\delta^{13}\text{C}$ and Sr input from different sources. $\delta^{13}\text{C}$ for the siderite in concretion A is indicative of a marine bicarbonate source (i.e. shell material dissolution and reprecipitation) and has the highest strontium concentration (661.7 ppm) and one of the lowest $^{87}\text{Sr}/^{86}\text{Sr}$ (0.7114) to support this. The siderites from concretions B and C have depleted $\delta^{13}\text{C}$ values and the bicarbonate supply is by reduction of iron oxides in the sediments which allows continued oxidation of organic matter and, where pyrite occurs by sulphate reduction processes, producing negative $\delta^{13}\text{C}$ values ($\delta^{13}\text{C} = -25‰$). Variable admixtures of these sources with marine bicarbonate ($\delta^{13}\text{C} \approx 0‰$, by shell dissolution and reprecipitation) gives the intermediate $\delta^{13}\text{C}$. High $^{87}\text{Sr}/^{86}\text{Sr}$ values are due to input of radiogenic strontium by leaching of biotite and other silicate detritus. This continually mixed with an increasing percentage of strontium from shell material, producing a two component mixing trend to calcite (Fig.4.16). Iron supply would be from biotites and interbedded argillaceous sediments. Pyrite observed with siderite signifies availability of dissolved sulphate and reactive organic matter for H_2S production. Pyrite constitutes <2% of any of the concretions and low availability of dissolved sulphate (possibly by meteoric influx) may have limited precipitation of pyrite. The oxygen isotope composition of siderite ($\delta^{18}\text{O} = -6.1$ to $-10.5‰\text{PDB}$) indicates a dominantly meteoric porewater during precipitation; with water of $\delta^{18}\text{O} = -7‰$ the calculated isotopic precipitation

temperatures are 14–33°C. Siderites are zoned and microprobe analyses show that the proportions of Mg and Ca increase relative to Fe in the outer (later) zones compared to the extremely Fe rich centre. The irregular edge of the inner Fe rich zone indicates that dissolution occurred prior to the precipitation of the Mg/Ca rich zones, so porewater chemistry was fluctuating during siderite formation.

4.11.2 CALCITE

According to Coleman (1985) and Froelich et al. (1979), if sufficient iron remains together with organic material after siderite precipitation, pyrite precipitates and the calcite cement which follows is non ferroan and has negative $\delta^{13}\text{C}$ compositions due to the processes of sulphate reduction. This sequence of events is observed within the concretions and the composition of the calcite $\text{Ca}_{96.3}\text{Fe}_{2.8}\text{Mg}_{0.9}$ (mol%), (Fig.4.11). Calcite $\delta^{13}\text{C}$ values (+2.1 to -10.4‰PDB) indicate a similar scenario to that observed in the siderites, with each concretion forming with varying sources of $\delta^{13}\text{C}$ and Sr. Concretion A has $\delta^{13}\text{C}$ values indicative of a marine signature (+1.8 and +2.1‰PDB) and has very high strontium concentrations suggestive of a source compatible with shell material (Table 4.2). Concretions B and C have contributions from sulphate reduction ($\delta^{13}\text{C}$ -25‰) which in variable mixtures with marine carbonate ($\delta^{13}\text{C} \approx 0\%$, i.e. shell dissolution and reprecipitation) produce intermediate values (-7.3 to -11.3% PDB). Strontium concentrations are high due to the contribution from shell material (555.8 - 2030.4 ppm, see Table 4.2). Porewater chemistry during calcite growth has homogenised in terms of $^{87}\text{Sr}/^{86}\text{Sr}$ (average value of 0.711), and also in terms of Ca, Fe and Mg regarding the microprobe analyses. Presumably the high ^{87}Sr mica sources were now exhausted, or the rate of ^{87}Sr supply had decreased, with a rapid calcite growth. The meteoric influence on the porewater was still present, $\delta^{18}\text{O} = -10.6$ to -12.6% PDB; isotopic temperatures of formation for the calcite are 31–45°C, assuming Jurassic meteoric water ($\delta^{18}\text{O} = -7\%$ SMOW). The meteoric water influx through the Brent sequence has the opportunity to incorporate bicarbonate with negative $\delta^{13}\text{C}$ values by oxidation of organic material in the delta top sediments of the Ness Formation and the underlying Dunlin shales, and also, to effect the dissolution and

reprecipitation of shell material (with a marine carbon signature) in the sediments. The high levels of radiogenic strontium due to leaching of silicate detritus are maintained. Supersaturation of the calcite occurred in areas where siderite already provided suitable reducing, alkaline substrate conditions for precipitation. The calcite occupies up to 58% of the sandstones studied and indicate precipitation at very shallow depths (<1.1km). The lack of a positive carbon signature at these depths suggests a deeply persisting sulphate reduction zone caused by the influxes of meteoric water during early diagenesis. Calcite precipitated by fermentation and abiotic processes produce ferroan calcite (Coleman 1985, Curtis 1977) in later stages of diagenesis and are not considered to be a major contributor of bicarbonate in these concretions.

The generation of siderite and non ferroan calcite by oxidation of organic material occurred in the presence of a dominantly meteoric fluid which penetrated down to 1.1km in an open system during early diagenesis, at temperatures between 14-45°C.

4.11.3 ANKERITE

Ankerite grew over a range of burial depths in a 'closing' system (Fig.4.18.b). Microprobe analysis of the ankerite in the centre of concretion B (9081'), is close to the ideal ankerite formula (Fig.4.15.c), whilst the remaining ankerites are dominantly Ca excess which supports the idea for partial replacement of calcite by ankerite (Fig.4.15.c). The source of the Fe and Mg is often considered to be from diagenetic reactions in surrounding shales (Boles 1978, Boles & Franks 1979). Kantorowicz (1985) suggests that the smectite to illite transition which sources Fe and Mg, was the supply of ions for ankerite precipitation. This occurs at temperatures marking the onset of hydrocarbon generation (Boles & Franks 1979), and is reported in the North Sea (Pearson et al 1982, 1983). Ankerite $\delta^{13}\text{C}$ indicates that it is a mixture of fermentation and decarboxylation processes, considering the calculated burial depth for ankerite formation is taken into account. Oxygen isotope ratios for the ankerite indicate precipitation at temperatures up to 102 C from an evolving meteoric porewater in a semi-closed system due to the decreasing water/rock ratio with burial. The depth of growth of ankerite is further constrained by

considering data on quartz overgrowths and illite (Fig.4.6) (Brint et al. this vol. Chap.3) which indicate that the latest stages of ankerite in the sandstones formed at temperatures of 99°C at burial depths 1.8 - 2.3km at the end-Cretaceous/Tertiary (cogenetic illite K/Ar date - 58Ma). The latest ankerite formed at elevated temperatures with respect to the expected temperature (68°C) for a burial depth of 1.8km (assumed geothermal gradient, 35°C/km). The strontium isotope signature of concretionary ankerite (0.7103 to 0.7113) indicates a contribution from silicate detritus (possibly feldspar dissolution), but strontium concentrations remain high and suggest a contribution from the shell material, which may come from replacement of the calcite. Strontium supply from the surrounding mudrocks is another possibility. Sullivan (1989) indicating that ankerite sourced from mudrocks has $^{87}\text{Sr}/^{86}\text{Sr}$ of 0.709 to 0.711 and Gallois (1978) reports strontium concentrations of 331ppm from the Kimmeridge Clay.

Overall, $^{87}\text{Sr}/^{86}\text{Sr}$ decreased with time (Fig.4.16.a), the dominance of radiogenic strontium from silicate detritus being lessened by shell dissolution and reprecipitation (high concentration, low $^{87}\text{Sr}/^{86}\text{Sr}$, 0.707, Middle Jurassic marine water), and becoming homogenised during calcite cementation. Progressive dilution of the radiogenic strontium occurred during ankerite precipitation along with a lowering in the concentration at the margins. It is possible that strontium was incorporated with Fe and Mg into the ankerite too. Figure 4.17 indicates that the strontium values and carbon values for siderite and calcite are not related, with no definite trend indicated for the ankerite. The two parameters are essentially decoupled.

4.12

CONCLUSIONS

- 1) Siderite-calcite concretions formed during early diagenesis at shallow burial depths (<1.1km) reducing porosity and permeability at an early stage (Fig.4.18.a).
- 2) Siderite forms at the sites of degrading biotites, with calcite forming more extensively, around these areas.
- 3) Carbon isotopes: Siderite, -0.1 to -11.6‰ PDB. Calcite, +2.1 to

-10.6‰ PDB). Bicarbonate supply is from variable admixtures of shell material (dissolution and reprecipitation) and oxidation of organic matter by iron and sulphate reduction.

4) Oxygen isotopes: Siderite, +24.4 to +19.9‰ SMOW. Calcite, +20.4 to +17.8‰ SMOW. The porewater during early diagenesis was dominantly meteoric ($\delta^{18}\text{O} = -7\text{‰ SMOW}$, Middle Jurassic). Isotopic precipitation temperatures for siderite are 14–33°C, and calcite, 31–45°C (supported by petrography and the paragenetic sequence).

5) Siderite has low strontium concentrations (74.2 to 661.7 ppm) and $^{87}\text{Sr}/^{86}\text{Sr}$ of 0.7114–0.7184 due to the incorporation of radiogenic strontium from degrading biotites and other silicate detritus. Calcite has lower $^{87}\text{Sr}/^{86}\text{Sr}$ (0.7109–0.7113) and higher concentrations of 555.8 – 2030.6 ppm due to the increased effects of dissolving shell material. Both end members were present during siderite and calcite growth, forming a two component mixing line. ^{13}C and $^{87}\text{Sr}/^{86}\text{Sr}$ are decoupled.

6) Meteoric water dominated early diagenesis in both the marine Tarbert and non marine Ness facies of the Brent sandstones (Fig.4.18.a). Water flowed through the sandstones leaching silicate detritus, so incorporating radiogenic strontium and dissolving carbonate shell debris (high strontium concentration). The system was open from the Middle Jurassic to around the middle Cretaceous when the Brent sequence was sealed from the surface (Brint et al. this vol. Chap. 3).

7) Ankerite growth occurred post siderite-calcite at burial depths between 1.1 and 1.7km (Fig.4.18.b). $\delta^{13}\text{C}$ values, -4.7 to -7.6‰ PDB, are indicative of mixtures of bicarbonate from fermentation and decarboxylation processes. Oxygen isotope ratios ($\delta^{18}\text{O} = +22.7$ to +19.1‰ SMOW) suggest that formation occurred from an isotopically evolved porewater at temperatures between 40–102 C. These temperatures imply an elevated geothermal gradient during final ankerite growth in the latest Cretaceous.

8) $^{87}\text{Sr}/^{86}\text{Sr}$ compositions indicate the presence of radiogenic strontium (0.7103–0.7113) and concentrations of 332.6–678.9 ppm. Concentrations may reflect dissolution of earlier calcite cement, the remnant effects of shell material, or possibly an input from

silicates in shales. Formation of the ankerite occurred in a semi-closed system, the $\delta^{18}\text{O}$ values indicate porewater evolution during burial diagenesis.

The authors wish to thank the technical staff at the Isotope Geology Unit, S.U.R.R.C., East Kilbride. Dr. W.E. Stephens and Donald Herd of the Geology department at St. Andrews University for access to the Jeol microprobe. Discussions with Graeme Rogers and Tim Dempster at S.U.R.R.C. proved helpful. We are grateful to the B.G.S. core store and to Dick Sutherland for access to core. J.F.B. acknowledges receipt of NERC grant no. GT4/85/GS/97. S. Brown publishes by permission of the Director of the B.G.S. (NERC). The Isotope Geology Unit is supported by the NERC and the Scottish Universities.

- BALDWIN, B., and BUTLER, C.O., 1985, Compaction curves: Am. Assoc. Petroleum Geologists Bull., v. 69, p. 622-626.
- BERG, R.R., 1986, Reservoir Sandstones: New Jersey, Prentice-Hall, 481p.
- BJORLYKKE, K. and BRENDSDAL, A., 1986, Diagenesis of the Brent sandstone in the Statfjord field, North Sea, in Gautier, D.L., ed., Roles of Organic Matter in Sediment Diagenesis, Soc. Econ. Palaeontologists Mineralogists Spec. Publ. 38, p.157 -167.
- BLANCHE, J.B., and WHITAKER, J.H.McD., 1978, Diagenesis of part of the Brent sand formation (Middle Jurassic) of the northern North Sea Basin: Jour. Geol. Soc. London, v. 135, p. 73-82.
- BOLES, J.R., 1978, Active ankerite cementation in the subsurface Eocene of Southwest Texas: Contrib. Mineral. Petrol. v. 68, p. 13-22.
- BOLES, J.R., and FRANKS, S.G., 1979, Clay diagenesis in Wilcox sandstones of southeast Texas: implications of smectite diagenesis on sandstone sedimentation: Jour. Sed. Petrology, v. 49, p. 55-70.
- BOLES, J.R., LANDIS, C.A., and DALE, P., 1985, The Moerake Boulders-anatomy of some septarian concretions: Jour. Sed. Petrology, v. 55, p. 398-406.
- BOWEN, J.M., 1975, The Brent Oilfield, in Woodland, W.A., ed., Petroleum and the Continental Shelf of North-West Europe, v. 1, Geology: Applied Science Publishers, Barking, p.353-362.
- BRINT, J.F., HASZELDINE, R.S., HAMILTON, P.J., FALLICK, A.E., and BROWN, S., Isotope diagenesis and palaeofluid movement in the Middle Jurassic Brent sands, northern North Sea, this vol. Chap.3.
- BROWN, S., RICHARDS, P.C., and THOMSON, A.R., 1987, Patterns in the deposition of the Brent Group (Middle Jurassic) UK North Sea, in Brooks, J., and Glennie, K., eds., Petroleum Geology of North West Europe: Graham & Trotman, London, p. 899-913.
- BUDDING, M.C., and INGLIN, H.F., 1981, A reservoir geological model

- of the Brent Sands in Southern Cormorant, in Illing, L.V., and Hobson, G.D., eds., Petroleum Geology of the Continental Shelf of North-West Europe, Heyden & Son, London, p. 326-334.
- BURKE, W.H., DENISON, R.E., HETHERINGTON, E.A., KOEPNICK, R.B., NELSON, H.F. and OTTO, J.B., 1982, Variation of seawater $^{87}\text{Sr}/^{86}\text{Sr}$ throughout Phanerozoic time: *Geology*, v. 10, p. 516-519.
- CARPENTER, S.J., ERICKSON, J.M., LOHMANN, K.C., and OWEN, M.R., 1988, Diagenesis of fossiliferous concretions from the Upper Cretaceous Fox Hills Formation, North Dakota: *Jour. Sed. Petrology*, v. 58, p. 706-723.
- CHAUVIN, A.L., and VALACHI, L.Z., 1980, Sedimentology of the Brent and Statfjord Formations of Statfjord Field, in, *The Sedimentation of the North Sea Reservoir Rocks*, Geilo, Norw. Petrol. Soc. p. 16/1-17.
- COLEMAN, M.L., 1985, Geochemistry of diagenetic non-silicate minerals: kinetic considerations: *Phil. Trans. R. Soc. London*, v. 315A, p.39-56
- COLEMAN, M.L., and RAISWELL, R., 1981, Carbon, oxygen and sulphur isotope variations in concretions from the Upper Lias of northeastern England: *Geochim. Cosochim. Acta*, v. 45, p. 329-340.
- CRAIG, H., 1957, Isotopic standards for carbon and oxygen correction factors for mass spectrometric analysis of carbon dioxide: *Geochim. Cosmochim. Acta*, v. 12, p. 133-149.
- CURTIS, C.D., 1977, Sedimentary geochemistry: environments and processes dominated by involvement of an aqueous phase: *Phil. Trans. R. Soc. London*, v.286A, p. 353-372.
- CURTIS, C.D., COLEMAN, M.L., and LOVE, L.G., 1986, Pore water evolution during sediment burial from isotopic and mineral chemistry of calcite, dolomite and siderite concretions: *Geochim. Cosmochim. Acta*, v. 50, p.
- DEEGAN, C.E., and SCULL, B.J., 1977, (Compilers), A standard lithostratigraphic nomenclature for the Central and Northern North Sea: *Rept. Inst. geol. Sci. 77/25*, HMSO Publications, 36p.

- DEER, W.A., HOWIE, R.A., and ZUSSMAN, J., 1962, Rock-forming Minerals, v. 5, p. 371 - non-silicates, John Wiley & Sons, New York.
- DIX, G.R., and MULLINS, H.T., 1987, Shallow, subsurface growth and burial alteration of Middle Devonian calcite concretions: Jour. Sed. Petrology, v. 57, p. 140-152.
- DOTT, R.H. Jr., 1964, Wacke, graywacke and matrix - what approach to immature sandstone classification?: Jour. Sed. Petrology, v. 34, p. 625-632.
- DUTTON, S.P. and LAND, L.S., 1985, Meteoric burial diagenesis of Pennsylvanian arkosic sandstones, southwestern Anadarko Basin, Texas: Am. Assoc. Petroleum Geologists Bull., v.69, p.22-38.
- FAURE, G., 1986, Principles of Isotope Geology, (2nd ed.): John Wiley & Sons, Canada, 589p.
- FISHER, R.S., and STUEBER, A.M., 1976, Strontium isotopes in selected streams within the Susquehanna river basin: Water Resources Research, v. 12, p. 1061-1068.
- FOLK, R.L., 1974, Petrology of Sedimentary Rocks: Hemphill Book Store, Austin, Texas, 174p.
- FRIEDMAN, I., and O'NEIL, J.R., 1977, Compilation of stable isotope fractionation factors of geochemical interest, in Fleischer, M., ed., Data of Geochemistry (6th ed.): United States Geological Survey Professional Paper 440-KK, 12p. + figures.
- FROELICH, P.N., KLINKHAMMER, G.P., BENDER, M.L., LUEDTKE, N.A., HEATH, G.R., CULLEN, D., DAUPHIN, P., HAMMOND, D., HARTMAN, B., and MAYNARD, V., 1979, Early oxidation of organic matter in pelagic sediments of the eastern equatorial Atlantic: Suboxic diagenesis: Geochim. Cosmochim. Acta, v. 43, p. 1075-1090. FROST, C.D., and O'NIONS, R.K., 1985, Caledonian magma genesis and crustal recycling: Jour. Petrology, v. 26, p. 515-544.
- GALLOIS, R.W., 1978, A pilot study of the oil shale occurrences in the Kimmeridge Clay: Rep. Inst. Geol. Sci., no. 78/13
- HALLET, D., 1981, Refinement of the geological model of the Thistle field, in Illing, L.V., and Hobson, G.D., eds., Petroleum Geology of

the Continental Shelf of North-West Europe, Heyden & Son, London, p. 315-325.

HAMILTON, P.J., FALLICK, A.E., MACINTYRE, R.M., and ELLIOTT, S., 1987, Isotopic tracing of the provenance and diagenesis of Lower Brent Group sands, North Sea, in Brooks, J., and Glennie, K., eds., Petroleum Geology of North West Europe, Graham & Trotman, London, p. 939-949.

HANCOCK, N.J., and TAYLOR, A.M., 1978, Clay mineral diagenesis and oil migration in the Middle Jurassic Brent Sand Formation: Jour. Geol. Soc. London, v. 135, p. 69-72.

IRWIN, H., CURTIS, C.D., and COLEMAN, M., 1977, Isotopic evidence for source of diagenetic carbonates formed during burial of organic-rich sediments: Nature, v. 269, p. 209-213.

JOURDAN, A., THOMAS M., BREVART, O., ROBSON, P., SOMMER, F., and SULLIVAN, M., 1987, Diagenesis as the control of the Brent sandstone reservoir properties in the Greater Alwyn area (East Shetland Basin), in Brooks, J., and Glennie, K., eds., Petroleum Geology of North West Europe, Graham & Trotman, London, p. 951-961.

KANTOROWICZ, J.D., 1985, The origin of authigenic ankerite from the Ninian field, UK North Sea: Nature, v. 315, p. 214-216.

KINSMAN, D.J.J., 1969, Interpretation of Sr^{2+} concentrations in carbonate minerals and rocks: Jour. Sed. Petrology, v. 39, p. 486-508.

LONGSTAFFE, F.J., 1986, Oxygen isotope studies of diagenesis in the Basal Belly River sandstone, Pembina I-Pool, Alberta: Jour. Sed. Petrology, v. 56, p. 78-88.

McCREA, J.M., 1950, On the isotope chemistry of carbonates and a paleotemperature scale: Jour. Chemical Physics, v. 18, p. 849-857.

MAYNARD, J.B., 1982, Extension of Berner's new geochemical classification of sedimentary environments' to ancient sediments: Jour. Sed. Petrology, v. 52, p. 1325-1331.

MOORE, L.J., MOODY, J.R., BARNES, I.L., GRAMICH, J.W., MURPHY, T.J., PAULSEN, P.J., and SHIELDS, W.R., 1973, Trace determination of

rubidium and strontium in silicate glass standard reference materials: Anal. Chemistry, v. 45, p. 2384-2387.

O'NEIL, J.R., CLAYTON, R.N., and MAYEDA, T.K., 1969, Oxygen isotope fractionation in divalent metal carbonates: Jour. Chem. Physics, v.51, p.5547-5558.

PARRY, C.C., WHITLEY, P.K.J., and SIMPSON, R.D.H., 1981, Integration of palynological and sedimentological methods in facies analysis of the Brent Formation, in, Illing, L.V., and Hobson, G.D., eds., Petroleum Geology of the Continental Shelf of North-West Europe, Heyden & Son, London, p. 205-215.

PEARSON, M.J., WATKINS, D., and SMALL, J.S., 1982, Clay diagenesis and organic maturation in northern North Sea sediments: Proc. Int. Clay Conf. Bologna & Pavia, p. 665-675.

PEARSON, M.J., WATKINS, D., PITTION, J.L., CASTON, D., and SMALL, J.S., 1983, Organofacies and early maturation effects in Upper Jurassic sediments from the Inner Moray Firth Basin, North Sea, in, Brooks, J., ed., Petroleum Geochemistry and Exploration of Europe, Jour. Geol. Soc. London. Spec. Pub. 12, Blackwell Scientific Publications, Oxford, p. 147-160.

PETTIJOHN, F.J., 1975, Sedimentary Rocks, 3rd Ed., Harper & Row, New York, 628p.

PRYOR, W.A., 1973, Permeability-porosity patterns and variations in some Holocene sand bodies: Am. Assoc. Petroleum Geologists Bull., v. 57, p. 162-189

RAINEY, S.C.R., 1987, Sedimentology, diagenesis and geochemistry of the Magnus sandstone member, northern North Sea: Unpubl. Ph.D thesis, Univ. of Edinburgh, 403p. RICHARDS, P.C., and BROWN, S., 1986, Shoreface storm deposits in the Rannoch Formation (Middle Jurassic), North West Hutton Oilfield: Scott. Jour. Geology, v. 22, p.367-375.

RICHARDS, P.C., BROWN, S., DEAN, J.M., and ANDERTON, R., 1988, A new palaeogeographic reconstruction for the Middle Jurassic of the northern North Sea: Jour. Geol. Soc. London, v. 145, p. 883-885.

RIECKE, III, H.H., and CHILINGARIAN, G.V., 1974, Compaction of Argillaceous Sediments, Developments in Sedimentology 16: Amsterdam,

Elsevier, 424p.

ROSENBAUM, J., and SHEPPARD, S.M.F., 1986, An isotopic study of sidreites, dolomites and ankerites at high temperatures: *Geochim. Cosmochim. Acta*, v. 50, p. 1147-1150.

SAMWAYS, G.M., 1986, Carbonate cementation in some Mid-Jurassic Brent Sands, UK, northern North Sea: Abstracts Annual Meeting British Sedimentology Research Group, Nottingham.

SOMMER, F., 1978, Diagenesis of Jurassic sandstones in the Viking Graben: *Jour. Geol. Soc. London*, v. 135, p. 63-67.

SULLIVAN, M., 1989, Diagenetic study of the Lower Permian Rotliegendes sandstone, Leman Field, Southern North Sea, Unpub. M.Sc thesis, Univ. of Glasgow, 148p.

THOMAS, M., 1986, Diagenetic sequences and K/Ar dating in Jurassic sandstones, Central Viking Graben: effects on reservoir properties: *Clay Minerals*, v. 21, p. 63-67.

VEIZER, J., 1983, Chemical diagenesis of carbonates: Theory and application of trace element technique, in, Arthur, M.A., Anderson, T.F., Kaplan, I.R., Veizer, J., and Land, L.S., eds., *Stable Isotopes in Sedimentary Geology*, Soc. Econ. Palaeontologists Mineralogists Short Course No.10, Dallas, p. 3-1, 3-100.

VEIZER, J., HOLSER, W.T., and WILGUS, C.K., 1980, Correlation of $^{13}\text{C}/^{12}\text{C}$ and $^{34}\text{S}/^{32}\text{S}$ secular variations: *Geochim. Cosmochim. Acta*, v. 44, p. 579-587

WALKER, J.C.G., 1984, Suboxic diagenesis in banded iron formations: *Nature*, v. 309, p. 340-342.

Figure 4.1: A - Location of Brent Province, East Shetland Basin, northern North Sea. (Inset refers to Fig.1B).

B - Location of Dunlin oilfield (211/23) with major structural features indicated, East Shetland Basin. (Inset refers to Fig. 1C).

C - Location of wells studied (211/23-3, -4) from the Dunlin oilfield, with the major structural elements.

Figure 4.2: Jurassic stratigraphy and facies in the East Shetland Basin, containing the Brent Group.

Figure 4.3: Sketch section of tilted fault blocks which characterise the Jurassic structural regime, East Shetland Basin.

Figure 4.4: A - Sedimentary log of Well 211/23-3, (Concretion A indicated), Key as Fig. 4.4B.

B - Sedimentary log of Well 211/23-4, (Concretions B and C indicated).

Figure 4.5: QFR plot for the framework grains of the concretions. Classification after Pettijohn (1975), modified from Dott (1964).

Figure 4.6: General paragenesis of diagenetic minerals, Brent sandstones.

Figure 4.7: a) Photomicrograph of kaolinite (Kaol.), as an alteration product of muscovite, pre-calcite cement, (Field of view = 0.5mm), cross-polars, Concretion C, 9278', (2827.8m), Tarbert Formation, 211/23-4.

b) Photomicrograph of vermiform kaolinite (Kaol.), pre-calcite cement, (Field of view = 0.2mm), cross-polars, Concretion A, 8883.5', (2707.6m), Tarbert Formation, 211/23-3.

c) E.M. Backscatter photomicrograph of K-feldspar overgrowths (K-Fsp o/g), pre-calcite cement, (scale bar - 10 microns), Concretion A, 8882' (2707.1m), Tarbert Formation, 211/23-3.

d) Photomicrograph of siderite aggregates (Sid.), pre calcite cement, (Field of view = 0.4mm), cross-polars, Concretion C, 9278' (2827.8m), Ness Formation, 211/23-4.

e) E.M. Backscatter photomicrograph showing siderite (sid.) and pyrite (Pyr.) growing between and forcing apart the individual biotite laths (scale bar - 100microns), Concretion C, 9285' (2829.9m), Ness Formation, 211/23-4.

f) Photomicrograph showing early aggressive calcite, with a floating grain texture developed, (Field of view = 2.5mm), cross-polars, Concretion C, 9278' (2827.8m), Ness Formation, 211/23-4.

g) Photomicrograph of intergranular calcite cement at the concretion edge, average size of individual crystals varies from 0.1 to 0.3mm, (Field of view = 1.5mm), cross-polars, Concretion C, 9278' (2827.8m), Ness Formation, 211/23-4.

h) Cathodoluminescence photomicrograph of poikilotopic calcite cement which has a uniform, unzoned orange luminescence, (Field of view = 2.5mm), Concretion B, 9081' (2767.8m), Tarbert Formation, 211/23-4.

Figure 4.8: Solidity-Depth plot for Concretions A,B and C, Dunlin oilfield. Siderite/Calcite growth occurred in an open system within 1.1 km of the surface (<50 C). Ankerite growth is difficult to constrain accurately between the maximum and minimum value, external evidence given later (isotopic section) indicates that the latest stages of growth occurred at 1.7-2.3 km. Individual points in the concretions are given in feet (present day burial depths). Note that it was not possible to calculate all points, cf. Table 1).

Figure 4.9: E.M. Backscatter photomicrograph of zoned rhombic siderite, showing three growth zones (pale-dark-pale). The innermost zone has a ragged outline, suggesting dissolution prior to formation of the second zone. Each zone is distinct in composition, (Fig.3.10). Concretion B, 9282' (2829.0m), Ness Formation, 211/23-4. Scale bar = 10 microns.

Figure 4.10: Siderite compositions (mole %) for Concretions A,B and C, Dunlin oilfield. Siderites may have three zones; I (inner), II (middle) and III (outer), or two zones; II (inner) and III (outer) developed. Zone I is not developed in the siderites with only two zones. The inset illustrates the evolution path of the siderite composition with precipitation, which reflects the changing porewater composition during early diagenesis.

Figure 4.11: Calcite composition field (mole %) from Concretions A,B and C, Dunlin oilfield. Data from microprobe analyses of all samples between 8882' (2707.1m) and 9285' (2829m). Total number of analyses = 29.

Figure 4.12: Ankerite compositions (mole %) from Concretion B, 9079 to 9084', Tarbert Formation, and 9276' and 9285', Concretion C, Ness Formation, Brent Group, Dunlin oilfield. At depth 9081', in Concretion B the ideal ankerite composition is approached, whilst the ankerite at the margins of Concretions B and C have a calcium excess. Number of analyses = 17

Figure 4.13: E.M. Backscatter photomicrograph of ankerite from 9084' (2768.7m), Tarbert Formation, 211/23-4. Ankerite displays a "stripe-like" zonation; analysis of the pale and dark areas showed no significant difference in Ca, Mg and Fe+Mn.

Figure 4.14: Plot of $\delta^{13}\text{C}$ versus $\delta^{18}\text{O}$ (PDB) for siderite, calcite and ankerite from Concretions A,B and C, Brent Group, Dunlin oilfield, and the area occupied by Rannoch concretions Thistle oilfield from Hamilton et al.(1987).

Figure 4.15.a - Siderite $\delta^{18}\text{O}$ versus Temperature and $\delta^{18}\text{O}$ porewater (all values reported against SMOW) from Concretions A,B and C, Brent Group, Dunlin oilfield (cf. Table 4.2, n = 7). The temperature range for siderite formation is illustrated for waters of $\delta^{18}\text{O} = -1.2\text{‰}$ and -7‰ SMOW. The meteoric water (-7‰) interpretation is preferred, 14 - 35°C.

$1000 \cdot \ln \alpha_{\text{Siderite-Water}} = 2.78 \cdot 10^6 \cdot T^{-2} - 2.89$, Friedman & O'Neil (1977), after O'Neil et al.(1969).

Figure 4.15.b - Calcite $\delta^{18}\text{O}$ versus Temperature and $\delta^{18}\text{O}$ porewater (all values reported against SMOW) from Concretions A,B and C, Brent Group, Dunlin oilfield (cf. Table 4.2, n = 7). The temperature range for the calcite cementation is illustrated for waters of $\delta^{18}\text{O} = -1.2\text{‰}$ and -7‰ SMOW. The meteoric water (-7‰) interpretation is preferred, 32 - 45°C.

$1000 \cdot \ln \alpha_{\text{Calcite-Water}} = 2.78 \cdot 10^6 \cdot T^{-2} - 2.89$, Friedman & O'Neil (1977), after O'Neil et al.(1969).

Fig.15.c - Ankerite $\delta^{18}\text{O}$ versus Temperature and $\delta^{18}\text{O}$ porewater (all values reported against SMOW) from Concretion B,

Tarbert Formation, Brent Group, Dunlin oilfield (cf. Table 4.2, n = 3). The temperature range for ankerite formation is illustrated for waters of $\delta^{18}\text{O} = -1.2\text{‰}$ and -7‰ SMOW. The interpretation is of growth from an isotopically evolving porewater at temperatures between 55 and 102°C.

$1000 \cdot \ln \alpha_{\text{Ankerite-Water}} = 2.78 \cdot 10^6 \cdot T^{-2} + 0.32$, Dutton & Land (1985).

Figure 4.16.a - Plot of $^{87}\text{Sr}/^{86}\text{Sr}$ versus $1/\text{Sr}$ ($\times 10^3$) using all data points from siderite, calcite and ankerite in Concretions A, B and C. The data illustrates the high $^{87}\text{Sr}/^{86}\text{Sr}$; low $1/\text{Sr}$ concentrations of siderite which evolves to lower $^{87}\text{Sr}/^{86}\text{Sr}$; higher $1/\text{Sr}$ concentrations of calcite. Ankerite suggests a trend to even lower $^{87}\text{Sr}/^{86}\text{Sr}$ which is displayed at the margins of Concretion B (9079', 9084').

The sub-diagram illustrates the evolutionary trend from a mica to shell dominated strontium source during early diagenesis. The trend to ankerite may suggest the input of strontium from feldspar in mudrocks (Sullivan 1989). Fig. 4.16.b - Two component mixing line illustrated by siderite from Concretion C, Ness Formation, 211/23-4. Strontium supply from 1) high $^{87}\text{Sr}/^{86}\text{Sr}$, low concentration source and 2) low $^{87}\text{Sr}/^{86}\text{Sr}$, high strontium concentration. Depths 9276' and 9278' illustrate the dominance of the former, whilst 9282' and 9285' illustrate a greater input of the latter, which finds 9282' falling into the area of diagenetically later calcite strontium compositions.

Figure 4.17: Plot of $^{87}\text{Sr}/^{86}\text{Sr}$ versus $\delta^{13}\text{C}$ (PDB) using all data from Concretions A, B and C, Brent Group. The data indicates that the two parameters are essentially decoupled both overall and on an individual concretion basis, (cf. Table 4.2).

Figure 4.18.a - Open system diagenetic regime during siderite and calcite precipitation: Meteoric water flows through the sequence from deposition until sealed off during the Cretaceous by overlying muds. Siderite precipitating at degrading biotite sites in reducing conditions which later nucleated calcite. Bicarbonate supply is local:- 1) shell material (marine Tarbert) and 2) oxidation of organic matter by sulphate reduction processes (delta plain Ness). Strontium was sourced from the biotites and the shells, and values

are uniform in both the Tarbert and Ness Formations suggesting that shell strontium was transported in the porewater.

Figure 4.18.b - Ankerite Formation: This schematic diagram illustrates the conditions at the end of ankerite precipitation in a semi-closed system. Ankerite precipitation was initiated immediately after the cessation of calcite growth ($T = 55^{\circ}\text{C}$) at 1.1 km, and continued to precipitate at increasing temperatures in an elevated geothermal gradient (102°C) from an isotopically evolving meteoric dominated porewater ($\delta^{18}\text{O} = -7$ to $= 1\%$). With burial the Brent Group became sealed from the surface. Fe and Mg may come from the surrounding muds, whilst Sr is sourced from the precursor calcite and possibly the muds.

Table 4.1: Point count data for Concretions A,B and C, 211/23-3, 211/23-4, Dunlin oilfield.

Table 4.2: Carbon, Oxygen and Strontium Isotope Data.

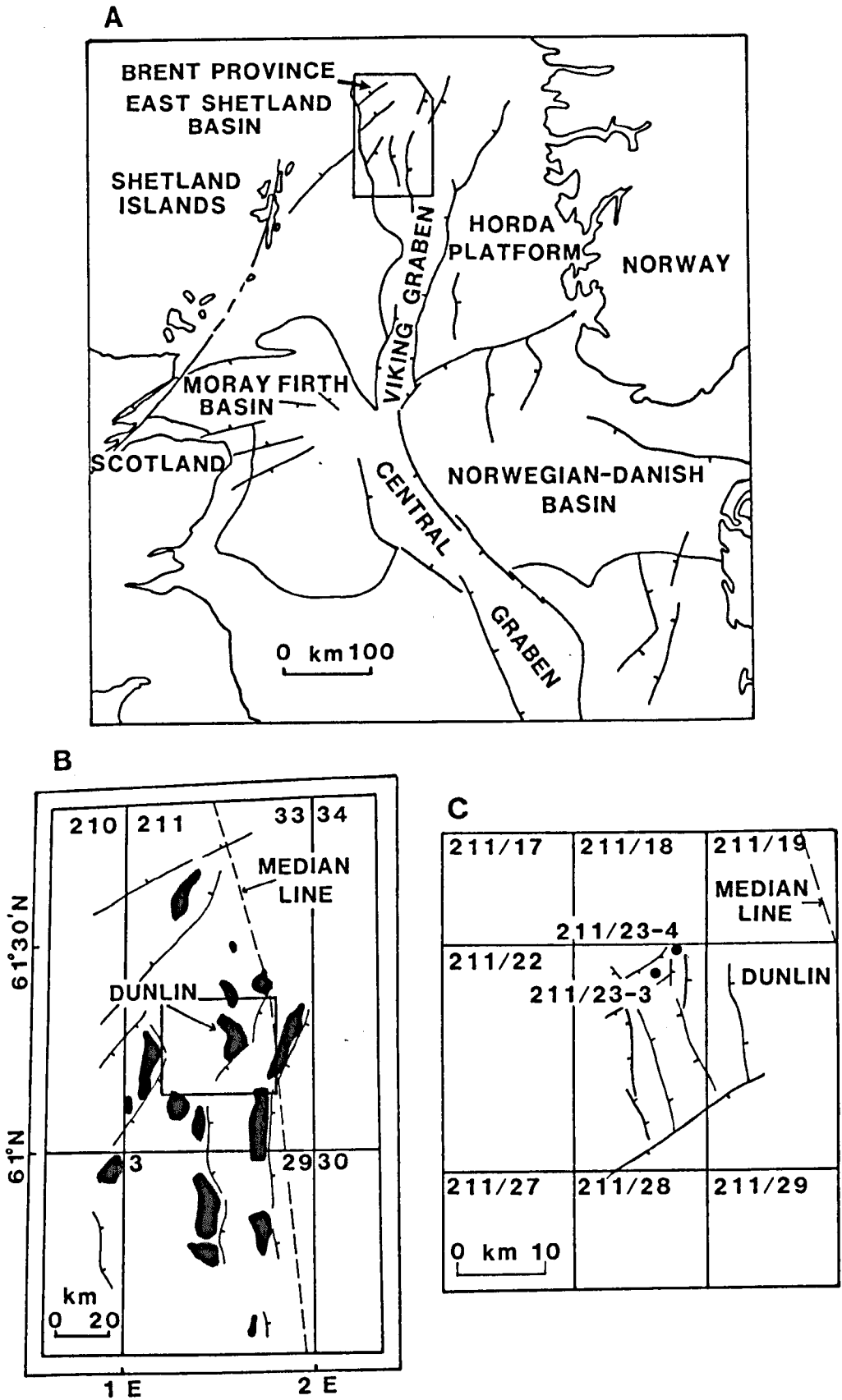


Figure 4.1

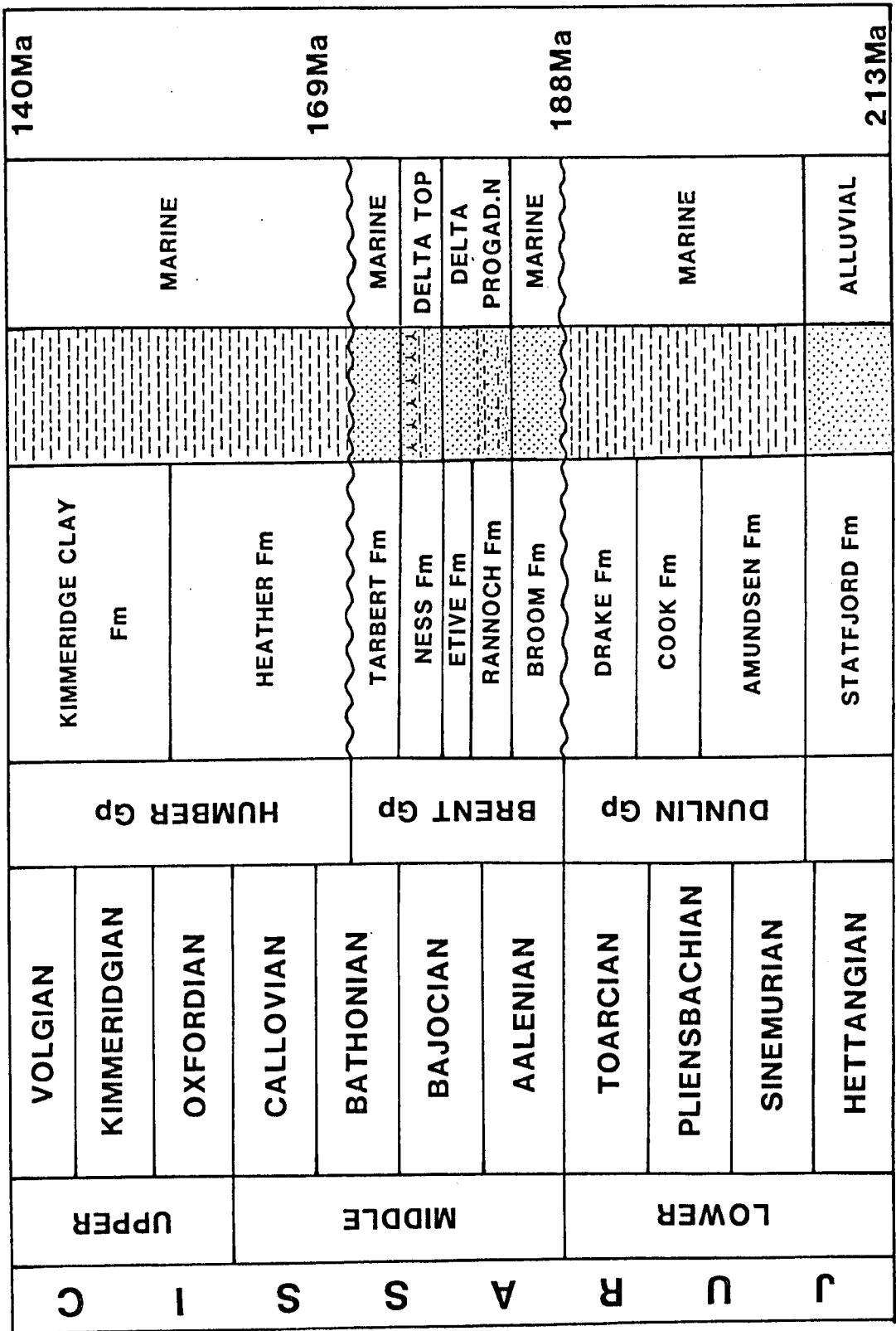


Figure 4.2

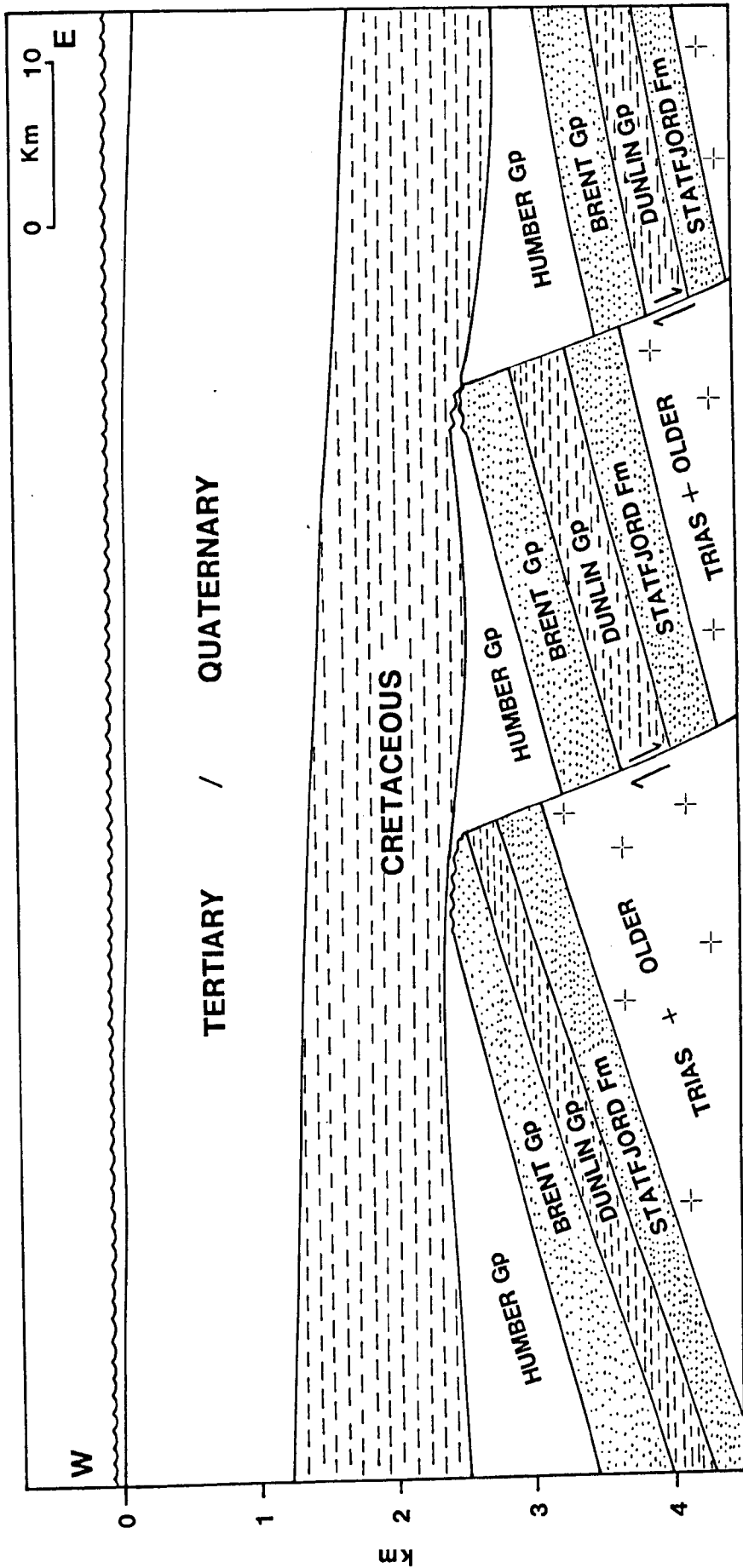
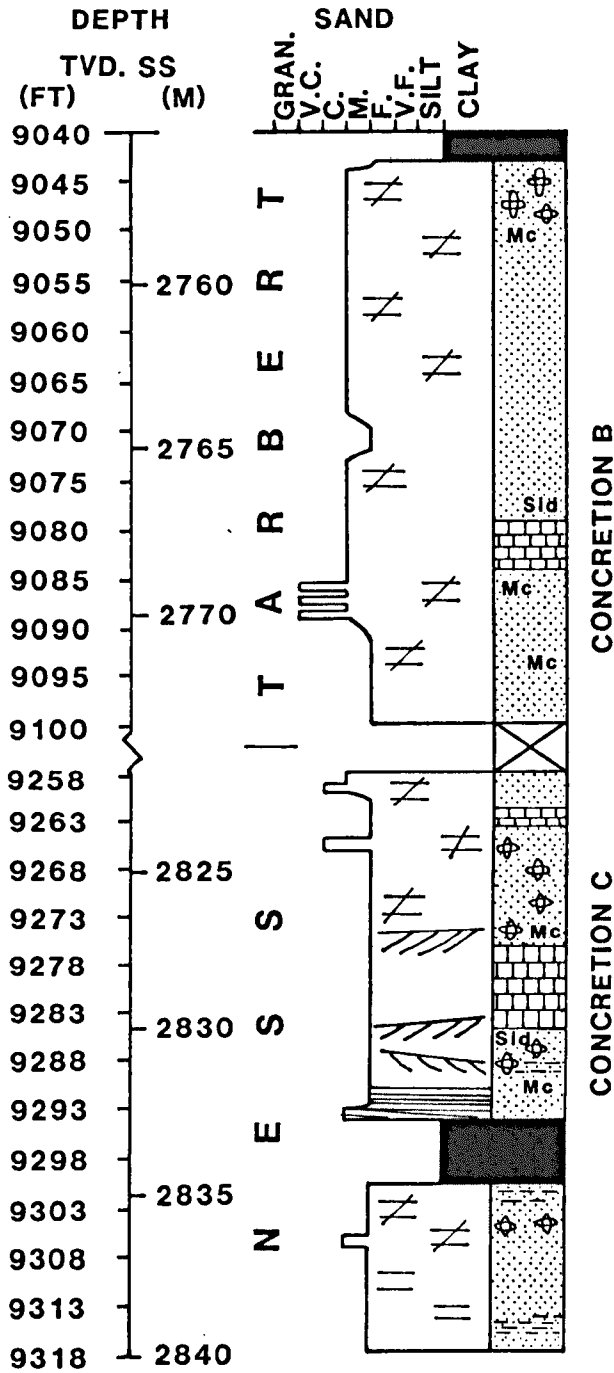


Figure 4.3

Figure 4.4.b

211/23-4



KEY :Figs. 4A and B

≠ Massive
No apparent bedding

(=) Slightly bedded

= Horizontal bedding

≈ Contorted bedding

/// Cross bedding

≡ Low angle lamination

∩ Ripple lamination

⊕ Bioturbated

■ Carbonaceous material

Sid Siderite

Mc Micaceous

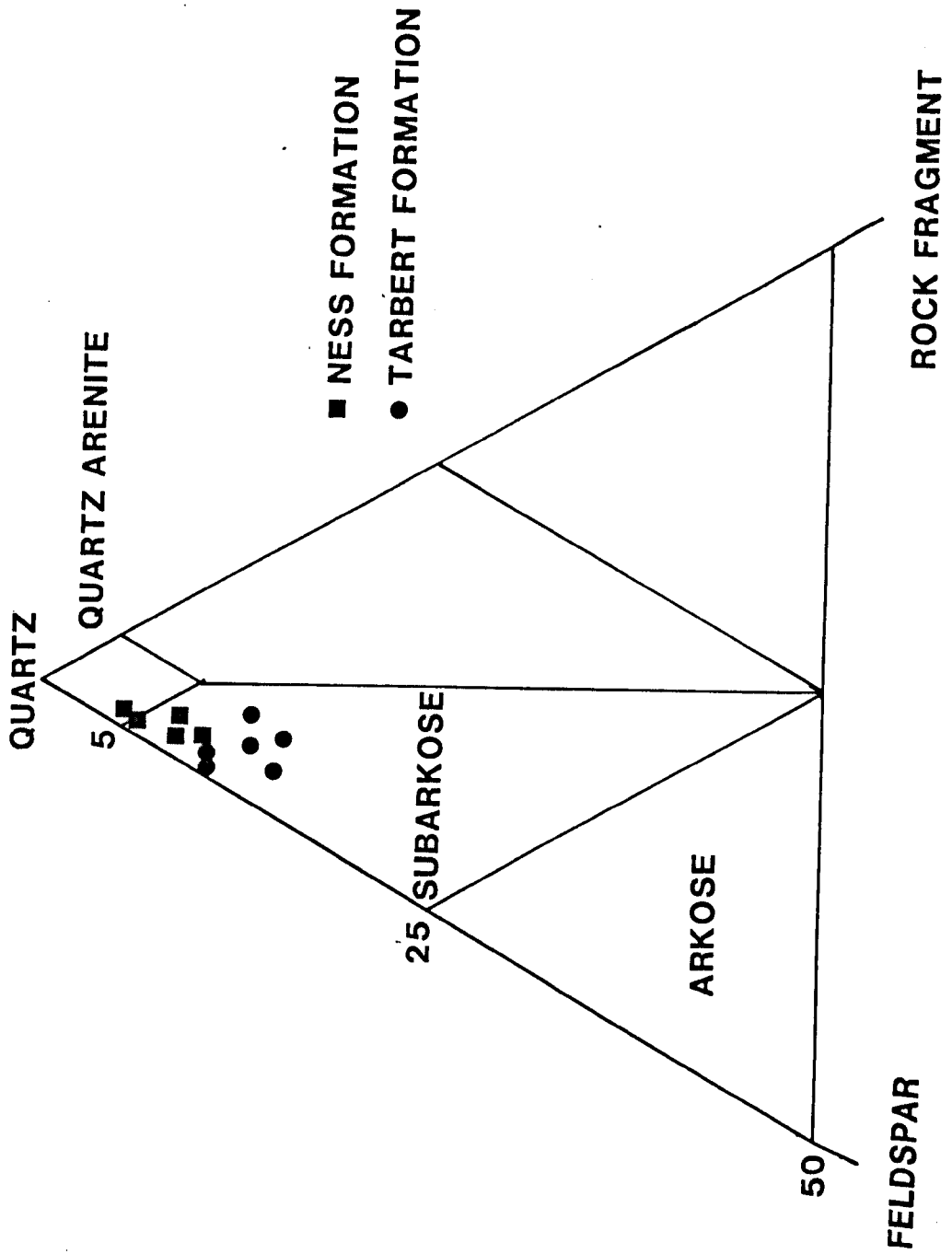


Figure 4.5

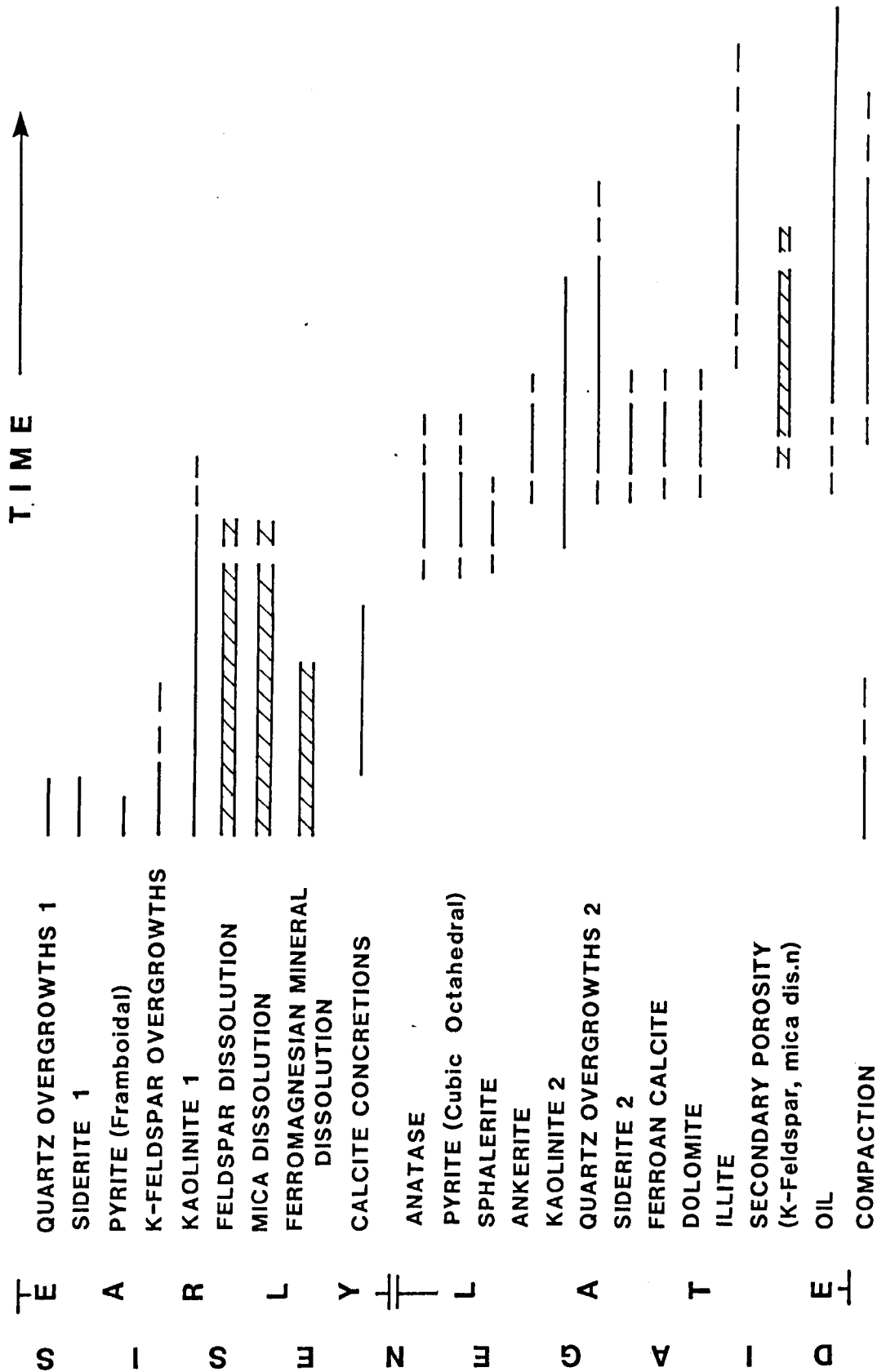


Figure 4.6

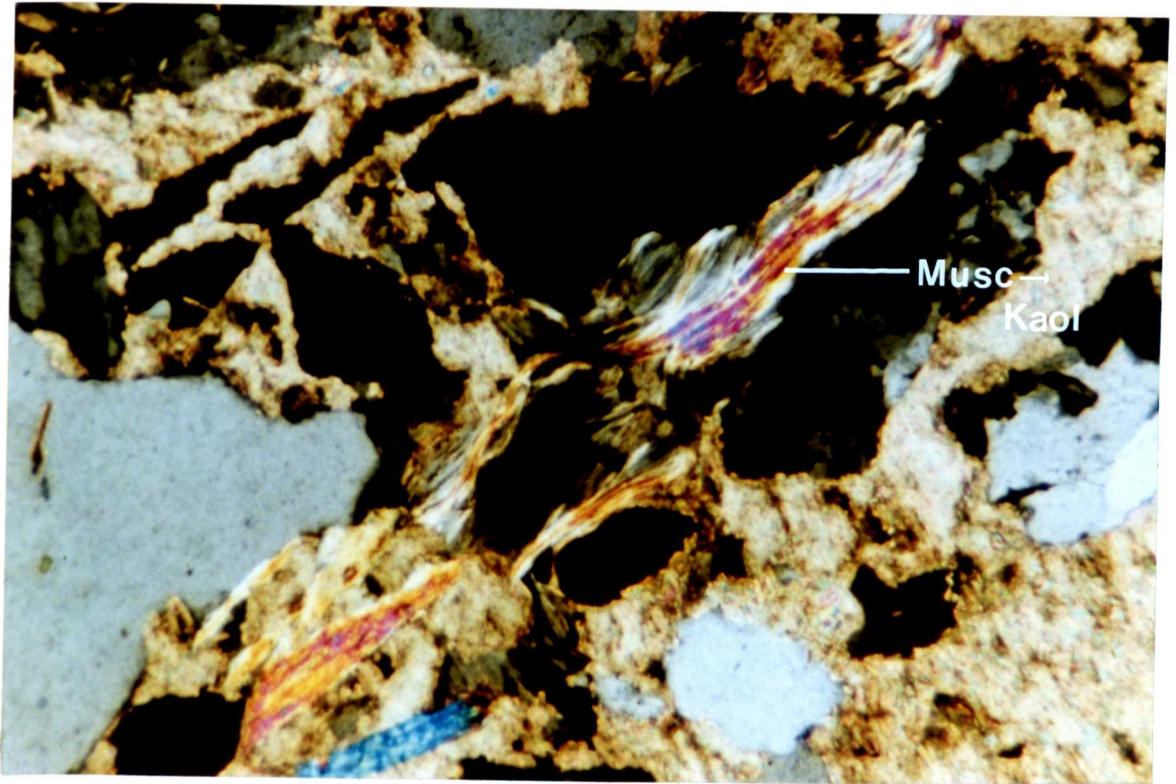


Figure 4.7.a

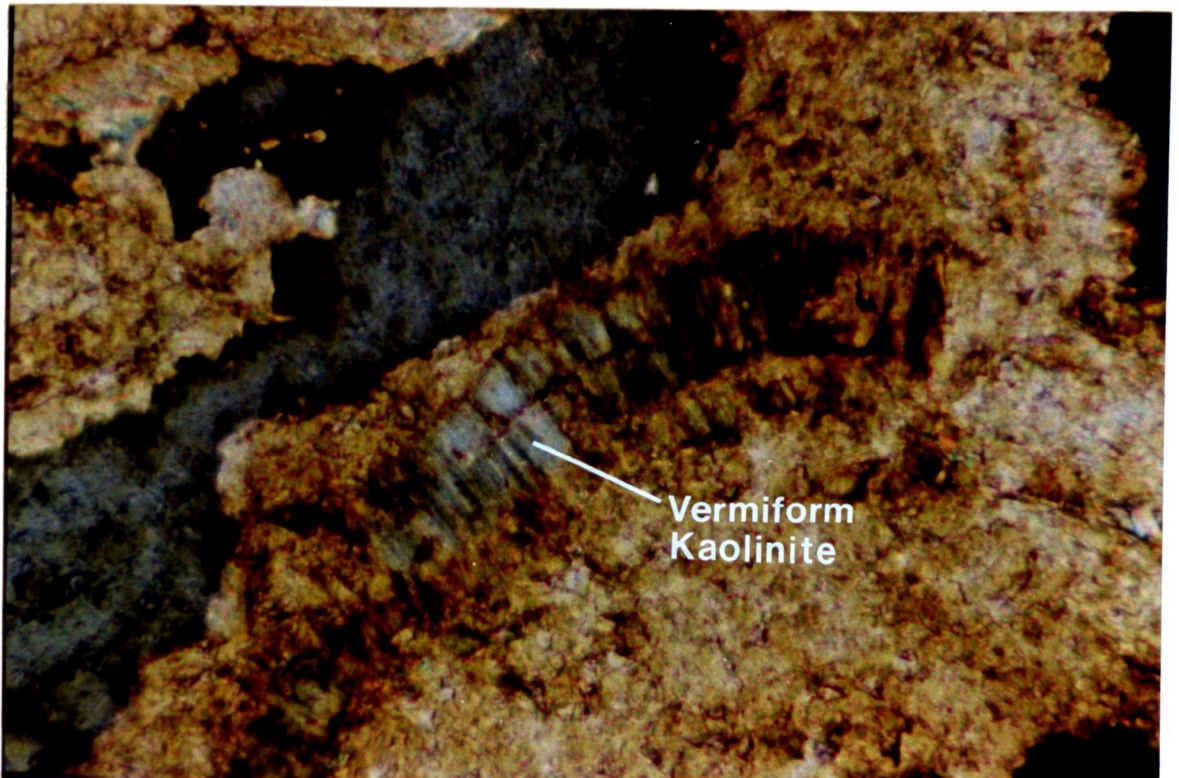


Figure 4.7.b

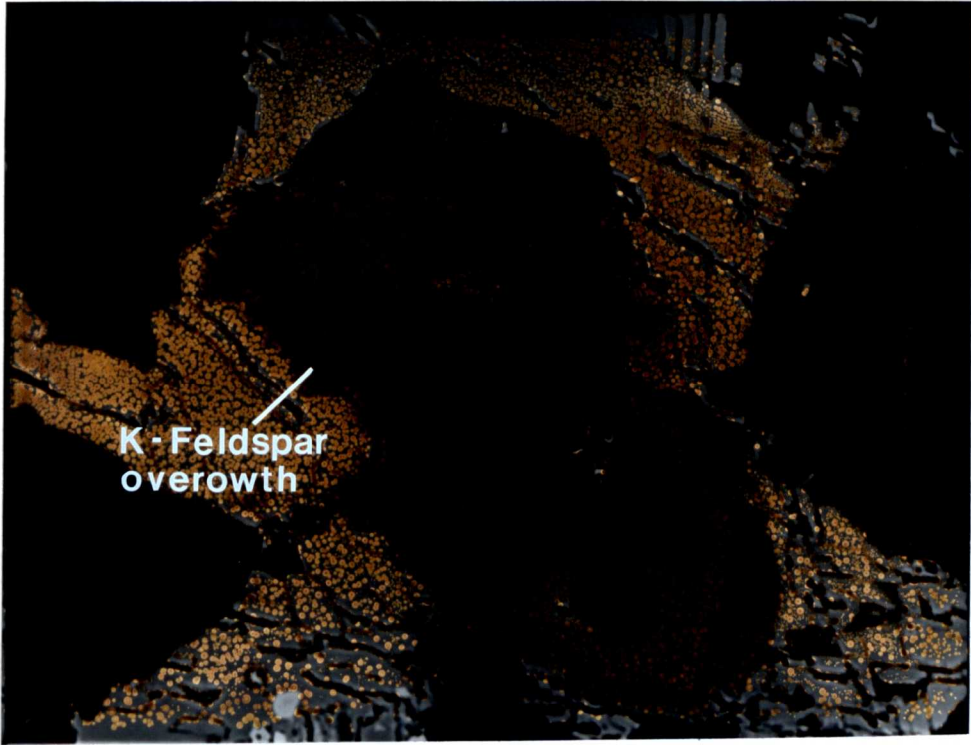


Figure 4.7.c

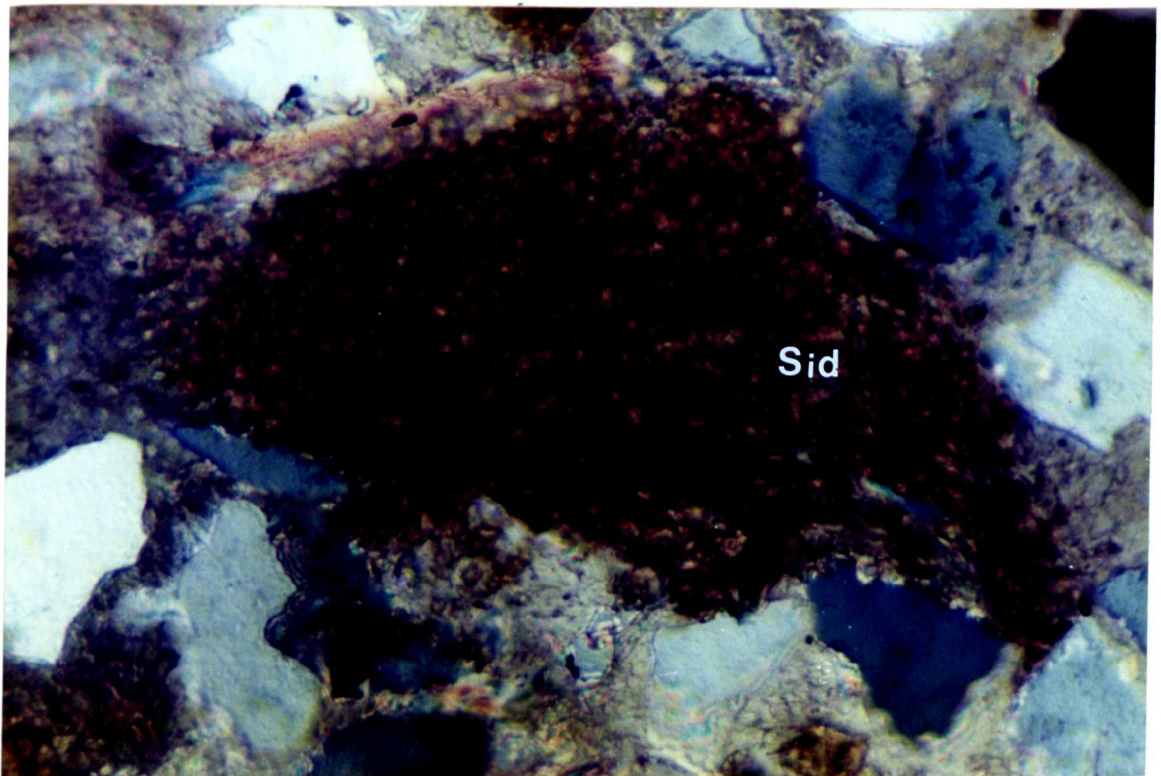


Figure 4.7.d

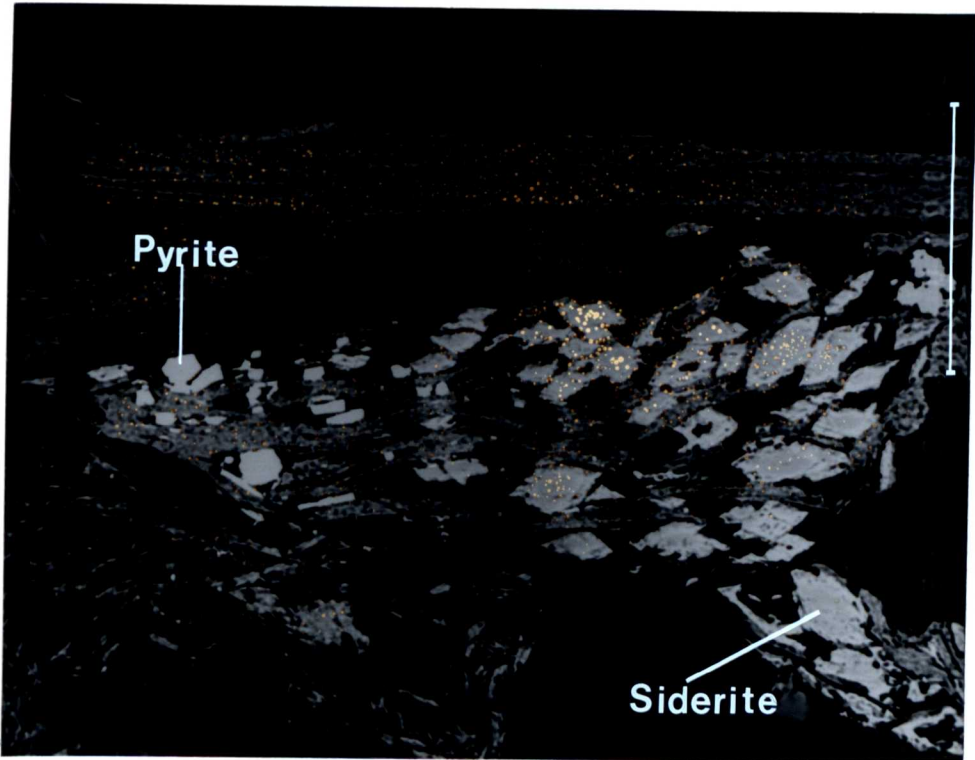


Figure 4.7.e

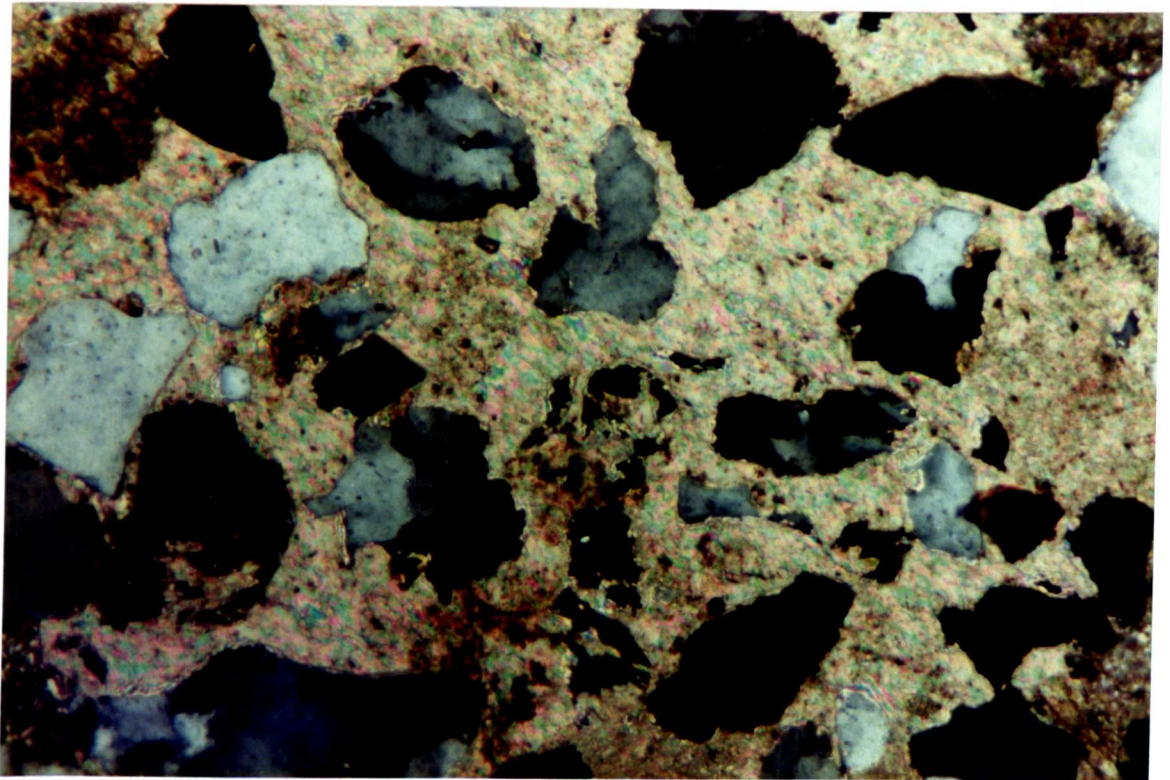


Figure 4.7.f

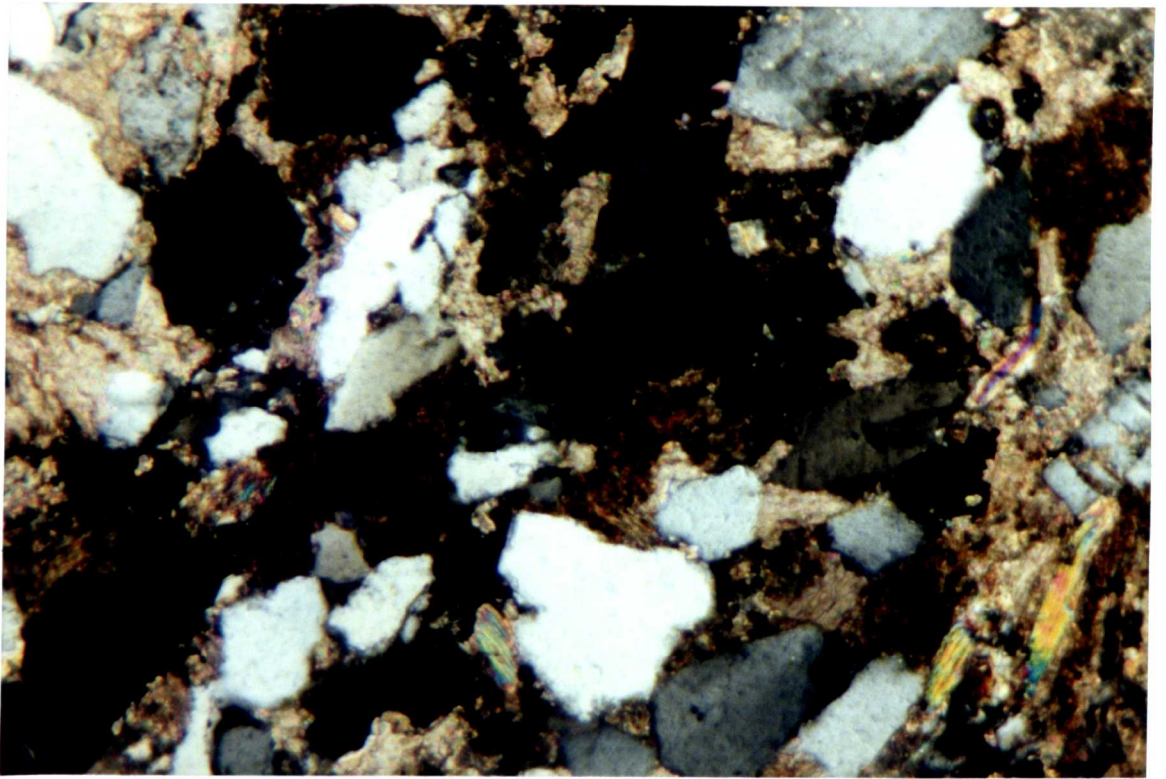


Figure 4.7.g

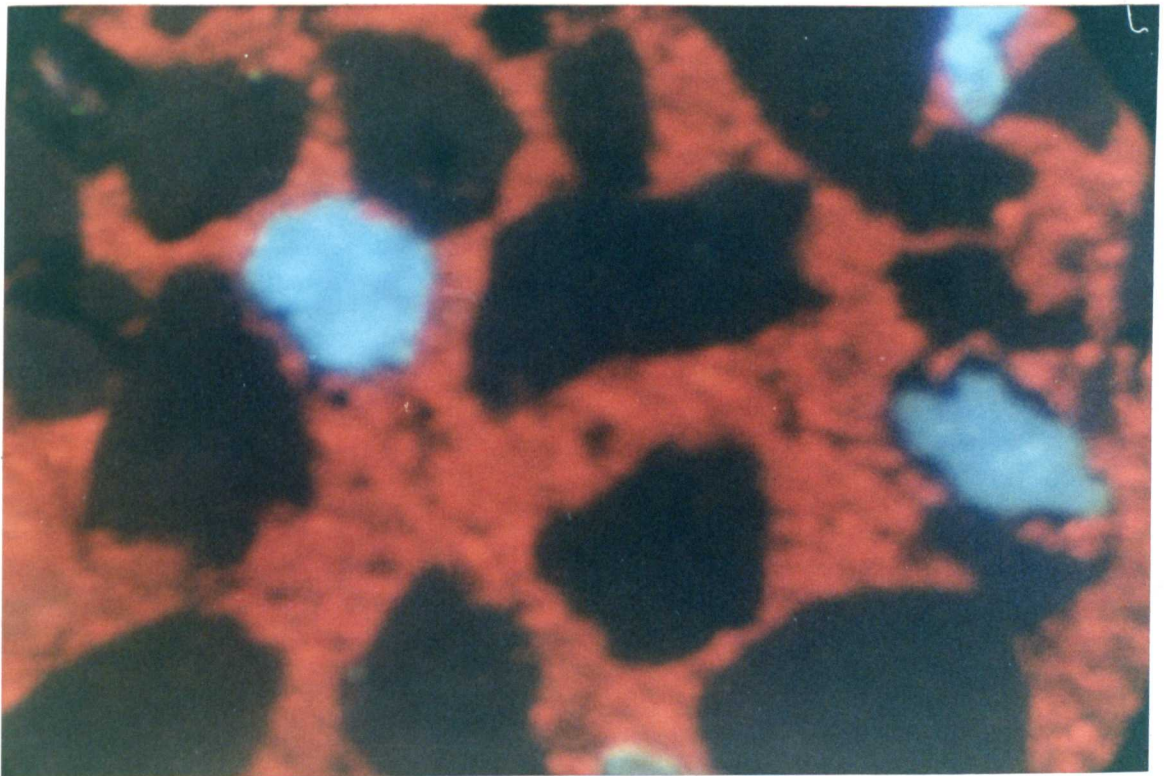


Figure 4.7.h

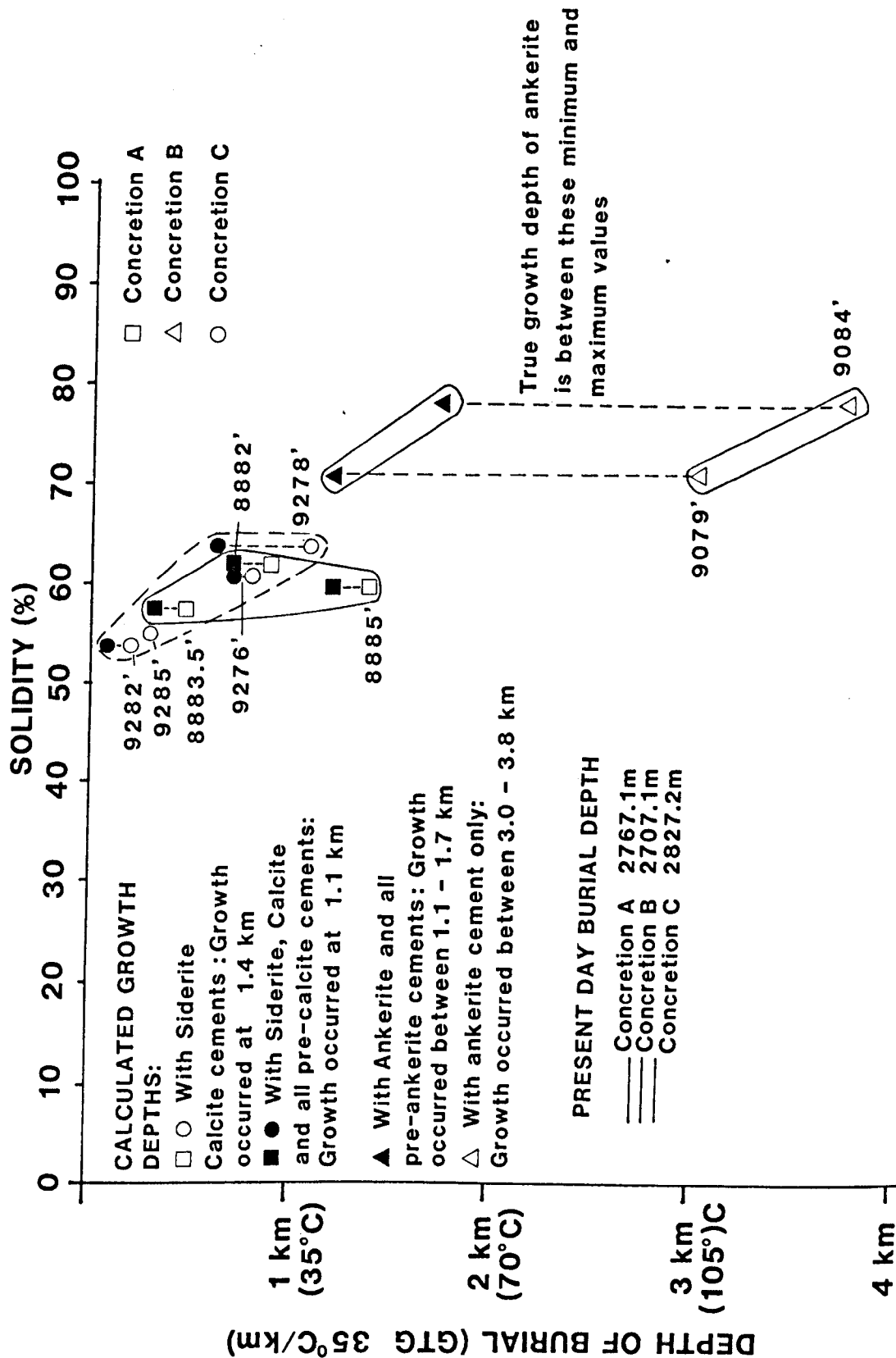


Figure 4.8

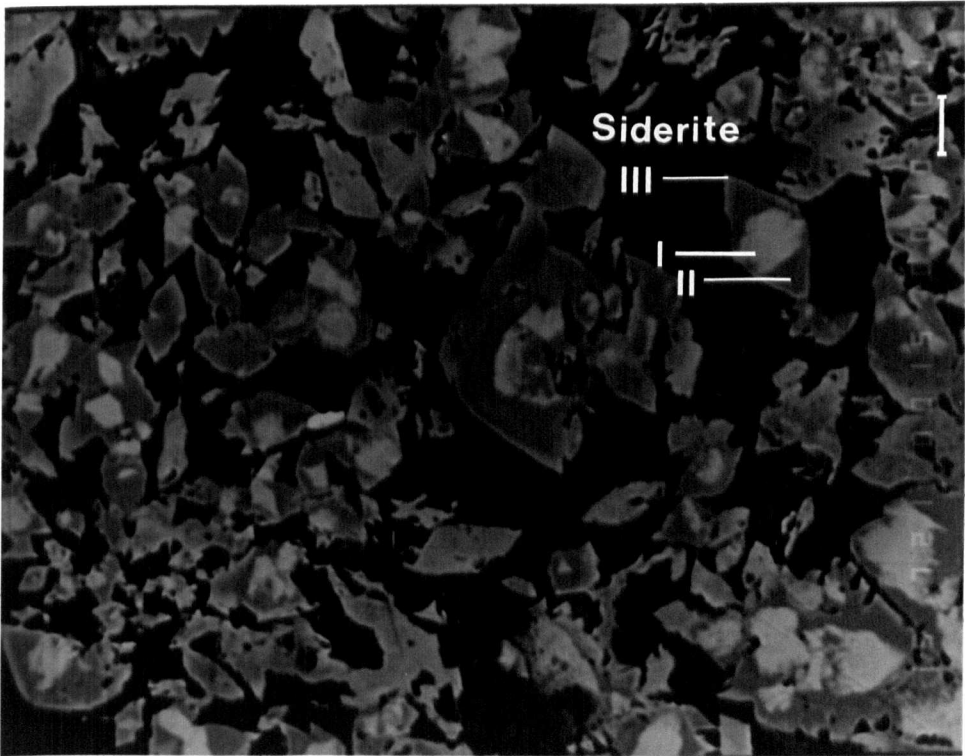


Figure 4.9

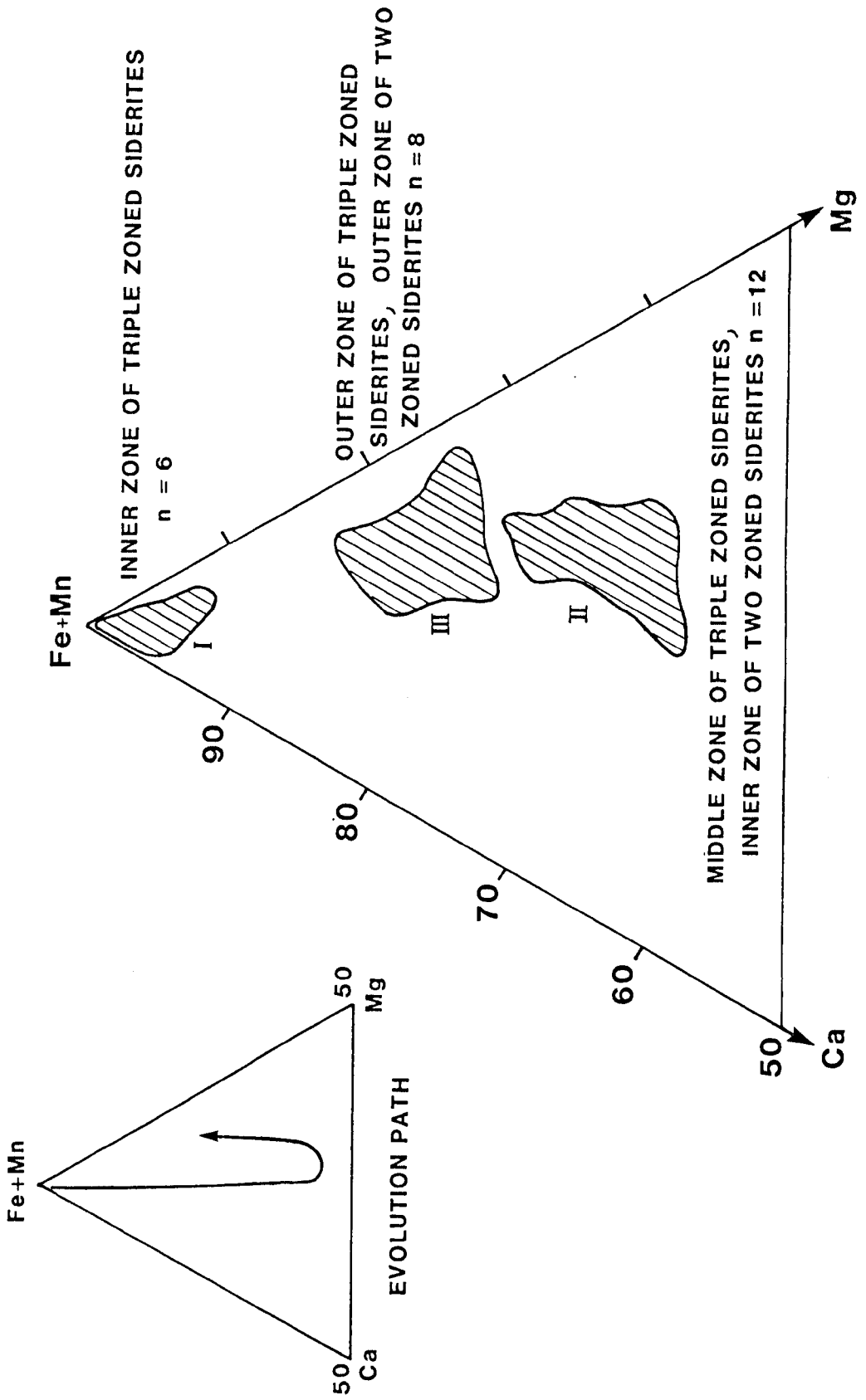


Figure 4.10

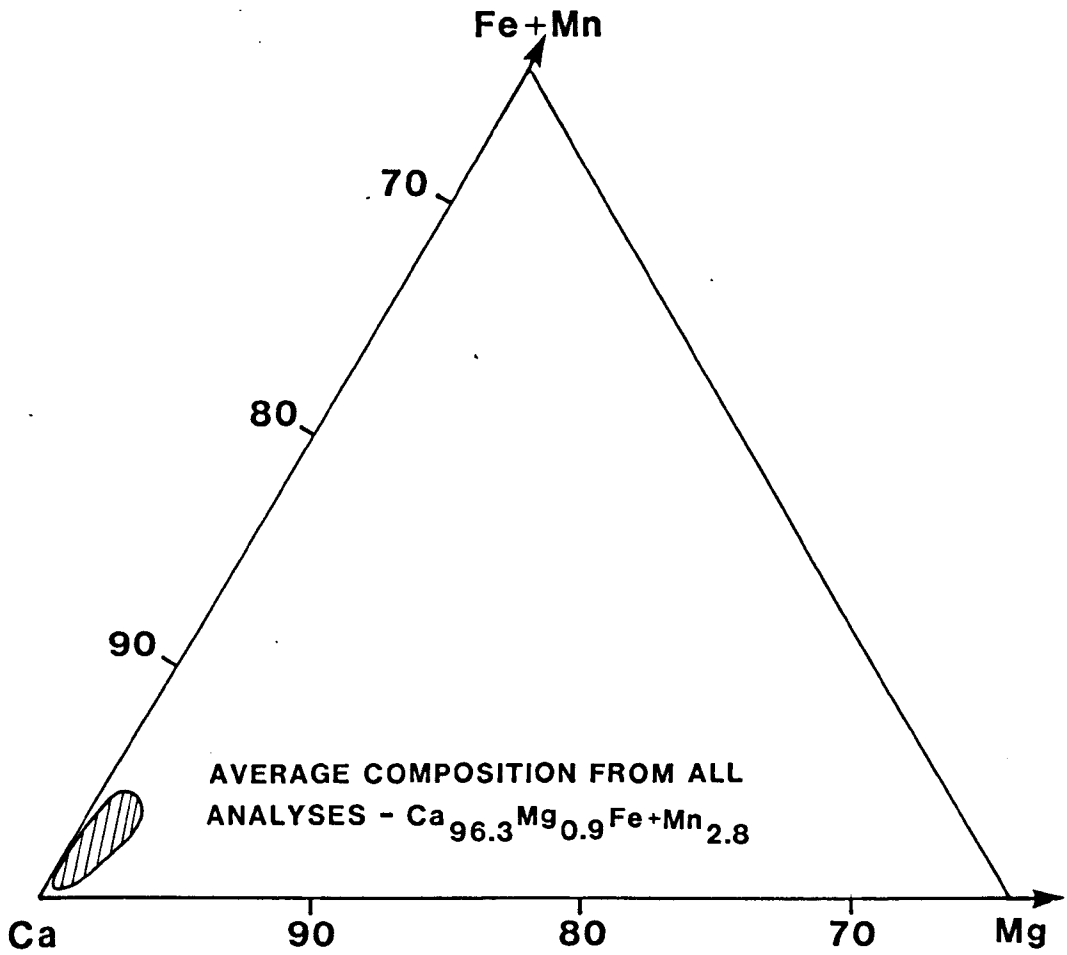


Figure 4.11

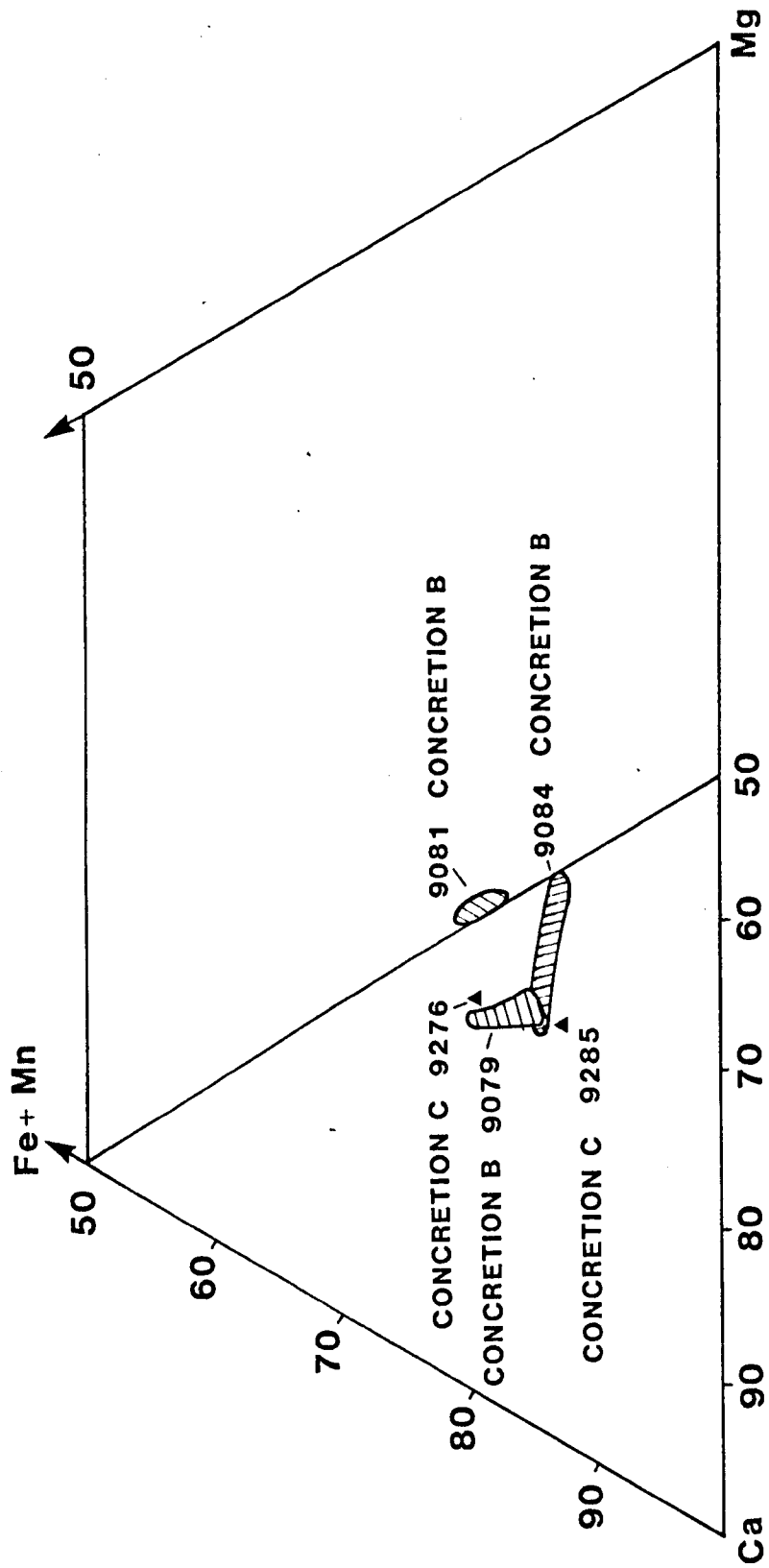


Figure 4.12

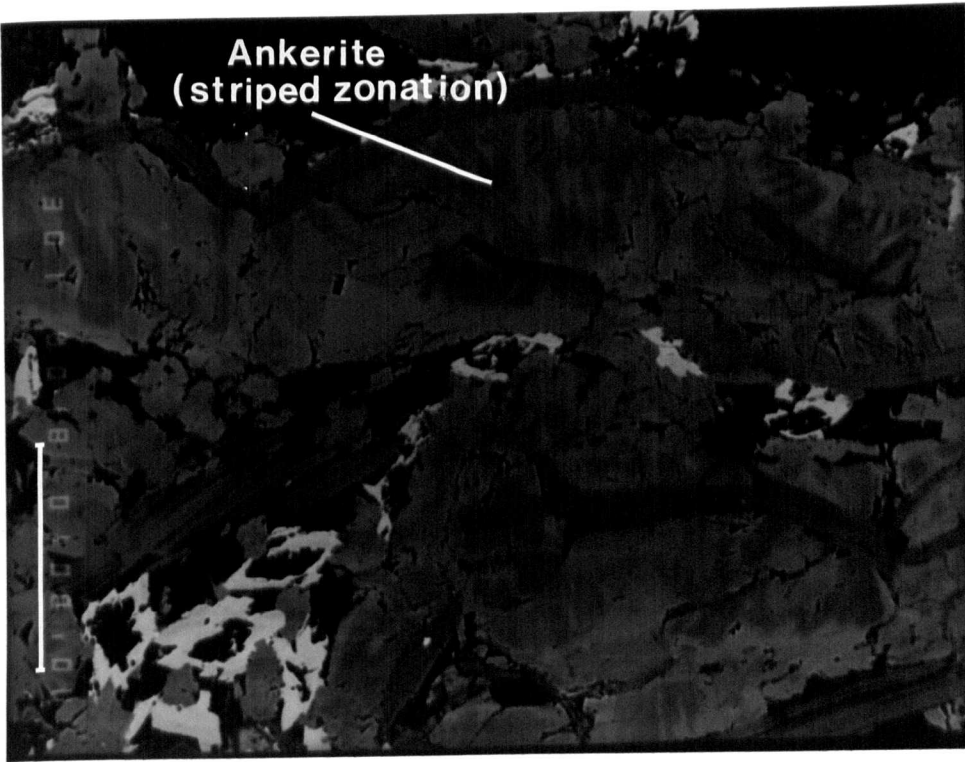


Figure 4.13

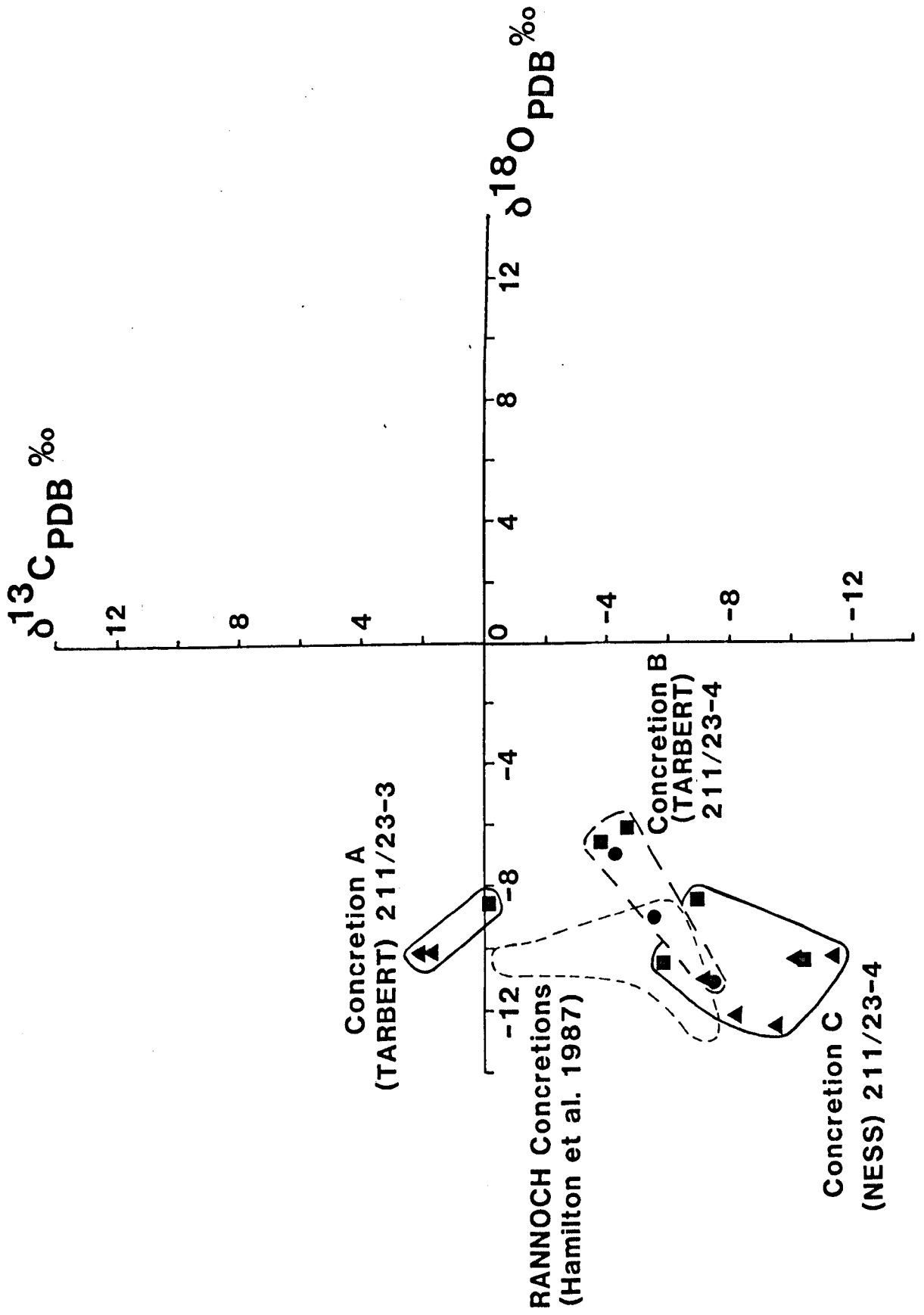


Figure 4.14

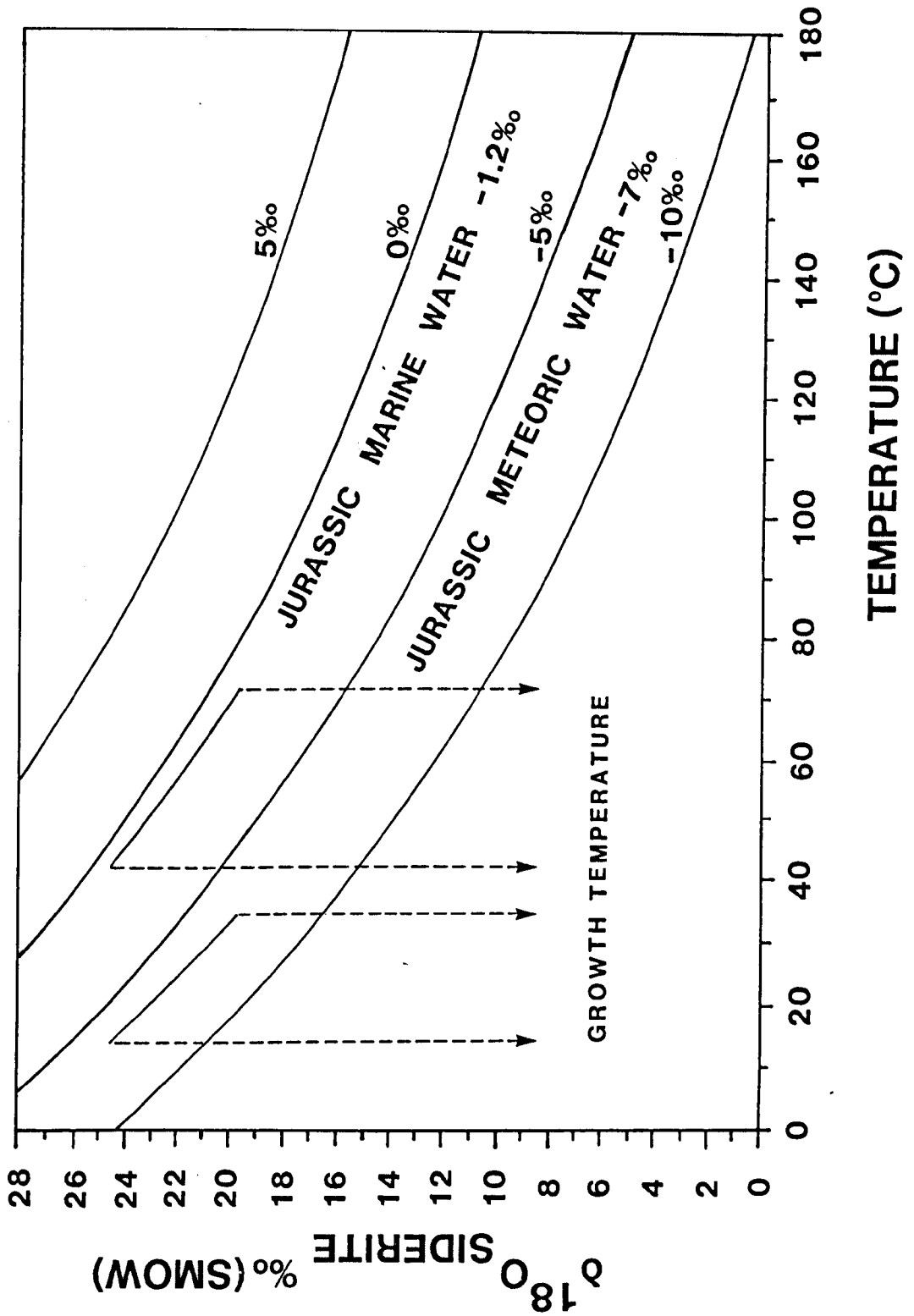


Figure 4.15.a

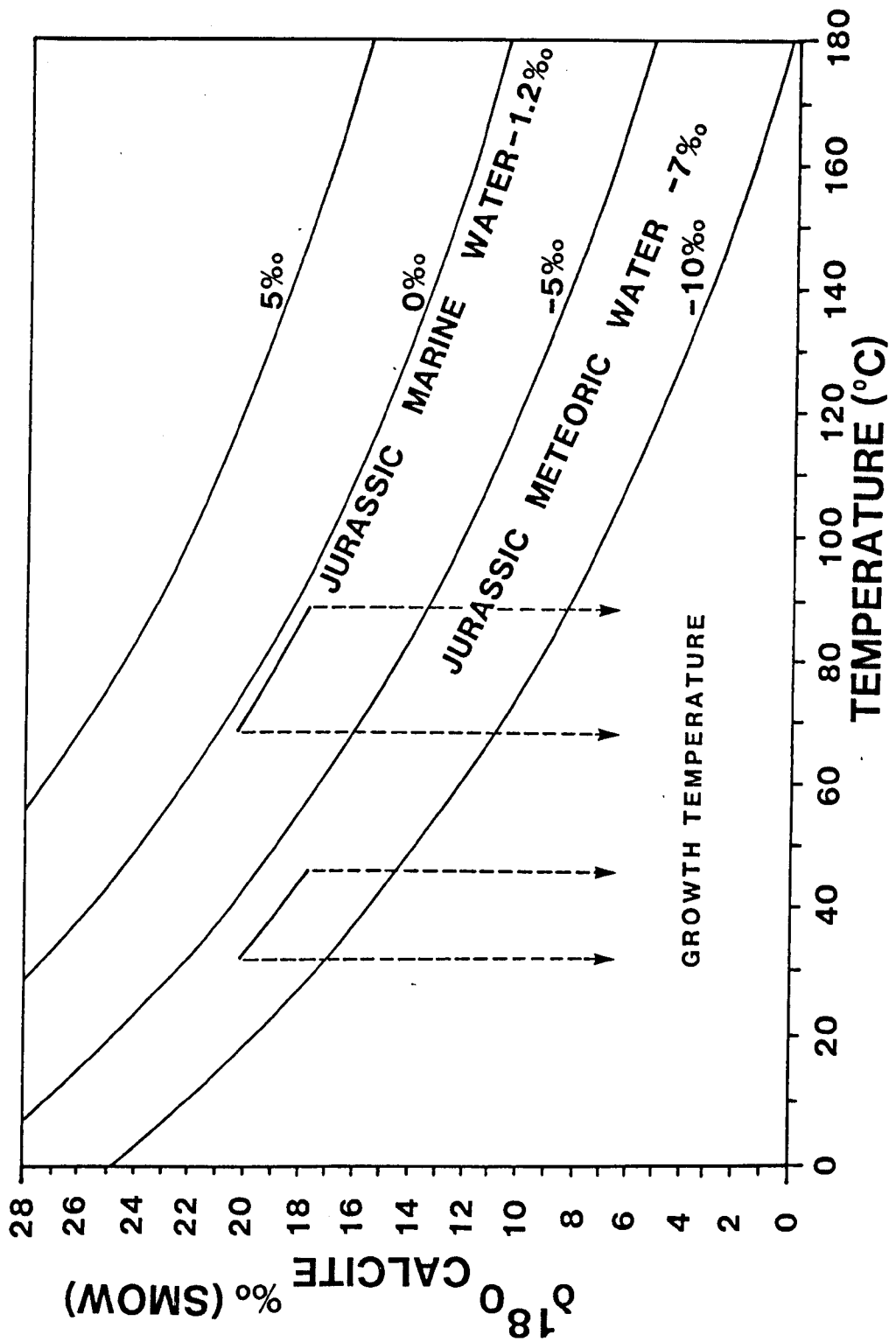


Figure 4.15.b

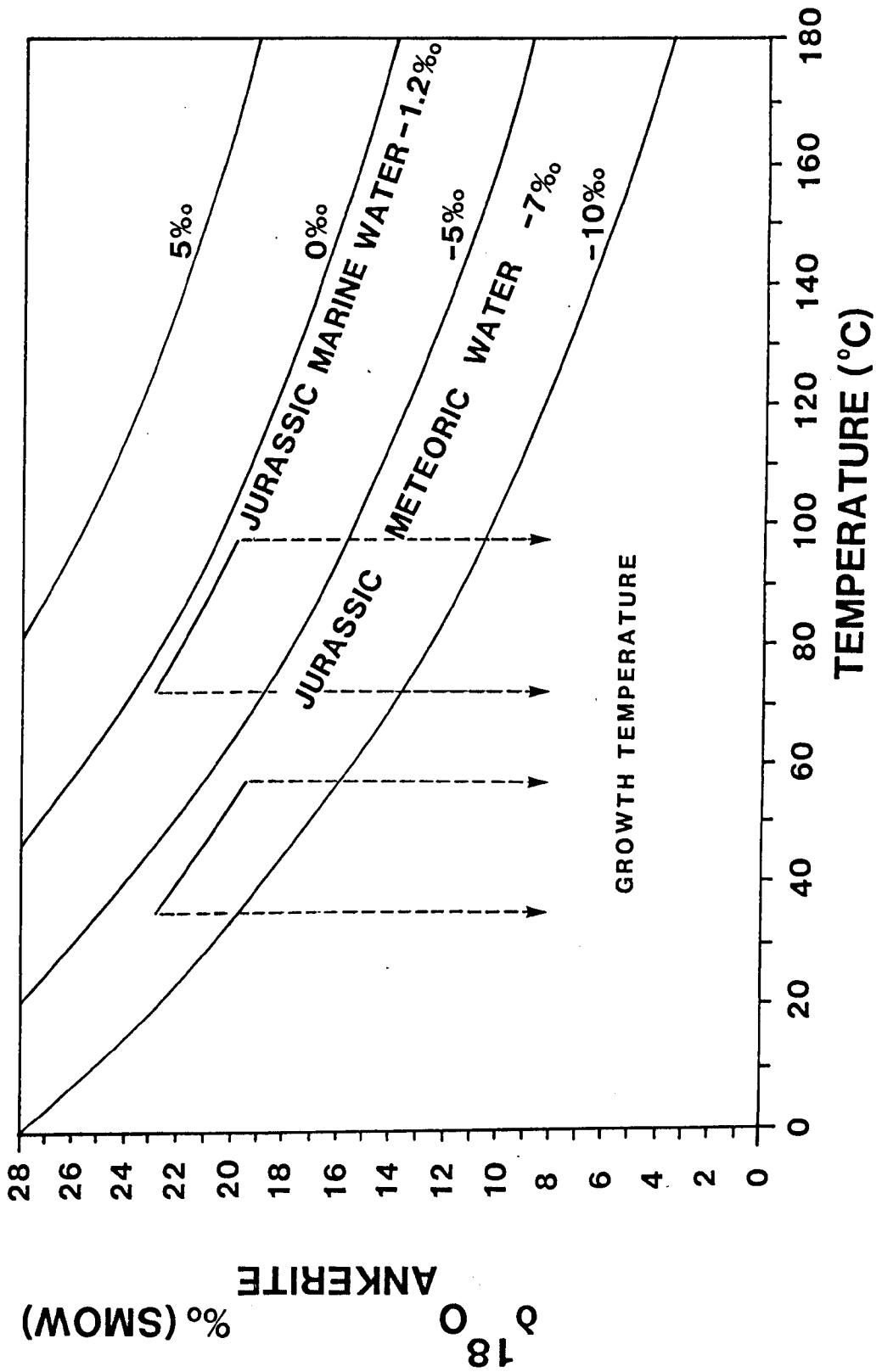
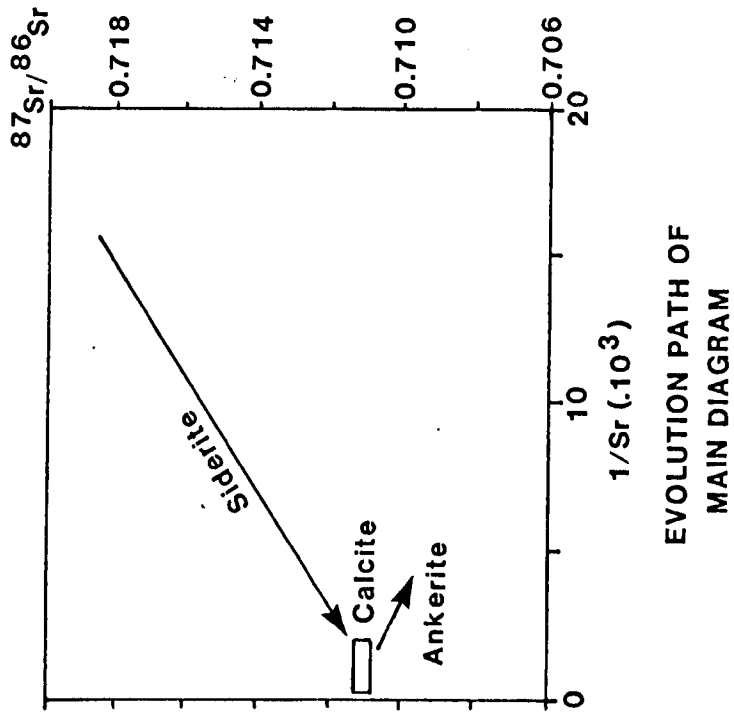
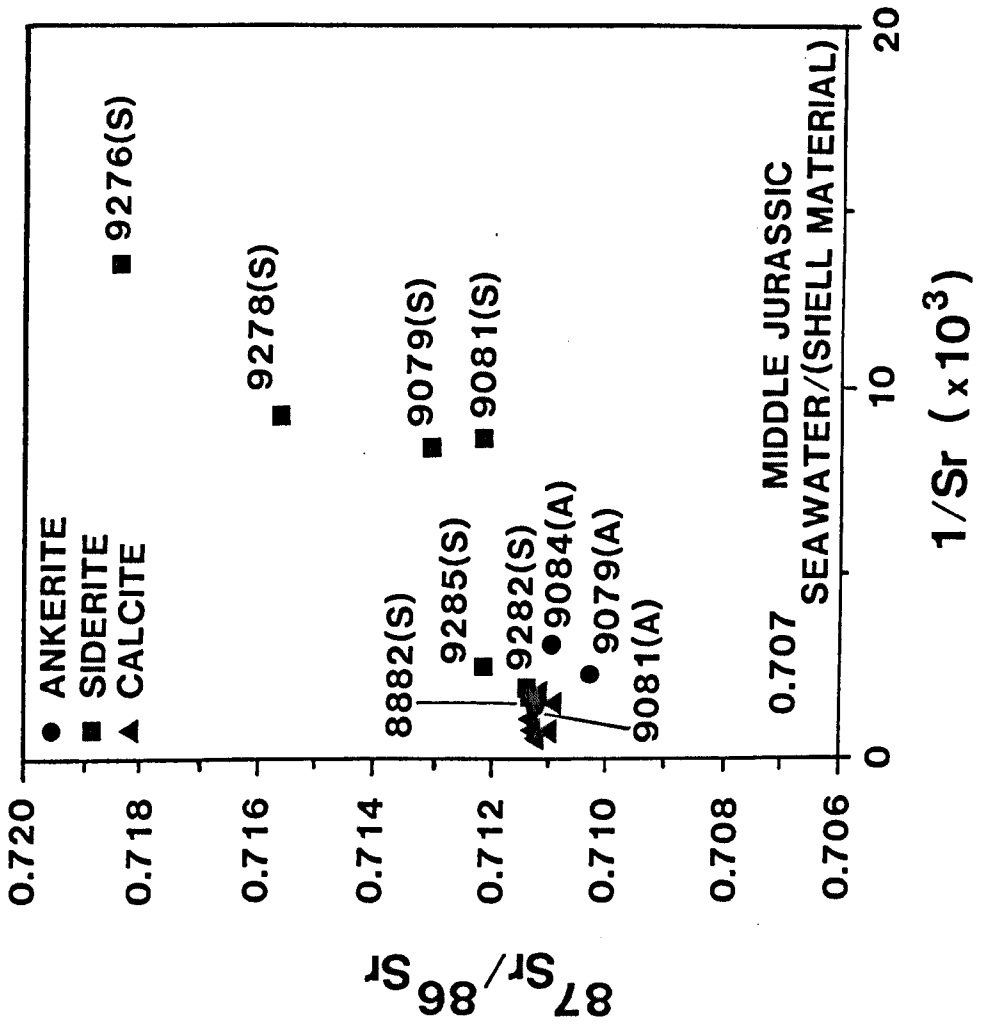


Figure 4.15.c

Figure 4.16.a



EVOLUTION PATH OF
MAIN DIAGRAM

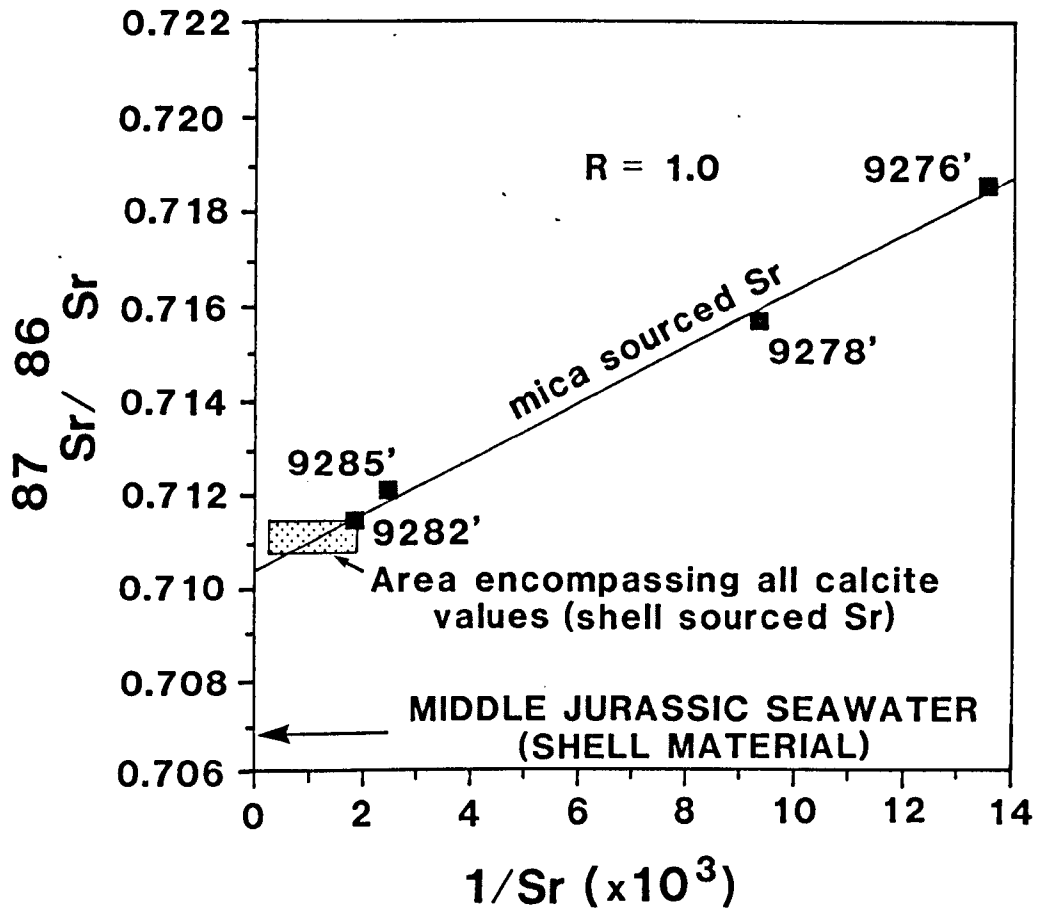


Figure 4.16.b

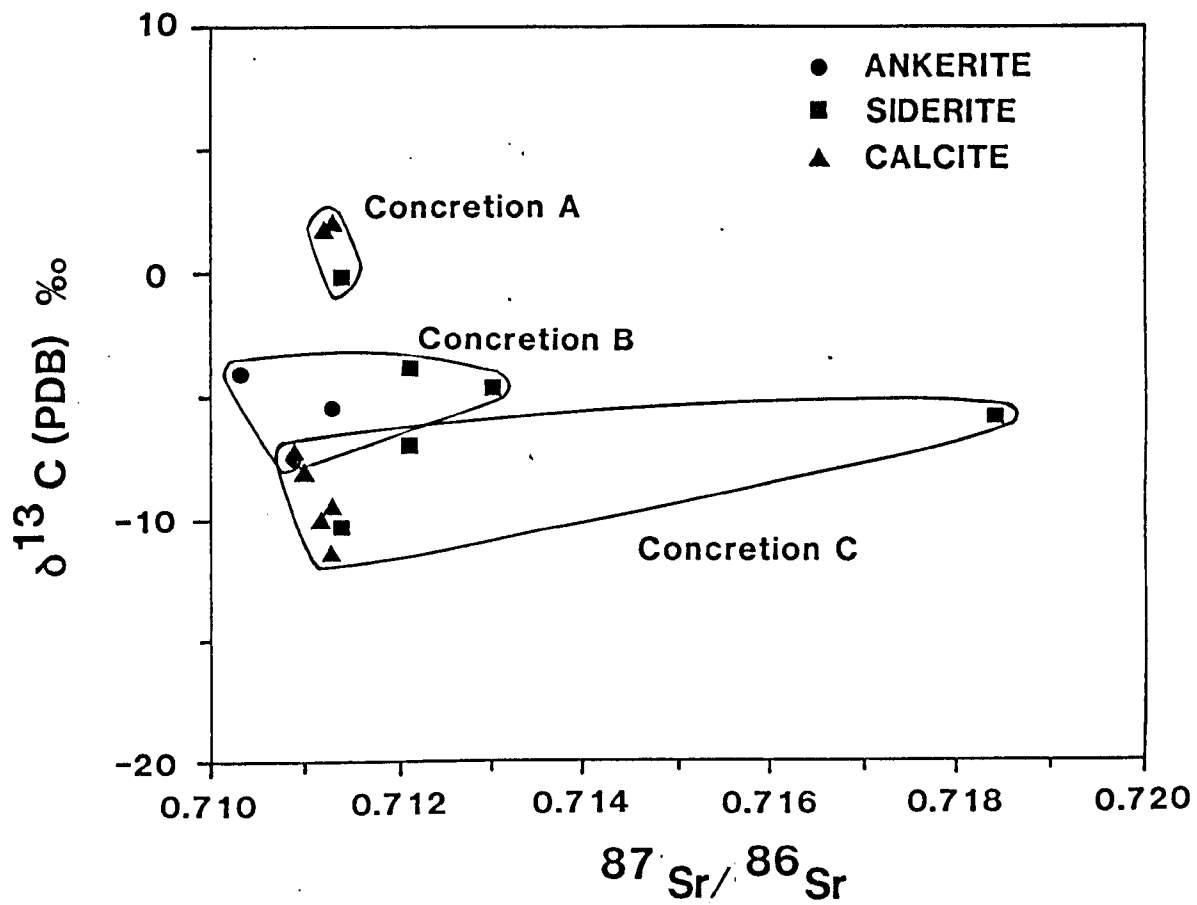


Figure 4.17

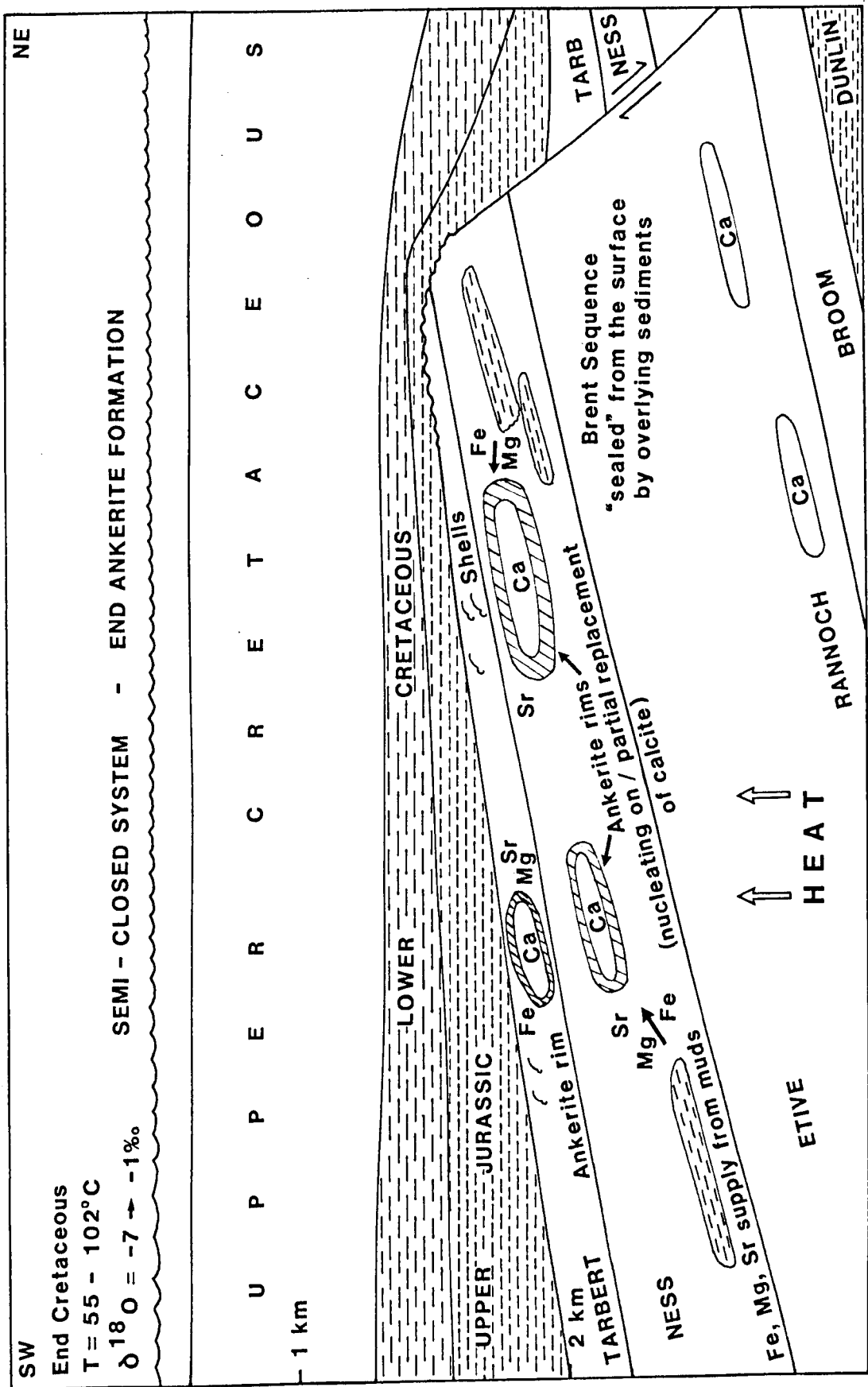


Figure 4.18.b

WELL	DEPTH (ft)	(TVD. SS) (m)	FORMATION	MEAN GRAIN SIZE (mm)	ANG.	SORT.	SPHER.	QTZ	PQTZ	K-FSP	PLAG	M.R.F.	I.R.F.	MUSC	BIOT	KAOL	CAL	SID	ANK	PYR	K-FSP O/G	CARB. MAT.	PRE-CEM. POROS.	DEPTH OF GTH CARB. CMT(km)	DEPTH OF GTH ALL CMTS (km)
211/23-3	8882	2707.1	TARBERT	0.4	SA-A	MOD	MOD	21.4	25.6	5.4	0.6	2.6	-	2.2	1.0	3.0	36.4	1.6	-	tr	tr	0.2	41.0	0.9	0.7
	8883.5	2707.6	TARBERT	0.5	SA-SR	P-M	MOD	22.0	25.0	4.2	0.2	2.4	-	0.8	-	2.6	41.8	0.4	-	tr	tr	0.6	44.8	0.5	0.3
	8885	2708.0	TARBERT	1.0	SA-SR	P-M	L-M	11.2	44.0	6.0	-	2.4	-	0.2	-	1.6	33.6	0.4	-	tr	tr	0.4	35.6	1.4	1.2
211/23-4	9079	2767.1	TARBERT	0.2	A-SA	MOD	L-M	37.1	10.3	4.6	1.0	4.0	-	5.0	1.3	7.6	-	7.1	21.7	0.3	tr	-	36.7	3.0	1.1
	9081	2767.8	TARBERT	0.3	A-SA	P-M	L-M	26.2	10.6	3.2	0.2	-	-	3.0	1.0	4.6	47.0	3.8	tr	0.4	tr	-	55.8	-	-
	9084	2768.7	TARBERT	0.2	A-SA	P-M	MOD	39.0	15.2	7.6	0.2	1.6	-	5.0	0.6	11.2	-	2.3	17.2	0.1	tr	-	30.8	3.8	1.7
	9276	2827.2	NESS	0.4	A-SA	POOR	MOD	39.2	8.8	3.4	0.6	1.2	-	2.8	3.0	0.8	37.8	1.4	tr	1.0	tr	-	41.0	0.8	0.7
	9278	2827.8	NESS	0.3	SA-SR	MOD	L-M	33.4	17.0	3.4	0.6	0.2	0.4	1.4	2.0	4.8	34.2	1.8	-	0.6	tr	-	41.4	1.1	0.6
	9282	2829.0	NESS	0.4	SA	POOR	L-M	30.6	17.0	2.6	0.6	1.2	-	-	-	1.2	45.2	1.0	-	tr	tr	0.6	47.4	0.2	0.1
	9282	2829.0	NESS	0.2	A-SA	M-W	L-M	21.8	4.2	0.8	0.2	0.4	-	5.4	9.0	1.8	39.8	16.0	-	0.4	tr	-	58.0	-	-
	9285	2829.9	NESS	0.1	A-SA	WELL	MOD	24.2	7.4	0.8	0.6	0.4	-	8.8	8.0	4.0	32.8	12.4	tr	0.6	tr	-	49.8	0.3	-

TABLE 1

KEY:

ANG - ANGULARITY, A - ANGULAR, SA - SUBANGULAR, SR - SUBROUNDED.

SORT - SORTING, P - POOR, M/MOD - MODERATE, W - WELL.

SPHER - SPHERICITY, L - LOW, M/MOD - MODERATE.

QTZ - QUARTZ, PQTZ - POLYCRYSTALLINE QUARTZ, K-FSP - K-FELDSPAR, PLAG - PLAGIOCLASE,

M.R.F. - METAMORPHIC ROCK FRAGMENT, I.R.F. - IGNEOUS ROCK FRAGMENT, MUSC - MUSCOVITE,

BIOT - BIOTITE, KAOL. - KAOLINITE, CAL - CALCITE, SID - SIDERITE, ANK - ANKERITE,

K-FSP O/G - K-FELDSPAR OVERGROWTH, PYR - PYRITE, POR - POROSITY, CARB. MAT.- CARBONACEOUS MATERIAL,

PRE-CEM. POR. - PRE-CEMENT POROSITY,

DEPTH OF FMN CARB CMT (km) - CALCULATED DEPTH OF GROWTH OF CONCRETION

USING CARBONATE CEMENT VALUE, (SEE FIG 8).

DEPTH OF FMN ALL CMTS (km) - CALCULATED DEPTH OF GROWTH OF CONCRETION USING ALL CEMENTS, (SEE FIG.8)

TABLE :2

WELL	DEPTH - TVD.	SS	FORMATION	MINERAL/ CONCRETION	$\delta^{13}\text{C}$ (PDB)	$\delta^{18}\text{O}$ (PDB)	$\delta^{18}\text{O}$ (SMOW)	$^{87}\text{Sr}/^{86}\text{Sr}$ (initial)	$^{87}\text{Sr}/^{86}\text{Sr}$ (corrected)	Sr ppm	1/Sr (.1000)	Rb ppm	Rb/Sr
211/23-3	8882	2707.1	TARBERT	SIDERITE (A)	-0.1	-8.7	+21.9	0.7114	0.7114	661.7	1.5	11.0	0.005
211/23-4	9079	2767.1	TARBERT	SIDERITE (B)	-4.6	-6.1	+24.5	0.7145	0.7130	118.4	8.5	26.4	0.646
	9081	2767.8	TARBERT	SIDERITE (B)	-3.9	-6.6	+24.0	0.7205	0.7121	116.0	8.6	47.3	1.181
	9276	2827.2	NESS	SIDERITE (C)	-5.9	-10.5	+19.9	0.7277	0.7184	74.3	13.5	111.2	4.339
	9278	2827.8	NESS	SIDERITE (C)	-	-	-	0.7207	0.7156	107.8	9.3	85.1	2.285
	9282	2829.0	NESS	SIDERITE (C)	-10.4	-10.4	+20.1	0.7189	0.7114	542.8	1.8	41.6	0.222
	9285	2829.9	NESS	SIDERITE (C)	-6.9	-8.5	+22.1	0.7131	0.7121	404.8	2.5	64.1	0.458
211/23-3	8882	2707.1	TARBERT	CALCITE (A)	+2.1	-10.1	+20.4	0.7113	0.7113	1372.6	0.7	-	-
	8885	2708.0	TARBERT	CALCITE (A)	+1.8	-10.1	+20.4	0.7112	0.7112	2030.4	0.5	1.1	0.001
211/23-4	9081	2767.8	TARBERT	CALCITE (B)	-7.3	-11.1	+19.4	0.7109	0.7109	691.7	1.4	6.5	0.027
	9276	2827.2	NESS	CALCITE (C)	-9.4	-12.6	+17.8	0.7114	0.7113	648.3	1.5	11.2	0.049
	9278	2827.8	NESS	CALCITE (C)	-8.1	-12.4	+18.1	0.7110	0.7110	1538.1	0.6	-	-
	9282	2829.0	NESS	CALCITE (C)	-11.4	-10.6	+19.9	0.7113	0.7113	1004.2	0.9	-	-
	9285	2829.9	NESS	CALCITE (C)	-10.1	-11.6	+18.8	0.7113	0.7112	555.7	1.8	4.4	0.023
211/23-4	9079	2767.1	TARBERT	ANKERITE (B)	-4.1	-7.6	+22.9	0.7104	0.7103	448.1	2.2	13.8	3.089
	9081	2767.8	TARBERT	ANKERITE (B)	-5.5	-8.9	+21.6	0.7115	0.7113	678.9	1.5	54.2	3.231
	9084	2768.7	TARBERT	ANKERITE (B)	-7.6	-11.3	+19.1	0.7111	0.7109	332.6	3.0	21.8	3.190

CHAPTER 5

A SULPHUR ISOTOPE STUDY OF LATE DIAGENETIC
PYRITE, MIDDLE JURASSIC BRENT SANDSTONES, NORTHERN NORTH SEA

J.F. BRINT
DEPARTMENT OF APPLIED GEOLOGY,
UNIVERSITY OF STRATHCLYDE,
GLASGOW, G1 1XJ

A.E. FALLICK
ISOTOPE GEOLOGY UNIT,
S.U.R.R.C.,
EAST KILBRIDE, G75 0QU

R.S. HASZELDINE
DEPARTMENT OF APPLIED GEOLOGY,
UNIVERSITY OF STRATHCLYDE,
GLASGOW, G1, 1XJ

Format: Journal of Sedimentary Petrology

Pyrite authigenesis associated with the burial stage of diagenesis occurs sporadically in wells 211/19-3 and 211/19-6 of the Murchison oilfield in the Middle Jurassic Brent Sandstone Group, northern North Sea. The pyrite occurs in cubic and octahedral forms and in places coalesces to form a porefilling cement in the sandstones. $\delta^{34}\text{S}$ analyses show a broad range of values from +0.9 to +28.7% relative to CDT. The majority of the samples are highly enriched in ^{34}S . A suggested simplistic model envisages pyrite formation by microbial sulphate reduction of seawater in a progressively closed system with respect to sulphate. Precipitation of early formed pyrite with light $\delta^{34}\text{S}$ values and the lack of replenishment of sulphate caused the residual sulphate to become enriched in $\delta^{34}\text{S}$. Consequently, later pyrite precipitated with increasingly enriched $\delta^{34}\text{S}$ values, which are dependent on the extent of earlier reduction processes and input from earlier pyrite. Formation may have taken place at up to ≈ 80 C. Input of sulphur by thermal maturation of organically bound sulphur and thermochemical sulphate reduction is difficult to assess, however these processes operate at higher temperatures and so were probably not important in this case.

The use of sulphur stable isotopes ($^{34}\text{S}/^{32}\text{S}$) in petroleum related studies has aided in the characterisation of the sulphur source in petroleum and its precipitation mechanism. Several investigations have shown its use in identifying oil from specific source rocks, in grouping oils into genetic families, and in constraining their migration and alteration (Harrison & Thode 1958a, Thode et al. 1958, LeIran 1971, LeIran et al. 1973, 1974, Orr 1974, 1975, Krouse 1977, Gaffney et al. 1979). Studies of sulphide minerals within hydrocarbon reservoirs (i.e. pyrite, anhydrite), Orr (1975), have been used to further elucidate the origin of the sulphur and the processes to which it has been subjected.

In the Middle Jurassic Brent Group of the northern North Sea (Fig. 5.1), sulphur only occurs sporadically and so any comprehensive study of the origin and precipitation mechanism would necessarily have to be of regional extent. In this limited sulphur isotope study of pyrite from hydrocarbon reservoir sandstones of the Brent Group, the analysed pyrite was recognised as a burial related diagenetic cement (Blanche & Whitaker 1978, Morton & Humphreys 1983) and placed into the paragenetic sequence. The $\delta^{34}\text{S}$ values range from +0.9 to +28.7% CDT. From the data it was hoped to ascertain the sulphur source and the mechanism of precipitation, and whether the porewater system was open or closed with respect to sulphur. Three models for the presence of pyrite are examined. These are -

- 1) Reduction of residual dissolved sulphate in the porefluid remaining from early diagenesis.

- 2) Production of H_2S by thermal maturation of organically bound sulphur.

- 3) Thermochemical reduction of sulphate.

Six $\delta^{34}\text{S}$ analyses were conducted on pyrite from two wells, 211/19-3 and 211/19-6 from the Murchison oilfield in the East Shetland Basin, the site of the Brent Province (Fig. 5.1).

The sandstones sampled are from the Middle Jurassic Brent Group, a sand dominated deltaic sequence (Brown et al. 1987) which is subdivided into five formations, the Broom, Rannoch, Etive, Ness and

Tarbert (Deegan & Scull 1977) (Fig.5.2). The Brent Group is underlain by the argillaceous Dunlin Group (Lower Jurassic) and overlain also by the argillaceous deposits of the Humber Group (Upper Jurassic), which contains the principal source rock of the Brent Province, the Kimmeridge Clay Formation (Goff 1983), (Fig.5.2). Structurally the East Shetland Basin is characterised by a dominantly westward dipping fault block regime for the Jurassic sediments (Brown 1984, Badley et al. 1988). The basin was filled in turn by Cretaceous and Cenozoic deposits which are up to 4 km thick (Parsley 1984). There are two major subparallel faults in the basin (Fig.5.1), the more westerly one of which controls the location of the Murchison oilfield.

The six samples come from the Ness and Etive Formations of the Brent Group (Fig.5.2). The Etive is considered to represent a barrier bar complex (Budding & Inglin 1981) consisting of thick structureless sandstones (Brown et al. 1987) whilst the Ness Formation is interpreted as a back barrier delta plain typified by interbedded sandstones, siltstones and mudstones and coal (Brown et al. 1987). Figure 5.3 illustrates the two well logs for 211/19-3 and 211/19-6 with the sample points indicated. The present day sample depth range is between 10155' and 10638' TVD.SS., (3095m, and 3242m).

5.4

PETROGRAPHY AND DIAGENESIS

The Brent sandstones are dominantly subarkoses and have a complicated paragenetic sequence (Fig.5.4), (Brint et al.Chap.3 this vol.) which is considered in two parts - 1) Early and 2) Late (burial) diagenesis. Early diagenesis (shallow burial) is dominated by the formation of kaolinite, siderite, minor (dominantly framboidal) pyrite, and in places by calcite concretionary horizons which are well developed in the Rannoch, Ness and Tarbert Formations (Hamilton et al. 1987a,b, Brint et al.Chap.4 this vol). Early framboidal pyrite (<1%), is found almost entirely within the calcite concretionary zones being observed in trace amounts outwith. Late (burial) diagenesis is typified by continued kaolinite authigenesis and the major cements of quartz overgrowths and illite (Fig.5.4). Pyrite, developed during the later stages of diagenesis, is considered on textural grounds to grow dominantly pre-dating quartz overgrowths (Fig.5.5.a) although it may have continued to form during the earliest stages of quartz authigenesis. The pyrite is also

observed as pre-dating secondary porosity (Fig.5.5.b).

In the six samples the late (burial related) pyrite was separated and analysed. The pyrite exists in a cubic and octahedral habit which in places coalesces to form a porefilling cement (up to 5.8%, on a thin section scale), (Fig.5.5.c),. Individual cubes and octahedra range in size from 50-100 microns.

5.5

SULPHUR ISOTOPES

5.5.1 PREPARATION

Each sandstone sample was disaggregated using a jaw crusher and sieved into the following fractions: >500 um, 250 - 500 um, 160 - 250 um, 85 - 160 um, 53 - 85 um, and <53 um. Each size fraction was inspected by binocular microscope and by X-ray diffraction to assess which fraction contained a significant quantity of pyrite for separation. Once this was ascertained, the selected size fraction was washed in distilled H₂O to remove clay material and dried prior to heavy liquid separation. 1,1,2,2, Tetrabromoethane was used to effect the separation of pyrite from the framework grains and succeeded in enhancing the proportion of pyrite. The samples were passed through a Frantz Isodynamic separator over a range of current and slope combinations to facilitate recovery of a pure pyrite separate. Finally the pyrite was hand picked to promote purity and examine the crystal habit.

For isotopic analyses the pyrite (≈ 5 mg) was reacted with excess Cu₂O, as an intimate mixture, at 1070 C (after Robinson & Kusakabe 1975) so producing SO₂. This usually failed to produce a 100% yield because of contamination by remnant host rock. The prepared gas was analysed on a 12 cm model double collector mass spectrometer (Isospec 44 modified for SO₂). Standard correction factors were applied to the raw $\delta^{34}\text{S}$ ratios (Craig 1957). The entire instrument is operated at 110 C. Within run precision of $\delta^{34}\text{S}$ ratios is typically $\pm 0.05\%$ or better and replicate analyses agree to within $\pm 0.2\%$. All $\delta^{34}\text{S}$ results are reported in ‰ relative to Canyon Diablo Troilite.

5.5.2 RESULTS

Figure 5.7 presents the $\delta^{34}\text{S}$ data for the six pyrite samples. Five of the six samples are extremely enriched in ^{34}S ; +16.0 to +28.7%. One value (10638', (3242m), 211/19-6) is distinct from the others with a $\delta^{34}\text{S}$ of +0.9‰ (Figure 5.6). Jurassic seawater sulphate had a $\delta^{34}\text{S} = +16\text{‰}$, and the majority of the pyrite values are also enriched with respect to this value.

5.6

DISCUSSION

The latest stages of pyrite development can be constrained in terms of temperature and the isotopic composition of the porefluid. As indicated earlier, the pyrite formed prior to and possibly during the earliest stages of quartz authigenesis (Fig. 5.4, 5.5.a). Fluid inclusion microthermometry on quartz overgrowths at 10500', in well 211/19-6, have a minimum temperature of formation of 84.2°C , (Brint et al. Chap.3 this vol.). So pyrite formation may have occurred at temperatures up to 80°C . The overall porefluid regime during diagenesis was a meteoric dominated water ($\delta^{18}\text{O} = -7$ SMOW), which evolved isotopically during burial to +2‰ as the final diagenetic cements precipitated (Fig.5.4). Present day formation water analyses in the Brent Province are between 0 and +2% (Brint et al. Chap.3 this vol.), Glassman et al.1989, in press). The present day reservoir temperature in the Murchison oilfield is 110°C (Engelstad 1987).

Early diagenesis of the Brent Group was affected by the influence of meteoric fluids (Brint et al. Chap.3 this vol.). Unless such fluids have passed through e.g. evaporites, fresh waters are generally considered to have very low dissolved sulphate concentrations (compared to seawater - 2712 ppm, Hanor 1987). Any dissolved sulphate would be reduced anaerobically by bacteria to sulphide (Thorstensen 1970) i.e. pyrite. In the Brent sequence early pyrite is typically framboidal with minor cubic crystal development. Calcite concretions which typically enclose early pyrite (Fig.5.4) began forming at 32°C (for a porefluid of $\delta^{18}\text{O} = -7\text{‰}$), (Brint et al. Chap.3 this vol.), so early pyrite development was initiated at temperatures lower than 32°C . For the formation of early pyrite the source of the sulphate would be from marine porewater. However this

statement would appear to be paradoxical as the $\delta^{18}\text{O}$ analyses of early diagenetic cements in the Brent sandstones indicate that the porewater was dominantly meteoric (Brint et al. Chap.3 this vol., Hamilton et al. 1987a,b.), and so of very low sulphate concentrations. Present day formation water analyses from the Columba oilfield (Fig. 5.1) in the Brent Province have dissolved sulphate concentrations of between 68 and 76 ppm, values that are considerably less than average seawater; $\text{SO}_4 = 2712$ ppm, Hanor (1987). The formation of the pyrite would require precipitation in vestiges of a marine water, which was undergoing dilution by the influxes of meteoric water in what was an open system. This leaves the question as to where the sulphur/sulphate came from for precipitation of the later pyrite.

The isotopic fractionation between the sulphate and bacterially generated H_2S causes the H_2S to be around 22% lighter than the associated sulphate (Harrison & Thode 1957). Jurassic seawater sulphate had a $\delta^{34}\text{S}$ of +16‰, Claypool et al.(1980), so initial pyrite would precipitate with $\delta^{34}\text{S}$ of around -6‰CDT, (Fig. 5.6).

With the incorporation of the ^{32}S into the sulphide, the residual reservoir of sulphate would become enriched in $\delta^{34}\text{S}$ if loss of sulphate by reduction exceeds replenishment of sulphate. The Brent sequence has undergone burial from the early Cretaceous to the present day and has become sealed from further influxes of meteoric dominated fluids so the sulphur/sulphate reservoir would not be renewed. Therefore with the reservoir closing to fluid influx with time and the temperature increasing the later cubic/octahedral pyrite would precipitate with increasingly enriched values of $\delta^{34}\text{S}$, (Figure 5.6), but by which precipitation mechanism.

5.7 PRECIPITATION MECHANISM FOR PYRITE

5.7.1 MICROBIAL SULPHATE REDUCTION OF RESIDUAL SULPHATE

For microbial reduction of sulphate to occur during early diagenesis, sulphate reducing bacteria require suitable organic matter, certain organic nutrients, water, temperatures <70 C, a sulphate source (e.g. marine water) and an anaerobic environment (Orr

1975). The H_2S generated is converted in the presence of free or reactive iron to pyrite. This pyrite will precipitate with light $\delta^{34}S$ values (as calculated above, -6% CDT). However, if as indicated above, the reservoir is closing with respect to sulphate, then continued sulphate reduction of residual sulphate would generate a progressively ^{34}S enriched reservoir (due to non-replenishment of sulphate and the precipitation of light $\delta^{34}S$ early pyrite). Later pyrite will then precipitate with enriched $\delta^{34}S$ values whose degree of enrichment is dependent on the extent of earlier reduction. Coleman & Raiswell (1981) observed that the variation in morphology from early framboids to later crystallised euhedra correlated with an enrichment in ^{34}S . This was ascribed to open system bacterial reduction of seawater sulphate during the formation of framboids followed by sulphate reduction in a partially closed system during shallow burial.

The data apart from 10638', (3242m) and 10458', (3187m), have extremely enriched values (Fig. 5.6), with reference to Jurassic seawater ($+16\%$) and would appear to follow this argument. The solitary light value ($+0.9\%$, 10638', (3242m), Table 5.1), may include a contribution from earlier pyrite (depleted in ^{34}S) which has formed the core of the crystal, with the later burial related pyrite nucleating around it. Similarly 10458' (3187m), ($+16\%$), may represent a mixture of early and later pyrite.

5.7.2 THERMAL MATURATION OF ORGANICALLY BOUND SULPHUR

Textural information indicates that pyrite formation occurred at maximum temperatures up to $80^\circ C$, prior to the main phase of quartz authigenesis (Brint et al. Chap.3 this vol). Fluid inclusions in the quartz overgrowths throughout the Brent Province have a proportion that are hydrocarbon rich (Brint et al. Chap.3 this vol., Cocker et al. in press, Glassman et al. 1989 in press, Jourdan et al. 1987). Homogenisation temperatures for hydrocarbon rich fluid inclusions within the overgrowths fall between 60 and 80 C. These inclusions may contain dissolved H_2S and so a source of sulphur for the burial related pyrite by the thermal decomposition of organic sulphur compounds (i.e. maturation). Orr (1975) indicates that the requirements for this mechanism are organic matter with bound sulphur

(oil, bitumens or kerogen) at temperatures $> 70^{\circ}\text{C}$. The H_2S content of the gas is limited by the amount of sulphur present in the organic matter and by dilution with light hydrocarbons formed concomitantly by thermal cracking. The $\delta^{34}\text{S}$ value of the H_2S is approximately the same as the combined sulphur in the source organic matter, which is typically $15\% \pm 5\%$ lower than associated sulphate (Orr 1975). This would give H_2S with a $\delta^{34}\text{S}$ of $\approx +1\%$ and consequently pyrite with a similar value (no significant fractionation is thought to occur with pyrite formation, Orr 1975). Therefore this mechanism would not explain the most enriched values, (Fig. 5.6). Also the mechanism occurs at temperatures predominantly above the upper temperature limit for pyrite formation in the samples studied.

5.7.3 THERMOCHEMICAL SULPHATE REDUCTION

A third possible mechanism which may have caused the late development of pyrite is thermochemical sulphate reduction. Requirements for this to occur are a source of sulphate, organic matter and temperatures in excess of $>70^{\circ}\text{C}$ (Orr 1975). This lower temperature limit is highly contentious and Krouse et al. (1988) consider it to be $> 90^{\circ}\text{C}$. In the Brent Group there is an abundance of organic material (Ness Formation), and also in the Upper Jurassic Kimmeridge Clay (the principal source rock, Cornford 1984). The amount of sulphate still available at these high temperatures ($>70^{\circ}\text{C}$) is unknown. Concentrations of the H_2S generated is limited by the availability of sulphate and organic matter. However the $\delta^{34}\text{S}$ of the H_2S is equivalent to the source sulphate, i.e. it occurs with little isotopic fractionation. No significant fractionation is thought to occur from H_2S to FeS_2 . This would give values of $+16\%$ and as with thermal maturation of organically bound sulphur fails to explain the most enriched values (Fig. 5.6). The hot temperature regime required however mitigates against thermochemical sulphate reduction as the mechanism for pyrite formation.

With limited data it is difficult to fully interpret such a small study. The highly enriched values of the pyrite are not easily explained by the three mechanisms considered. The latter two precipitation mechanisms (i.e. thermal decomposition of organic sulphur compounds and thermochemical sulphate reduction) are unlikely as their effective temperature range is higher than the envisaged reservoir temperature during pyrite formation. Also the expected $\delta^{34}\text{S}$ values would not explain the most enriched pyrite values of this study. There being no significant isotopic fractionation between the original sulphate and the generated H_2S .

A simplistic model for pyrite formation in the reservoir may involve the precipitation of early (dominantly framboidal) pyrite with typically light $\delta^{34}\text{S}$ values (relative to Jurassic seawater sulphate, $\delta^{34}\text{S} = +16\%$) by microbial sulphate reduction of seawater at low temperatures (30 C) in an open system. Then as the Brent sequence underwent burial it became "sealed off" from the overlying sulphate reservoir which was also undergoing dilution by the influxes of meteoric water which occurred during early diagenesis (Brint et al. Chap. 3, this vol.). With the reservoir becoming sealed, loss of sulphate by reduction exceeded replenishment of sulphate so the system became partially closed with respect to sulphate. The later cubic/octahedral pyrite precipitated with enriched $\delta^{34}\text{S}$ values dependent on the extent of earlier reduction processes and input from earlier pyrite. This earlier pyrite may have acted as nucleation sites for the later pyrite and consequently lowered the measured sulphur value i.e. $+0.9\%$, 10638', (3242m), 211/19-6. This model for formation of pyrite may be viewed as a continuous process by microbial sulphate reduction from framboidal to cubic/octahedral habit as temperature increased. Inferring a continuous process would suggest that the most enriched values formed last from the increasingly enriched sulphate reservoir. Availability of sulphate for precipitation of the later pyrite is however problematic, considering that the porefluid is dominated by meteoric water which have and will cause low sulphate concentrations. But as marine water compacts out of mudrocks, the system may receive an extra input of sulphate during burial diagenesis, and Rainey (1987)

reports the availability of excess sulphur within the Kimmeridge Clay at the present day. Termination of pyrite formation occurred prior to 80°C by the cessation of bacterial activity.

The iron required for precipitation of the pyrite is available from free or reactive sources and from the surrounding mud sequence.

Such a model requires to be tested by considerably more data to assess its validity and to determine if other precipitation mechanisms have contributed to the formation of pyrite.

The authors would like to thank Adrian Boyce for conducting the analyses. J.F.B. acknowledges receipt of N.E.R.C. grant no. GT4/85/GS/97. The Isotope Geology Unit is supported by the NERC and the Scottish Universities.

- BADLEY, M.E., PRICE, J.D., DAHL, C.R., and AGDESTAIN, T., 1988, The structural evolution of the North Viking Graben and its bearing upon extensional modes of basin formation: Jour. Geol. Soc. London, v. 145, p. 455-462
- BLANCHE, J.B., and WHITAKER, J.H.McD., 1978, Diagenesis as part of the Brent sand formation (Middle Jurassic) of the northern North Sea Basin: Jour. Geol. Soc. London, v. 135, p. 73-82.
- BRINT, J.F., HASZELDINE, R.S., HAMILTON, P.J., FALLICK, A.E., and BROWN, S., 1989, Isotope diagenesis and palaeofluid movement in the Middle Jurassic Brent sands, northern North Sea, Chapter 3, this volume.
- BRINT, J.F., HASZELDINE, R.S., HAMILTON, P.J., FALLICK, A.E., and BROWN, S., 1989, The formation and origin of carbonate cemented zones in the Brent sandstones of the Dunlin field, northern North Sea: Chapter 3, this volume.
- BROWN, S., 1984, Jurassic: In, Glennie, K.W., ed., Introduction to the Petroleum Geology of the North Sea, Blackwell Scientific Publications, p. 133-160.
- BROWN, S., RICHARDS, P.C., and THOMSON, A.R., 1987, Patterns in the deposition of the Brent Group (Middle Jurassic) UK North Sea, in Brooks, J., and Glennie, K., eds., Petroleum Geology of North West Europe: Graham & Trotman, London, p. 899-913.
- BUDDING, M.C., and INGLIN, H.F., 1981, A reservoir geological model of the Brent Sands in Southern Cormorant, in Illing, L.V., and Hobson, G.D., eds., Petroleum Geology of the Continental Shelf of North-West Europe, Heyden & Son, London, p. 326-334.
- CLAYPOOL, G.E., HOLSER, W.T., KAPLAN, I.R., SAKAI, H., and ZAK, I., 1980, The age curves of sulphur and oxygen isotopes in marine sulphate and their mutual interpretation: Chemical Geology, v. 28, p. 199-260.
- COCKER, J.D., CLAUER, N., JSUI, T-F., and SWARBRICK, R.E., 1989 A Diagenetic model for the Northwest Hutton Field: Clay Minerals in

press.

COLEMAN, M.L., and RAISWELL, R., 1981, Carbon, oxygen and sulphur isotope variations in concretions from the Upper Lias of N.E. England: *Geochim. Cosmochim. Acta*, v. 45, p. 329-340.

CORNFORD, C., 1984, Source Rocks and Hydrocarbons of the North Sea, in Glennie, K., ed., *Introduction to the Petroleum Geology of the North Sea*, Blackwell Scientific Publications, p. 171-204.

CRAIG, H., 1957, Isotopic standards for carbon and oxygen and correction factors for mass-spectrometric analysis of carbon dioxide: *Geochim. Cosmochim. Acta*, v. 12, p. 133-149.

DEEGAN, C.E., and SCULL, B.J., 1977, (Compilers), *A standard lithostratigraphic nomenclature for the Central and Northern North Sea: Rept. Inst. geol. Sci. 77/25.*, H.M.S.O Publications, London, 35p.

ENGELSTAD, N., 1987, Murchison, in Spencer., A. M., ed., *Geology of the Norwegian Oil and Gas Fields*, Graham & Trotman, London, p. 295-306.

GAFFNEY, J.S., PREMUZIC, E.T., and MANOWITZ, B., 1979, On the usefulness of sulphur isotope ratios in crude oil correlations: *Geochim. Cosmochim. Acta*, v. 44, p.135-139.

GLASSMAN, J.R., LUNDEGARD, P.D., CLARK, R.A., PENNY, B.K., and COLLINS, I.D., 1989, *Geochemical evidence for the history of diagenesis and fluid migration: Brent sandstone, Heather Field, North Sea: Clay Minerals in press.*

COFF, J.C., 1983, Hydrocarbon generation and migration from Jurassic source rocks in the East Shetland Basin and Viking Graben of the northern North Sea: *Jour. Geol. Soc. London*, v. 140, p. 445-474.

HAMILTON, P.J., BRINT, J., HASZELDINE, R.S., FALLICK, A.E., and BROWN, S., 1987a, Formation of calcite cemented zones, Brent Group, North Sea: *Terra Cognita*, v. 7, p.342.

HAMILTON, P.J., FALLICK, A.E., MACINTYRE, R.M., and ELLIOTT, S., 1987b, Isotopic tracing of the provenance and diagenesis of Lower Brent Group sands, North Sea, in Brooks, J., and Glennie, K., eds.,

Petroleum Geology of North West Europe, Graham & Trotman, London, p. 939-949.

HANOR, J.S., 1988, Origin and Migration of Subsurface Sedimentary Brines, Soc. Econ. Palaeontologists Mineralogists Short Course Lecture Notes No. 21, Tulsa, 247p.

HARRISON, A.G., and THODE, H.G., 1957, The kinetic isotope effect in the chemical reduction of sulphate: Trans. Faraday Soc., v. 53, p. 1-4.

HARRISON, A.G., and THODE, H.G., 1958, Sulphur isotope abundances in hydrocarbons and source rocks of Uinta basin, Utah: Am. Assoc. Petrol. Geologists. Bull., v. 42, p. 2642-2649.

JOURDAN, A., THOMAS, M., BREVART, O., ROBSON, P., SOMMER, F., and SULLIVAN, M., 1987, Diagenesis as the control of the Brent sandstone reservoir properties in the Greater Alwyn area (East Shetland Basin), in Brooks, J., and Glennie, K., eds., Petroleum Geology of North West Europe, Graham & Trotman, London, p. 951-961.

KROUSE, H.R., 1977, Sulphur isotope studies and their role in petroleum exploration: Jour. Geochem. Explor., v. 7, p. 189-211.

KROUSE, H.R., VIAU, C.A., ELIUK, L.S., UEDA, A., and HALAS, S., 1988, Chemical and isotopic evidence of thermochemical sulphate reduction by light hydrocarbon gases in deep carbonate reservoirs: Nature, v. 333, p. 415-419.

Le TRAN, K., 1971, Geochemical study of hydrogen sulphide sorbed in sediments, in, Advances in Organic Geochemistry, Pergamon Press, p. 717-726.

Le TRAN, K., 1974, Diagenesis of organic matter and occurrence of hydrocarbons and hydrogen sulphide in the SW Aquitaine Basin (France): Bull. Centre Rech. Pau., v. 8, p. 111-137.

Le TRAN, K., CANNAN, J., and VAN DER WEIDE, B., 1973, Diagenesis of the organic matter and formation of hydrocarbons and of hydrogen sulphide in the southwest Aquitaine Basin: Proc. of 6th International Conference of Organic Geochemistry, Paris.

ORR, W.L., 1974, Changes in sulphur content and isotopic ratios of

- sulphur during petroleum migration: A study of Big Horn Basin Palaeozoic oils: Am. Assoc. Petrol. Geologists Bull., v. 50, p. 2295-2318.
- ORR, W.L., 1975, Geologic and geochemical controls on the distribution of hydrogen sulphide in natural gas: in, Advances in Organic Geochemistry, Proc. of 7th International Meeting on Organic Geochemistry, Madrid, p.571-597.
- PARSLEY, A.J., 1984, North Sea Hydrocarbon Plays, in, Glennie, K.W., ed., Introduction to the Petroleum Geology of the North Sea, Blackwell Scientific Publications, London, p. 205-230.
- RAINEY, S.C.R., 1987, Sedimentology, diagenesis and the geochemistry of the Magnus sandstone member, northern North Sea: Unpubl. Ph.D thesis, Univ. of Edinburgh, 403p.
- ROBINSON, B.W., and KUSAKABE, M., 1975, Quantitative preparation of sulphur dioxide, for sulphur - 34/ sulphur - 32 analysis, from sulphides by combustion with cuprous oxide: Anal. Chem., v. 47, p. 1179-1181.
- SIMPSON, R.D.H., and WHITLEY, P.K.J., 1981, Geological Input to Reservoir Simulation of the Brent Formation, in Illing, L.V., and Hobson, G.D., eds., Petroleum Geology of the Continental Shelf of North-West Europe, Heyden & Son, London, p. 310-314.
- THODE, H.G., MONSTER, J., and DUNFORD, H.B., 1958, Sulphur-isotope abundance in petroleum and associated materials: Am. Assoc. Petrol. Geologists Bull., v. 42, p. 2619-2641.
- THURSTENSON, D.C., 1970, Equilibrium distribution of small organic molecules in natural waters: Geochim. Cosmochim. Acta, v. 34, p. 745-770.

Figure 5.1.a : Location of the Brent Province, East Shetland Basin, northern North Sea.

Figure 5.1.b : Location of the Murchison oilfield within the Brent Province, East Shetland Basin.

Figure 5.1.c : Location of the two wells (211/19-3 and 211/19-6) within the Murchison oilfield. Contours to Top Brent, (after Simpson & Whitley 1981).

Figure 5.2 : Jurassic stratigraphy and facies in the East Shetland Basin containing the Brent succession.

Figure 5.3.a : Sedimentary log of well 211/19-3, indicating sample points.

Figure 5.3.b : Sedimentary log of well 211/19-6, indicating sample points.

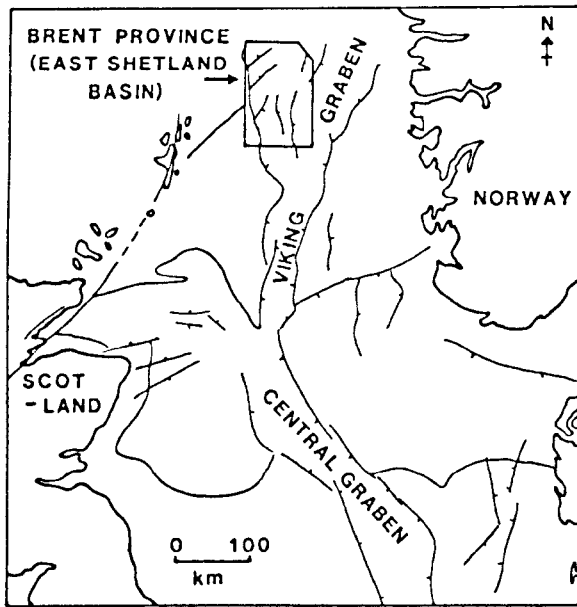
Figure 5.4 : Diagenetic sequence for the Brent sandstones (from Brint et al. Chap. 3, this vol.) indicating the relative timing of pyrite formation.

Figure 5.5.a : Photomicrograph of a pyrite cube pre-dating quartz overgrowth, scale bar - 20 microns, 10580' (3228m), Ness Formation, 211/19-6, Murchison oilfield.

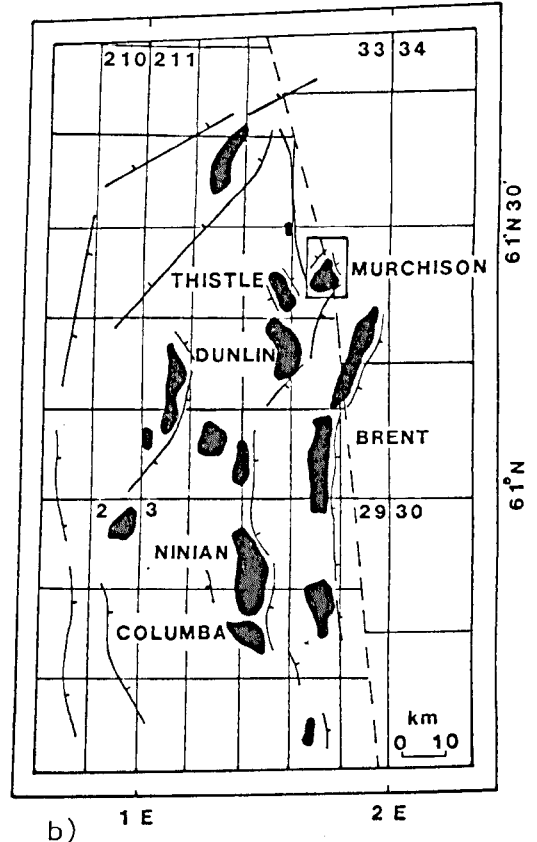
Figure 5.5.b : Photomicrograph of porefilling pyrite pre-dating secondary porosity, field of view - 1.0mm, 10458' (3187m), Ness Formation, 211/19-6, Murchison oilfield.

Figure 5.5.c : Photomicrograph of porefilling pyrite (reflected light), 10622' (3237m), Etive Formation, 211/19-6, Murchison oilfield.

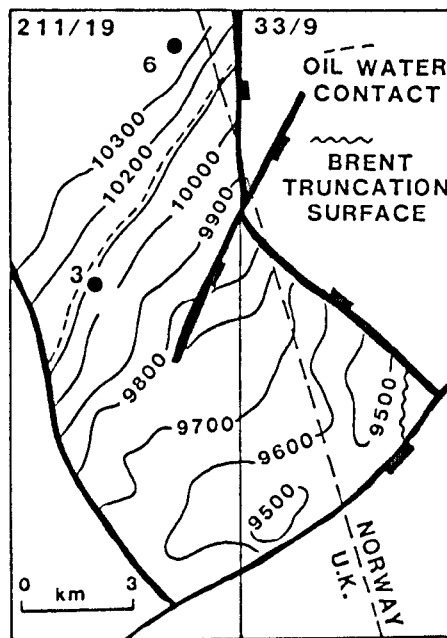
Figure 5.6 : $\delta^{34}\text{S}$ values for late pyrite, Murchison oilfield with the $\delta^{34}\text{S}$ range for possible precipitation mechanisms indicated.



a)



b)



c)

Figure 5.1

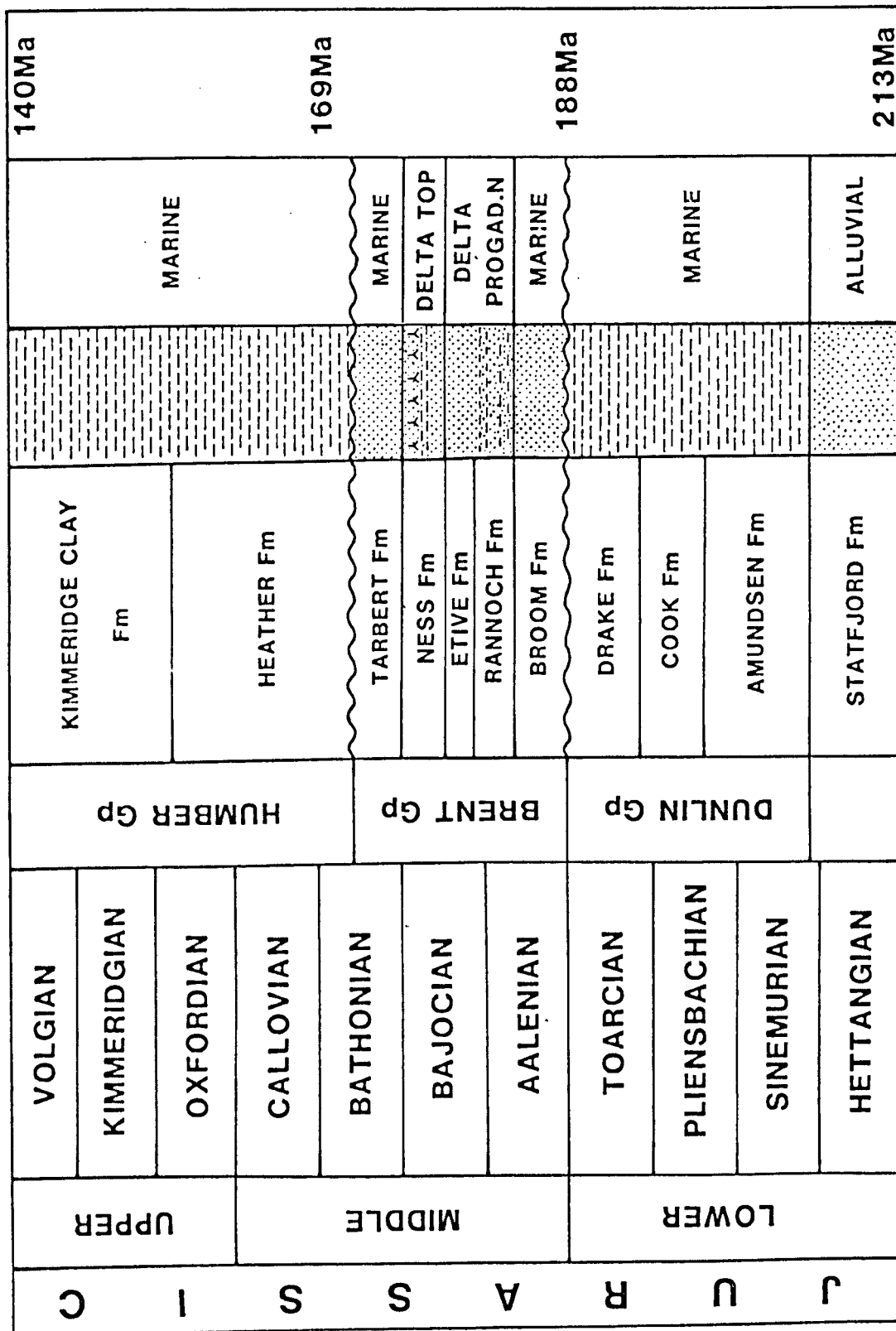
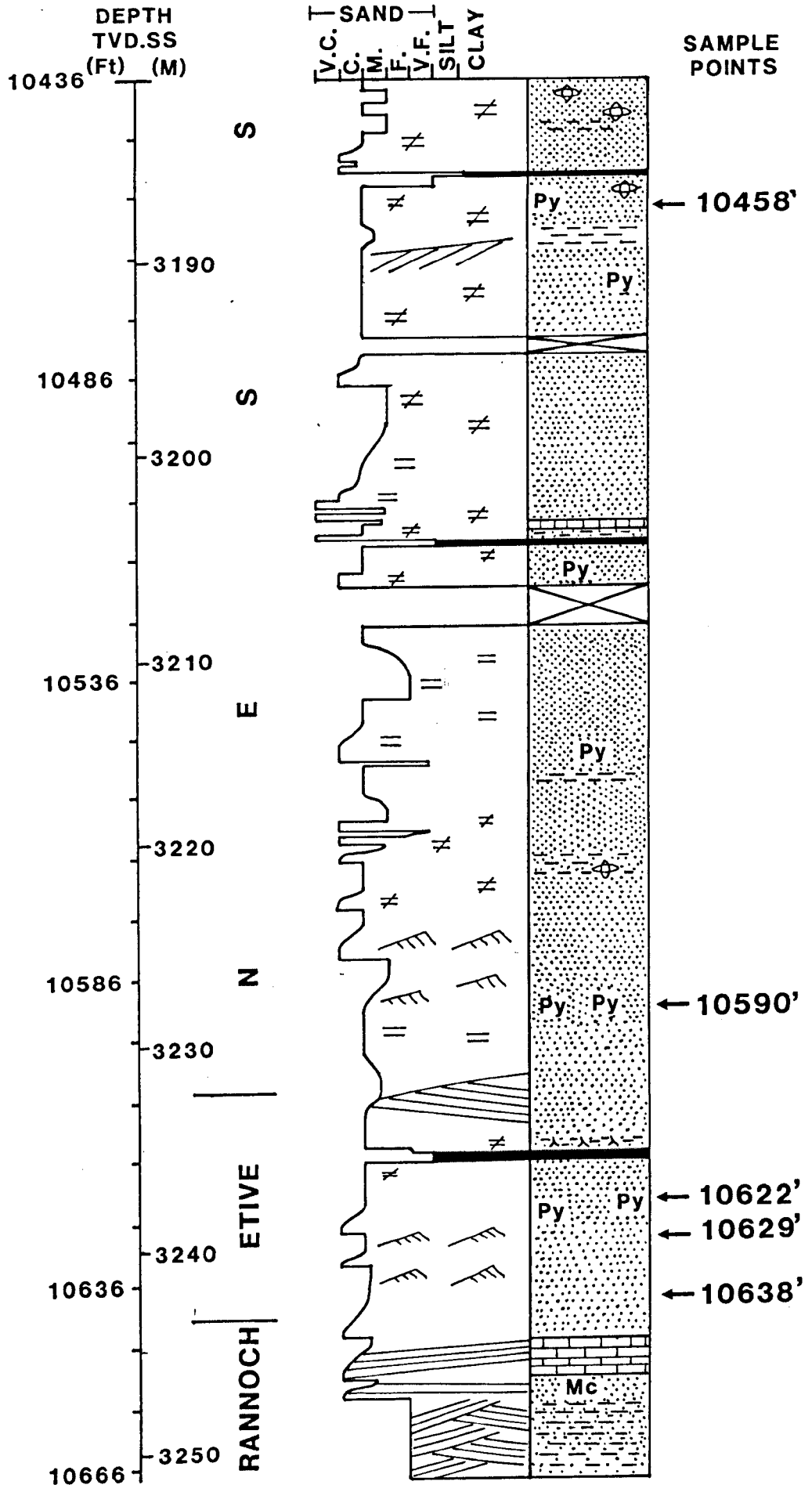


Figure 5.2

Figure 5.3.b

211/19-6



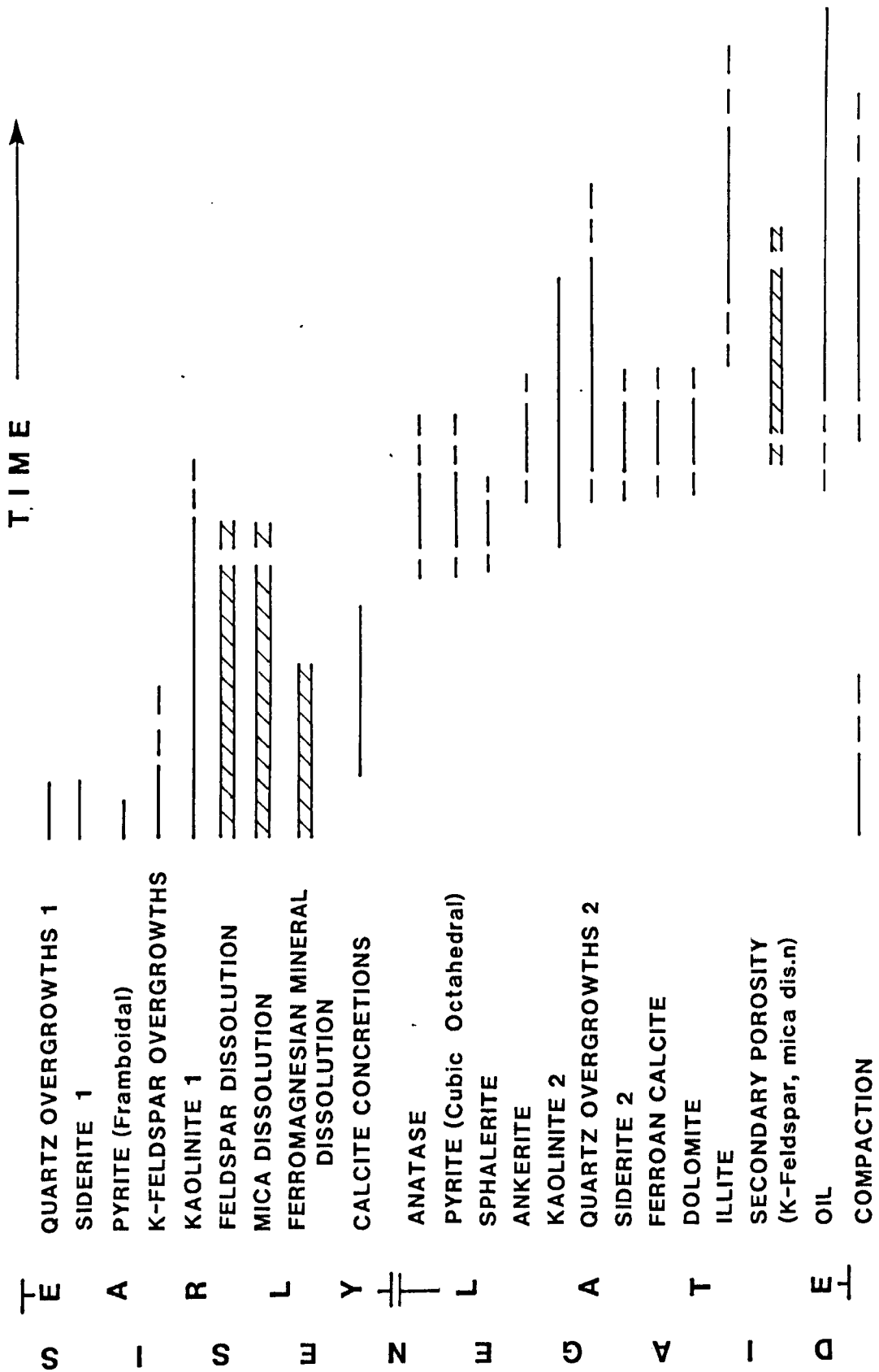


Figure 5.4

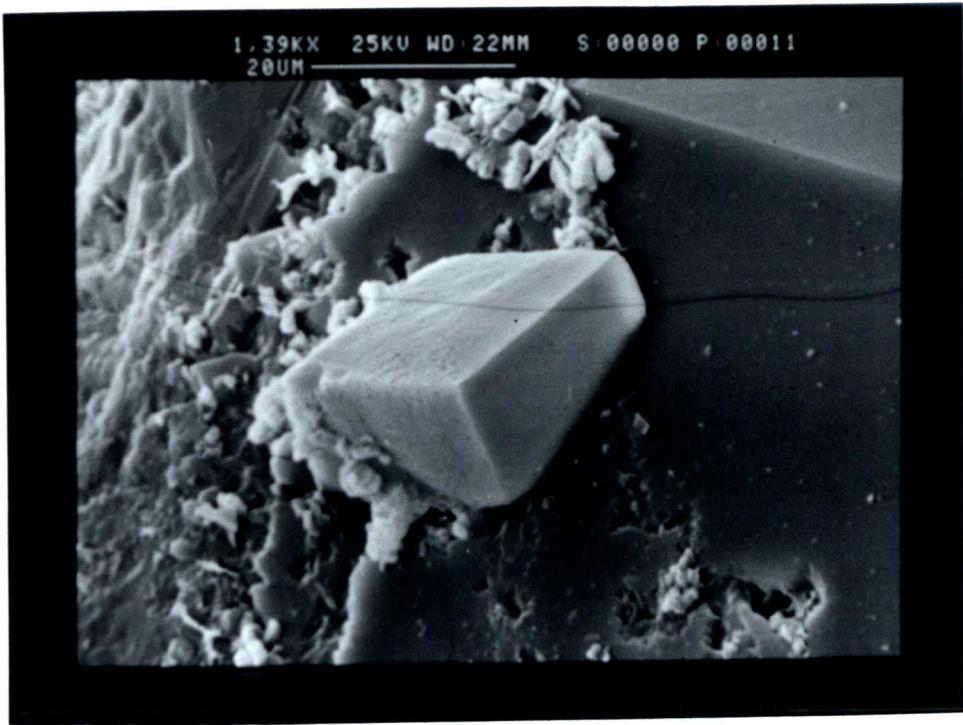


Figure 5.5.a

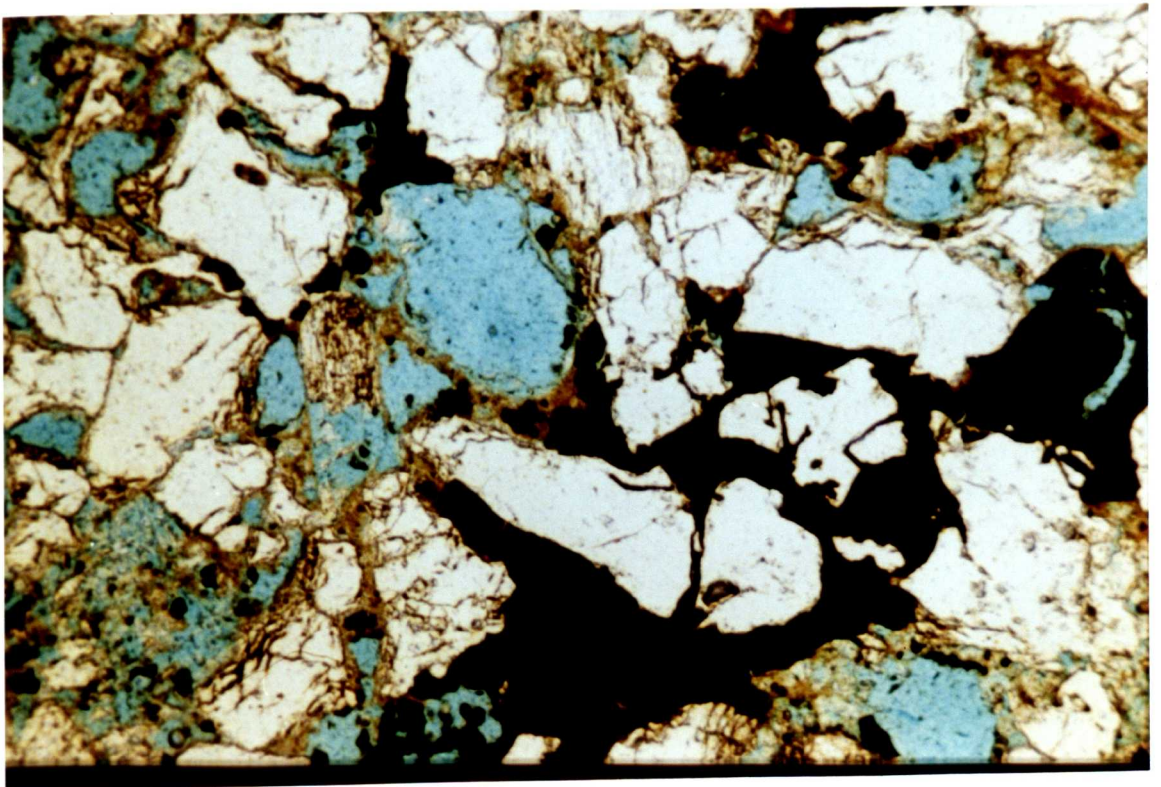


Figure 5.5.b

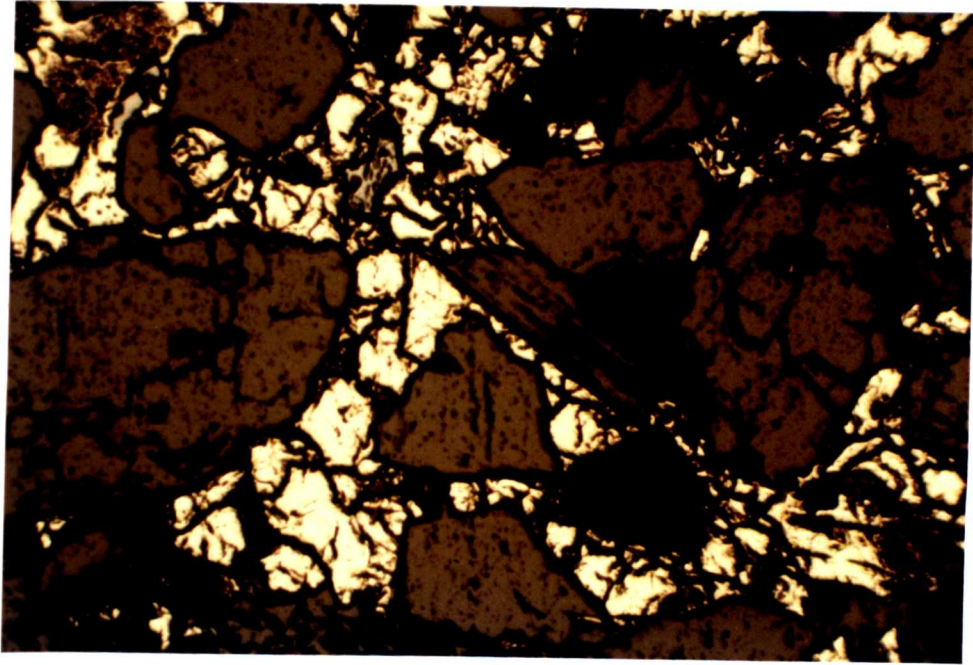


Figure 5.5.c

$\delta^{34}\text{S}$ VALUES FOR LATE PYRITE, MURCHISON OILFIELD

WELL	FORMATION	DEPTH		$\delta^{34}\text{S}$ ‰ CDT
		(FT)	(M)	
211/19-6	NESS	10458'	3187	16.0
	NESS	10590'	3228	28.7
	ETIVE	10622'	3237	19.9
	ETIVE	10629'	3239	27.3
	ETIVE	10638'	3242	0.9
211/19-3	NESS	10155'	3095'	20.7

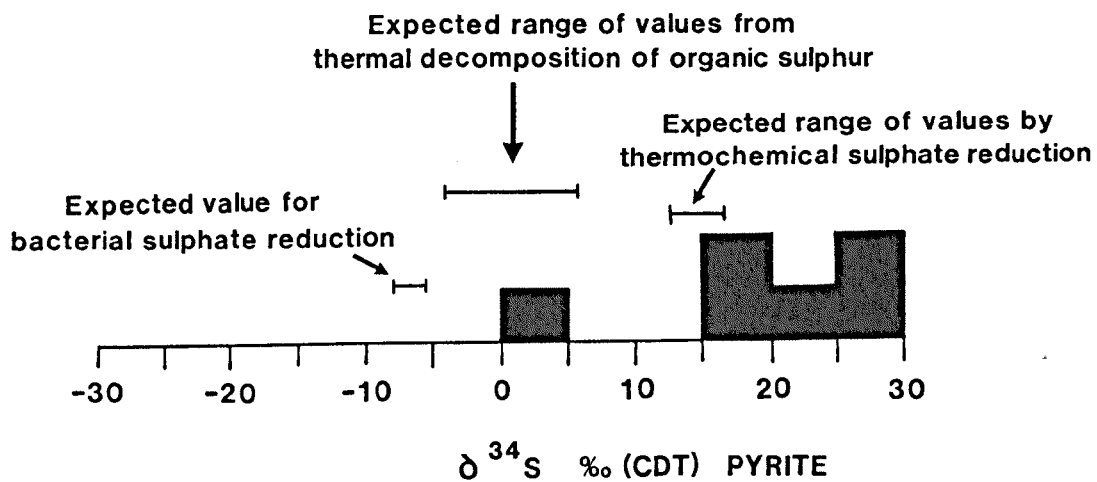










Figure 5.6

APPENDICES

APPENDIX A

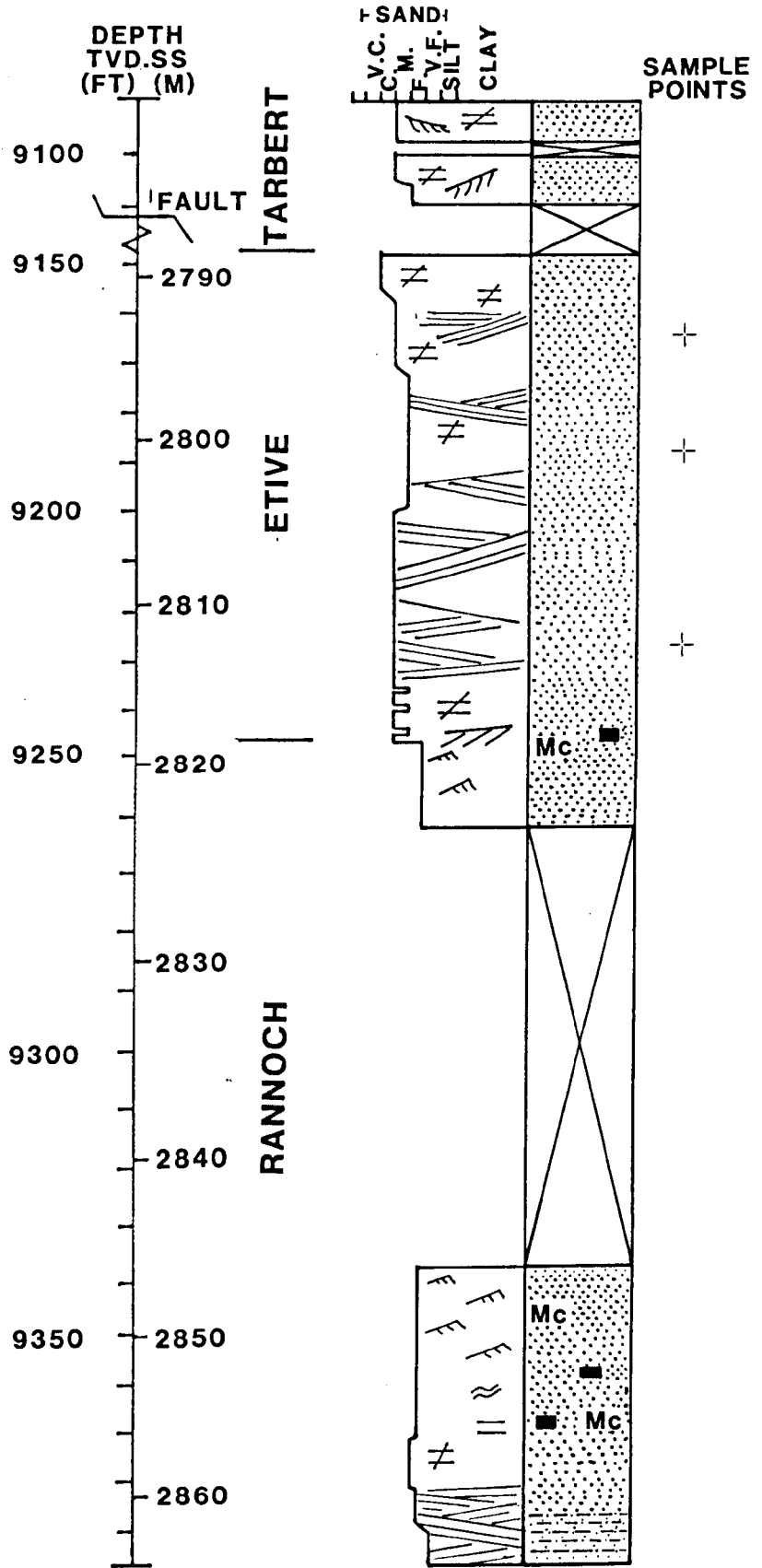
Well logs and sample points.

KEY

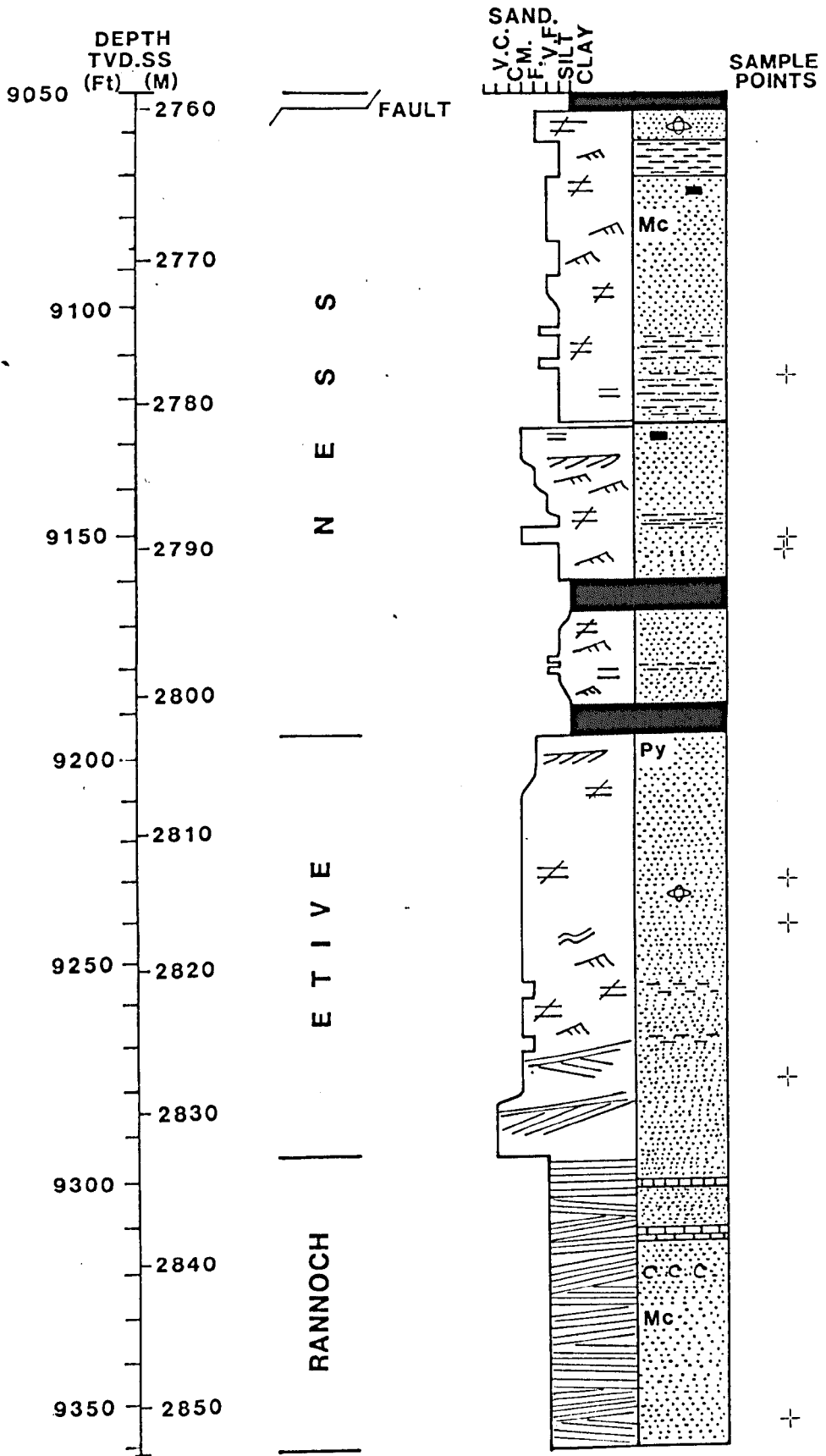
	Massive No apparent bedding		Bioturbated
	Slightly bedded	Mc	Micaceous
	Horizontal bedding	Py	Pyrite
	Cross bedding	Sid	Siderite
	Contorted Bedding		
	Low angle lamination		
	Ripple lamination		

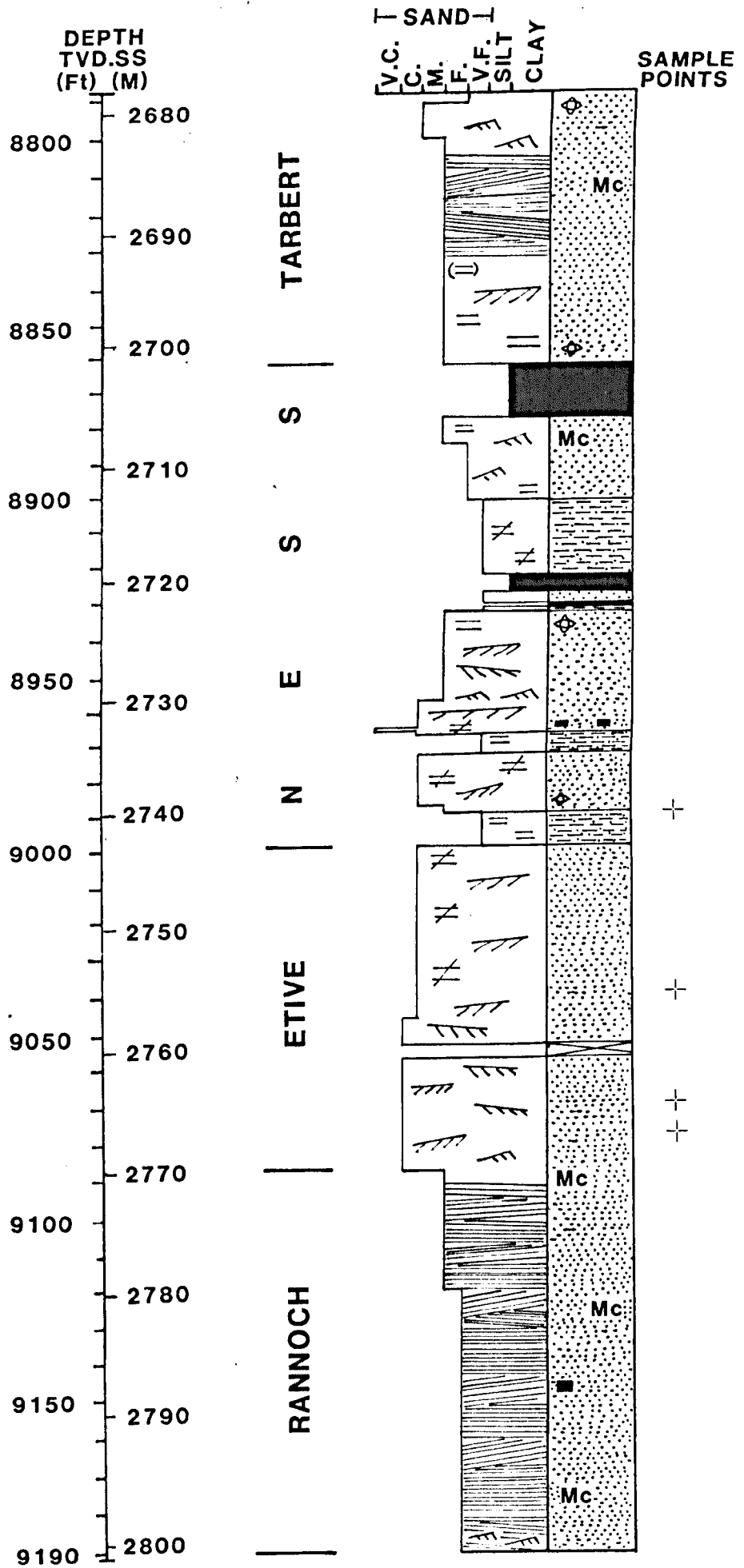
(No well log available for 211/18-A45)

211/18-A30

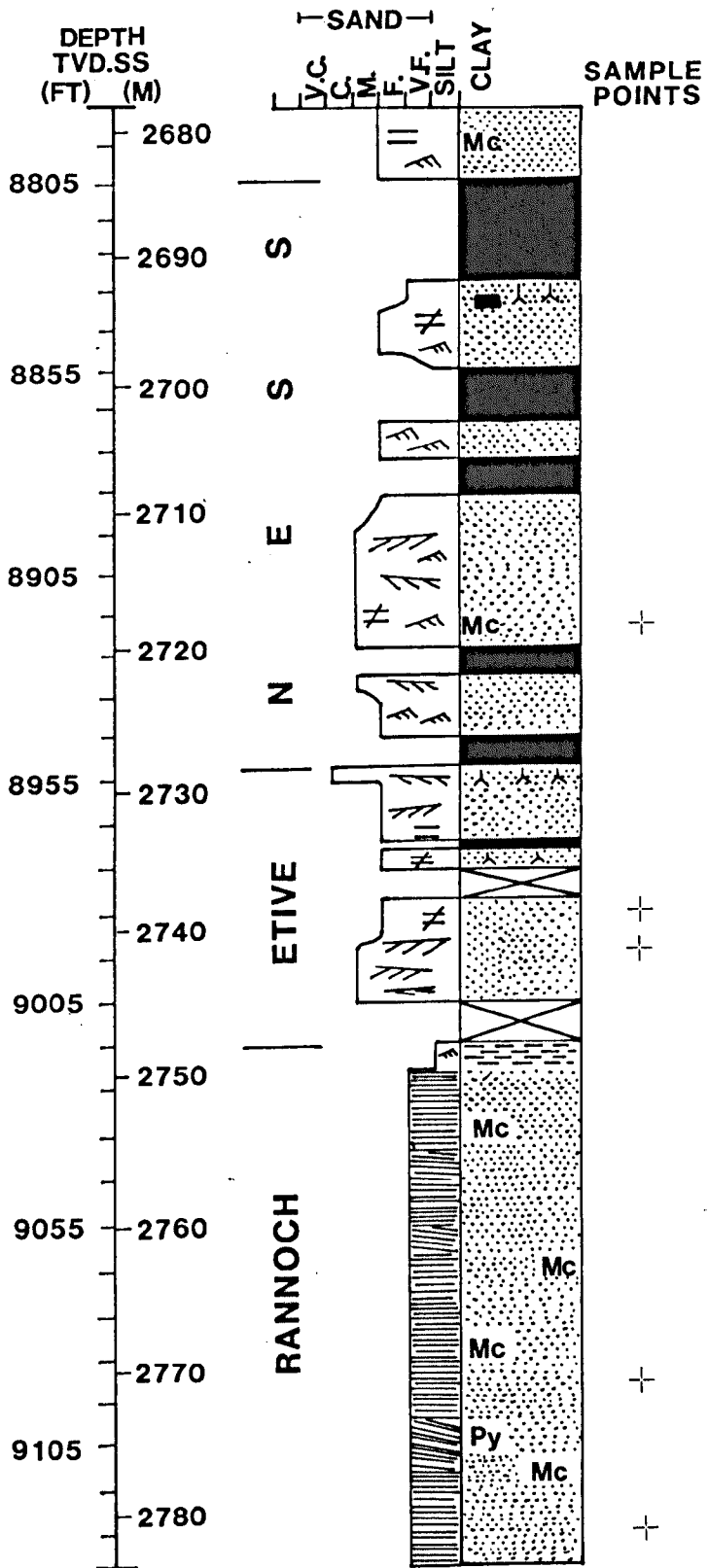


211/18-A30ST

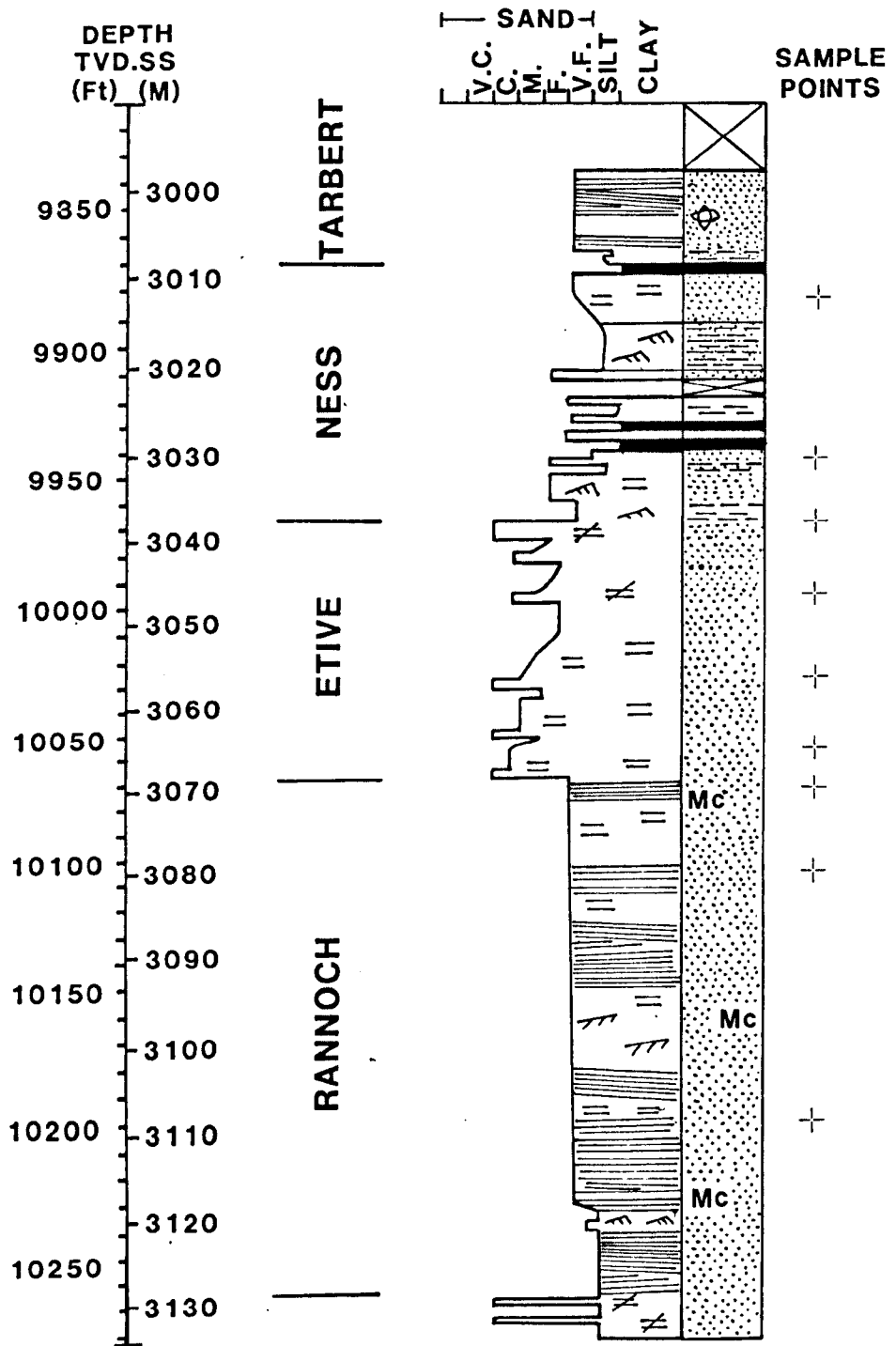




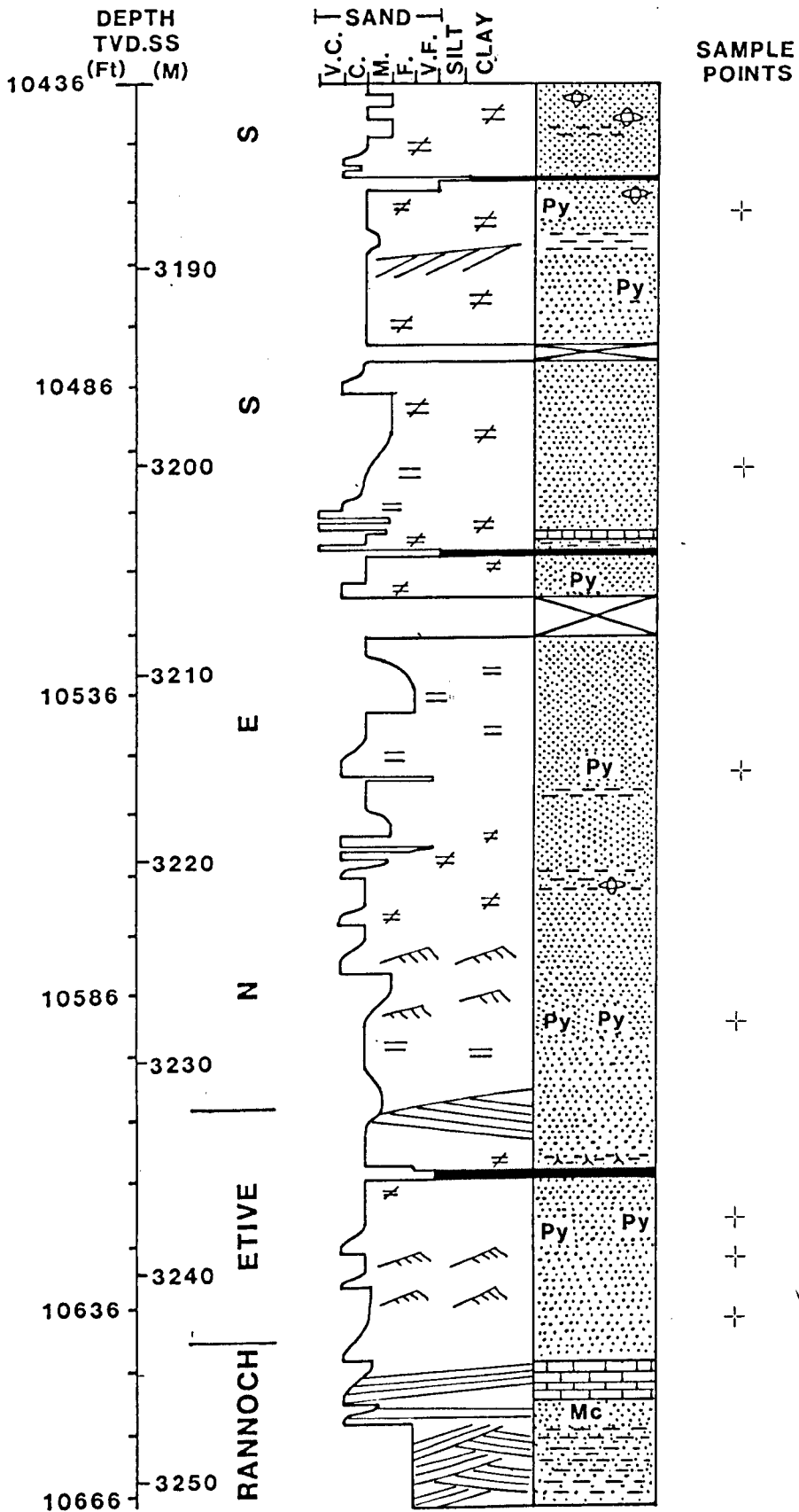
211/18-A33

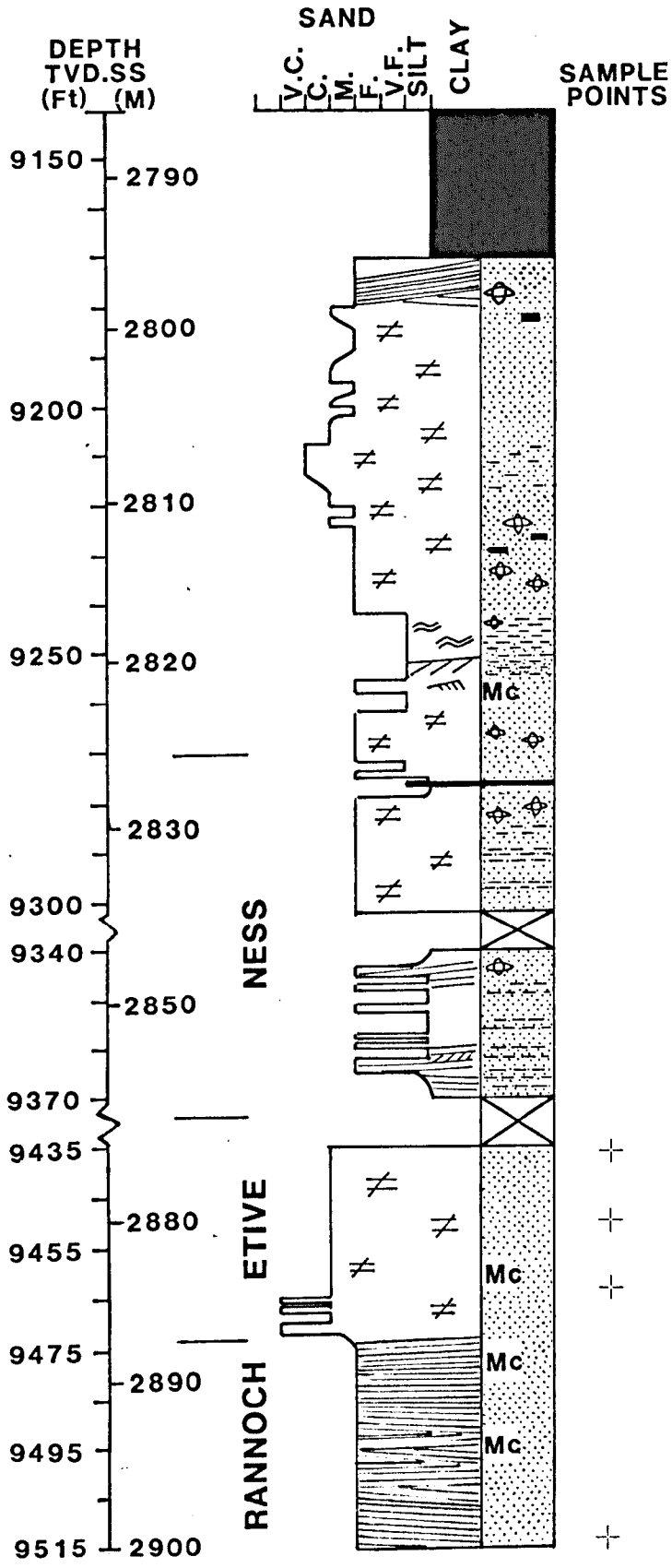


211/19-4

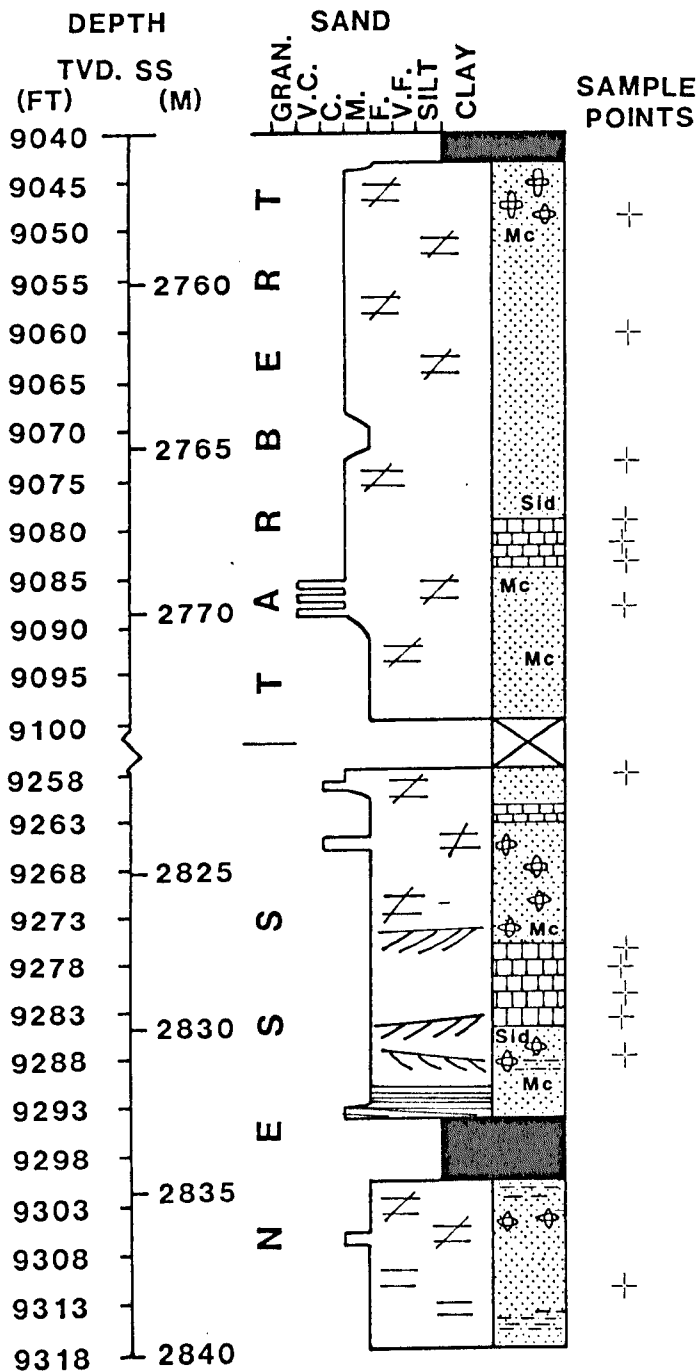


211/19-6

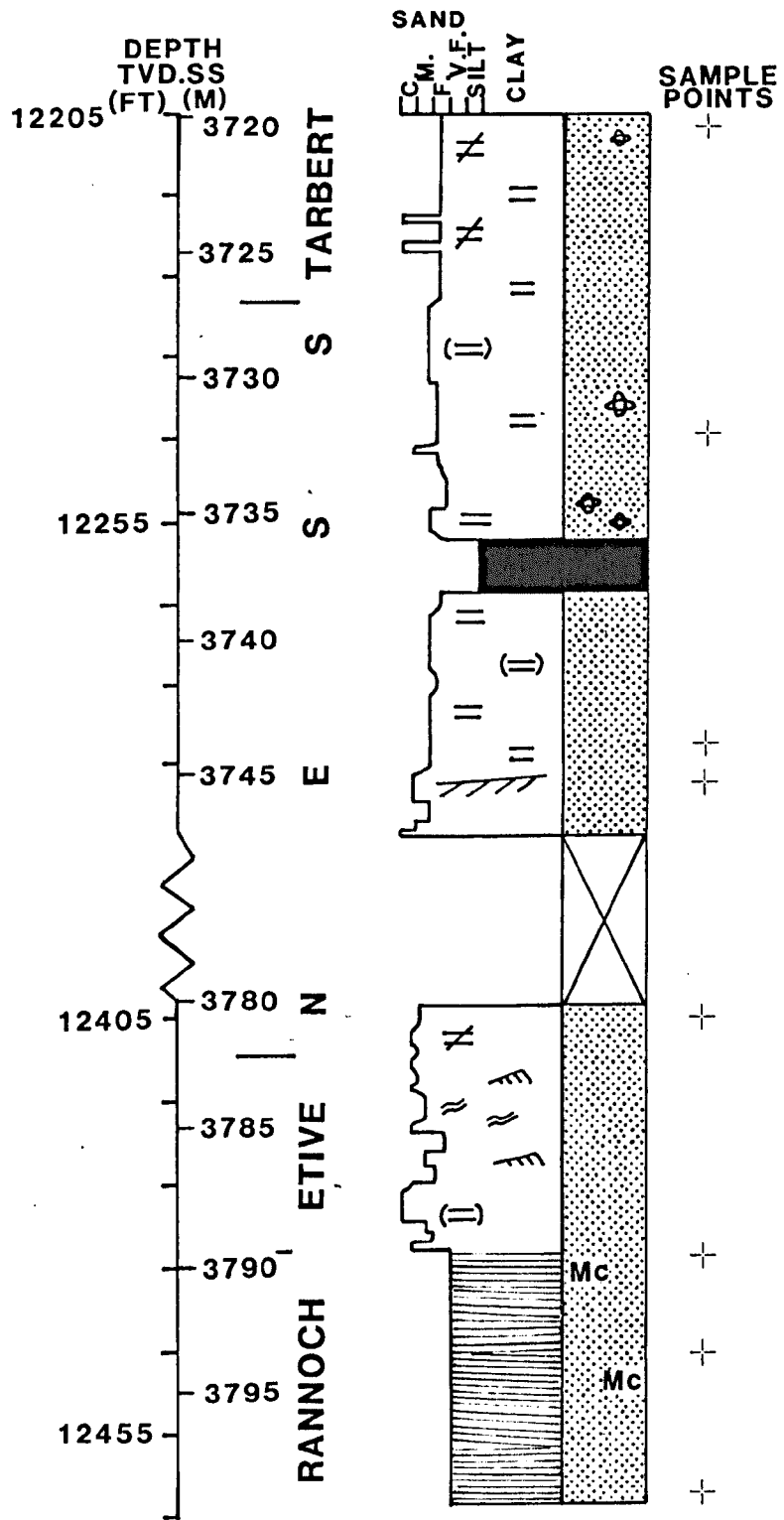




211/23-2



3/13a-1



MICROTHERMOMETRIC STUDIES

Equipment and sample preparation

The measurement of low and high temperature phase changes in fluid inclusions was made on a Linkam TH 600 heating - freezing stage (Shepherd 1981). The stage has a working temperature range of -180°C to $+600^{\circ}\text{C}$ with heating - cooling rates that may be varied between 0.1 and 90°C per minute. The ability to use such slow heating rates allows accurate measurement of the temperature of the phase changes in the inclusions. The stage was used in conjunction with a Leitz Dialux 20 - EB binocular microscope equipped with $\times 25$ eyepieces and $\times 32$ and $\times 50$ objectives, giving a maximum magnification of $\times 1250$. During the course of measurements the rate never exceeded $10^{\circ}\text{C}/\text{min}$ and when measuring phase transitions it was reduced to 0.2°C for homogenisation and 0.1°C for low temperature melting.

MacDonald & Spooner (1981) measured vertical and horizontal thermal gradients within the area of the sample block. Vertical thermal gradients were undetectable over a height of 300 microns above the stage, but horizontal gradients could be as high as 1.5°C at -95°C over the illuminated area of the block. Over the temperature range of interest (-50 to $+200^{\circ}\text{C}$) however, such discrepancies are insignificant when compared with the errors arising from imprecise calibration of the stage.

Samples containing quartz overgrowths which had usable inclusions were assessed prior to preparation of doubly polished wafers (40 - 100 microns thick) using the technique of Crosbie (1981).

CALIBRATION

1. LOW TEMPERATURE

Calibration of the stage was undertaken at low temperatures using the melting points of pure organic liquids and de-ionised water. These covered a temperature between -50 to 0°C . The liquid

standards were put into glass capillary tubes and cooled until frozen. Each sample was in turn heated at a rate corresponding to that used for actual inclusions. The melting point taken as the temperature at which the solid phase finally disappeared. Table 1 presents the liquids, along with their melting characteristics. The deviation between the true and measured melting point temperatures is used to construct the calibration curve (Fig.1).

2. HIGH TEMPERATURE

Calibration to 300°C was achieved using OMPS melting standards obtained from Omega Engineering Corporation of Stamford, U.S.A. A very small amount of the solid was placed between the cover slips and heated at similar rates to actual inclusions until it melted. The compounds are listed in Table 1 with their melting characteristics. Again the deviation between true and measured melting point temperatures was used to generate the calibration curve.

Calibration of the stage was fully checked every month, and prior to every period of use five of the standards verified. During periods of extended use the standards were checked once a week.

REFERENCES

CROSBIE, T.R., 1981, Polished wafer preparation for fluid inclusion and other studies: *Trans. Inst. Min. Metall. (Sect. B: Appl. earth sci.)*, v. 90, B82-B83.

MacDONALD, A.J., and SPOONER, E.T.C., 1981, Calibration of a LINKAM TH600 programmable heating - cooling stage for microthermometric analysis of fluid inclusions: *Econ. Geol.*, v. 76, p. 1248-1258.

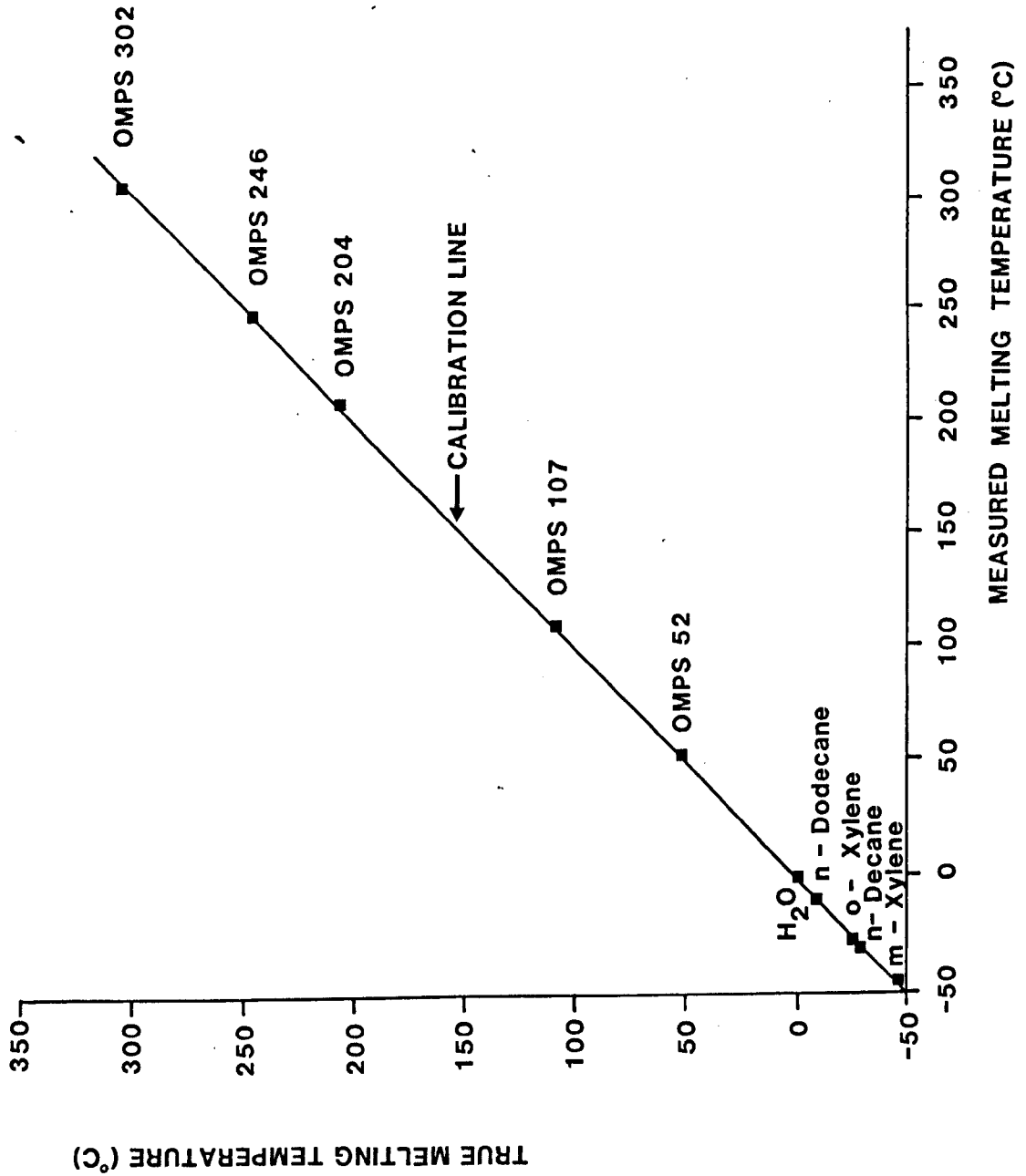
TABLE 1

Calibration compounds used and their melting behaviour

COMPOUNDS	TRUE T _m (°C)	MEASURED T _m (°C)	MELTING BEHAVIOUR
m-Xylene	-47.9	-48.4	Slow melting over a 1°C interval.
n-Decane	-29.7	-30.3	Protracted melting interval commencing 31°C.
o-Xylene	-25.2	-25.8	Protracted melting interval commencing at 27°C.
n-Dodecane	-9.6	-10.3	Very rapid melting.
Water (deionised)	0.0	-0.8	Almost isothermal melting
OMPS 52	51.1	50.7	Rapid melting of translucent laths.
OMPS 107	106.9	107.3	Rapid melting of semi-translucent prisms.
OMPS 204	205.6	207.3	Rapid melting of coarse prisms.
OMPS 246	245.6	247.9	Protracted melting of fine crystals.
OMPS 302	304.0	306.2	Protracted melting of fine dark brown crystals.

OMPS = Omega Melting Point Standard

Figure 1: Calibration curve for the LINKAM TH600 heating/
freezing stage



APPENDIX B

FLUID INCLUSION DATA: QUARTZ OVERGROWTHS II

MURCHISON 211/19-6

FORMATION	DEPTH (FT)	TVD.SS (M)	T _h (°C)	SALINITY (wt.% eq. NaCl)	T _m (°C)	T _e (°C)
NESS	10500'	3200	86.4	5.5	-3.4	-22.7
			93.6	-	-	-
			96.5	-	-	-
			84.2	-	-	-
			84.2	-	-	-
			95.2	-	-	-
			99.7	-	-	-
			102.1	-	-	-
			105.4	-	-	-
			107.9	-	-	-
			98.7	-	-	-
			122.4	-	-	-
			110.8	-	-	-
			111.7	-	-	-
			88.2	4.0	-2.4	-35.0
			96.2	-	-	-
			95.7	3.4	-2.0	-22.3
			91.7	-	-	-
			94.0	-	-	-
			99.7	-	-	-

WELL 3/13a-1

FORMATION	DEPTH (FT)	TVD.SS (M)	T _h (°C)	SALINITY (wt.% eq. NaCl)	T _m (°C)	T _e (°C)
TARBERT	12207'	3720	93.6	-	-	-
			97.2	-	-	-
			105.6	-	-	-
			98.5	-	-	-
			99.7	-	-	-
			97.2	-	-	-
			101.2	-	-	-
			103.3	-	-	-
			108.3	-	-	-
			107.8	-	-	-
			118.0	-	-	-
			101.1	-	-	-
			103.9	3.2	-1.9	-13.5
			112.5	-	-	-
			98.9	-	-	-
			98.3	-	-	-
131.1	2.9	-1.7	-13.6			
NESS	12267'	3739	105.2	-	-	-
			111.1	2.7	-1.6	-22.7
NESS	12283'	3743	119.5	-	-	-
			101.2	1.9	-1.1	-36.2

THISTLE

WELL 211/18-A45

FORMATION	DEPTH (FT)	TVD.SS (M)	T _h (°C)	SALINITY (wt.% eq. NaCl)	T _m (°C)	T _e (°C)
ETIVE	8624'	2628	87.4	6.4	-4.0	-48.1
ETIVE	8629'	2630	117.9	-	-	-
			121.6	-	-	-
			106.2	-	-	-
ETIVE	8631'	2631	109.4	-	-	-
			116.4	-	-	-
			103.9	-	-	-
			110.6	-	-	-
			100.2	-	-	-
			101.3	-	-	-

211/18-A30

ETIVE	9164'	2793	80.4	5.8	-3.6	-35.1
			82.8	-	-	-
			86.6	7.7	-4.9	-50.5
			87.5	-	-	-
			94.1	7.1	-4.5	-53.4
			81.1	-	-	-
			92.2	-	-	-
			105.4	-	-	-
			105.7	-	-	-
			109.4	-	-	-
			105.7	-	-	-
			117.8	-	-	-
			75.5	-	-	-
			80.1	-	-	-
			73.5	-	-	-
			73.6	-	-	-
			76.9	-	-	-
			79.7	-	-	-
			81.1	-	-	-

FORMATION	DEPTH	TVD.SS	T _h	SALINITY	T _m	T _e
	(FT)	(M)	(°C)	(wt.% eq. Na Cl)	(°C)	(°C)
			83.9	-	-	-
			84.1	-	-	-
			85.2	-	-	-
	9187'	2800	83.6	-	-	-
			83.7	-	-	-
			84.8	-	-	-
			89.4	-	-	-
			90.9	-	-	-
			82.4	-	-	-
			77.9	-	-	-
			95.3	-	-	-
	9227'	2812	82.9	-	-	-
			78.1	-	-	-
			74.9	6.1	-3.8	-36.0
			102.7	-	-	-
211/18-A30ST						
ETIVE	9223'	2811	90.9	-	-	-
			91.3	-	-	-
			87.1	-	-	-
			90.8	-	-	-
			87.7	-	-	-
ETIVE	9246'	2818	87.1	-	-	-
			91.7	5.7	-3.4	-14.1
			92.4	-	-	-
			94.2	3.5	-2.1	-
			109.1	3.7	-2.2	-
			94.2	3.9	-2.3	-
			82.9	-	-	-
			72.4	-	-	-
			80.9	-	-	-
			79.7	-	-	-
			86.2	8.6	-5.6	-
			91.9	3.2	-1.9	-

APPENDIX C - ELECTRON PROBE MICROANALYSES

SIDERITE: TRIPLE ZONED

WELL	FORMATION	DEPTH (FT)	TVD.SS (M)	Ca	Mg	Fe	Mn	ZONE
211/23-3	TARBERT	8885'	2707.1	2.0	0.4	96.1	1.5	I
211/23-4	TARBERT	9079'	2767.1	3.8	2.0	93.5	0.7	I
	TARBERT	9079'	2767.1	14.7	27.1	57.5	0.7	II
	TARBERT	9079'	2767.1	3.3	14.7	80.6	1.4	III
	NESS	9282'	2829.0	4.4	4.1	90.5	1.0	I
	NESS	9282'	2829.0	13.4	27.1	58.8	0.7	II
	NESS	9282'	2829.0	4.2	20.6	73.9	1.3	III
	NESS	9282'	2829.0	1.4	0.9	97.0	0.7	I
	NESS	9282'	2829.0	23.3	19.9	57.0	0.8	II
	NESS	9282'	2829.0	10.3	12.5	76.3	0.9	III
	NESS	9282'	2829.0	1.2	0.2	97.4	1.2	I
	NESS	9282'	2829.0	13.2	27.0	58.2	0.8	II
	NESS	9282'	2829.0	2.8	24.2	72.7	0.7	III
	NESS	9285'	2829.9	4.0	1.5	90.6	3.9	I
	NESS	9285'	2829.9	10.6	23.3	65.4	0.7	II
	NESS	9285'	2829.9	11.1	16.1	71.9	0.9	III

SIDERITE: TWO ZONES

211/23-4	TARBERT	9079'	2767.1	13.5	22.8	63.2	0.5	II
	TARBERT	9079'	2767.1	10.2	15.4	72.3	2.1	III
	NESS	9276'	2827.2	8.7	21.8	68.3	1.2	II
	NESS	9276'	2827.2	9.7	11.3	77.5	1.5	III
	NESS	9285'	2827.2	11.3	25.9	62.1	0.7	II
	NESS	9285'	2827.2	12.4	16.5	70.4	0.7	III

TARBERT	9081'	2768.0	12.8	19.1	67.0	1.1	II	*
TARBERT	9081'	2768.0	14.0	21.2	64.1	0.7	II	*
TARBERT	9081'	2768.0	16.1	21.7	61.5	0.7	II	*
TARBERT	9084'	2768.7	10.0	25.0	64.5	0.5	II	*

(* - The outer zone (III) was present but too thin to be analysed)

CALCITE

WELL	FORMATION	DEPTH (FT)	TVD.SS (M)	Ca	Mg	Fe	Mn
211/23-3	TARBERT	8885'	2708.0	96.2	1.3	2.3	0.2
	TARBERT	8885'	2708.0	96.5	1.2	2.0	0.3
	TARBERT	8885'	2708.0	97.7	0.7	1.4	0.2
211/23-4	TARBERT	9081'	2767.7	98.9	0.2	0.6	0.3
	TARBERT	9081'	2767.7	97.1	0.7	1.8	0.4
	TARBERT	9081'	2767.7	97.1	0.9	1.9	0.2
	TARBERT	9081'	2767.7	97.1	0.7	1.8	0.4
	TARBERT	9081'	2767.7	96.9	1.2	1.4	0.5
	NESS	9276'	2827.2	97.7	0.5	1.3	0.5
	NESS	9276'	2827.2	97.1	0.8	1.5	0.6
	NESS	9276'	2827.2	98.3	0.5	0.9	0.3
	NESS	9276'	2827.2	95.7	1.5	2.5	0.3
	NESS	9278'	2827.8	96.9	0.8	1.8	0.5
	NESS	9278'	2827.8	98.0	0.4	1.3	0.3
	NESS	9278'	2827.8	97.4	0.6	1.7	0.3
	NESS	9282'	2829.0	97.3	0.7	1.6	0.4
	NESS	9282'	2829.0	96.7	0.7	2.0	0.6
	NESS	9282'	2829.0	95.0	1.1	0.5	3.4
	NESS	9282'	2829.0	93.3	1.5	4.6	0.6
	NESS	9282'	2829.0	93.3	1.1	5.1	0.5
	NESS	9282'	2829.0	92.4	1.4	5.6	0.6
	NESS	9282'	2829.0	97.1	0.5	2.0	0.4
	NESS	9282'	2829.0	93.3	1.4	4.7	0.6
	NESS	9285'	2829.9	96.1	0.9	2.6	0.4
	NESS	9285'	2829.9	96.4	0.8	2.5	0.3
	NESS	9285'	2829.9	96.8	0.9	1.9	0.4
	NESS	9285'	2829.9	96.8	0.7	2.1	0.4
	NESS	9285'	2829.9	92.9	2.2	0.3	4.6

NESS	9285'	2829.9	96.6	0.7	2.3	0.4
NESS	9285'	2829.9	95.9	0.8	2.8	0.5

ANKERITE:

WELL	FORMATION	DEPTH (FT)	TVD.SS (M)	Ca	Mg	Fe	Mn
211/23-4	TARBERT	9079'	2767.1	58.8	25.9	14.3	1.0
	TARBERT	9079'	2767.1	58.2	27.6	13.7	0.5
	TARBERT	9079'	2767.1	58.6	26.1	14.6	0.7
	TARBERT	9079'	2767.1	58.4	26.5	14.5	0.6
	TARBERT	9079'	2767.1	58.6	27.1	13.6	0.7
	TARBERT	9079'	2767.1	58.6	26.6	13.9	0.9
	TARBERT	9079'	2767.1	57.8	27.8	13.5	0.9
	TARBERT	9079'	2767.1	56.9	24.6	17.5	1.0
	TARBERT	9079'	2767.1	57.5	26.4	15.2	0.9
	TARBERT	9081'	2768.0	49.0	31.7	18.5	0.8
	TARBERT	9081'	2768.0	49.7	32.8	16.8	0.7
	TARBERT	9081'	2728.0	49.2	30.7	19.1	1.0
	TARBERT	9084'	2768.7	59.7	26.4	13.2	0.7
	TARBERT	9084'	2768.7	50.6	37.5	11.5	0.4
	TARBERT	9084'	2768.7	56.7	29.7	12.6	1.0
	NESS	9276'	2827.2	56.0	24.3	18.9	0.8
	NESS	9285'	2829.9	60.0	27.0	12.3	0.7